

RADIOLOGY AND ONCOLOGY

vol.50 no.2

june 2016



NOVA SMER DO PODALJŠANJA CELOKUPNEGA PREŽIVETJA



Prva in edina samostojna kemoterapija, ki v primerjavi z ostalimi možnostmi zdravljenja z enim zdravilom, pri bolnicah s predhodno že večkratno zdravljenim metastatskim rakom dojke, dokazano značilno podaljša celokupno preživetje.^{1,2}



- **Halaven** (eribulin): ne-taksanski zaviralec dinamike mikrotubulov, prvo zdravilo iz nove skupine kemoterapevtikov, imenovanih *halihondrini*.
- Zdravilo HALAVEN je indicirano za zdravljenje bolnic z lokalno napredovalim ali metastatskim rakom dojke, ki je napredoval po vsaj enem režimu kemoterapije za napredovalo bolezen. Predhodna zdravljenja morajo vključevati antraciklin in taksan, bodisi kot adjuvantno zdravljenje ali za zdravljenje metastatskega raka dojke, razen če to zdravljenje za bolnice ni bilo primerno.¹
- Priporočeni odmerek 1,23 mg/m², intravensko, v obliki 2- do 5-minutne infuzije, 1. in 8. dan vsakega 21-dnevnega cikla.
- Ena 2 ml viala vsebuje 0,88 mg eribulina.
- Rastvorina, pripravljena za uporabo, redčenje ni potrebno.

SKRAJŠAN POVZETEK GLAVNIH ZNAČILNOSTI ZDRAVILA

HALAVEN 0,44 mg/ml raztopina za injiciranje (eribulin)
TERAPEVTSKE INDIKACIJE: Zdravljenje lokalno napredovalega ali metastatskega raka dojke, ki je napredoval po vsaj enem režimu kemoterapije za napredovalo bolezen vključno z antraciklinom in taksanom (adjuvantno zdravljenje ali zdravljenje metastatskega raka dojke), razen če to ni bilo primerno. **ODMERJANJE IN NAČIN UPORABE:** Halaven se daje v enotah, specializiranih za dajanje citotoksične kemoterapije, in le pod nadzorom usposobljenega zdravnika z izkušnjami v uporabi citotoksičnih zdravil. **Odmernje:** Priporočeni odmerek eribulina v obliki raztopine je 1,23 mg/m² i.v. v obliki 2- do 5-minutne infuzije 1. in 8. dan vsakega 21-dnevnega cikla. Bolnikom je lahko slabo ali bruhanje. Treba je razmisлити o antiemetični profilaksi, vključno s kortikosteroidi. **Preložitev odmerka med zdravljenjem:** Dajanje Halavena je treba preložiti, če se pojavi kaj od naslednjih: absolutno število nevtrofilcev (ANC) < 1 x 10⁹/l, trombociti < 75 x 10⁹/l ali nehematološki neželeni učinki 3. ali 4. stopnje. **Zmanjšanje odmerka med zdravljenjem:** Za priporočila za zmanjšanje odmerka ob pojavu hematoloških ali nehematoloških neželenih učinkov glejte celoten povzetek glavnih značilnosti zdravila. **Okvara jeter zaradi zasevkov:** Priporočeni odmerek pri blagi okvari jeter (stopnje A po Child-Pughu) je 0,97 mg/m² v obliki 2- do 5-minutne i.v. infuzije 1. in 8. dan 21-dnevnega cikla. Priporočeni odmerek pri zmernih okvari jeter (stopnje B po Child-Pughu) je 0,62 mg/m² v obliki 2- do 5-minutne i.v. infuzije 1. in 8. dan 21-dnevnega cikla. Pri hudi okvari jeter (stopnje C po Child-Pughu) se pričakuje, da je treba dati še manjši odmerek eribulina. **Okvara jeter zaradi ciroze:** Zgornje odmerke se lahko uporabi za blago do zmerno okvaro, vendar se priporoča skrbno nadziranje, saj bo odmerek morda treba ponovno prilagoditi. **Okvara ledvic:** Pri hudi okvari ledvic (očistek kreatinina < 40 ml/min) bo morda treba odmerek zmanjšati. Priporočila se skrbno nadzirajo v skladu s kliničnimi podatki. **Okvara ledvic:** Odmerek se lahko razrediži z do 100 ml 0,9 % raztopine natrijevega klorida (9 mg/ml) za injiciranje. Ne sme se ga redčiti v 5 % infuzijski raztopini glukoze. Pred dajanjem glejte navodila glede redčenja zdravila v celotnem povzetku glavnih značilnosti zdravila ter se prepričajte, da obstaja dober periferni venski dostop ali prehodna centralna linija. Ni znakov, da bi eribulin povzročal mehurje ali dražlj. V primeru ekstravazacije mora biti zdravljenje simptomatsko. **KONTRAINDIKACIJE:** Preobčutljivost na zdravilno učinkovino ali katerokoli pomožni snov. Dojenje. **POSEBNA OPOZORILO IN PREVIDNOSTNI UKREPI:** Mielosupresija je odvisna od odmerka in se kaže kot nevropatija. Pred vsakim odmerkom eribulina je treba opraviti pregled celotne krvne slike. Zdravljenje z eribulinom se lahko uvede le pri bolnikih z vrednostmi ANC $\geq 1,5 \times 10^9/l$ in s trombociti > 100 x 10⁹/l. Bolnike, pri katerih se pojavijo febrilna nevropatija, huda nevropatija ali trombotična, je treba zdravljenje v skladu s priporočili v celotnem povzetku glavnih značilnosti zdravila. Hudo nevropatijo se lahko zdravi z uporabo G-CSF ali enakovrednim zdravilom v skladu s smernicami. Bolnike je treba skrbno nadzirati za znake periferne motorične in senzorične nevropatije. Pri razvoju hude periferne nevrotoksičnosti je treba odmerek prestativati ali zmanjšati. Če začnemo zdravljenje pri bolnikih s kongestivnim srčnim popuščanjem, z bradibradijami ali sočasno z zdravili, za katera je znano, da podaljšujejo interval QT, vključno z antiaritmiki razreda la in III, in z

elektrolitskimi motnjami, je priporočljivo spremljanje EKG. Pred začetkom zdravljenja s Halavenom je treba popraviti hipokallemijo in hipomagnezijo in te elektrolite je treba občasno kontrolirati med zdravljenjem. Eribulina ne smemo dajati bolnikom s prirojenim sindromom dolgega intervala QT. To zdravilo vsebuje majhne količine etanola (alkohola), manj kot 100 mg na odmerek. Eribulin je pri podganah embriotoksičen, fetotoksičen in teratogen. Halavena se ne sme uporabljati med nosečnostjo, razen kadar je to nujno potrebno. Ženske v rodni dobi naj ne zanosi v času, ko same ali njihov moški partner dobivajo Halaven, in naj med zdravljenjem in še do 3 mesece po njem uporabljajo učinkovito kontracepcijo. Moški naj se pred zdravljenjem posvetujejo o shranjevanju sperme zaradi možnosti nepopravljive neplodnosti. **INTERAKCIJE:** Eribulin se izloča do 70 % prek žolča. Sočasna uporaba učinkovin, ki zavirajo jetrne transportne beljakovine, kot so beljakovine za prenos organskih anionov in beljakovine, odporne na številna zdravila, z eribulinom se ne priporoča (npr. ciklosporin, ritonavir, sakvinavir, lopinavir in nekateri drugi zaviralci proteaze, efavirenz, emtricitabin, verapamil, klaritromicin, kinin, kinidin, dipiramidid). Sočasno zdravljenje z indukcijami učinkovinami, kot so rifampicin, karbamazepin, fenitoin, šentjanževka, lahko povzroči znižanje koncentracij eribulina v plazmi, zato je ob sočasni uporabi indikatorjev potrebna previdnost. Eribulin je blag inhibitor encima CYP3A4. Priporočila je previdnost in spremljanje glede neželenih učinkov pri sočasni uporabi snovi, ki imajo ozko terapevtsko okno in se odstranjujejo iz telesa predvsem preko CYP3A4 (npr. alfentanil, ciklosporin, ergotamin, fentanyl, pimožid, kinidin, sirolimus, takrolimus). **NEŽELENI UČINKI:** **Povzetek varnostnega profila** Neželeni učinek, o katerem najpogosteje poročajo v zvezi s Halavenom, je supresija kostnega mozga, ki se kaže kot nevropatija, levkopenija, anemija, trombocitopenija s pridruženimi okužbami. Poročali so tudi o novem začetku ali poslabšanju že obstoječe periferne nevropatije. Med neželenimi učinki, o katerih poročajo, je toksičnost za prebavila, ki se kaže kot anoreksija, navzea, bruhanje, driska, zaprtost in stomatitis. Med drugimi neželenimi učinki so utrujenost, alopecija, zvečani jetrni encimi, sepsa in mišičnoskeletni bolečinski sindrom. **Seznam neželenih učinkov:** **Zelo pogosti ($\geq 1/10$):** nevropatija (57,0 %) (3/4. stopnje: 49,7 %), levkopenija (29,3 %) (3/4. stopnje: 17,3 %), anemija (20,6 %) (3/4. stopnje: 2,0 %), zmanjšani apetit (21,9 %) (3/4. stopnje: 0,7 %), periferne nevropatije (35,6 %) (3/4. stopnje: 7,6 %), glavobol (17,2 %) (3/4. stopnje: 0,8 %), dispneja (13,9 %) (3/4. stopnje: 3,1 %), kašelj (13,6 %) (3/4. stopnje: 0,6 %), navzea (33,8 %) (3/4. stopnje: 1,1 %), zaprtost (19,6 %) (3/4. stopnje: 0,6 %), driska (17,9 %) (3/4. stopnje: 0,8 %), bruhanje (17,6 %) (3/4. stopnje: 0,9 %), alopecija, artralgijska in mialgijska (19,4 %) (3/4. stopnje: 1,1 %), bolečina v hrbtu (13,0 %) (3/4. stopnje: 1,5 %), bolečina v udih (10,0 %) (3/4. stopnje: 0,7 %), utrujenost/astenija (47,9 %) (3/4. stopnje: 7,8 %), pireksija (20,4 %) (3/4. stopnje: 0,6 %), zmanjšanje telesne mase (11,3 %) (3/4. stopnje: 0,3 %). **Pogosti ($\geq 1/100$ do < 1/10):** okužba sečil (8 %) (3/4. stopnje: 0,5 %), pljučnica (1,2 %) (3/4. stopnje: 0,8 %), ustna kandidiaza, ustni herpes, okužba zgornjih dihal, nazofarngitis, rinitis, limfopenija (4,9 %) (3/4. stopnje: 1,4 %), febrilna nevropatija (4,7 %) (3/4. stopnje: 4,5 %), trombotična (4,3 %) (3/4. stopnje: 0,7 %), hipokallemija (6,1 %) (3/4. stopnje:

1,7 %), hipomagnezija (2,9 %) (3/4. stopnje: 0,2 %), dehidracija (2,8 %) (3/4. stopnje: 0,5 %), hiperglikemija, hipofosfatemija, nespečnost, depresija, disgezija, omotičnost (7,9 %) (3/4. stopnje: 0,5 %), hipoestezija, letargija, nevrotoksičnost, obilnejše solzenje (6,0 %) (3/4. stopnje: 0,1 %), konjunktivitis, vrtoglavica, tahikardija, vročinski valovi, orofaringealna bolečina, epistaksa, rinoreja, bolečina v trebuhu, stomatitis (9,3 %) (3/4. stopnje: 0,8 %), suha usta, dispneja (5,9 %) (3/4. stopnje: 0,2 %), gastroezofagealna refluksna bolezen, razjede v ustih, distenzija trebuha, zvišanje alanin-aminotransferaze (7,6 %) (3/4. stopnje: 2,1 %), zvišanje aspartat-aminotransferaze (7,4 %) (3/4. stopnje: 1,5 %), zvišanje gama-glutamyltransferaze (1,8 %) (3/4. stopnje: 0,9 %), hiperbilirubinemija (1,5 %) (3/4. stopnje: 0,3 %), izpuščaji, pruritus (3,9 %) (3/4. stopnje: 0,1 %), boleznino nohtov, nočno potenje, suha koža, eritem, hiperhidroza, bolečina v kosteh (9,6 %) (3/4. stopnje: 1,7 %), mišični spazmi (5,1 %) (3/4. stopnje: 0,1 %), mišično-skeletna bolečina in mišično-skeletna bolečina v prsih, mišična oslabelost, disurija, vnetje sluznice (8,3 %) (3/4. stopnje: 1,1 %), periferni edem, bolečina, mrzlica, bolečina v prsih, gripi podobna bolezen. **Občasni ($\geq 1/1.000$ do < 1/100):** sepsa (0,5 %) (3/4. stopnje: 0,2 %), nevropenična sepsa (0,1 %) (3/4. stopnje: 0,1 %), herpes zoster, tinitus, globoka venska tromboza, pljučna embolija, hepatotoksičnost (1,0 %) (3/4. stopnje: 0,6 %), palmarno-plantarna eritrodisezija, hematurnija, proteinurija, odpoved ledvic. **Redki ($\geq 1/10.000$ do < 1/1.000):** diseminirana intravaskularna koagulacija, intersticijska pljučna bolezen, pankreatitis, angioedem. Za popoln opis neželenih učinkov glejte celoten povzetek glavnih značilnosti zdravila. Vrstna ovjavnine in vsebina: viala z 2 ml raztopine. **Režim izdaje:** H Imetnik dovoljenja za promet: Eisai Europe Ltd, European Knowledge Centre, Mosquito Way, Hatfield, Hertfordshire, AL10 9SN, Velika Britanija HAL-270614, julij 2014

Pred predpisovanjem in uporabo zdravila prosimo preberite celoten povzetek glavnih značilnosti zdravila!

Viri: (1) Povzetek glavnih značilnosti zdravila Halaven, junij 2014; (2) Cortes J et al. *Lancet* 2011; 377: 914–23.


PharmaSwiss
Choose More Life

Odgovoren za trženje v Sloveniji:
PharmaSwiss d.o.o., Brodišče 32, 1236 Trzin
telefon: +386 1 236 47 00, faks: +386 1 283 38 10

HAL-0714-01, julij 2014



Publisher

Association of Radiology and Oncology

Affiliated with

Slovenian Medical Association – Slovenian Association of Radiology, Nuclear Medicine Society,
Slovenian Society for Radiotherapy and Oncology, and Slovenian Cancer Society
Croatian Medical Association – Croatian Society of Radiology
Societas Radiologorum Hungarorum
Friuli-Venezia Giulia regional groups of S.I.R.M.
Italian Society of Medical Radiology

Aims and scope

Radiology and Oncology is a journal devoted to publication of original contributions in diagnostic and interventional radiology, computerized tomography, ultrasound, magnetic resonance, nuclear medicine, radiotherapy, clinical and experimental oncology, radiobiology, radiophysics and radiation protection.

Editor-in-Chief

Gregor Serša, Institute of Oncology Ljubljana,
Department of Experimental Oncology, Ljubljana,
Slovenia

Executive Editor

Viljem Kovač, Institute of Oncology Ljubljana,
Department of Radiation Oncology, Ljubljana, Slovenia

Deputy Editors

Andrej Čör, University of Primorska, Faculty of
Health Science, Izola, Slovenia

Maja Čemažar, Institute of Oncology Ljubljana,
Department of Experimental Oncology, Ljubljana,
Slovenia

Igor Kocijančič, University Medical Centre
Ljubljana, Institute of Radiology, Ljubljana, Slovenia

Karmen Stanič, Institute of Oncology Ljubljana,
Department of Radiation Oncology, Ljubljana, Slovenia

Primož Strojjan, Institute of Oncology Ljubljana,
Department of Radiation Oncology, Ljubljana, Slovenia

Editorial Board

Sotirios Bisdas, National Hospital for Neurology
and Neurosurgery, University College London
Hospitals, London, UK

Karl H. Bohuslavizki, Facharzt für
Nuklearmedizin, Hamburg, Germany

Serena Bonin, University of Trieste, Department of
Medical Sciences, Trieste, Italy

Boris Brkljačić, University Hospital "Dubrava",
Department of Diagnostic and Interventional
Radiology, Zagreb, Croatia

Luca Campana, Veneto Institute of Oncology
(IOV-IRCCS), Padova, Italy

Christian Dittrich, Kaiser Franz Josef - Spital,
Vienna, Austria

Metka Filipič, National Institute of Biology,
Department of Genetic Toxicology and Cancer Biology,
Ljubljana, Slovenia

Maria Gódeny, National Institute of Oncology,
Budapest, Hungary

Janko Kos, University of Ljubljana, Faculty of
Pharmacy, Ljubljana, Slovenia

Robert Jeraj, University of Wisconsin, Carbone
Cancer Center, Madison, Wisconsin, USA

Advisory Committee

Tullio Girdali, University of Trieste, Faculty of
Medicine and Psychology, Trieste, Italy

Vassil Hadjidekov, Medical University,
Department of Diagnostic Imaging, Sofia, Bulgaria

Tamara Lah Turnšek, National Institute of
Biology, Ljubljana, Slovenia

Damijan Miklavčič, University of Ljubljana,
Faculty of Electrical Engineering, Ljubljana, Slovenia

Luka Milas, UT M. D. Anderson Cancer Center,
Houston, USA

Damir Miletić, Clinical Hospital Centre Rijeka,
Department of Radiology, Rijeka, Croatia

Håkan Nyström, Skandionkliniken,
Uppsala, Sweden

Maja Osmak, Ruder Bošković Institute,
Department of Molecular Biology, Zagreb, Croatia

Dušan Pavčnik, Dotter Interventional Institute,
Oregon Health Science University, Oregon,
Portland, USA

Geoffrey J. Pilkington, University of
Portsmouth, School of Pharmacy and Biomedical
Sciences, Portsmouth, UK

Ervin B. Podgoršak, McGill University,
Montreal, Canada

Matthew Podgorsak, Roswell Park Cancer
Institute, Departments of Biophysics and Radiation
Medicine, Buffalo, NY, USA

Marko Hočevar, Institute of Oncology Ljubljana,
Department of Surgical Oncology, Ljubljana, Slovenia

Miklós Kásler, National Institute of Oncology,
Budapest, Hungary

Csaba Polgar, National Institute of Oncology,
Budapest, Hungary

Dirk Rades, University of Lubeck, Department of
Radiation Oncology, Lubeck, Germany

Mirjana Rajer, Institute of Oncology Ljubljana,
Department of Radiation Oncology, Ljubljana, Slovenia

Luis Souhami, McGill University, Montreal,
Canada

Borut Štabuc, University Medical Centre Ljubljana,
Department of Gastroenterology, Ljubljana, Slovenia

Katarina Šurlan Popovič, University Medical
Center Ljubljana, Clinical Institute of Radiology,
Ljubljana, Slovenia

Justin Teissié, CNRS, IPBS, Toulouse, France

Gillian M. Tozer, University of Sheffield,
Academic Unit of Surgical Oncology, Royal
Hallamshire Hospital, Sheffield, UK

Andrea Veronesi, Centro di Riferimento
Oncologico - Aviano, Division of Medical Oncology,
Aviano, Italy

Branko Zakotnik, Institute of Oncology Ljubljana,
Department of Medical Oncology, Ljubljana, Slovenia

Stojan Plesničar, Institute of Oncology Ljubljana,
Department of Radiation Oncology, Ljubljana, Slovenia

Tomaž Benulič, Institute of Oncology Ljubljana,
Department of Radiation Oncology, Ljubljana, Slovenia

Editorial office

Radiology and Oncology

Zaloška cesta 2

P. O. Box 2217

SI-1000 Ljubljana

Slovenia

Phone: +386 1 5879 369

Phone/Fax: +386 1 5879 434

E-mail: gsera@onko-i.si

Copyright © Radiology and Oncology. All rights reserved.

Reader for English

Vida Kološa

Secretary

Mira Klemenčič

Zvezdana Vukmirović

Design

Monika Fink-Serša, Samo Rován, Ivana Ljubanović

Layout

Matjaž Lužar

Printed by

Tiskarna Ozimek, Slovenia

Published quarterly in 400 copies

Beneficiary name: DRUŠTVO RADIOLOGIJE IN ONKOLOGIJE

Zaloška cesta 2

1000 Ljubljana

Slovenia

Beneficiary bank account number: SI56 02010-0090006751

IBAN: SI56 0201 0009 0006 751

Our bank name: Nova Ljubljanska banka, d.d.,

Ljubljana, Trg republike 2,

1520 Ljubljana; Slovenia

SWIFT: LJBASIX

Subscription fee for institutions EUR 100, individuals EUR 50

The publication of this journal is subsidized by the Slovenian Research Agency.

Indexed and abstracted by:

- *Celdes*
- *Chemical Abstracts Service (CAS)*
- *Chemical Abstracts Service (CAS) - SciFinder*
- *CNKI Scholar (China National Knowledge Infrastructure)*
- *CNPIEC*
- *DOAJ*
- *EBSCO - Biomedical Reference Collection*
- *EBSCO - Cinahl*
- *EBSCO - TOC Premier*
- *EBSCO Discovery Service*
- *Elsevier - EMBASE*
- *Elsevier - SCOPUS*
- *Google Scholar*
- *J-Gate*
- *JournalTOCs*
- *Naviga (Softweco)*
- *Primo Central (ExLibris)*
- *ProQuest - Advanced Technologies Database with Aerospace*
- *ProQuest - Health & Medical Complete*
- *ProQuest - Illustrata: Health Sciences*
- *ProQuest - Illustrata: Technology*
- *ProQuest - Medical Library*
- *ProQuest - Nursing & Allied Health Source*
- *ProQuest - Pharma Collection*
- *ProQuest - Public Health*
- *ProQuest - Science Journals*
- *ProQuest - SciTech Journals*
- *ProQuest - Technology Journals*
- *PubMed*
- *PubsHub*
- *ReadCube*
- *SCImago (SJR)*
- *Summon (Serials Solutions/ProQuest)*
- *TDOne (TDNet)*
- *Thomson Reuters - Journal Citation Reports/Science Edition*
- *Thomson Reuters - Science Citation Index Expanded*
- *Ulrich's Periodicals Directory/ulrichsweb*
- *WorldCat (OCLC)*

This journal is printed on acid-free paper

On the web: ISSN 1581-3207

<http://www.degruyter.com/view/j/raon>

<http://www.radioloncol.com>

contents

review

- 129 **Malignant gliomas: old and new systemic treatment approaches**
Tanja Mesti, Janja Ocvirk
- 139 **Early medical rehabilitation after neurosurgical treatment of malignant brain tumours in Slovenia**
Natasa Kos, Boris Kos, Mitja Benedicic

radiology

- 145 **Screen-detected ductal carcinoma in situ found on stereotactic vacuum-assisted biopsy of suspicious microcalcifications without mass: radiological-histological correlation**
Bartłomiej Szynglarewicz, Piotr Kasprzak, Przemyslaw Biecek, Agnieszka Halon, Rafal Matkowski

nuclear medicine

- 153 **^{18}F -FET and ^{18}F -FCH uptake in human glioblastoma T98G cell lines**
Marco Giovanni Persico, Federica Eleonora Buroni, Francesca Pasi, Lorenzo Lodola, Carlo Aprile, Rosanna Nano, Marina Hodolic

experimental oncology

- 159 **Imaging of human glioblastoma cells and their interactions with mesenchymal stem cells in the zebrafish (*Danio rerio*) embryonic brain**
Miloš Vittori, Barbara Breznik, Tajda Gredar, Katja Hrovat, Lilijana Bizjak Mali, Tamara Turnsek Lah
- 168 **Identification of differentially expressed genes associated with the enhancement of X-ray susceptibility by RITA in a hypopharyngeal squamous cell carcinoma cell line (FaDu)**
Jinwei Luan, Xianglan Li, Rutao Guo, Shanshan Liu, Hongyu Luo, Qingshan You
- 175 **Diffusion tensor MR microscopy of tissues with low diffusional anisotropy**
Franci Bajd, Carlos Mattea, Siegfried Stapf, Igor Serša

clinical oncology

- 188 **The prognostic value of whole blood *SOX2*, *NANOG* and *OCT4* mRNA expression in advanced small-cell lung cancer**
Eva Sodja, Matija Rijavec, Ana Koren, Aleksander Sadikov, Peter Korosec, Tanja Cufer

- 197 **Tenckhoff tunneled peritoneal catheter placement in the palliative treatment of malignant ascites: technical results and overall clinical outcome**
Geert Maleux, Inge Indesteege, Annouschka Laenen, Chris Verslype, Ignace Vergote, Hans Prenen
- 204 **CA19-9 serum levels predict micrometastases in patients with gastric cancer**
Tomaz Jagric, Stojan Potrc, Katarina Mis, Mojca Plankl, Tomaz Mars
- 212 **Hepatic splenosis mimicking liver metastases in a patient with history of childhood immature teratoma**
Sara Jereb, Blaz Trotovsek, Breda Skrbinc
- 218 **Treatment of nasopharyngeal carcinoma using simultaneous modulated accelerated radiation therapy via helical tomotherapy: a phase II study**
Lei Du, XinXin Zhang, LinChun Feng, Jing Chen, Jun Yang, HaiXia Liu, ShouPing Xu, ChuanBin Xie, Lin Ma
- 226 **Bevacizumab plus chemotherapy in elderly patients with previously untreated metastatic colorectal cancer: single center experience**
Janja Ocvirk, Maja Ebert Moltara, Tanja Mesti, Marko Boc, Martina Rebersek, Neva Volk, Jernej Benedik, Zvezdana Hlebanja

radiophysics

- 232 **The dosimetric significance of using 10 MV photons for volumetric modulated arc therapy for post-prostatectomy irradiation of the prostate bed**
Henry Kleiner, Matthew B. Podgorsak,
- 238 **Effect of photon energy spectrum on dosimetric parameters of brachytherapy sources**
Mahdi Ghorbani, Mohammad Mehrpouyan, David Davenport, Toktam Ahmadi Moghaddas

| *slovenian abstracts*

Malignant gliomas: old and new systemic treatment approaches

Tanja Mesti¹, Janja Ocvirk^{1,2}

¹ Department of Medical Oncology, Institute of Oncology Ljubljana, Ljubljana, Slovenia

² Faculty of Medicine, University of Ljubljana, Ljubljana, Slovenia

Radiol Oncol 2016; 50(2): 129-138.

Received 30 June 2014

Accepted 29 September 2014

Correspondence to: Asisst. Prof. Janja Ocvirk, M.D., Ph.D., Institute of Oncology Ljubljana, Zaloška 2, SI-1000 Ljubljana, Slovenia.
Phone: +386 1 5879 220; Fax: +386 1 5879 305; E-mail: jocvirk@onko-i.si

Disclosure: No potential conflicts of interest were disclosed.

Background. Malignant (high-grade) gliomas are rapidly progressive brain tumours with very high morbidity and mortality. Until recently, treatment options for patients with malignant gliomas were limited and mainly the same for all subtypes of malignant gliomas. The treatment included surgery and radiotherapy. Chemotherapy used as an adjuvant treatment or at recurrence had a marginal role.

Conclusions. Nowadays, the treatment of malignant gliomas requires a multidisciplinary approach. The treatment includes surgery, radiotherapy and chemotherapy. The chosen approach is more complex and individually adjusted. By that, the effect on the survival and quality of life is notable higher.

Key words: malignant gliomas; systemic treatment; multidisciplinary; survival; quality of life

Introduction

Malignant (high-grade) gliomas are rapidly progressive brain tumors comprising of anaplastic oligodendroglioma, anaplastic astrocytoma, mixed anaplastic oligoastrocytoma (all grade III, World Health Organization [WHO]) and glioblastoma (grade IV, WHO).¹

The incidence of malignant gliomas is approximately 5/100,000. Malignant gliomas constitute 35–45% of primary brain tumors. Glioblastomas account for approximately 60 to 70% of malignant gliomas, while anaplastic astrocytomas represent 10 to 15%, and anaplastic oligodendrogliomas and anaplastic oligoastrocytomas 10% of malignant gliomas.¹⁻³ The incidence of these tumors has increased slightly over past two decades, especially in the elderly. The peak incidence is in the fifth and sixth decade of life. The median age of patients at the time of diagnosis in the case of glioblastoma is 64 years and in the case of anaplastic gliomas 45 years. Malignant gliomas are 40% more frequent in men than in women and twice more frequent in white population than in black one.^{2,4,5}

In Slovenia from 1991 till 2005, a total of 1636 patients (878 males and 758 females) were diagnosed with brain cancer. Since 2001 till 2005 the microscopical verification was performed in 83% of cases: 82% were gliomas, of which two thirds were glioblastoma, 14% astrocytoma and 10% oligodendroglioma. Approximately 60% of the patients were diagnosed at age between 50 to 74 years, and 25% at age between 20 to 49 years.⁶

The only established environmental risk factor identified for the majority of malignant gliomas is exposure to ionizing radiation.⁴ There is suggestive evidence with unclear importance of and association of immunologic factors in the development of malignant gliomas, as patients with atopy have a reduced risk of gliomas⁷ and patients with glioblastoma with elevated IgE levels appear to live longer than those with normal levels.⁸ Also gene polymorphisms that affect detoxification, DNA repair, and cell cycle regulation have also been implicated in the development of gliomas.⁴

Few genetic syndromes are associated with the increased risk for malignant gliomas.⁹ Five percent of patients with malignant gliomas have a family

history of gliomas, such as neurofibromatosis 1 and 2, retinoblastoma, the Li-Fraumeni syndrome, the Turcot's syndrome (the inherited mutations are presented in the Table 1).¹⁰

Molecular pathology

The malignant gliomas arise from neural progenitor cells. Malignant gliomas contain multipotent tumour stem cells that are responsible for populating and repopulating the tumours.^{11,12}

Classical cytogenetic and array – based comparative genomic hybridization studies of gliomas have identified copy number changes (deletions, amplification, gains) in several regions; deletions

and loss of heterozygosity in tumours might point to genes involved in tumour initiation or progression (e.g. oncogenes). The chromosomal alterations that are mostly observed in gliomas are presented in Table 2.¹⁰

The transition from low grade to anaplastic astrocytoma is associated with inactivation of tumour suppressor genes on chromosomes 9p, 12q and 19q. Loss of chromosome 13q, which includes the retinoblastoma (RB) gene focus, occurs in approximately 30% of higher-grade astrocytic tumours. Two-thirds of malignant astrocytomas and glioblastomas have homozygous deletions of the region of chromosome 9p that includes the cyclin-dependent kinase inhibitor 2A (CDKN2A) and CDKN2B genes. In general, RB, CDKN2A and cyclin- dependent kinase (CDK)4 gene alterations are mutually exclusive in glioblastomas.¹³ Malignant progression to glioblastoma is also associated with inactivation of the phosphatase and tensin homolog (PTEN) tumour suppressor gene on chromosome 10 and amplification of the epidermal growth factor receptor (EGFR) gene.¹⁴ The loss of chromosome 10 occurs in 60% to 85% of glioblastomas, with approximately 25% of cases having PTEN mutation.¹⁵ In approximately 40% of glioblastomas the EGFR gene is amplified, resulting in overexpression of EGFR.¹⁶

Glioblastomas can be classified as primary or de novo and secondary or progressive. Primary glioblastomas comprises the majority of cases (60%), develop in older patients (> 50y), without prior clinical history of less malignant tumours, presenting after the short medical history (less than 6 months). Secondary or progressive glioblastomas (40%) are common among younger people (< 45y) and arise through the progression from lower-grade astrocytomas (WHO grade II) or anaplastic astrocytomas (WHO grade III), with varying time for the progression, between less than 1 year to more than 10 years. Primary and secondary glioblastomas obviously constitute distinct disease entities that evolve through different genetic pathways. CDKN2A deletions, PTEN alterations and EGFR amplification are more prevalent among de novo glioblastomas and less frequently, mouse double minute 2 homolog (MDM2) amplification, whereas p53 mutations develop as earliest detectable alteration in secondary glioblastomas (Figure 1).¹⁷

TABLE 1. Inherited mutation present in patients with malignant gliomas

Syndrome	Gene name	Chromosomal location
Neurofibromatosis 1	Neurofibromin 1 (NF1)	17q11
Neurofibromatosis 2	Neurofibromin 2 (NF2)	22q12
Tuberous sclerosis	Tuberous sclerosis 1 (TSC1) Tuberous sclerosis 2 (TSC2)	9q34 16p13
Retinoblastoma	Retinoblastoma 1 (RB1)	13q14
Li-Fraumeni syndrome	Tumor suppressor p53 (TP53)	17p13
Turcot's syndrome and multiple hamartoma	Adenomatous polyposis coli (APC) DNA mismatch repair genes: Recombinant human MutL homolog-1 (hMLH2) MutS homolog 2 (hMSH2) Mismatch repair endonuclease (PMS2) Phosphatase and tensin homolog (PTEN)	5q21 3p21.3 2p22-21 7p22 10q23.3

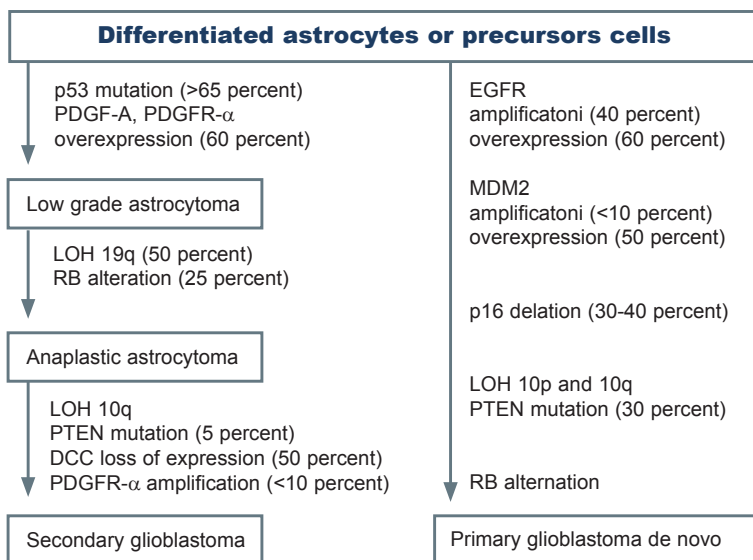


FIGURE 1. Development of primary and secondary glioblastoma

DCC = deleted in colon cancer gene; LOH = loss of heterozygosity; PDGF = platelet-derived growth factor; PDGFR = platelet-derived growth factor receptor; RB = retinoblastoma gene

Prognostic factors

Age, tumour grade (anaplastic gliomas *versus* glioblastoma) and performance status are three most

TABLE 2. The chromosomal alterations, mostly observed in gliomas

Chromosomal region	Type of alteration	Candidate gliomas genes
1p36.31-pter	Gains and deletions	Not known
1p36.22-p36.31	Gains and deletions	Not known
1p34.2-p36.1	Gains and deletions	Not known
1q32	Gains	Receptor interacting protein kinase 5 (RIPK5), mouse double minute 4 (MDM4), phosphatidylinositol-4-phosphate 3-kinase, catalytic subunit type 2 beta (PIK3C2B) and others
4q	Deletions	NIMA-related kinase 1 (NEK1), NIMA
7p11.2-p12	Amplifications or gains	<i>Epidermal growth factor receptor</i> (EGFR)
9p21-p24	Deletions	Cyclin-dependent kinase inhibitor 2A (CDKN2)
10q23	Deletions	Phosphatase and tensin homolog (PTEN)
10q25-q26	Deletions	O-6-methylguanine-DNA methyltransferase (MGMT)
11p	Deletions	Between cyclin-dependent kinase inhibitor 1C (CDKN1C) and related RAS viral (r-ras) oncogene homolog 2 (RRAS2)
12q13.3-q15	Amplifications	Mouse double minute 2 homolog (MDM2), cyclin-dependent kinase 4 (CDK4) and others
13p11-p13 and 13q14-q34	Loss	Retinoblastoma 1 (RB1)
19q13	Loss	Glioma tumor suppressor candidate region gene 1 (GLTSCR1), GLTSCR2, ligase I, DNA, ATP-dependent (LIG1), cytohesin 2 (CYTH2) and many others
22q11.21-q12.2	Loss	28 genes, including integrase interactor 1 (INI1)
22q13.1-q13.3	Loss	Not known

important prognostic factors affecting response to the treatment, along with extend of initial surgical resection.^{5,18,19} Lamborn *et al.* showed the aforementioned by study of 832 patients with glioblastoma in which the outcome was analysed by the recursive partitioning analysis.²⁰

Also for patients with newly diagnosed glioblastoma, nomograms that incorporate patient age, extent of resection, use of postoperative (adjuvant) temozolomide, mental status and corticosteroid use as a baseline for prognostic factors, have been developed for estimation of the median survival and two year survival probability, as a helpful tool in decision making for individual patients.²¹ Nomograms have been developed on the bases of Stupp *et al.*, temozolomide adjuvant trial from 2005.²²

Prognostic and predictive markers

Oligodendrogliomas with 1p/19q deletions have been recognized as distinct pathologic entities with particular sensitivity to RT and chemotherapy (ChT). In the retrospective analysis, the patients with tumours' epigenetic silencing of the methylguanine methyl transferase (MGMT) gene promoter by methylation benefited from temozolomide.

The tumours were unable to repair ChT induced DNA damage.²³

IDH1 (NADP⁺-dependent isocitrate dehydrogenases) mutation occurs in the vast majority of WHO grade II or III gliomas and secondary glioblastomas.²⁴ The p.Arg132His mutation (substitution of arginine with histidine) of isocitrate dehydrogenase 1 (IDH1^{R132H}) is not only a frequent alteration (>70%) but also a major prognostic marker in gliomas.²⁵ Patients with IDH1 mutation have a better treatment outcome and a better survival.²⁶

Diagnosis

Clinical manifestations

Clinical manifestations of malignant gliomas depend on the localization and size of the tumour. The variety of symptoms may be present, such as headaches and seizures (50–60%), focal neurologic deficits, confusion, memory loss and personality changes (20%).²⁷

The classic headache suggestive of increased intracranial pressure is most severe in the morning and may be associated with nausea and vomiting.²⁸

Rarely meningeal dissemination may be the first presentation of malignant gliomas as back pain

TABLE 3. Symptoms at presentation of glioblastoma

Headache
Nausea/vomiting
Cognition changes
Personality changes
Gait imbalance
Urinary incontinence
Hemiparesis
Aphasia
Hemineglect
Visual field defect
Seizures

with or without radicular symptoms, mental status changes, cranial nerve palsies, and myelopathy or cauda equina syndrome (Table 3).^{29,30}

Imaging

Diagnosis and staging are made by imaging of the brain and tumour histopathologic verification. For imaging the magnetic resonance (MRI) is preferred, but computed tomography may also be used. Additional biopsy or tumour resection follows afterwards.

Imaging studies show heterogeneously enhancing mass with surrounding oedema. Glioblastomas frequently have central areas of necrosis and more extensive peritumoral oedema than in anaplastic gliomas.³¹

Tissue diagnosis is essential, it can be attended either at the time of surgical resection or by separate procedure named frameless stereotactic biopsy. In the case of frameless stereotactic biopsy, the neurosurgeon is aware of the three dimensional positions of surgical instruments inside the intracranial space during the biopsy, because it is MRI or CT guided.³² The procedure related mortality is 1–2%.³³

Positron emission tomography (PET)³⁴ and magnetic resonance spectroscopy (MRS) can be used to identify metabolically active areas of different tumours, and by that increasing the accuracy of stereotactic brain biopsy. PET can be integrated with the use of 18F-labeled fluorodeoxyglucose (FDG-PET) or L-[methyl-(11) C]-methionine (MET-PET) increasing the diagnostic sensitivity and specificity. The both image procedures MET-PET and FDG-PET correspond with each other.³⁵

Systemic treatment for malignant gliomas

Postoperative (adjuvant) therapy

Glioblastoma

Because of their infiltrative nature, malignant gliomas cannot be completely eliminated with surgery. The standard treatment after surgery today for *glioblastoma* is concomitant RT-ChT with temozolomide (RT of 60 Gy and temozolomide 75 mg/m²/day for 6 weeks), followed by the adjuvant temozolomide therapy (150–200 mg/m²/day for 5 days every 28 days for 6 cycles). As reported by Stupp *et al.*²², this RT-ChT combination has an acceptable side effect profile and as compared with RT alone (60 Gy for 6 weeks), increased the median survival (14.6 months vs. 12.1 months, $p < 0.001$). The survival rate among the patients treated with RT/ChT was significantly higher than the rate among the patients that received RT alone at two and five years, respectively (26.5% vs. 10.4% and 10% vs. 2%).

MGMT promoter methylation was a major prognostic factor for the improved survival and was predictive of benefit from the therapy. For those with MGMT methylation, the two years survival rates were 49% and 24% with combination therapy and RT alone respectively, while for those without MGMT methylation, the two year survival rates were 15% and 2% respectively.

The 5-year overall survival analysis of the European Organisation for Research and Treatment of Cancer (EORTC) and National Cancer Institute of Canada (NCIC) trial has shown benefit for patients treated with RT and temozolomide compared with only irradiated patients (9.8% vs. 1.9%), the median survival after the progression remains only 6.2 months, regardless of the initial treatment.³⁶

Adjuvant ChT with procarbazine, lomustine (CCNU) and vincristine (PCV regimen) has failed to improve the survival in individual prospective randomized studies, both in grade IV and in grade III tumours. One large meta-analysis has showed that nitrosourea based ChT marginally improves the survival. Namely, individual patient data from 3004 patients enrolled in 12 randomized controlled trials comparing RT alone or with ChT, were included, ChT was associated with a 15% decrease in the risk of death, which translated to a 6% absolute increase in one year survival (from 40% to 46%) and a two month improvement in the median survival.³⁷

There are no randomized trials that have compared temozolomide with a nitrosourea-based

TABLE 4. Summary of current treatments for malignant gliomas* (Adapted from ref.28)

Type of Tumour	Therapy
Newly diagnosed tumours	
Glioblastoma (WHO grade IV)	Maximal surgical resection, plus radiotherapy, plus concomitant and adjuvant TMZ **
Anaplastic astrocytoma (WHO grade III)	Maximal surgical resection, with the following options after surgery (no accepted standard treatment): radiotherapy, plus concomitant and adjuvant TMZ or adjuvant TMZ alone**
Anaplastic oligodendroglioma and anaplastic oligoastrocytoma (WHO grade III)	Maximal surgical resection, with the following options after surgery (no accepted standard treatment): radiotherapy alone, TMZ or PCV with or without radiotherapy afterward, radiotherapy plus concomitant and adjuvant TMZ, or radiotherapy plus adjuvant TMZ**+
Recurrent tumours	Reoperation in selected patients, conventional chemotherapy (e.g., lomustine, carmustine, PCV, carboplatin, irinotecan, etoposide), bevacizumab plus irinotecan, experimental therapies +

* Additional data are from Sathornsumettee *et al.*⁴⁷, Furnari *et al.*⁴⁸, Chi and Wen⁴⁹ and Sathornsumettee *et al.*⁵⁰; ** Radiotherapy is administered at a dose of 60 Gy given in 30 fractions over a period of 6 weeks. ; Adjuvant TMZ = adjuvant temozolomide, beginning 4 weeks after radiotherapy, 150 mg/m²/day on days 1 to 5 of the first 28-day cycle, followed by 200 mg/m²/day on days 1 to 5 of each subsequent 28-day cycle, if the first cycle was well tolerated; Concomitant TMZ = concomitant temozolomide, 75 mg/m²/day for 42 days with radiotherapy; PCV = lomustine (CCNU), 110 mg/m², on day 1; procarbazine, 60 mg/m² on days 8 to 21; vincristine, 1.5 mg/m² (maximum dose, 2 mg), on days 8 and 29; WHO = World Health Organization

combination regimen when given concurrently with RT followed by the adjuvant therapy.

Another chemotherapeutic approach involves the implantation of biodegradable polymers containing carmustine (Gliadel Wafers, MGI Pharma) into the tumour bed after the resection of the tumour. The aim of the treatment with these polymers, which release carmustine gradually over the course of several weeks, is to kill residual tumour cells. In a randomized, placebo-controlled trial that investigated the use of these polymers in patients with newly diagnosed malignant gliomas, the median survival increased from 11.6 months to 13.9 months ($p = 0.03$).³⁸ This survival advantage was maintained at 2 and 3 years.³⁹

The newest phase III study data, in patients with newly diagnosed patients with glioblastoma, are coming from Radiation Therapy Oncology Group (RTOG) 0825 and Avastin in Glioblastoma (AVAGLIO) studies. In RTOG 0825 study, 637 newly diagnosed patients were randomly assigned to receive either standard ChT-RT (with temozolomide plus bevacizumab (10 mg/kg intravenous [IV], q 2 weeks), or standard ChT-RT plus placebo). The progression-free survival was significantly improved in the bevacizumab arm: 10.7 months vs. 7.3 months for placebo. However, the overall survival was slightly (although not significantly) worse in the bevacizumab arm: 15.7 months vs. 16.1 months for placebo. In addition, patients in the bevacizumab arm had a greater symptom burden and worse neurocognitive functioning, and they scored worse on several measures of health-related quality of life (QOL) than did patients who received only a standard therapy.⁴⁰

The AVAGLIO trial, which had a study design very similar to that of RTOG 0825 and which in-

involved 921 patients, also showed an improvement in progression-free survival (10.6 months in the bevacizumab arm vs. 6.2 months in the placebo arm) but virtually identical overall survival (16.8 months vs. 16.7 months, respectively). However, the QOL outcome in the bevacizumab arm was more favourable than in RTOG 0850 and time to the initiation of the corticosteroid treatment to manage adverse effects was also significantly longer in the patients who received bevacizumab (a median of 12.3 months vs. 3.7 months for placebo).⁴¹

Anaplastic astrocytoma

The standard therapy after surgery for *anaplastic astrocytoma* is still RT up to 60 Gy after the surgery. Currently, there are no findings from controlled trials that support the use of concurrent temozolomide in patients with anaplastic astrocytomas.⁴²

Anaplastic oligodendrogliomas and anaplastic oligoastrocytomas

Anaplastic oligodendrogliomas and anaplastic oligoastrocytomas are generally more responsive to therapy than are pure astrocytic tumours.⁴³ Nearly 90% of patients with anaplastic oligodendrogliomas and 20% patients with anaplastic oligoastrocytomas has a co-deletion of chromosomes 1p and 19q, mediated by an unbalanced translocation of 19p to 1q.⁴⁴ Tumours in patients with the LOH 1p/19q co-deletion are particularly sensitive to CHT with PCV with response rates of up to 100%, as compared with response rates of 23 to 31% among patients without the deletion LOH of 1p/19q.

Two large phase III studies of PCV ChT with RT, as compared with RT alone, in patients with newly diagnosed anaplastic oligodendrogliomas or anaplastic oligoastrocytomas, have been reported. In

both studies, the addition of ChT to RT increased the time to tumour progression by 10 to 12 months, but, did not improve the overall survival (median, 3.4 and 4.9 years).^{45,46} No difference in efficacy was apparent between PCV and temozolomide ChT⁴³, however, studies directly comparing the two regimens have not been performed (Table 4).

Pseudo progression

In patients with malignant gliomas, treated with temozolomide and RT, have been described with sub-acute treatment-related reactions with or without clinical deterioration, showing oedema and sometimes contrast enhancement on MRI, suggestive of tumour progression.⁵¹⁻⁵³ The occurrence of pseudo progression is mostly within the first 2 months after temozolomide ChT-RT.

In a prospective phase III trials with RT only, pseudo progression occurred in three of 32 (9%) patients.⁵⁴ More recent study on 85 patients with malignant gliomas treated with temozolomide ChT-RT, pseudo progression occurred in 18 (21%) patients.⁵⁵ In one third of patients treated with temozolomide ChT-RT, the increase in radiological abnormalities was accompanied by new focal signs, but in most patients the increase in radiological abnormalities was clinically asymptomatic.⁵⁵ In the study involving 103 patients, pseudo progression was noted in 32 patients (31%), and was clinically symptomatic in 11 (34%) of these patients. Patients with MGMT have more frequent pseudo progression and it was connected with better overall survival.⁵⁶

Most likely, pseudo progression is induced by a pronounced local tissue reaction with an inflammatory component, oedema, and abnormal vessel permeability causing new or increased contrast enhancement on neuroimaging. In less severe cases, this event can subside without the further treatment, but in more severe cases it can result, over time, in true treatment-related necrosis.

The possibilities of a good functional outcome in patients with malignant gliomas could be increased with good early medical rehabilitation treatment.⁵⁷

Treating the recurrent malignant gliomas

For glioblastoma, median time to progression after the treatment with RT and temozolomide is 6.9 months.³⁶ In case of symptomatic disease from mass effect, reoperation may be indicated (Table 4), with limited prolongation of survival afterwards.⁵⁸

The treatment of recurrent malignant gliomas with RT is controversial. Some data have suggest-

ed that fractionated stereotactic reirradiation (SRT) and stereotactic radiosurgery (SRS) may be beneficial.⁵⁹ Observational series of patients with recurrent malignant gliomas, treated with SRT showed the median survival of 12 months for patients with grade III tumours and eight months for those with grade IV lesions.⁶⁰ The one-year survival rates were 65% and 23 % for patients with grade III and IV lesions, respectively. Kong DS *et al.* in patients with recurrent gliomas treated with SRS has achieved progression free survival for patients with grade III and grade IV of 8.6 and 4.6 months, respectively.⁶¹ All patients were treated with SRS treatments delivered by gamma knife, except for 5 patients treated by linear accelerator.

The conventional ChT is more effective for anaplastic gliomas than for glioblastomas. In general, the conventional ChT has modest value for recurrent malignant gliomas. There is no established ChT regimen available and patients are best treated within investigational clinical protocols. Temozolomide was evaluated in a phase II study in patients with recurrent anaplastic gliomas who had previously been treated with nitrosoureas.⁶² The response rate was 35%, and the 6-month rate of progression-free survival was 46%, comparing favourably with the 31% rate of progression-free survival at 6 months for therapies that were reported to be ineffective.⁶³ In patients with recurrent glioblastomas, temozolomide has only limited activity, with response rate of 5.4% and 6-month rate of progression-free survival of 21%.⁶⁴ Different temozolomide doses and administration regimens have been developed. With the aim of depleting MGMT, Brock *et al.*⁶⁵ conducted a phase I trial of continuous temozolomide administration, demonstrating that a dose of 75 mg/m² daily up to 49 days is safe. Continuous dose-dense temozolomide administration at a dose of 100 mg/m² for 3 weeks out of 4 or 150 mg/m² 1 week out of 2 will double the dose intensity and deplete peripheral blood mononuclear cells of MGMT.^{66,67} Continuous temozolomide administration is associated with profound lymphocytopenia and an increased risk for opportunistic infections.^{68,69}

Other chemotherapeutic agents that are used for recurrent gliomas include nitrosoureas, carboplatin, procarbazine, irinotecan, and etoposide. Nitrosoureas (carmustine, fotemustine) either as single agents or in combination regimens as procarbazine, lomustine and vincristine (PCV) have shown activity in phase II studies in previously treated patients. Brandes *et al.* conducted a phase II study on 40 patients with recurrent glioblastoma

following surgery and standard RT, treated with carmustine as monotherapy. Median time to progression was 13.3 weeks and progression-free survival at 6 months was 17.5%.⁷⁰

As combination regiment PCV, Schmidt F *et al.*, has applied to 86 patients with recurrent glioblastoma. There were three partial responses, but no complete responses. Median progression-free survival was 17.1 weeks and progression-free survival at 6 months was 38.4%.⁷¹

Bevacizumab is a monoclonal antibody, which binds to vascular endothelial growth factor (VEGF), the key driver of neovascularization, and thereby inhibits the binding of VEGF to its receptors, VEGFR-1 and VEGFR-2, on the surface of endothelial cells. It demonstrated significant clinical activity in phase II studies using bevacizumab as a single agent or in combination with ChT agents such as irinotecan for patients with grade 3 and grade 4 malignant gliomas (higher objective response, progression-free survival and overall survival) in recurrent glioblastomas⁷²⁻⁷⁴ and has been approved by Food and Drug Administration (FDA) for the secondary treatment of glioblastoma in USA⁷⁵, but it is not approved yet by European Medicines Agency (EMA).⁷⁶

The most extensive experience with bevacizumab comes from a noncomparative phase II trial, in which 167 patients with recurrent glioblastomas, priory treated with ChT with temozolomide, were randomly assigned to bevacizumab, either as a single agent or at the same dose in conjunction with irinotecan.⁷³ Treatment cycles were repeated every two weeks. The objective response rates with bevacizumab alone or in combination with irinotecan were 28% and 38%, respectively, and the six-month progression-free survival rates and overall survival were 43% and 50 %, and 9.2 and 8.7 months, respectively. An update of the results was presented at the 2010 American Society of Clinical Oncology (ASCO) meeting.⁷⁴ Overall safety and efficacy were similar to that previously presented; the 12 and 24-month survival rates were 38% and 16% to 17% on both treatment arms, which appear to be better than historical control series.

According to our experience, at Institute of Oncology Ljubljana, we treated 19 patients with recurrent malignant gliomas with bevacizumab and irinotecan, from August 2008 to November 2011. The objective response rates were 47.4 % and 10.5% after 3 and 6 months respectively. The six-month time to progression interval rate and overall survival were 52.6% and 68.4% and 6.8 and 7.7 months, respectively (Figure 1).⁷⁷

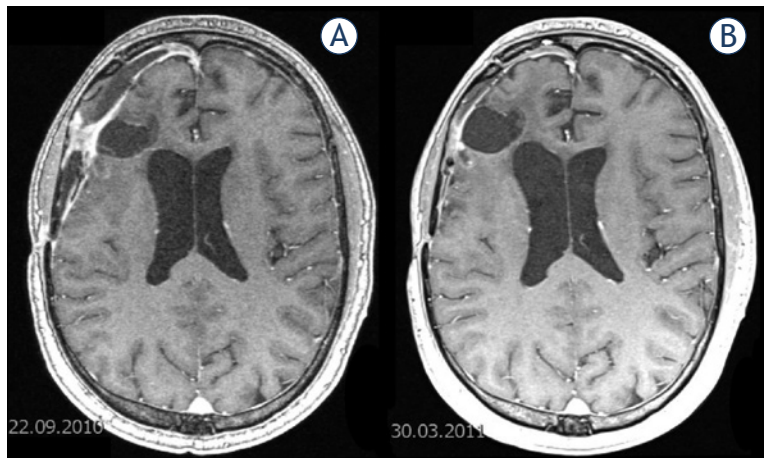


FIGURE 2. Magnetic resonance imaging (MRI) in recurrent glioblastoma patient, treated at Institute of Oncology Ljubljana, with bevacizumab/irinotecan, (A) before and (B) after six months of treatment.

Bevacizumab alone or in combination with ChT has not been demonstrated to prolong the overall survival. Pivotal studies to determine the impact of this agent on overall survival are ongoing.

Treating the elderly

According to the Central Brain Tumor Registry of United States of America (CBTRUS), in one series of over 14,000 cases, 44% of cases were patients aged 65 years or more.⁷⁸ Older age and poor performance status are associated with shorter survival.

RT among patients older than 70 years has a modest benefit in the median survival (29.1 weeks) as compared with supportive care (16.9 weeks).⁷⁹ Older patients tolerate therapy less well than younger patients, so the treatment regimen should be adjusted. RT applied as abbreviated course (40 Gy in 15 fractions over a period of 3 weeks) or temozolomide as monotherapy has similar outcomes as conventional RT regimens.^{80,81}

Two contemporary randomized trials conducted exclusively in older patients have new data about the optimal treatment approach. Both trials, Methusalem trial (NOA-08)⁷⁸ and Nordic Elderly Trial⁸² have compared initial ChT as monotherapy with RT alone. In the Methusalem Trial the median age was 72 years.⁷⁸ Patients treated with RT has a better survival, the median survival was 293 vs. 245 days, one year survival was 38% vs. 31%, the toxicity was more severe in patients treated with ChT. In Nordic Elderly Trial the median age was 70 years. Patients were treated with RT 60 Gy (6 weeks), 34 Gy (6 weeks) and temozolomide as monothera-

TABLE 5. Selected investigational therapies for malignant gliomas* (Adapted from ref. 28)

Type of treatment	Example
Convection enhanced surgical delivery of pharmacologic agent	Cintredekin besudotox
Drugs to overcome resistance to TMZ	
Dose dense TMZ	O ⁶ -benzylguanine
MGMT inhibitors	BSI-201, ABT-888
PARP inhibitors	RTA 744, ANG 1005
New chemotherapies	
Antiangiogenic therapies	
Anti-avb5 integrins	Cilengitide
Anti-hepatocyte growth factor	AMG-102
Anti-VEGF	Bevacizumab, aflibercept (VEGF-trap)
Anti-VEGFR	Cediranib, pazopanib, sorafenib, sunitinib, vandetinib, vatalanib, XLI 84, CT-322
Other agents	Thalidomide
Targeted molecular therapies	
Akt	Perifosine
EGFR inhibitors	Erlotinib, gefitinib, lapatinib, BIBW2992, nimotuzumab, cetuximab
FTI inhibitors	Tipifarnib, lonafanib
HDAC inhibitors	Vorinostat, depeptide, LBH589
HSP90 inhibitors	ATI3387
Met	XLI84
mTOR inhibitors	Everolimus, sirolimus, temsirolimus, deforolimus
PI3K inhibitors	BEZ235, XL765
PKCb	Enzastaurin
PDGFR inhibitors	Dasatinib, imatinib, tandutinib
Proteasome	Bortezomib
Raf	Sorafenib
Src	Dasatinib
TGF-b	API2009
Combination therapies	Erlotinib plus temsirolimus, gefitinib plus everolimus, gefitinib plus sirolimus, saorafenib plus temsirolimus, erlotinib, or tipifarnib, pazopanib plus lapatinib
Immunotherapies	
Dendritic cell and EGFRvIII peptide vaccines	DCVax, CDX-110
Monoclonal antibodies	¹³¹ I-anti-tenascin antibody
Gene therapy	
Other therapies	¹³¹ I-TM-601

* Additional data are from Sathornsumetee *et al.*⁴⁷, Furnari *et al.*⁴⁸, Chi and Wen⁴⁹, Sathornsumetee *et al.*⁵⁰; EGFR = epidermal growth factor; FTI = farnesyltransferase; HDAC = histone deacetylase; HSP90 = heat-shock protein 90; MGMT = O⁶-methylguanine-DNA methyltransferase; mTOR = mammalian target of rapamycin; PARP = poly (ADP-ribose) polymerase; PDGFR = platelet-derived growth factor receptor; PI3K = phosphatidylinositol 3-kinase; PKCb = protein kinase Cb; TGF = transforming growth factor; TMZ = temozolomide; VEGFR = vascular endothelial growth factor receptor; WHO = World Health Organization

py. In this trial patients treated with CTh had a better survival, with the overall survival of 6, 7.5 and 8.3 months, respectively. It seems that there might be benefit from systemic treatment over RT in patients with MGMT methylated tumours.

Experimental approaches

Increased understanding of the molecular pathways involved in signal transduction, angiogenesis and cell growth has led to the development of a number of targeted agents, which are now under active evaluation, alone and in various combinations for patients with malignant gliomas and other tumours. Other investigational therapies for malignant gliomas include chemotherapeutic agents that cross the blood-tumour barrier more effectively, gene therapy, peptide and dendritic-cell vaccines, radiolabeled monoclonal antibodies against the extracellular matrix protein tenascin, synthetic chlorotoxins (¹³¹I-TM-601), and infusion of radiolabeled drugs and targeted toxins into the tumour and surrounding brain by means of convection-enhanced delivery. Promising investigational therapies are selected in Table 5.²⁸

Conclusions

Malignant gliomas remains difficult to treat, and despite the efforts to improve the treatment outcome, the survival of patients with malignant gliomas is poor, with median survival of slightly above one year.

After revolutionary change in the postoperative setting with RT-ChT with Temozolomide has been achieved, mostly negative trials follow. AVAGLIO and RTOG 0825 trials were negative. Even though the AVAGLIO trial kind of suggests progression-free survival and QOL improvement, these are not clear cut results and upon review the actual progression-free survival benefit was smaller, while QOL results are completely contradictory. In the recurrent malignant glioma setting, still nothing significant has been achieved.

The optimal management requires a multidisciplinary approach and knowledge of potential complications from both the disease and its treatment. In the future, with the better understanding of the molecular pathogenesis of malignant gliomas, it may be possible to select the most appropriate therapies on the basis of the patient's tumour genotype and in that way more effective therapies can be developed for malignant gliomas. Most of

all, further targeted therapy approaches should be biomarker driven.

References

1. WHO Classification of tumours of the central nervous system. Louis DN, Ohgaki H, Wiestler OD, Cavenee WK, editors. Lyon: IARC Press; 2007.
2. CBRUS, Central Brain Tumor Registry of the United States. 2007–2008. Primary brain tumors in the United States. Statistical report. 2000–2004 years of data collected. Available from: <http://www.cbrus.org/reports/2007-2008/2007report.pdf>. Accessed on 10 November 2013.
3. Kase M, Minajeva A, Niinepuu K, Kase S, Vardja M, Asser T, et al. Impact of CD133 positive stem cell proportion on survival in patients with glioblastoma multiforme. *Radiol Oncol* 2013; **47**: 405-10.
4. Fisher JL, Schwartzbaum JA, Wrensch M, Wiemels JL. Epidemiology of brain tumors. *Neurol Clin* 2007; **25**: 867-90.
5. Smrdel U, Kovac V, Popovic M, Zwitter M. Glioblastoma patients in Slovenia from 1997 to 2008. *Radiol Oncol* 2014; **48**: 72-9.
6. Zakej MP, Zadnik V, Zagar T, Zakotnik B. *Survival of cancer patients, diagnosed in 1991-2005 in Slovenia*. Ljubljana: Institute of Oncology Ljubljana, Epidemiology and Cancer Registry, Cancer Registry of Republic of Slovenia; 2009. p. 229.
7. Linos E, Raine T, Alonso A, Michaud D. Atopy and risk of brain tumours: a metaanalysis. *J Natl Cancer Inst* 2007; **99**: 1544-50.
8. Wrensch M, Wiencke JK, Wiemels J, Miike R, Patoka J, Moghadassi M, et al. Serum IgE, tumour epidermal growth factor receptor expression and inherited polymorphisms associated with gliomas survival. *Cancer Res* 2006; **66**: 4531-41.
9. Farell CJ, Plotkin SR. Genetic causes of brain tumors: neurofibromatosis, tuberous sclerosis, von Hippel-Lindau and other syndromes. *Neurol Clin* 2007; **25**: 925-46.
10. Schwartzbaum JA, Fisher JL, Kenneth DA, Wrensch M. Epidemiology and molecular pathology of gliomas. *Nature* 2006; **2**: 494-503.
11. Galli R, Binda E, Orfanelli U, Cipelletti B, Gritti A, De Vitis S, et al. Isolation and characterization of tumorigenic, stem-like neural precursors from human glioblastoma. *Cancer Res* 2004; **64**: 7011-21.
12. Singh SK, Hawkins C, Clarke ID, Squire JA, Bayani J, Hide T, et al. Identification of human brain tumor initiating cells. *Nature* 2004; **432**: 396-401.
13. Ueki K, Ono Y, Henson JW, Efrid JT, von Deimling A, Louis DN. CDKN2A (p16) or RB alterations occur in majority of glioblastomas and are inversely correlated. *Cancer Res* 1996; **56**: 150-3.
14. Fujisawa H, Kurrer M, Reis RM, Yonekawa Y, Kleihues P, Ohgaki H. Acquisition of the glioblastoma phenotype during astrocytoma progression is associated with loss of heterozygosity on 10q25-qter. *Am J Pathol* 1999; **155**: 387-94.
15. Li J, Yen C, Liaw D, Podsypanina K, Bose S, Wang SI, et al. PTEN, a putative protein tyrosine phosphatase gene mutated in human brain, breast, and prostate cancer. *Science* 1997; **275**: 1943-7.
16. Watanabe K, Tachibana O, Sata K, Yonekawa Y, Kleihues P, Ohgaki H. Overexpression of the EGFR receptor and p53 mutations are mutually exclusive in the evolution of primary and secondary glioblastomas. *Brain Pathol* 1996; **6**: 217-23.
17. Kleihues P, Ohgaki H. Primary and secondary glioblastomas: from concept to clinical diagnosis. *Neuro Oncol* 1999; **1**: 44-51.
18. Devaux BC, O'Fallon JR, Kelly PJ. Resection, biopsy, and survival in malignant glial neoplasms. A retrospective study of clinical parameters, therapy and outcome. *J Neurosurg* 1993; **78**: 767-75.
19. Laws ER, Parney IF, Huang W, Anderson F, Morris AM, Asher A, et al. Survival following surgery and prognostic factors for recently diagnosed malignant gliomas: data from the Glioma Outcomes Project. *J Neurosurg* 2003; **99**: 467-73.
20. Lamborn KR, Chang SM, Prados MD. Prognostic factors for survival of patients with glioblastoma: recursive partitioning analysis. *Neuro Oncol* 2004; **6**: 227-35.
21. Gorlia T, van den Bent MJ, Hegi ME, Mirimanoff RO, Weller M, Cairncross JG, et al. Nomograms for predicting survival of patients with newly diagnosed glioblastoma: prognostic factor analysis of EORTC and NCIC trial 26981-22981/CE.3. *Lancet Oncol* 2008; **9**: 29-38.
22. Stupp R, Mason WP, van den Bent MJ, Weller M, Fisher B, Taphoorn MJB, et al. Radiotherapy plus concomitant and adjuvant temozolomide for glioblastoma. *N Engl J Med* 2005; **352**: 987-96.
23. Hegi ME, Dierens AC, Gorlia T, Hamou MF, de Tribolet N, Weller M, et al. MGMT gene silencing and benefit from temozolomide in glioblastoma. *N Engl J Med* 2005; **352**: 997-1003.
24. Yan H, Parsons DW, Jin G, McLendon R, Rasheed BA, Yuan W, et al. IDH1 and IDH2 Mutations in Gliomas. *N Engl J Med* 2009; **360**: 765-73.
25. Boisselier B, Marie Y, Labussière M, Ciccarino P, Desestret V, Wang X, et al. COLD PCR HRM: a highly sensitive detection method for IDH1 mutations. *Hum Mutat* 2010; **31**: 1360-5.
26. Labussiere M, Sanson M, Idbaih A, Delattre JY. IDH1 gene mutations: a new paradigm in glioma prognosis and therapy? *Oncologist* 2010; **15**: 196-9.
27. Chang SM, Parney IF, Huang W, Anderson FA Jr, Asher AL, Bernstein M, et al. Patterns of care for adults with newly diagnosed malignant gliomas. *JAMA* 2005; **293**: 557-64.
28. Wen PY, Kesari S. Malignant gliomas in adults. *N Engl J Med* 2008; **359**: 492-507.
29. Wheen LC, Anderson NE, Baker PC, Singh VK, Synek BJ. Leptomeningeal infiltration as the presenting manifestation of a malignant gliomas. *J Clin Neurosci* 2006; **13**: 298-301.
30. Omuro A, DeAngelis LM. Glioblastoma and other malignant gliomas: a clinical review. *JAMA* 2013; **310**: 1842-50.
31. Cha S. Update on brain tumour imaging: from anatomy to physiology. *AJNR Am J Neuroradiol* 2006; **27**: 475-87.
32. Paleologos TS, Dorward NL, Wadley JP, Thomas DG. Clinical validation of true frameless stereotactic biopsy: analysis of the first 125 consecutive cases. *Neurosurgery* 2001; **49**: 835-7.
33. Bernays RL, Kollias SS, Khan N, Brandner S, Meier S, Yonekawa Y. Histological yield, complications and technological considerations in 114 consecutive frameless stereotactic biopsy procedures aided by open intraoperative magnetic resonance imaging. *J Neurosurg* 2002; **97**: 354-62.
34. Maza S, Buchert R, Brenner W, Munz DL, Thiel E, Korfel A, et al. Brain and whole-body FDG-PET in diagnosis, treatment monitoring and long-term follow-up of primary CNS lymphoma. *Radiol Oncol* 2013; **47**: 103-10.
35. Pirotte B, Goldman S, Massager N, David P, Wikler D, Vandesteene A, et al. Comparison of 18F-FDG and 11C-methionine for PET-guided stereotactic brain biopsy of gliomas. *J Nucl Med* 2004; **45**: 1293-8.
36. Stupp R, Hegi EM, Mason PW, van den Bent MJ, Taphoorn JBM, Janzer CR, et al. Effects of radiotherapy with concomitant and adjuvant temozolomide versus radiotherapy alone on survival in glioblastoma in a randomised phase III study: 5-year analysis of the EORTC-NCIC trial. *Lancet Oncol* 2009; **10**: 459-66.
37. Stewart LA. Chemotherapy in adult high-grade gliomas: a systematic review and meta-analysis of individual patient data from 12 randomised trials. *Lancet* 2002; **359**: 1011-8.
38. Westphal M, Hilt DC, Bortey E, Delavault P, Olivares R, Warnke PC, et al. A phase 3 trial of local chemotherapy with biodegradable carmustine (BCNU) wafers (Gliadel wafers) in patients with primary malignant gliomas. *Neuro Oncol* 2003; **5**: 79-88.
39. Westphal M, Ram Z, Riddle V, Hilt D, Bortey E. Gliadel wafer in initial surgery for malignant gliomas: long-term follow-up of a multicenter controlled trial. *Acta Neurochir (Wien)* 2006; **148**: 269-75.
40. Gilbert MR, Dignam J, Won M, Blumenthal DT, Vogelbaum MA, Aldape KD, et al. RTOG 0825: phase III double-blind placebo-controlled trial evaluating bevacizumab (Bev) in patients (Pts) with newly diagnosed glioblastoma (GBM). [Abstract]. 2013 ASCO Annual Meeting. *J Clin Oncol* 2013; **31(18 Suppl)**: Abstract No. 1.
41. Henriksson R, Bottomley A, Mason W, Saran F, Wick W, Nishikawa R, et al. Progression-free survival (PFS) and health-related quality of life (HRQoL) in AVAglio, a phase III study of bevacizumab (Bv), temozolomide (T), and radiotherapy (RT) in newly diagnosed glioblastoma (GBM). [Abstract]. 2013 ASCO Annual Meeting. *J Clin Oncol* 2013; **31(18 Suppl)**: Abstract No. 2005.

42. Brem SS, Bierman PJ, Brem H, Butowski N, Chamberlain MC, Chiocia EA, et al. Central nervous system cancers. *J Natl Compr Canc Netw* 2011; **9**: 352-400.
43. van den Bent MJ. Anaplastic oligodendroglioma and oligoastrocytoma. *Neurol Clin* 2007; **25**: 1089-109.
44. Jenkins RB, Blair H, Ballman KV, Giannini C, Arusell RM, Law M, et al. A t(1;19)(q10;p10) mediates the combined deletions of 1p and 19q and predicts a better prognosis of patients with oligodendroglioma. *Cancer Res* 2006; **66**: 9852-61.
45. Intergroup Radiation Therapy Oncology Group Trial 9402, Cairncross G, Berkey B, Shaw E, Jenkins R, Scheithauer B, et al. Phase III trial of chemotherapy plus radiotherapy compared with radiotherapy alone for pure and mixed anaplastic oligodendroglioma: Intergroup Radiation Therapy Oncology Group Trial 9402. *J Clin Oncol* 2006; **24**: 2707-14.
46. van den Bent MJ, Carpentier AF, Brandes AA, Sanson M, Taphoorn MJ, Bernsen HJ, et al. Adjuvant procarbazine, lomustine, and vincristine improves progression-free survival but not overall survival in newly diagnosed anaplastic oligodendrogliomas and oligoastrocytomas: a randomized European Organisation for Research and Treatment of Cancer phase III trial. *J Clin Oncol* 2006; **24**: 2715-22.
47. Sathornsumetee S, Rich JN, Reardon DA. Diagnosis and treatment of high grade astrocytoma. *Neurol Clin* 2007; **25**: 1111-39.
48. Furnari FB, Fenton T, Bachoo RM, Mukasa A, Stommel JM, Stegh A, et al. Malignant astrocytic glioma: genetics, biology, and paths to treatment. *Genes Dev* 2007; **21**: 2683-710.
49. Chi AS, Wen PY. Inhibiting kinases in malignant gliomas. *Expert Opin Ther Targets* 2007; **11**: 473-96.
50. Sathornsumetee S, Reardon DA, Desjardins A, Quinn JA, Vredenburgh JJ, Rich JN. Molecularly targeted therapy for malignant gliomas. *Cancer* 2007; **110**: 13-24.
51. Fiegler W, Langer M, Scheer M, Kazner E. [Reversible computed tomographic changes following brain tumour irradiation induced by the "early-delayed reaction" after radiation]. [German]. *Radiologe* 1986; **26**: 206-9.
52. Watne K, Hager B, Heier M, Hirschberg H. Reversible oedema and necrosis after irradiation of the brain. Diagnostic procedures and clinical manifestations. *Acta Oncol* 1990; **29**: 891-5.
53. Griebel M, Friedman HS, Halperin EC, Wiener MD, Marks L, Oakes WJ, et al. Reversible neurotoxicity following hyperfractionated radiation therapy of brain stem gliomas. *Med Pediatr Oncol* 1991; **19**: 182-6.
54. de Wit MC, de Bruin HG, Eijkenboom W, Sillevs Smitt PA, van den Bent MJ. Immediate post-radiotherapy changes in malignant gliomas can mimic tumour progression. *Neurology* 2004; **63**: 535-7.
55. Taal W, Brandsma D, de Bruin HG, Bromberg JE, Swaak-Kragten AT, Smitt PA, et al. The incidence of pseudoprogression in a cohort of malignant gliomas patients treated with chemo-radiation with temozolomide. [Abstract]. *Proc Am Soc Clin Oncol* 2007; **25**: Abstract No. 2009.
56. Brandes AA, Franceschi E, Tosoni A, Blatt V, Pession A, Tallini G, et al. MGMT promoter methylation status can predict the incidence and outcome of pseudoprogression after concomitant radiochemotherapy in newly diagnosed glioblastoma patients. *J Clin Oncol* 2008; **26**: 2192-7.
57. Kos N, Kos B, Benedicic M. Early medical rehabilitation after neurosurgical treatment of malignant brain tumours in Slovenia. *Radiol Oncol* 2015; **49**: in press.
58. Keles GE, Lamborn KR, Chang SM, Prados MD, Berger MS. Volume of residual disease as a predictor of outcome in adult patients with recurrent supratentorial glioblastomas multiforme who are undergoing chemotherapy. *J Neurosurg* 2004; **100**: 41-6.
59. Tsao MN, Mehta MP, Whelan TJ, Morris DE, Hayman JA, Flickinger JC, et al. The American Society for Therapeutic Radiology and Oncology (ASTRO) evidence-based review of the role of radiosurgery for malignant gliomas. *Int J Radiat Oncol Biol Phys* 2005; **63**: 47-55.
60. Combs SE, Thilmann C, Edler L, Debus J, Schulz-Ertner D. Efficacy of fractionated stereotactic reirradiation in recurrent gliomas: long-term results in 172 patients treated in a single institution. *J Clin Oncol* 2005; **23**: 8863-9.
61. Kong DS, Lee JI, Park K, Kim JH, Lim DH, Nam DH. Efficacy of stereotactic radiosurgery as a salvage treatment for recurrent malignant gliomas. *Cancer* 2008; **112**: 2046-51.
62. Prados MD, Yung WKA, Fine HA, Greenberg HS, Junck L, Chang SM, et al. Phase 2 study of BCNU and temozolomide for recurrent glioblastoma multiforme: North American Brain Tumor Consortium study. *Neuro Oncol* 2004; **6**: 33-7.
63. Wong ET, Hess KR, Gleason MJ, Jaecle KA, Kyritsis AP, Prados MD, et al. Outcomes and prognostic factors in recurrent gliomas patients enrolled onto phase II clinical trials. *J Clin Oncol* 1999; **17**: 2572-8.
64. Yung WK, Albright RE, Olson J, Fredericks R, Fink K, Prados MD, et al. A phase II study of temozolomide vs. procarbazine in patients with glioblastoma multiforme at first relapse. *Br J Cancer* 2000; **83**: 588-93.
65. Brock CS, Newlands ES, Wedge SR, Bower M, Evans H, Colquhoun I, et al. Phase I trial of temozolomide using an extended continuous oral schedule. *Cancer Res* 1998; **58**: 4363-7.
66. Tolcher AW, Gerson SL, Denis L, Geyer C, Hammond LA, Patnaik A, et al. Marked inactivation of O6-alkylguanine-DNA alkyltransferase activity with protracted temozolomide schedules. *Br J Cancer* 2003; **88**: 1004-11.
67. Wick W, Steinbach JP, Kuker WM, Dichgans J, Bamberg M, Weller M. One week on/one week off: a novel active regimen of temozolomide for recurrent glioblastoma. *Neurology* 2004; **62**: 2113-5.
68. Su YB, Sohn S, Krown SE, Livingston PO, Wolchok JD, Quinn C, et al. Selective CD4+ lymphopenia in melanoma patients treated with temozolomide: a toxicity with therapeutic implications. *J Clin Oncol* 2004; **22**: 610-6.
69. Wick W, Weller M. How lymphotoxic is dose-intensified temozolomide? The glioblastoma experience. *J Clin Oncol* 2005; **23**: 4235-6; author reply 4236.
70. Brandes AA, Tosoni A, Amistà P, Nicolardi L, Grosso D, Berti F, et al. How effective is BCNU in recurrent glioblastoma in the modern era? A phase II trial. *Neurology* 2004; **63**: 1281-4.
71. Schmidt F, Fischer J, Herrlinger U, Dietz K, Dichgans J, Weller M. PCV chemotherapy for recurrent glioblastoma. *Neurology* 2006; **66**: 587-9.
72. Kreisl TN, Kim L, Moore K, Duic P, Royce C, Stroud I, et al. Phase II trial of single-agent bevacizumab followed by bevacizumab plus irinotecan at tumor progression in recurrent glioblastoma. *J Clin Oncol* 2009; **27**: 740-5.
73. Friedman HS, Prados MD, Wen PY, Mikkelsen T, Schiff D, Abrey LE, et al. Bevacizumab alone and in combination with irinotecan in recurrent glioblastoma. *J Clin Oncol* 2009; **27**: 4733-40.
74. Cloughesy T, Vredenburgh JJ, Day B, Das A, Friedman HS. Updated safety and survival of patients with relapsed glioblastoma treated with bevacizumab in the BRAIN study. [Abstract]. *J Clin Oncol* 2010; **28(15 Suppl)**: Abstract No. 3085.
75. NCCN clinical practical guidelines in oncology. Central nervous system cancer. Version 2.2013. Available from: http://www.nccn.org/professionals/physician_gls/f_guidelines.asp#site. Accessed on 7 August 2012.
76. Stupp R, Tonn JC, Brada M, Pentheroudakis G. High grade malignant glioma: ESMO clinical practice guidelines for diagnosis, treatment and follow-up. *Ann Oncol* 2010; **21(Suppl 5)**: v190-3.
77. Mesti T, Ebert Moltara M, Boc M, Reberšek M, Ocvirk J. Bevacizumab and irinotecan in recurrent malignant glioma, a single institution experience. *Radiol Oncol* 2014. Ahead of print. doi:10.2478/raon-2014-0021
78. Wick W, Engel C, Combs SE, Nikkhah G, Steinbach J, Kortmann R, et al. NOA-08 randomized phase III trial of 1 week on/1 week off temozolomide versus involved-field radiotherapy in elderly (older than age 65) patients with newly diagnosed anaplastic astrocytoma or glioblastoma (Methusalem). [Abstract]. *J Clin Oncol* 2010; **28**: 949s. Abstract No. LBA2001.
79. Keime-Guibert F, Chinot O, Taillandier L, Cartalat-Carel S, Frenay M, Kantor G, et al. Radiotherapy for glioblastoma in the elderly. *N Engl J Med* 2007; **356**: 1527-35.
80. Roa W, Brasher PM, Bauman G, Anthes M, Bruera E, Chan A, et al. Abbreviated course of radiation therapy in older patients with glioblastoma multiforme: a prospective randomized clinical trial. *J Clin Oncol* 2004; **22**: 1583-8.
81. Glantz M, Chamberlain M, Liu Q, Litofsky NS, Recht LD. Temozolomide as an alternative to irradiation for elderly patients with newly diagnosed malignant gliomas. *Cancer* 2003; **97**: 2262-6.
82. Malmstrom A, Gronberg BH, Stupp R, Marosi C, Frappaz D, Schultz HP, et al. Glioblastoma (GBM) in elderly patients: a randomized phase III trial comparing survival in patients treated with 6-week radiotherapy (RT) versus hypofractionated RT over 2 weeks versus temozolomide single agent chemotherapy (TMZ) for glioblastoma (GBM) in the elderly. [Abstract]. *J Clin Oncol* 2010; **28(18 Suppl)**: 949s. Abstract No. LBA2002

Early medical rehabilitation after neurosurgical treatment of malignant brain tumours in Slovenia

Natasa Kos¹, Boris Kos², Mitja Benedicic³

¹ Medical Rehabilitation Unit, University Medical Centre, Ljubljana, Slovenia

² Zdravstveni dom dr. Julija Polca Kamnik, Slovenia

³ Department of Neurosurgery, University Medical Centre, Ljubljana, Slovenia

Radiol Oncol 2016; 50(2): 139-144.

Received 23 September 2014

Accepted 3 December 2014

Correspondence to: Mitja Benedičič, M.D., Ph.D., Department of Neurosurgery, University Medical Centre Ljubljana, Zaloška 2, SI-1000 Ljubljana, Slovenia. E-mail: mitja.benedicic@kclj.si

Disclosure: No potential conflicts of interest were disclosed.

Background. The number of patients with malignant brain tumours is on the rise, but due to the novel treatment methods the survival rates are higher. Despite increased survival the consequences of tumour properties and treatment can have a significant negative effect on the patients' quality of life. Providing timely and appropriate rehabilitation interventions is an important aspect of patient treatment and should be started immediately after surgery. The most important goal of rehabilitation is to prevent complications that could have a negative effect on the patients' ability to function.

Conclusions. By using individually tailored early rehabilitation it is often possible to achieve the patients' independence in mobility as well as in performing daily tasks before leaving the hospital. A more precise evaluation of the patients' functional state after completing additional oncologic therapy should be performed to stratify the patients who should be directed to complex rehabilitation treatment. The chances of a good functional outcome in patients with malignant brain tumours could be increased with good early medical rehabilitation treatment.

Key words: malignant brain tumour; surgery; early rehabilitation

Introduction

Malignant brain tumours have a very high likelihood of producing disabling effects on a patient's life. The indirect effects of chemotherapy and radiation therapy add to the functional deficits which are usually caused by the tumour itself (mass effect). Neurological deficits are related to the area of the brain that the tumour invades. The most common neurological complications of primary brain tumours are cognitive deficits (80%), motor deficits (78%), visual-perceptual deficits (53%), sensory loss (38%), bowel/bladder impairment (37%), cranial nerve palsy (29%), dysarthria (27%), dysphagia (26%), aphasia (24%) and ataxia (20%).¹ The observed preoperative and postoperative neu-

rological deficits have an important impact on patients' daily life functions and result in diminished ability to perform usual family and social roles. Furthermore, most of the patients experience progressive neurological decline as their disease progresses.²

Brain tumours occur over the life span with higher incidence in advanced age.³ The survival rates have increased due to early diagnostics and up-to-date multidisciplinary treatment involving neurologists, neuroradiologists, neurosurgeons, oncologists and the medical rehabilitation specialists.^{4,5} However, besides prolonged survival⁶, the contemporary approach is the maintained or improved quality of life, which can be much contributed to by the rehabilitation processes, which

needs to be adjusted to the individual's abilities. The purpose of rehabilitation is restoring independence with the emphasis on activities of daily living, mobility, cognition and communication. Interventions can be applied in all stages of the disease but the rehabilitation goals adjust according to the patient's problems. The rehabilitation needs to start early enough in order to reach the established goals, prevent the complications and achieve better functional outcome.⁷

Symptoms of brain tumours

The symptoms of brain tumours are dependent on the size and location of the tumour. They are caused by mass effect of the tumour and by the surrounding vasogenic brain oedema. First symptom is usually headache, which is usually worse in the morning and can be accompanied by nausea and vomiting.⁸ Sometimes an epileptic seizure is the first and only symptom. Each person may experience symptoms differently, but motor deficits and speech disturbances are the most unpleasant because they interfere with patient's independence. Cognitive deficits are common and important because they have effect on quality of life and on the efficiency of specific rehabilitation programme, but can go unnoticed for longer periods of time.^{9,10}

Operative treatment of brain tumours

Surgery is usually the first choice of treatment; the goal of surgery is maximal tumour resection, but it is also important to provide the diagnosis and prevent symptoms of the mass effect.¹¹ In addition to microsurgery, several new techniques are used in brain tumour surgery, such as frameless, image-guided neuronavigation, preoperative functional MRI, fiber tracking and transcranial magnetic stimulation, intraoperative ultrasound and MRI, intraoperative neurophysiological monitoring (including direct cortical stimulation), fluorescence-guided removal of malignant gliomas, stereotactic needle biopsy, neuroendoscopy, awake surgery and brachytherapy. These novel techniques can help the surgeon to facilitate tumour removal, minimize the injury of the surrounding brain tissue and the occurrence of postoperative neurological deficit, thus resulting in better patient outcome.¹¹

Postoperative period

The most common complaint after surgery is fatigue, which improves over time, but can be intense

during first weeks after surgery and also during chemotherapy or radiation therapy.¹² Relatively little research on fatigue in patients undergoing surgery for malignant brain tumours has been performed to date.¹³ More severe fatigue significantly correlate with poor functional status and poorer quality of life due to impaired physical functioning and sleep disturbances.¹³ Patients with fatigue have problems with routine tasks - these tasks require greater concentration and effort as usually. These problems need to be considered when deciding upon the intensity of activity during the rehabilitation program. Therefore, we plan short periods of rest during the program and assure that the patients stop with the activity before becoming overtired.

Besides fatigue, cognitive functions such as attention, concentration and memory can be affected to a varying degree. The deficits may be temporary or more permanent, depending on whether the cause is permanent and structural or transient due to temporary brain swelling. Affective disorders must be considered immediately after surgery - they are more common in patients with the history of depression and those with coincidental physical disability.¹⁴ It is important to determine the severity of the cognitive impairments and to accordingly modify the rehabilitation planning.⁸

Headache can last for a few days after the operation and can interfere with the patients' ability to participate in activities. Neurological deficits (paralysis, weakness and balance disturbances) may also persist after the surgery.

Early medical rehabilitation in Slovenia

Recovery time after surgery is different for each individual. The goal of postoperative rehabilitation is to prevent complications and to maximize the patient's functional abilities. Early rehabilitation at our institution is provided by the rehabilitation team, consisting of the occupational therapist working together with the physiotherapist, while the consultant of physical and rehabilitation medicine is responsible for proper rehabilitation procedures used to help the patient return to normal activities. The rehabilitation procedures are started as soon as possible because the length of hospital stay is short (usually around 1 week) and time to achieve the goal is limited. The content, intensity and frequency of the rehabilitation programme are tailored to the individual patient's clinical needs. Patient and his relatives are also included in the rehabilitation team, while consultants of other specialisations are included as needed.

On the first postoperative day, provided that the control CT scan of the brain shows no significant postoperative hematoma or oedema, we start with progressive mobilisation. This is possible when the patient has good physical stamina and is without motor deficits. We evaluate the patient's independence in basic daily activities and Karnofsky performance scale (KPS) is used for evaluation of patient's functional abilities. This scale allows patients to be classified as to their functional impairment. The Karnofsky score runs from 100 to 0, where 100 is "perfect" health and 0 is death - the lower the score, the bigger the impairment.¹⁵ KPS may be used to determine patient's prognosis or to measure changes in a patient's ability to function and is often used with patients suffering from malignant brain tumours.^{16,17}

Often the patients present with cognitive deficits despite the lack of motor impairment. They would benefit from early neuropsychological treatment or at least early neuropsychological evaluation. However, this can rarely be achieved in the acute phase due to lack of clinical psychologists in hospital setting in Slovenia. Neuropsychological assessment helps to determine whether treatment, in the form of cognitive rehabilitation or psychotherapy, may be useful after discharge from the acute hospital. Outpatient programs to address cognitive deficits in brain tumour survivors, including cognitive therapy and pharmacologic strategies, have shown to be beneficial.⁹

Patients who experience temporary or permanent speech difficulties require specialised therapy by the speech therapist. The speech therapist is invited into the rehabilitation team early after the operation if speech and swallowing difficulties are detected, but sufficient patient's cooperation must be assured.¹⁸

Preliminary results of our retrospective review focusing on neurological deficits after surgery for malignant brain tumours during the past three years show that the proportion of patients with persistent neurological deficits is substantial even after surgery and in about 30% percent of patients neurological deficits could be identified at discharge. Neurological deficits can often be multiple, Mukand *et al.* described that 74.5% of patients had three or more concurrent neurologic deficits, and 39% of patients had five or more deficits, which is in accordance to our preliminary results.¹

Patient with neurological deficits need special rehabilitation while they are in the acute hospital. Usually, the most important deficit for patients is motor impairment and problems with walking.

Such a patient is bed-ridden and the resulting complications need to be prevented. In this setting, verticalization is very important and there are usually no contraindications for it. We use different equipment to help patients sit on their bed, the tilt table is used to achieve standing and the wheelchairs are used for sitting. With the wheelchair, we enable the patient to be driven out from the room. This has a positive effect on the patient's wellbeing, preventing social isolation which may occur when the patient is constantly in bed and alone in the room.

With the help of a chosen neuro-physiotherapeutic technique we opt to maintain a good passive range of movement in the joints of the limbs where active movement is not possible. When increased muscle tone is present, these techniques also contribute to its normalization and help the patient to start using paretic limbs. Occupational therapist evaluates and treats difficulties, related to self-care and daily living and plays an important role in helping the patient develop new ways of doing different daily tasks, such as dressing, undressing, washing and eating. Often, while in the acute hospital, the patient is provided with individually tailored accessories to facilitate functioning at home (thickened cutlery handles, equipment to assist with putting on footwear etc.). Additional instructions are provided to the patient and their relatives in order to improve the organization of daily living at home.

Rehabilitation does not end with the patient's discharge from the acute hospital. Hospital stays are short; at our institution, the average length of stay in the acute hospital is 9 days, which often means that the rehabilitations goals are not fully met. The patients are either discharged home or transferred to other hospitals and most of them must continue with additional oncologic treatment.

University Rehabilitation Institute of the Republic of Slovenia is the only tertiary institution performing complex rehabilitation in Slovenia. Direct transferral of patient with malignant brain tumours from the acute hospital to this institution are rare, since most patients need further oncologic treatment; transferrals are thus only possible after the oncologic treatment is complete.

Some patients remain very weak, dependant and immobile due to the extent of neurological and cognitive impairment. When it comes to extensive neurological deficits and disturbances of consciousness with poor cooperation, our actions are mainly focused on preventing complications arising from constantly lying in bed. Special emphasis is put on respiratory physiotherapy. It is

necessary to regularly turn the patient, put him in proper positions and perform neuro-physiotherapy; electronic devices that enable joint movements and prevent contractures can also be used. Even patients in the minimally conscious state can use the wheelchair, provided it has been adapted to accommodate for passive sitting. Patients in the minimally conscious state can be stimulated with different sensory stimuli in the appropriate environmental settings, minimising additional disruptive stimuli from the surroundings. Relatives help in picking the appropriate stimuli and can also perform sensory stimulation during visiting hours. It is extremely important to educate the family to be able to offer good care and support to the patient, especially when patients are bedridden and dependant in daily activities needing the help of other people. Often, it is also necessary to arrange for proper utilities the patient will need at home, such as an adopted bed, wheelchair, walker or lift for easier handling with bedridden patients. Such equipment can be prescribed when the patient is discharged from the hospital.

Discussion

Increasing incidence of brain tumours has been observed in many countries over the last thirty years.¹⁹ In assessing the outcome of malignant brain tumour patients, life expectancy as well as direct and indirect functional impairment must also be taken into consideration. Giordana *et al.* have reviewed several studies dealing with the functional outcome of brain tumour patients and have shown that rehabilitation intervention offers significant benefit to these patients.²⁰ The rehabilitation process is therefore of paramount importance in brain tumour patients when compared to other malignancies because of their extremely high rate of associated disability.³ Similarly, preliminary results of our retrospective review have shown that approximately 30% of 200 patients being treated annually for malignant brain tumours have post-operative neurological deficits. Patients usually receive further oncologic treatment and we can assume that their functional status might worsen during additional therapy due to brain oedema or tumour progression. Recent progress in the multimodal treatment of brain tumour patients has improved 5 year survival rate, which has resulted in an increased number of patients requiring rehabilitation support.³ Nowadays cancer is viewed as a chronic disease where rehabilitation becomes

an important aspect of care. However, despite the high incidence of neurological and functional deficits in brain tumour patients, rehabilitation treatment in this population is not as well established as it is for patients with other neurological conditions.⁷ In a study comparing brain tumour patients and patients with traumatic brain injury the authors found no significant differences in mobility and independence in activities of daily living between both groups of patients.²¹ Functional improvements are also comparable to those achieved in stroke patients.²⁰ Clinical guidelines suggest that rehabilitation should begin early in stroke patients in order to improve the recovery process and reduce disability.^{22,23} In brain tumour patients, where deterioration is often faster than in stroke patients, the need for early intervention is even more pressing.⁷ Rehabilitation, especially during the acute phase and immediately postoperatively can improve functional outcome.⁷ The review of the literature by Khan *et al.* failed to identify any high quality studies evaluating the effectiveness of multidisciplinary rehabilitation care in patients with brain tumours.²⁴ On the other hand, there is strong evidence that unidisciplinary interventions (exercise, physical therapy...) enhance functional outcome and improve quality of life.²⁴

Rehabilitation is recommended in early stages of the disease for function restoration after surgery and in more advanced stages as an important part of palliative care with the aim to prevent complications, control the symptoms and maintain patients' independence and quality of life regardless of life expectancy.²⁵ In brain tumour patients, specificity of medical treatment, complication of surgery and side effects of irradiation and chemotherapy have to be taken into consideration.²⁶ Side effects of corticosteroids and anticonvulsants are also important, because their chronic use can be associated with myopathy, osteoporosis, behavioural changes and psychiatric disorders.²⁷ Anticonvulsants can affect cognitive functions, alter the reaction time and in some instances cause movement disorders such as ataxia; all of these side effects influence the rehabilitation process.²⁶ In the acute phase of rehabilitation, flexibility and frequent reassessments are required.²⁸ Oncologic and other treatments may impact the timing of physical therapy interventions, which should be performed in a phase of patient's peak performance.²⁸ Because of diverse clinical picture and varying levels of disability among brain tumour patients an individualised approach is always warranted.²⁹

With proper early medical rehabilitation in the postoperative settings we enable the patients to become more independent, prevent complications and increase baseline conditions for further rehabilitation. The length of stay in the acute hospital setting is short and we start with rehabilitation procedures immediately after surgery; these procedures should be carried out throughout the additional oncologic therapy. After finishing the treatment, the patients should be evaluated and the neurological impairments, influencing daily functioning, should be identified. Further complex rehabilitation could be arranged at the University Rehabilitation Institute of the Republic of Slovenia. Several studies have shown significant improvement in the functional state of brain tumour patients as a result of inpatient rehabilitation.^{30,31} In the institutions providing inpatient rehabilitation, patients are offered individually adapted treatment programs based on their deficit, ability to cooperate and set goals. The challenge is not just to help the patients overcome their disabilities and improve performance status but also to help them stay independent in the community and lower the family burden. After finishing the inpatient rehabilitation, the patients may also receive appropriate rehabilitation devices to facilitate care giving at home and prolong their independency.

We must emphasize that an article by Goljar from 2008 shows that only about 10 patients treated for malignant brain tumours are admitted to the University Rehabilitation Institute of the Republic of Slovenia yearly.³² Considering large number of patients undergoing surgery and a significant proportion of postoperative neurological symptoms it remains unclear what type of rehabilitation is offered to them after completion of the oncologic treatment.

Besides motor impairments, an important potential long-term deficit of the surviving patients is cognitive deterioration, which is related to tumour location, surgical morbidity and oncologic treatment.⁹ Problems related to cognitive impairment are well documented and present even in the tumour remission period.³³ However, only few studies have focused on strategies to prevent and treat cognitive deficits in brain tumour patients and many of them have serious methodological limitations, such as too small of a sample or retrospective study design, so further studies are necessary.^{33,34} Regardless of the severity, cognitive deficits have a significant negative impact on patient's daily living.³⁵ In 2003, Hahn and as-

sociates published a prospective study, in which they performed standardised neuropsychological testing and life quality evaluation in primary brain tumour patients.³⁶ The study has shown that individually tailored rehabilitation programs can increase the patient's quality of life.³⁶ Gehring *et al.* have in 2008 established that we are at a relatively early stage of development of effective pharmacological and behavioural approaches towards treatment and prevention of cognitive deficits in this group of patients, although the approaches used might have a positive effect on other areas of patient's functioning and well-being.³³ Cognitive deficits interfere significantly with familial, social and career-related activities.³⁷ Recent systematic review of the literature established that neurocognitive symptoms and personality changes irreversibly altered the relationship between the patient and the caregiver, giving the caregiver the sense of total responsibility.³⁸ For the patient, however, loss of autonomy and coping with restriction seem to be the most difficult.³⁸ Early identification of neuropsychological changes may lead to improved effectiveness of cognitive training.³³ It has been shown that early cognitive training in the postsurgical period markedly improves cognitive functioning.³³ Taking into account and treating these impairments can enhance the patients' quality of life. Therefore, more precise evaluation of patients' functional and cognitive state after completion of the oncologic therapy is warranted to establish criteria for further complex medical rehabilitation.

Conclusions

Rehabilitation of patients suffering from malignant brain tumours is an important part of treatment. By starting treatment early during hospitalization and by continuing the treatment in qualified institutions later on we can raise the quality of the patient's life and achieve higher levels of independence. Considering the high number of patients in Slovenia the percentage of those referred to the University Rehabilitation Institute of Slovenia after oncologic treatment is low. We believe that a more precise evaluation of the patients' functional state after finishing additional tumour related treatments should be performed and more patients directed to the complex rehabilitation treatment. In addition to retrospective reviews, a well-designed study should be performed in Slovenia to establish the effect of inpatient postoperative rehabilitation on the quality of life in this group of patients.

References

- Mukand JA, Blackinton DD, Cirncoli MG, Lee JJ, Santos BB. Incidence of neurologic deficits and rehabilitation of patients with brain tumors. *Am J Phys Med Rehabil* 2001; **80**: 346-50.
- Hansen A, Rosenbek Minet LK, Sogaard K, Jarden JO. The effect of an interdisciplinary rehabilitation intervention comparing HRQoL, symptom burden and physical function among patients with primary glioma: an RTC study protocol. *BMJ Open* 2014; **4**(10): e005490.
- Vargo M. Brain tumor rehabilitation. *Am J Phys Med Rehabil* 2011; **90**(5 Suppl 1): S50-62.
- Kase M, Minajeva A, Niinepuu K, Kase S, Vardja M, Asser T, et al. Impact of CD133 positive stem cell proportion on survival in patients with glioblastoma multiforme. *Radiol Oncol* 2013; **47**: 405-10.
- Maza S, Buchert R, Brenner W, Munz DL, Thiel E, Korfel A, et al. Brain and whole-body FDG-PET in diagnosis, treatment monitoring and long-term follow-up of primary CNS lymphoma. *Radiol Oncol* 2013; **47**: 103-10.
- Smrdel U, Kovac V, Popovic M, Zwitter M. Glioblastoma patients in Slovenia from 1997 to 2008. *Radiol Oncol* 2014; **48**: 72-9.
- Bartolo M, Zucchella C, Pace A, Lanzetta G, Vecchione C, Bartolo M, Grillea G, Serrao M, Tassorell C, Sandrini G, Pierelli F. Early rehabilitation after surgery improves functional outcome in inpatients with brain tumours. *J Neurooncol* 2012; **107**: 537-44.
- Cheville AL. Cancer rehabilitation. In: Braddon LB, Chan L, Harrast MA, et al, editors. *Physical medicine and rehabilitation*. 4th edition, Philadelphia: Saunders 2011. p. 1371-401.
- Shen C, Bao WM, Yang BJ, Xie R, Cao XY, et al. Cognitive deficits in patients with brain tumor. *Chin Med J* 2012; **125**: 2610-7.
- Giovagnoli AR. Investigation of cognitive impairments in people with brain tumors. *J Neurooncol* 2012; **108**: 277-83.
- Vranic A. New developments in surgery of malignant gliomas. *Radiol Oncol* 2011; **45**: 159-65.
- Tuna-Malak A, Diramali A. Radiotherapy-related tiredness in patients with glioblastoma multiforme (GBM). *Asian Pac J Cancer Prev* 2008; **9**: 497-500.
- Kim RB, Chun MH, Han EY. Fatigue assessment and rehabilitation outcomes in patients with brain tumors. *Support Care Cancer* 2012; **20**: 805-12.
- Mainio A, Hakko H, Niemela A, Koivukangas J, Rasanen P. Depression and functional outcome in patients with brain tumours: a population-based 1-year follow-up study. *J Neurosurg* 2005; **103**: 841-7.
- Vincent Mor V, Laliberte L, Morris JN, Wiemann M. The Karnofsky performance status scale: An examination of its reliability and validity in a research setting. *Cancer* 1984; **53**: 2002-7.
- Schag CC, Heinrich RL, Ganz PA. Karnofsky performance status revisited: Reliability, validity, and guidelines. *J Clin Oncol* 1984; **2**: 187-93
- O'Toole DM, Golden AM. Evaluating cancer patients for rehabilitation potential. *West J Med* 1991; **155**: 384-7.
- Kos N. [Early medical rehabilitation after surgery of central nervous system tumors]. [Slovenian]. In: Marinček Č, Burger H, editors. *19th rehabilitation medicine days*, Ljubljana, March 28-29, 2008. *Rehabilitacija* 2008; **7**(Suppl 2): 49-51.
- Wrensch M, Minn Y, Chew T, Bondy M, Berger MS. Epidemiology of primary brain tumors: Current concepts and review of the literature. *Neuro Oncol* 2002; **4**: 278-99.
- Giordana MT, Clara E. Functional rehabilitation and brain tumour patients. A review of outcome. *Neurol Sci* 2006; **27**: 240-4.
- Huang ME, Cifu DX, Keyser-Marcus L. Functional outcomes in patients with brain tumor after inpatient rehabilitation: comparison of traumatic brain injury. *Am J Phys Med Rehabil* 2000; **79**: 327-35.
- Duncan PW, Zorowitz R, Bates B, Choi JY, Glasberg JJ, Graham GD, Katz RC, Lamberty K, Reker D. Management of adult stroke rehabilitation care: a clinical practice guideline. *Stroke* 2005; **36**: 2100-43.
- Bates B, Choi JY, Duncan PW, Glasberg JJ, Graham GD, Katz RC, Lamerty K, Reker D, Zorowitz R. Veterans Affairs/Department of Defense Clinical Practice Guideline for the Management of Adult Stroke rehabilitation care: executive summary. *Stroke* 2005; **36**: 2049-56.
- Khan F, Amatya B, Ng L, Drummond K, Olver J. Multidisciplinary rehabilitation after primary brain tumour treatment (review). *Top Geriatr Rehabil* 2011; **27**: 184-92.
- Bartolo M, Zucchella C, Pace A, De Nunzio AM, Serrao M, Sandrini G, et al. Improving neuro-oncological patients care: basic and practical concepts for nurse specialist in neuro-rehabilitation. *J Exp Clin Cancer Res* 2012; **31**: 82.
- Ching W, Luhmann M. Neuro-oncological physical therapy for older person. *Top Geriatr Rehabil* 2011; **27**: 184-92.
- Pace A, Metro G, Fabi A. Supportive care in neurooncology. *Curr Opin Oncol* 2010; **22**: 621-6.
- Kirshblum S, O'Dell MW, Ho C, Barr K. Rehabilitation of persons with central nervous system tumors. *Cancer* 2001; **92**(4 Suppl): 1029-38.
- Sherwood PR, Given BA, Given CW, Schiffman RF, Murman DL, Lovely M, et al. Predictors of distress in caregivers of persons with a primary malignant brain tumor. *Res Nursing Health* 2006; **29**: 105-20.
- O'Dell MW, Barr K, Spanier D, Warnick RE. Functional outcome of inpatient rehabilitation in persons with brain tumors. *Arch Phys Med Rehabil* 1998; **97**: 1530-4.
- Marciniak CM, Sliwia JA, Heinemann AW, Semik PE. Functional outcomes of persons with brain tumors after inpatients rehabilitation. *Arch Phys Med Rehabil* 2001; **82**: 457-63.
- Goljar N. [Comprehensive rehabilitation of patients with brain tumours]. [Slovenian]. In: Marinček Č, Burger H, editors. *19th rehabilitation medicine days*, Ljubljana, March 28-29, 2008. *Rehabilitacija* 2008; **7**(Suppl 2): 52-5.
- Gehring K, Sitskoom MM, Aaronson N, Tophoom MJB. Interventions for cognitive deficits in adult with brain tumours. *Lancet Neurol* 2008; **7**: 548-60.
- Weitzner MA, Meyers CA. Cognitive functioning and quality of life in malignant glioma patients: A review of the literature. *Psychooncology* 1997; **6**: 169-77.
- Zucchella C, Capone A, Codella V, De Nunzio AM, Vecchione C, Sandrini G, et al. Cognitive rehabilitation for early post-surgery inpatients affected by primary brain tumor: a randomized, controlled trial. *J Neurooncol* 2013; **114**: 93-100.
- Hahn CA, Dunn RH, Logue PE, King JH, Edwards CL, Halperin EC. Prospective study of neuropsychologic testing and quality-of-life assessment of adults with primary malignant brain tumors. *Int J Radiat Oncol Biol Phys* 2003; **55**: 992-9.
- Biegler KA, Chaoul MA, Cohen L. Cancer, cognitive impairment and medication. *Acta Oncol* 2009; **48**: 18-26.
- Sterckx W, Coolbrandt A, Dierckx de Casterle B, Van den Heede K, Decruyenaere M, et al. The impact of high-grade glioma on everyday life: A systematic review from patient's and caregiver's perspective. *Eur J Oncol Nurs* 2013; **17**: 107-17.

Screen-detected ductal carcinoma in situ found on stereotactic vacuum-assisted biopsy of suspicious microcalcifications without mass: radiological-histological correlation

Bartłomiej Szynglarewicz¹, Piotr Kasprzak², Przemysław Biecek³, Agnieszka Halon⁴, Rafał Matkowski^{1,5}

¹ Breast Unit, Department of Surgical Oncology, Lower Silesia Oncology Centre, Wrocław, Poland

² Department of Breast Imaging, Lower Silesia Oncology Centre, Wrocław, Poland

³ Faculty of Mathematics, Informatics and Mechanics, University of Warsaw, Warsaw, Poland

⁴ Department of Pathomorphology and Oncological Cytology, Wrocław Medical University, Poland

⁵ Department of Oncology, Wrocław Medical University, Poland

Radiol Oncol 2016; 50(2): 145-152.

Received 30 November 2015

Accepted 26 January 2016

Correspondence to: Bartłomiej Szynglarewicz, M.D., Lower Silesian Oncology Centre, Plac Hirszfelda 12, 53-413 Wrocław, Poland. Phone: +48 071 368 9333; Fax: +48 071 799 8600. E-mail: szynglarewicz.b@dco.com.pl

Disclosure: No potential conflicts of interest were disclosed.

Background. Commonly identified on screening mammography breast microcalcifications are the predominant manifestation of ductal carcinoma *in situ* (DCIS). The aim of this study was to investigate the association between clinico-radiological features and histological findings in patients with screen-detected DCIS.

Patients and methods. Consecutive 127 patients with pure DCIS found on stereotactic vacuum-assisted biopsy of screen-detected suspicious microcalcifications without mass entered the study. Patient age, type and distribution of microcalcifications, DCIS nuclear grade (NG) and the presence of comedonecrosis were investigated. Association between parameters was statistically analysed with $P < 0.05$ as a significance level.

Results. Powdery microcalcifications were most often clustered while regional were most common of casting-type ($P < 0.001$). High, intermediate and low NG of DCIS was significantly related to casting-type, crushed stone-like and powdery microcalcifications, respectively ($P < 0.01$). Low and intermediate NG DCIS were the most common in clustered and grouped microcalcifications while high NG DCIS was the most often when regional distribution was observed ($P < 0.05$). Comedonecrosis was significantly more common in high NG DCIS ($P < 0.01$). The association between comedonecrosis and type of microcalcifications was not significant, but with their distribution was close to the significance level ($P = 0.07$). Patient age was not significantly related to imaging or histological findings.

Conclusions. The association between pattern of mammographic microcalcifications and histological findings related to more aggressive disease can be helpful in optimal surgery planning in patients with screen-detected DCIS, regarding the extent of breast intervention and consideration of synchronous sentinel node biopsy.

Key words: breast cancer screening; mammographic microcalcifications; ductal carcinoma *in situ*

Introduction

The development of imaging techniques and the widespread adoption of screening programs resulted in dramatically increased incidence of ductal carcinoma *in situ* (DCIS), which currently accounts

for about 20–25% of newly diagnosed breast cancer cases.¹ The most common clinical presentation of DCIS are mammographically visible microcalcifications. Although being present in about 30% of all breast cancers and in approximately 55% of non-palpable breast malignancies, they are responsible

for the detection of 85–95% of cases of DCIS by screening mammography.^{2,3}

The microcalcifications associated with the development of DCIS arise in the lumen of the terminal ducts, by calcium production on the secretion material or on the zones of necrosis.⁴ They only indirectly attest to the cell proliferation of the carcinoma, that will then progress in the ducts in an anterograde direction toward the nipple or in a retrograde direction, within the lobule.⁵ The microcalcifications are commonly discontinuous, which may indicate multifocality. However, since the true multifocal DCIS is currently believed to be a relatively rare condition, they most often correspond to a single lesion extending to several ducts by contiguity.^{4,7} With the introduction of stereotactic minimal-invasive biopsy (core-needle or vacuum-assisted) it has become possible to obtain a preoperative diagnosis of suspicious breast microcalcifications not visible on ultrasound. As most DCIS lesions are nonpalpable and some are more extensive than suspected on the mammogram, evaluation of imaging-pathologic correlation by a multidisciplinary team is essential in the assessment of patients to determine their eligibility for breast conserving surgery as well as to achieve in these cases a complete excision with negative margins and good cosmetic outcomes.⁸

The aim of this study was to investigate the clinical and histological features, and to evaluate the association among these findings in screen-detected DCIS found on stereotactic vacuum-assisted biopsy of suspicious microcalcifications.

Patients and methods

Screening program

Nation-wide and population-based breast cancer screening program is targeting women aged 50–69, with exclusion of females undergoing treatment or being followed-up due to breast cancer. Two-view mammography (cranio-caudal and oblique) is used as a standard screening test. High-quality analogue (screen-film) or full field digital mammography (FFDM) are both allowed in screening program in Poland. Routine round length of the program is two years. All women with radiological findings categorised as suspicious of malignancy (BIRADS 4) or highly suggested for cancer (BIRADS 5) are referred to further assessment and invasive investigations. In patients with masses ultrasound-guided core-needle or vacuum-assisted biopsy is carried out, whereas in patients with oth-

er lesions, not well seen in ultrasound, a stereotactic biopsy under digital mammography guidance is performed.

Patients

A cohort of 127 consecutive non-symptomatic patients with screen-detected DCIS diagnosed in years 2009–2014 was enrolled. All of them fulfilled the study entering criteria: BIRADS category 4 or 5 microcalcifications without mass or architectural distortion, pure DCIS found on histological examination, lack of invasion or microinvasion (≤ 1 mm in the longest diameter), absence of any other breast malignancy or border-line lesion. Median (mean, range) patient age was 60 years (59.6, 50–69). All the patients underwent the same type of minimal-invasive biopsy under the stereotactic guidance. Study was approved by the Independent Ethics Committee (UMED KB-376) and the Institutional Board (NDOK/668). Patients signed the informed consent.

Biopsy

In each case an informed consent to undergo biopsy was obtained. All the procedures were performed by one breast-dedicated radiologist (PK), in the same breast care unit, according to the same standardised protocol to assure quality control. Five specimens was the minimal number of tissue cores. Each biopsy was done under the local anaesthesia using 10 cm³ of 1% lidocaine in two-step approach: 5 cm³ superficially and 5 cm³ deeply. Biopsies were completed under digital mammography guidance using a designated prone table unit (Mammotest Plus / S, Fisher Imaging, Denver, USA) with 10-G needle (EnCore Breast Biopsy System, SenoRx Inc., Irvine, CA or EnCore Enspire Breast Biopsy System, C.R. Bard Inc., Tempe, AZ).

Pathology

All hematoxylin and eosin stained slides of formalin-fixed and paraffin-embedded tissue blocks were assessed by board-certified pathologists experienced in breast cancer. In all the cases pathological examination reported pure DCIS without invasive or microinvasive component. In cases with any doubt about the origin E-cadherin immunohistochemistry was used to exclude a pleomorphic type of lobular carcinoma *in situ*. Evaluation of DCIS histology was performed according to the well-defined and widely accepted criteria.

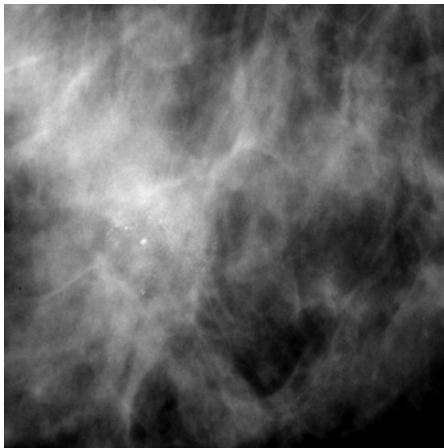


FIGURE 1. Powdery microcalcifications (cotton ball-like, indistinct, amorphous).

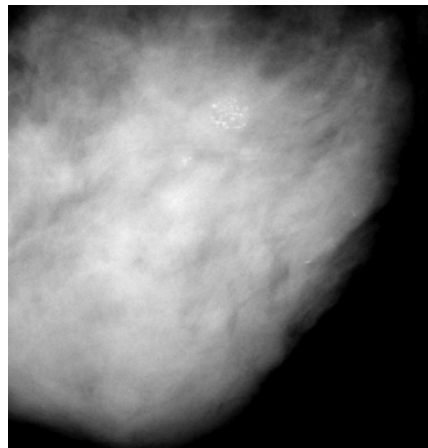


FIGURE 2. Crushed stone-like microcalcifications (pleomorphic).

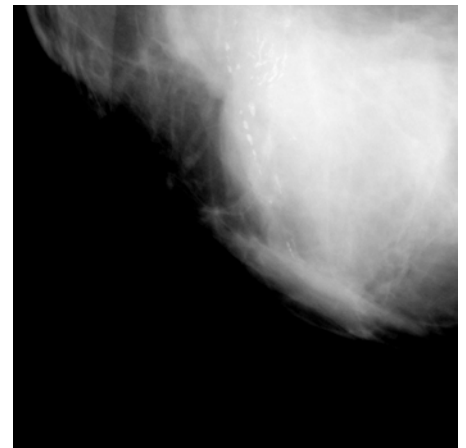


FIGURE 3. Casting-type microcalcifications (linear, branching).

Comedonecrosis was determined as present if the central areas of necrosis with ghost outlines of cells and cellular debris were found. Grading system was expressed by the assessment of nuclear grade (NG) categorising DCIS as low, intermediate, and high grade, based on the recommendations of the College of American Pathologists.^{9,10} Finally, all the slides were reviewed and re-evaluated by study supervising pathologist (AH) to confirm the original diagnosis of DCIS and its histological features as well as the absence of invasion or micro-invasion.

Statistical analysis

Data were collected in a prospective manner and entered a computer database. Statistical analysis was performed by professional statistician (PB). Following features were investigated: patient age, DCIS nuclear grade and the presence of comedonecrosis (as described above) as well as distribution pattern and morphology of microcalcifications. With regard to distribution pattern microcalcifications were classified as clustered (< 1 cm), grouped (1–2 cm), and regional (> 2 cm). Morphological type was categorised according to Tabar classification (Figure 1–3) as powdery (cotton ball-like: indistinct, amorphous), crushed stone-like (pleomorphic), and casting-type (linear, branching).¹¹ Mammographic appearance was assessed before biopsy (without knowledge of the histopathological diagnosis) by two board-certified radiologists with special expertise in breast imaging (double reading) and then reviewed and re-evaluated by study supervising radiologist (PK) using analogue microfocus magnification techniques in orthogo-

TABLE 1. Baseline characteristics

Features	n (%)
Patient age	
50–60	67 (53)
61–69	60 (47)
Microcalcifications type	
Powdery	19 (15)
Crushed stone-like	81 (64)
Casting-type	27 (21)
Microcalcifications distribution	
Clustered	85 (67)
Grouped	31 (24)
Regional	11 (9)
Nuclear grade (NG)	
NG 1 (Low)	71 (56)
NG 2 (Intermediate)	38 (30)
NG 3 (High)	18 (14)
Comedonecrosis	
Absent	58 (46)
Present	69 (54)

nal planes or, in cases of FFDM, on-screen magnification. Baseline characteristics are presented in Table 1. Association between investigated variables was analysed using Pearson’s chi-square test. P values less than 0.05 were considered statistically significant.

Results

Microcalcifications type - distribution

84% (n = 16) of powdery microcalcifications were clustered, 16% (3) were grouped, while none had regional distribution. Considering crushed stone-like and casting-type morphology 75% (61) and 30% (8) of microcalcifications were clustered, 20% (16) and 44% (12) were grouped, 5% (4) and 26%

TABLE 2. Association between microcalcifications distribution and type

Features	Microcalcifications distribution, n (%)			
	Clustered	Grouped	Regional	
Microcalcifications type, n [%]				
Powdery	16 (19) [84]	3 (10) [16]	0 (-) [-]	[100%]
Crushed stone-like	61 (72) [75]	16 (51) [20]	4 (36) [5]	[100%]
Casting type	8 (9) [30]	12 (39) [44]	7 (64) [26]	[100%]
	(100%)	(100%)	(100%)	P < 0.001

TABLE 3. Association between nuclear grade and microcalcifications

Features	Nuclear grade, n (%)			
	I (Low)	II (Intermediate)	III (High)	
Microcalcifications Type, n [%]				
Powdery	14 (20) [74]	3 (8) [16]	2 (11) [10]	[100%]
Crushed stone-like	47 (66) [58]	27 (71) [33]	7 (39) [9]	[100%]
Casting type	10 (14) [37]	8 (21) [30]	9 (50) [33]	[100%]
	(100%)	(100%)	(100%)	P < 0.01
Distribution, n [%]				
Clustered	54 (76) [64]	23 (60) [27]	8 (44) [9]	[100%]
Grouped	14 (20) [45]	12 (32) [39]	5 (28) [16]	[100%]
Regional	3 (4) [27]	3 (8) [27]	5 (28) [46]	[100%]
	(100%)	(100%)	(100%)	P < 0.05

(7) had regional pattern, respectively. With regard to clustered and grouped microcalcifications 19% (16) and 10% (3) were powdery, 72% (61) and 51% (16) were crushed stone-like, while 9% (8) and 39% (12) were casting-type, respectively. None of regional microcalcifications had powdery morphology, 36% (4) were crushed stone-like, and 64% (7) were casting-type. To sum up, powdery microcalcifications were most often clustered, never regional. Similarly, just one-fourth of crushed stone-like microcalcifications were grouped or regional. Clustered microcalcifications were most rarely of casting-type while regional were most commonly. The association between morphology and distribution of microcalcifications was of very high statistical significance ($t1$ X-squared = 25.281, $df = 4$, $P = 4.416e-05$) (Table 2).

Microcalcifications type - nuclear grade

All over 74% (14) of powdery microcalcifications revealed DCIS with low NG, 16% (3) intermediate, and 10% (2) high NG. Crushed stone-like micro-

calcifications were related to low NG in 58% (47), intermediate in 33% (27), and high in 9% (7). In contrast, 33% (9) of casting-type microcalcifications had high NG DCIS, 30% (8) intermediate, while 37% (10) had low NG DCIS. 50% (9) of high NG DCIS were presenting as casting-type microcalcifications, 39% (7) as crushed stone-like, and 11% (2) as powdery. 21% (8) of DCIS with intermediate NG was found in casting-type microcalcifications, 71% (27) in crushed stone-like, and 8% (3) in powdery. With regard to low NG DCIS, 14% (10) was detected in casting-type microcalcifications, while 66% (47) and 20% (14) in crushed stone-like and powdery, respectively. In summary, high NG DCIS was most commonly related to casting-type microcalcifications while low NG DCIS most rarely. DCIS with intermediate NG was most often found in crushed stone-like microcalcifications. Just one-fourth of powdery microcalcifications revealed DCIS with NG other than low. The association between morphology of microcalcifications and NG of DCIS was statistically significant ($t1$ X-squared = 13.363, $df = 4$, $P = 0.009632$) (Table 3).

Microcalcifications type - comedonecrosis

Comedonecrosis was found in 47% (9) of powdery microcalcifications, 57% (46) of crushed stone-like, and in 52% (14) of casting-type. DCIS with comedonecrosis was presenting as powdery in 13% (10), crushed stone-like in 67% (46), and casting-type microcalcifications in 20% (14) of cases. Considering DCIS without comedonecrosis, powdery microcalcifications were detected in 17% (10) of patients while crushed stone-like and casting-type in 60% (35) and 23% (13), respectively.

Microcalcifications type - patient age

58% (11) of patients with powdery microcalcifications were 50-60 years old, whereas 54% (44) and 44% (12) of those with crushed stone-like and casting-type, respectively (Table 4). Patients aged 50–60 years had powdery microcalcifications in 16% (11), crushed stone-like in 66% (44), and casting-type in 18% (12). Among older patients (61–69) powdery microcalcifications were present in 13% (8), crushed stone-like in 62% (37), and casting-type in 25% (15) of cases. Neither patient age nor the presence of comedonecrosis was significantly related to morphology of microcalcifications (t1 X-squared = 1.0293, df = 2, P = 0.5977; t1 X-squared = 0.63551, df = 2, P = 0.7278; respectively).

Microcalcifications distribution - nuclear grade

In 64% (54) of clustered microcalcifications low NG DCIS was found, whereas intermediate and high NG DCIS in 27% (23) and 9% (8), respectively. Grouped microcalcifications revealed low, intermediate and high NG DCIS in 45% (14), 39% (12), and 16% (5) of cases while regional microcalcifications in 27% (3), 27% (3), and 46% (5), respectively. 76% (54) and 60% (23) of DCIS with low and intermediate NG were presenting as clustered microcalcifications, 20% (14) and 32% (12) as grouped, and 4% (3) and 8% (3) as regional, respectively. Among patients with high NG DCIS 44% (8) had clustered, while 28% (5) each had grouped and regional microcalcifications. Summarising, low NG DCIS was the most common in clustered microcalcifications and very rare in regional, where high NG DCIS was the most often, being found in nearly half of cases. The association between distribution of microcalcifications and NG of DCIS was statis-

TABLE 4. Association between comedonecrosis and microcalcifications

Features	Comedonecrosis, n (%)		
	Absent	Present	
Microcalcifications Type, n [%]			
Powdery	10 (17) [53]	9 (13) [47]	[100%]
Crushed stone-like	35 (60) [43]	46 (67) [57]	[100%]
Casting type	13 (23) [48]	14 (20) [52]	[100%]
	(100%)	(100%)	P > 0.5
Distribution, n [%]			
Clustered	44 (76) [52]	41 (59) [48]	[100%]
Grouped	12 (21) [39]	19 (28) [61]	[100%]
Regional	2 (3) [18]	9 (13) [82]	[100%]
	(100%) (100%)		P 0.07

tically significant (t1 X-squared = 13.233, df = 4, P = 0.01019) (Table 3).

Microcalcifications distribution - comedonecrosis

In 48% (41) of patients with clustered, 61% (19) with grouped and 82% (9) with regional microcalcifications DCIS with comedonecrosis was found. Among patients with non-comedo DCIS 76% (44) had clustered, 21% (12) had grouped, and 3% (2) had regional microcalcifications. 59% (41) of DCIS with comedonecrosis was presenting as clustered microcalcifications, while 28% (19) and 13% (9) as grouped and regional. In summary, three-fourths of patients without comedonecrosis had clustered microcalcifications while in the vast majority of patients with regional microcalcifications DCIS with comedonecrosis was diagnosed. The association between distribution of microcalcifications and the presence of comedonecrosis was close but did not reach the statistical significance (t1 X-squared = 5.2275, df = 2, P = 0.07326) (Table 4).

Microcalcifications distribution - patient age

All over 58% (49) of patients with clustered, 39% (12) with grouped, and 55% (6) with regional microcalcifications were 50–60 years old. Considering these younger patients (50–60), 73% (49), 18% (12), and 9% (6) had clustered, grouped and regional microcalcifications, respectively. Among older ones (61–69) clustered microcalcifications were found in 60% (36) while grouped and regional in 32% (19) and 8% (5), respectively. Patient age was not sig-

TABLE 5. Association between nuclear grade and comedonecrosis

Features	Nuclear grade, n (%)			P < 0.01
	I (Low)	II (Intermediate)	III (High)	
Comedonecrosis, n [%]				
Absent	37 (52) [64]	20 (53) [34]	1 (6) [2]	[100%]
Present	34 (48) [49]	18 (47) [26]	17 (94) [25]	[100%]
	(100%)	(100%)	(100%)	

TABLE 6. Statistical significance of dependency (chi-square test, P value)

Features	Patient age	Microcalcifications type	Microcalcifications distribution	Nuclear grade	Comedonecrosis
Patient age	—	0.5977	0.1936	0.9098	1
Microcalcifications type	0.5977	—	< 0.001	< 0.01	0.7278
Microcalcifications distribution	0.1936	< 0.001	—	< 0.05	0.0733
Nuclear grade	0.9098	< 0.01	< 0.05	—	< 0.01
Comedonecrosis	1	0.7278	0.0733	< 0.01	—

nificantly related to the distribution of microcalcifications (t1 X-squared = 3.2839, df = 2, P = 0.1936).

Nuclear grade - comedonecrosis

In 94% (17) of high NG DCIS the comedonecrosis was present, whereas in 47% (18) and 48% (34) of intermediate and low NG, respectively. Among patients without comedonecrosis 2% (1) had high NG, while 34% (20) and 64% (37) had intermediate and low NG DCIS, respectively. In the group with comedonecrosis high, intermediate, and low NG DCIS were diagnosed in 25% (17), 26% (18), and 49% (34) of cases, respectively. In summary, almost all the patients with high NG DCIS had comedonecrosis while just less than half of others. In almost all the patients without comedonecrosis DCIS of low or intermediate NG was found. The association between NG and the presence of comedonecrosis was statistically significant (t1 X-squared = 13.604, df = 2, P = 0.001112) (Table 5).

Nuclear grade - patient age

Younger patients (50–60) had low, intermediate, and high NG DCIS in 57% (38), 28% (19), and 15% (10), while older women (61–69) in 55% (33), 32% (19), and 13% (8), respectively. In cases of high, intermediate, and low NG DCIS 56% (10), 50% (19), and 54% (38) of patients were in younger age. Patient age was not significantly related to NG of DCIS (t1 X-squared = 0.18908, df = 2, P = 0.9098).

Comedonecrosis - patient age

Comedonecrosis was present in 54% (36) of younger patients and in 55% (33) of those aged 61–69 years. When comedonecrosis was absent 53% (31) of patients were 50–60 years old. Similarly, among patients with comedonecrosis 52% (36) was in younger group. The association was not significant (t1 X-squared = 0, df = 1, P = 1).

Significance level of correlation between investigated variables is presented in Table 6.

Discussion

Surgery, sometimes followed by radiotherapy in cases with breast conservation, remains the treatment of choice in DCIS patients. Since it is highly favourable disease, there is no difference in mortality rate regardless of which treatment is chosen.¹² On the other hand, the extent of surgical intervention and the need of postoperative radiotherapy depend on some well-defined factors known to be important in predicting of local recurrence. The most significant and independent variables are quantified by the University of California/Van Nuys Prognostic Index (USC/VNPI), which is widely used in clinical practice. USC/VNPI is a numerical algorithm combining the following prognostic factors: age at diagnosis (older age is better), tumour size (smaller size is better), surgical margin width (wider margin is better), NG

(lower grade is better), and the presence or absence of comedonecrosis (no necrosis is better). Each of the four predictors (NG and comedonecrosis both determine pathologic classification) is scored 1 (the most favourable), 2, or 3 (the least favourable), and then added together to give an overall score, ranging from a low of 4 (least likely to recur) to a high of 12 (most likely to recur).¹²

However, not all these variables are available before operation (e.g. microscopic lesion diameter, surgical margin width). Moreover, some of features available before surgery can be underestimated in specimens from minimal-invasive biopsy (e.g. low/intermediate nuclear grade, absence of comedonecrosis) and eventually upgraded in the final examination of postoperative specimen. It would be helpful in surgical treatment planning if the histological characteristics could be predicted from the mammogram, particularly from the type and distribution of microcalcifications, which are the most common imaging presentation of DCIS.

There are conflicting reports on whether the histological features of DCIS can be estimated by the pattern of microcalcifications found on mammography. Dinkel *et al.* found that linear branching microcalcifications tended to be associated with higher pathological grading. However, correlation was poor and not statistically significant.¹³ Also in a series of Slanetz and co-workers (75 cases, 62 with calcifications alone) histological grade of DCIS could not be accurately determined prospectively based on the mammographic appearance of microcalcifications.¹⁴ In contrast, in a study of Holland and Hendriks well-differentiated DCIS was most commonly associated with multiple clusters of fine granular microcalcifications while poorly differentiated DCIS usually appeared on the mammogram as either linear branching or as coarse granular microcalcifications.¹⁵ It corresponds to our observation that low NG DCIS is usually found in clustered microcalcifications of crushed stone-like or powdery type whereas high NG DCIS is most common in casting type microcalcifications with regional distribution.

Results of more recent studies support these findings. In the large dataset consisting of 1783 DCIS (Sloane Project) casting-type microcalcifications were more frequently seen in the higher grade of DCIS, occurring in 58% of high grade while in 26% of low grade cases. Moreover, casting-type microcalcifications were increasingly common with increasing lesion size.¹⁶ These associations were of high statistical significance ($P < 0.001$). De Roos *et al.* reported significant association between linear

microcalcifications and high grade ($P < 0.001$) as well as between fine granular type and low grade of DCIS ($P < 0.05$).⁸ Barreau *et al.* studied a large cohort of 909 cases and found that granular or linear branching type and a number of microcalcifications higher than 20 were correlated with high grade of DCIS and the presence of comedonecrosis.¹⁷ Evans *et al.* noticed that when the comedonecrosis was present following features were seen more commonly: abnormal mammogram (95% vs. 7%, $P < 0.001$), mammogram with calcifications (96% vs. 61%, $P < 0.001$), calcifications with a ductal distribution (80% vs. 45%, $P < 0.005$), and rod-shaped calcifications (83% vs. 45%, $P < 0.001$). In contrast, DCIS without comedonecrosis was associated with mammogram without calcifications (39% vs. 4%, $P < 0.001$) and predominantly punctate calcifications (36% vs. 13%, $P < 0.05$).¹⁸ In a series of Stomper and Connolly predominantly linear calcifications were present in 47% of DCIS with comedonecrosis compared to 18% of DCIS without comedonecrosis ($P = 0.01$) while the predominantly granular calcifications in 53% and 82% ($P = 0.01$), respectively.¹⁹

Mammogram with microcalcifications is the most common imaging appearance of DCIS. Nevertheless, in some cases calcifications are not present. Interesting issue is to compare histological characteristics of calcified and non-calcified DCIS. As mentioned above, Evans and colleagues found that non-calcified DCIS was less commonly associated with comedonecrosis.¹⁸ Tang *et al.* reported that comedo DCIS had higher frequency of histologically seen calcifications in the ducts, however, when compared to other types it was easier to detect on ultrasound with not significant differences on mammography and MRI.²⁰ Slanetz *et al.* noticed that DCIS presenting on mammography as only a mass was usually well-differentiated.¹⁴ In contrast, Cho *et al.* observed that 59% of non-calcified DCIS lesions were high grade or comedonecrosis type.²¹ Supporting this finding, in numerous recent studies the presence of accompanying mass was related to the increased risk of invasive ductal component, which can reflect more aggressive behaviour of DCIS.²²⁻²⁵ In the series of Rauch *et al.* DCIS more frequently visible on sonography was ER-negative type, which also tended to be larger, was more likely to be high grade (93% vs. 44%, $P < 0.0001$) and associated with comedonecrosis (64% vs. 29%, $P < 0.0001$).²⁶

Considering screen-detected DCIS, the presence of calcifications seems to be related to less favourable histology and features associated with more aggressive behaviour. In the analysis of 217 DCIS

cases in 212 asymptomatic patients by Mun *et al.* high nuclear grade ($P < 0.05$), comedonecrosis ($P < 0.001$), and the presence of HER2/neu oncogene ($P < 0.001$) were more common in the calcified lesions.²⁷ Similarly, Kim *et al.* noticed that calcified DCIS was significantly more often HER2-positive than ER-positive or triple-negative. Histopathologically, HER2-positive DCIS and triple-negative DCIS were more commonly associated with high nuclear grade and comedonecrosis when compared to ER-positive DCIS.²⁸

In the era of screening programmes, advanced diagnostic tools, image-guided minimal-invasive biopsies and oncoplastic surgery a very close cooperation in multidisciplinary team is essential for the optimum management of breast cancer patients. The correlation between pattern of mammographic microcalcifications and histological features related to more aggressive disease can be helpful in optimal surgery planning in patients with screen-detected DCIS, with regard to the extent of breast intervention and the consideration of synchronous sentinel node biopsy.

Acknowledgements

Authors would like to thank Ewa Kowalska for her excellent assistance in data collection and management.

References

- Ernster VL, Ballard-Barbash R, Barlow WE, Zheng Y, Weaver DL, Cutter G, et al. Detection of ductal carcinoma in situ in women undergoing screening mammography. *J Natl Cancer Inst* 2002; **94**: 1546-54.
- Gajdos C, Tartter PI, Bleiweiss IJ, Hermann G, de Csepel J, Estabrook A, et al. Mammographic appearance of nonpalpable breast cancer reflects pathologic characteristics. *Ann Surg* 2002; **235**: 246-51.
- de Roos MA, van der Vegt B, de Vries J, Wesseling J, de Bock GH. Pathological and biological differences between screen-detected and interval ductal carcinoma in situ of the breast. *Ann Surg Oncol* 2007; **14**: 2097-104.
- Holland R, Hendriks JH, Vebeek AL, Mruvanac M, Schuurmans Stekhoven JH. Extent, distribution, and mammographic/histological correlation of breast ductal carcinoma in situ. *Lancet* 1990; **335**: 519-22.
- Henrot P, Leroux A, Barlier C, Genin P. Breast microcalcifications: The lesions in anatomical pathology. *Diagn Interv Imaging* 2014; **95**: 141-52.
- Faverly DR, Burgers L, Bult P, Holland R. Three dimensional imaging of mammary ductal carcinoma in situ: clinical implications. *Semin Diagn Pathol* 1994; **11**: 193-8.
- Mai KT, Yazdi HM, Burns BF, Perkins DG. Pattern of distribution of intraductal and infiltrating ductal carcinoma: a three-dimensional study using serial coronal giant sections of the breast. *Hum Pathol* 2000; **31**: 464-74.
- de Ross MAJ, Pijnappel RM, Post WJ, de Vries J, Baas PC, Groote LD. Correlation between imaging nad pathology in ductal carcinoma in situ of the breast. *World J Surg Oncol* 2004; **2**: 4.
- Lester SC, Bose S, Chen YY, Connolly JL, de Baca ME, Fitzgibbons PL, et al. Protocol for the examination of specimens from patients with ductal carcinoma in situ of the breast. *Arch Pathol Lab Med* 2009; **133**: 15-25.
- Schwartz GF, Lagios MD, Carter D, Connolly J, Ellis IO, Eusebi V, et al. Consensus conference on the classification of ductal carcinoma in situ. *Cancer* 1997; **80**: 1798-802.
- Tabar L, Tot T, Dean PB. *Breast Cancer: The art and science of early detection with mammography*. Stuttgart, New York: Thieme; 2005.
- Silverstein MJ, Lagios MD. Treatment selection for patients with ductal carcinoma in situ (DCIS) of the breast using the University of Southern California/Van Nuys (USC/VNPI) Prognostic Index. *Breast J* 2015; **21**: 127-32.
- Dinkel HP, Gassel AM, Tschammler A. Is the appearance of microcalcifications on mammography useful in predicting histological grade of malignancy in ductal cancer in situ? *Br J Radiol* 2000; **73**: 938-44.
- Slanetz PJ, Giardino AA, Oyama T, Koerner FC, Halpern EF, Moore RH, et al. Mammographic appearance of ductal carcinoma in situ does not reliably predict histologic subtype. *Breast J* 2001; **7**: 417-21.
- Holland R, Hendriks JH. Microcalcifications associated with ductal carcinoma in situ: mammographic-pathologic correlation. *Semin Diagn Pathol* 1994; **11**: 181-92.
- Evans A, Clements K, Maxwell A, Bishop H, Hanby A, Lawrence G, et al. Sloane Project Steering Group: Lesion size is major determinant of the mammographic features of ductal carcinoma in situ: findings from the Sloane Project. *Clin Radiol* 2010; **65**: 181-4.
- Barreau B, de Mascarel I, Feuga C, MacGrogan G, Dilhuydy MH, Picot V, et al. Mammography of ductal carcinoma in situ of the breast: review of 909 cases with radiographic-pathologic correlations. *Eur J Radiol* 2005; **54**: 55-61.
- Evans A, Pinder S, Wilson R, Sibbering M, et al. Ductal carcinoma in situ of the breast: correlation between mammographic and pathologic findings. *AJR Am J Roentgenol* 1994; **162**: 1307-11.
- Stomper PC, Connolly JL. Ductal carcinoma in situ of the breast: correlation between mammographic calcification and tumor subtype. *AJR Am J Roentgenol* 1992; **159**: 483-5.
- Tang X, Yamashita T, Hara M, Kumaki N, Tokuda Y, Masuda S. Histopathological characteristics of breast ductal carcinoma in situ and association with imaging findings. *Breast Cancer* 2015; Feb 3 [DOI:10.1007/s12282-015-0592-0 Epub ahead of print].
- Cho KR, Seo BK, Kim CH, Whang KW, Kim YH, Woo OH, et al. Non-calcified ductal carcinoma in situ: ultrasound and mammographic findings correlated with histological findings. *Yonsei Med J* 2008; **49**: 103-10.
- Schulz S, Sinn P, Golatta M, Rauch G, Junkermann H, Schuetz F, et al. Prediction of underestimated invasiveness in patients with ductal carcinoma in situ of the breast on percutaneous biopsy as rationale for recommending concurrent sentinel lymph node biopsy. *Breast* 2013; **22**: 537-42.
- Park HS, Park S, Cho J, Park JM, Kim SI, Park BW. Risk predictors of underestimation and the need for sentinel node biopsy in patients diagnosed with ductal carcinoma in situ by preoperative needle biopsy. *J Surg Oncol* 2013; **107**: 388-92.
- Szynglarewicz B, Kasprzak P, Halon A, Matkowski R. Preoperatively diagnosed ductal cancers in situ of the breast presenting as even small masses are of high risk for the invasive foci in postoperative specimen. *World J Surg Oncol* 2015; **13**: 218.
- Bae S, Yoon JH, Moon HJ, Kim MJ, Kim EK. Breast microcalcifications: diagnostic outcomes according to image-guided biopsy method. *Korean J Radiol* 2015; **16**: 996-1005.
- Rauch GM, Kuerer HM, Scoggins ME, Fox PS, Benveniste AP, Park YM, et al. Clinicopathologic, mammographic, and sonographic features in 1,187 patients with pure ductal carcinoma in situ of the breast by estrogen receptor status. *Breast Cancer Res Treat* 2013; **139**: 639-47.
- Mun HS, Shin HJ, Kim HH, Cha JH, Kim H. Screening-detected calcified and non-calcified ductal carcinoma in situ: differences in the imaging and histopathological features. *Clin Radiol* 2013; **68**: e27-35.
- Kim MY, Kim HS, Choi N, Yang JH, Yoo YB, Park KS. Screening mammography-detected ductal carcinoma in situ: mammographic features based on breast cancer subtypes. *Clin Imaging* 2015; **39**: 983-6.

^{18}F -FET and ^{18}F -FCH uptake in human glioblastoma T98G cell lines

Marco Giovanni Persico¹, Federica Eleonora Buroni¹, Francesca Pasi², Lorenzo Lodola¹, Carlo Aprile¹, Rosanna Nano³, Marina Hodolic⁴

¹ Department of Oncohaematology, Nuclear Medicine Unit, IRCCS San Matteo Hospital Foundation, Pavia, Italy

² Department of Oncohaematology, Radiotherapy Unit, IRCCS San Matteo Hospital Foundation, Pavia, Italy

³ Department of Biology and Biotechnology "Lazzaro Spallanzani", University of Pavia, Pavia, Italy

⁴ Nuclear medicine research department, Iason, Graz, Austria

Radiol Oncol 2016; 50(2): 153-158.

Received 26 November 2015

Accepted 18 March 2016

Correspondence to: Lorenzo Lodola, Fondazione IRCCS Policlinico San Matteo, V. le Golgi 19, 27100 Pavia, Italy. Phone: +39 038 250 1666; Fax: +39 0382501669; E-mail: l.lodola@smatteo.pv.it

Disclosure: No potential conflicts of interest were disclosed.

M.G.P., F.E.B. and F.P. have contributed equally.

Background. Despite complex treatment of surgery, radiotherapy and chemotherapy, high grade gliomas often recur. Differentiation between post-treatment changes and recurrence is difficult. ^{18}F -methyl-choline (^{18}F -FCH) is frequently used in staging and detection of recurrent prostate cancer disease as well as some brain tumours; however accumulation in inflammatory tissue limits its specificity. The ^{18}F -ethyl-tyrosine (^{18}F -FET) shows a specific uptake in malignant cells, resulting from increased expression of amino acid transporters or diffusing through the disrupted blood-brain barrier. ^{18}F -FET exhibits lower uptake in macrophages and other inflammatory cells. Aim of this study was to evaluate ^{18}F -FCH and ^{18}F -FET uptake by human glioblastoma T98G cells.

Material and methods. Human glioblastoma T98G or human dermal fibroblasts cells, seeded at a density to obtain 2×10^5 cells per flask when radioactive tracers were administered, grew adherent to the plastic surface at 37°C in 5% CO_2 in complete medium. Equimolar amounts of radiopharmaceuticals were added to cells for different incubation times (20 to 120 minutes) for ^{18}F -FCH and ^{18}F -FET respectively. The cellular radiotracer uptake was determined with a gamma counter. All experiments were carried out in duplicate and repeated three times. The uptake measurements are expressed as the percentage of the administered dose of tracer per 2×10^5 cells. Data (expressed as mean values of % uptake of radiopharmaceuticals) were compared using parametric or non-parametric tests as appropriate. Differences were regarded as statistically significant when $p < 0.05$.

Results. A significant uptake of ^{18}F -FCH was seen in T98G cells at 60, 90 and 120 minutes. The percentage uptake of ^{18}F -FET in comparison to ^{18}F -FCH was lower by a factor of more than 3, with different kinetic curves. ^{18}F -FET showed a more rapid initial uptake up to 40 minutes and ^{18}F -FCH showed a progressive rise reaching a maximum after 90 minutes.

Conclusions. ^{18}F -FCH and ^{18}F -FET are candidates for neuro-oncological PET imaging. ^{18}F -FET could be the most useful oncological PET marker in the presence of reparative changes after therapy, where the higher affinity of ^{18}F -FCH to inflammatory cells makes it more difficult to discriminate between tumour persistence and non-neoplastic changes. Additional studies on the influence of inflammatory tissue and radionecrotic cellular components on radiopharmaceutical uptake are necessary.

Key words:

Introduction

The human brain is made up of approximately 100 billion nerve cells. Already in 19th century

there was a statement that nervous system is held together by specific cells called glia (in Greek language: glia=glue). More than insulating one neuron from another and prevent neuronal injury, glia

supply oxygen and nutrients to neurons, destroy pathogens and remove dead neurons. In the brain, glial cells are more numerous than nerve cells (ratio of app. 3:1).¹

Approximately 30% of all brain tumours and app. 80% of malignant ones arise from glial cell (gliomas). Different oncogenes and genetic disorders are most commonly mentioned as causes of gliomas. Despite complex treatment of surgery, radiotherapy and chemotherapy, high grade gliomas almost always recur.^{2,3} Before additional systemic or local therapies are performed, precise localization of recurrent tumour is essential. Differentiation between postsurgical, postradiotherapy changes and recurrent tumour is still a difficult diagnostic task.

Magnetic resonance imaging (MRI) is well established imaging modality for diagnosis of recurrent disease in patients with gliomas.^{4,6} ^{18}F -fluorodeoxyglucose (^{18}F -FDG) Positron Emission Tomography (PET) in brain tumours was the first application of this modality in oncology^{7,8}, however because of the high physiologic glucose uptake of normal brain tissue, ^{18}F -FDG did not gain widespread use in brain tumours imaging.^{9,10}

PET imaging with [^{11}C]- and [^{18}F]-labelled choline derivatives is frequently used in the staging and detection of recurrent prostate cancer disease due to the increased choline kinase expression in this malignancy. Moreover, choline kinase dysregulation can be frequently found, not only in prostate cancer cells but in a large panel of human tumours such as lung, colorectal, and brain tumours.¹¹⁻¹³ Following intravenous injection of choline derivatives in rats and mice, the brain uptake is less than 0.2% of the injected dose.¹⁴ However, choline accumulation in inflammatory tissue limits the specificity of choline PET for tumour detection.¹⁵

In the last decades, radiolabelled amino acids are attracting increasing interest in nuclear medicine because amino acid tracers appear to be more specific for brain tumour imaging than tracers like [^{11}C]- and [^{18}F]-labelled choline derivatives or 3,4-Dihydroxy-6-[^{18}F]fluoro-L-phenylalanine (^{18}F -DOPA). Results on cellular uptake of O-(2-[^{18}F]fluoroethyl)-L-tyrosine (^{18}F -FET) has been studied in vitro and in vivo already in the 1960's.¹⁶ The uptake mechanism of ^{18}F -FET in malignantly transformed cells can either be active or probably result from increased expression of amino acid transporters or passive, whereby the accumulation is slightly higher in tumour tissue with a disrupted blood-brain barrier. In contrast to ^{18}F and ^{11}C -choline, ^{18}F -FET exhibits lower uptake in macrophages and other inflammatory cells.^{17,18} Also ^{11}C -methionine, la-

belled amino acid for PET imaging of central nervous system tumours, showed very good results. But because of short half-life of ^{11}C (20.4 min), this tracer can be used just in the centres with on-site cyclotron. In the last years many articles supported statement that ^{18}F -FET PET/CT is valuable modality for individual treatment decision in patients with low grade gliomas.¹⁹⁻²⁴ The T98G cells are the most radio resistant cell line available derived from a human glioblastoma multiform tumour.²⁵ T98G are arrested in G1 phase under stationary phase conditions, so they also exhibit the transformed characteristics of anchorage independence and immortality.²⁶

In our previous study²⁷, we compared the uptake of ^{18}F -FCH and ^{18}F -FDG by T98G cells and fibroblasts; also for evaluation its influence on cellular radiopharmaceutical uptake competition experiments with cold choline were performed.

Aim of this study was to evaluate ^{18}F -FCH and ^{18}F -FET uptake on T98G cell lines derived from a human glioblastoma multiforme tumour.

Material and methods

Cell lines

Human glioblastoma T98G cells were purchased from the European Collection of Cell Cultures (ECACC, Salisbury, UK) and cultured in Eagle's Minimum Essential Medium (EMEM, Euroclone SpA, MI, Italy) supplemented with 10% fetal bovine serum, 100 units/mL penicillin/streptomycin, 2 mM L-glutamine and 0.01% sodium pyruvate at 37°C in a humidified atmosphere of 5% CO_2 in air. Human dermal fibroblasts were used as non-pathological control cell types. Primary cultures of human dermal fibroblasts were derived from biopsies of healthy donors after obtaining informed consent. Primary cultures of fibroblasts were cultured in Dulbecco's modified Eagle's medium (DMEM, Euroclone SpA, MI, Italy) supplemented with 10% fetal bovine serum, 100 units/mL penicillin, 100 g/mL streptomycin, 2 mM L-glutamine at 37°C in a humidified atmosphere of 5% CO_2 in air. Stock cultures of both cell lines were maintained in exponential growth as monolayers in 25 cm^2 Corning plastic tissue-culture flasks (Sigma-Aldrich, St Louis, MO, USA).

Radioactive tracer incubation

^{18}F -FCH and ^{18}F -FET were obtained from IASON GmbH (Graz-Seiersberg, Austria). Synthesis of ^{18}F -FCH was performed as follows: The precu-

sor was reacted with ¹⁸F and the intermediate was evaporated via a solid phase cartridge. After the gas phase reaction, the product was trapped and purified by solid phase cartridges and passed through a sterilized filter, synthesis of ¹⁸F-FET was performed as follows: The precursor (in acetonitrile) was reacted with ¹⁸F. After ¹⁸F incorporation, acetonitrile was removed under pressure, and hydrolysis was carried out with 1 M HCl. The final solution was neutralized and purified by solid phase cartridges and passed through a sterilized filter.

Cells, seeded at a density to obtain 2×10^5 cells per flask when radioactive tracers were administered, grew adherent to the plastic surface at 37°C in 5% CO₂ in complete medium. Radioactive tracer experiments were performed 20-22 hours post-seeding in order to use the cells in the exponential phase of growth. The medium was renewed before performing studies. Cells were incubated at 37°C with 100 kBq (100 μL) equimolar amounts of ¹⁸F-FCH or ¹⁸F-FET, added in 2 mL of medium in each flask for varying incubation times (20, 40, 60, 90, 120 min for ¹⁸F-FCH; 20, 40, 60, 80, 100, 120 min for ¹⁸F-FET) under 5% CO₂ gaseous conditions. For experiments with ¹⁸F-FCH and ¹⁸F-FET, radiotracer incubation was done in complete medium. Control samples underwent the same procedure as other samples, but they were incubated with 100 μL of saline instead of a radiotracer.

Cell kinetic studies and uptake evaluation

The cellular radiotracer uptake was determined with a 3 x 3" NaI(Tl) pinhole 16 x 40 mm gamma counter (Raytest, Straubenhardt, Germany). All measurements were carried out under the same counting position along with a standardized source to verify the counter's performance and the data were corrected for background and decay. Total radioactivity was counted when the radiotracer was added to the medium in each flask (time 0). After 20, 40, 60, 90, 120 min for ¹⁸F-FCH and 20, 40, 60, 80, 100, 120 min for ¹⁸F-FET from time 0, the medium was harvested, the cells were rapidly washed three times with 1 mL of phosphate-buffered saline (PBS) and radiopharmaceutical uptake for each sample was assessed. All experiments were carried out in duplicate and repeated three times. The uptake measurements are expressed as the percentage of the administered dose of tracer per 2×10^5 cells after correction for negative control uptake (flasks containing no cells with complete medium and incubated with radiopharmaceutical).

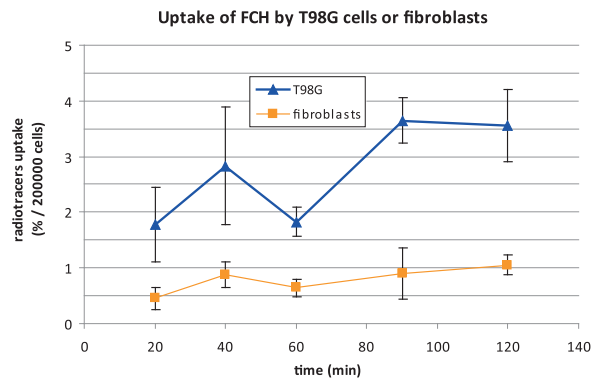


FIGURE 1. Uptake of ¹⁸F-methyl-choline (¹⁸F-FCH) by T98G cells and human dermal fibroblasts.

Cell viability assay

At the end of quantitative gamma spectrometry, adherent cells were harvested with 1% trypsin-EDTA solution and supernatants with adherent cells were counted with Burker's chamber. Trypan Blue dye assay was performed to assess cell viability as standard protocol.

Statistical analysis

In vitro binding experiments were conducted in duplicate and repeated three times. Data (expressed as mean values of % uptake of radiopharmaceuticals) were compared using parametric or non-parametric tests as appropriate. Differences were regarded as statistically significant when $p < 0.05$. All values are expressed as mean values with confidence interval CI 95% and report the uptake of radiotracers as a function of the incubation period. All values are shown as a percentage of the administered dose per 200,000 cells (mean ± CI 95%). Therefore, if error bars on the Y axis do not overlap, the two points are considered significantly different.

Results

Radiopharmaceuticals binding assay

A significant uptake of ¹⁸F-FCH was seen in T98G cells after 60 minutes, with a percentage of uptake of $1.8 \pm 0.3\%$, $3.6 \pm 0.4\%$ and $3.6 \pm 0.6\%$ at 60, 90 and 120 min respectively. Human dermal fibroblasts did not seem to accumulate ¹⁸F-FCH specifically; at each incubation time the percentage of the administered dose in the cells was lower than 1%. Human dermal fibroblast uptake was significantly lower than in the T98G cell uptake in all incubation times (Figure 1).

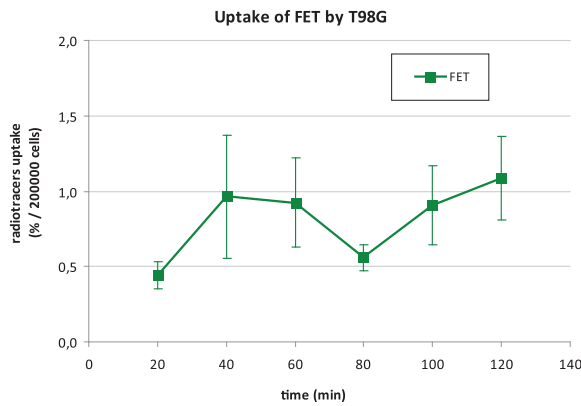


FIGURE 2. Uptake of ^{18}F -ethyl-tyrosine (^{18}F -FET) by T98G cells.

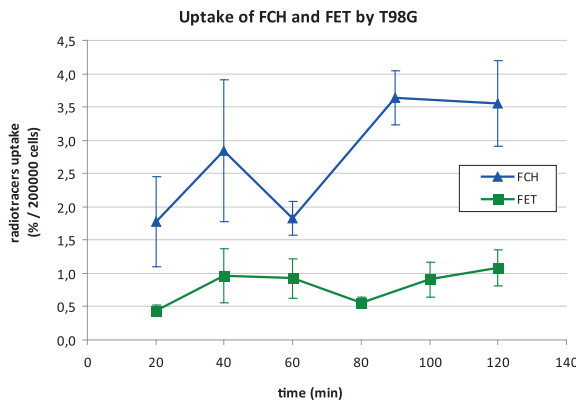


FIGURE 3. Uptake of ^{18}F -methyl-choline (^{18}F -FCH) and ^{18}F -ethyl-tyrosine (^{18}F -FET) by T98G cells.

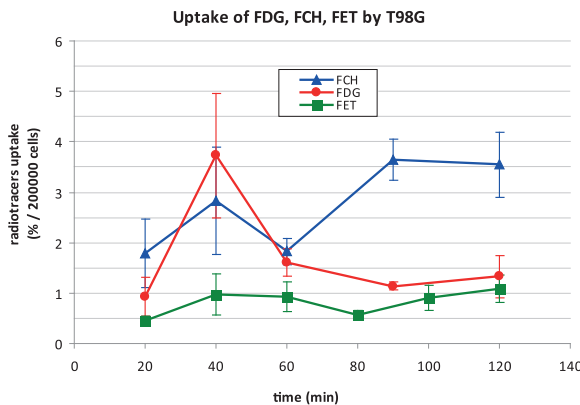


FIGURE 4. Uptake of ^{18}F -fluorodeoxyglucose (^{18}F -FDG), ^{18}F -methyl-choline (^{18}F -FCH) and ^{18}F -ethyl-tyrosine (^{18}F -FET) by T98G cells.

Figure 2 shows the kinetic uptake of ^{18}F -FET by T98G cells. Despite the trend represented by the curve, the uptake is quite low in terms of radiotracer uptake (% / 200000 cells).

Figure 3 shows that the uptake by T98G cells is increased for ^{18}F -FCH in comparison to ^{18}F -FET. The trend of the two kinetic curves are quite different: the uptake by T98G cells is increased for ^{18}F -FCH over ^{18}F -FET and the accumulation kinetic is not superimposable (see discussion).

Figure 4 illustrates the comparison of ^{18}F -FDG (data derived from our previous study²⁷, ^{18}F -FCH and ^{18}F -FET uptake in T98G cells. At 40 min and at the following time points there is not overlapping of the confidence bars for ^{18}F -FDG and ^{18}F -FET, and the ^{18}F -FET uptake is always lower than ^{18}F -FDG. ^{18}F -FCH uptake at time points after 60 min, is higher in comparison to the other radiopharmaceuticals.

As a negative control, flasks containing medium without cells were incubated under the same conditions and did not show a significant uptake of radiotracers.

Cell viability

Exposure to the gaseous mixture was maintained throughout the experiment and the cells' viability was calculated to be approximately 90% under all experimental conditions (data not shown).

Discussion

Our research data on T98G human glioblastoma cell lines underscores the affinity of ^{18}F -FET for neoplastic tissue, confirming its potential as a viable oncological PET marker. However, two aspects need to be discussed.

The percentage uptake of ^{18}F -FET in comparison to ^{18}F -FCH was lower by a factor of more than 3. Furthermore, both tracers showed a lower uptake of radioactivity under 60 minutes in comparison to values previously reported for ^{18}F -FDG.²

A thorough literature search did not find any studies with direct comparisons between ^{18}F -FCH and ^{18}F -FET uptake in glioma cell cultures. However, papers related to in vivo uptake in experimental rat gliomas indicate a higher accumulation of ^{18}F -FET in terms of Standard Uptake Value (SUV) as seen in both transplanted C6²⁸ or F98 glioma models^{29,30} in comparison to radio-labelled choline. Despite the different amounts of ^{18}F -FCH and ^{18}F -FET taken up by the same cell culture, the in vitro kinetic uptake is quite similar. ^{18}F -FET did show a more rapid initial uptake up to 40 minutes and ^{18}F -FCH showed a more progressive, continuous rise reaching a maximum activity plateau after

90 minutes. Several factors render the comparison between our results and data found in the literature difficult, due to the differing characteristics of our T98G cells and other experimental cell lines. In particular, the accumulation kinetics of ^{18}F -FET in T98G cells is quite different from that described in the 9L cancer cell line, where a wash-out is observable after 60 min of incubation.³¹ This phenomenon is less evident in F98 cell culture, with an initially fast uptake, peaking at 10 min, and followed by a nearly constant or slow wash-out rate during the incubation period of 60 min.³² On the other hand, Habermeier *et al.* described a progressive accumulation of non-radioactive FET in a NL229 human glioblastoma line up to 4 hours.³³

Both Hebermaier *et al.*³³ and Heiss *et al.*³⁴ tested the release of FET. Heiss *et al.*³⁴ demonstrated a quick efflux of ^{18}F -FET from porcine SW707 colon cancer cells, only 7% of the original activity remained in the experimental cells after 6 min incubation time, when the culture medium was replaced with a new tracer-free medium. Different results were reported by Habermeier *et al.*³³ demonstrating that, although ^{18}F -FET is not incorporated into proteins, an intracellular metabolism could lead to another impermeable derivative trapped within the glioma cells. This would suggest an asymmetry of intra- and extracellular recognition by LAT1. The ^{18}F -FCH kinetic pattern in our study was quite similar to that seen in 9L glioma cells³⁵, both in the normoxic or hypoxic conditions, reaching maximum activity at 120 minutes. Bansal *et al.*³⁵ reported a negligible washout of ^{18}F -FCH of about 13% after 2 hours in the release experiments because this radiopharmaceutical remains trapped in the cells as phospho-FCH. This demonstrates the slow rate of dephosphorylation. Conversely, apparent discrepancies between our in vitro observations and the in vivo glioma rat model emerged, both in terms of relative uptake and tracer kinetics. These mismatches could be explained by different causes, including radiotracer accumulation detected by the external imaging device or direct measurement of the pathological specimen, which provides information not only of the true tumour uptake but also of the inflammatory cells. In this setting, ^{18}F -FET accumulates predominantly in the tumour rather than in inflammatory cells, differing from ^{11}C -MET and suggesting that different subtypes of the L system are involved.³⁶ Contrarily, ^{18}F -FCH accumulation has been demonstrated in brain radiation injuries and in murine atherosclerotic plaques - probably mediated by macrophages - as well as in a turpentine-induced sterile abscess.^{37,38} In a rat

model of acute brain injury (cryolesion and proton-induced necrosis) ^{18}F -FET uptake was mainly due to the disruption of the blood-brain-barrier while ^{18}F -FCH was additionally taken up by inflammatory cells.³⁹ Similarly, a comparison of ^{18}F -FCH and ^{18}F -FET in a rat glioma radionecrosis indicated ^{18}F -FET as the superior discriminant between viable tumour and inflammatory changes³⁰, although evidence of increased ^{18}F -FET uptake in perilesional reactive astrogliosis after radiotherapy could lead to an overestimation of tumor size.⁴⁰

Conclusions

The in vitro model used in these experiments allows direct comparison of different radiopharmaceuticals as potential candidates for neuro-oncological PET imaging. The results obtained indicate a superiority of ^{18}F -FCH in terms of absolute uptake and in obtaining an optimal target to non-target ratio in the brain, whereas the major limitation of ^{18}F -FDG is its physiological parenchymal uptake. However, a direct translation to clinical application is hampered by certain conflicting results reported in the literature. ^{18}F -FET could be more useful in the presence of reparative changes after therapy, where the higher affinity of ^{18}F -FCH to inflammatory cells makes it more difficult to discriminate between tumour persistence and non-neoplastic changes. Additional studies on the influence of inflammatory tissue and radionecrotic cellular components on radiopharmaceutical uptake will be necessary to elucidate these topics.

References

1. Purves D, Augustine GJ, Fitzpatrick D, Katz LC, LaMantia AS, McNamara JO, et al. *Neuroscience (2nd edition)*. Sunderland (MA): Sinauer Associates; 2001.
2. Park JK, Hodges T, Arko L, Shen M, Dello Iacono D, McNabb A, et al. Scale to predict survival after surgery for recurrent glioblastoma multiforme. *J Clin Oncol* 2010; **28**: 3838-43.
3. Chaichana KL, McGirt MJ, Latterra J, Olivi A, Quiñones-Hinojosa A. Recurrence and malignant degeneration after resection of adult hemispheric low-grade gliomas. *J Neurosurg* 2010; **112**: 10-7.
4. Wick W, Stupp R, Beule AC, Bromberg J, Wick A, Ernemann U, et al. A novel tool to analyze MRI recurrence patterns in glioblastoma. *Neuro Oncol* 2008; **10**: 1019-24.
5. Barajas RF Jr, Chang JS, Segal MR, Parsa AT, McDermott MW, Berger MS, et al. Differentiation of recurrent glioblastoma multiforme from radiation necrosis after external beam radiation therapy with dynamic susceptibility-weighted contrast-enhanced perfusion MR imaging. *Radiology* 2009; **253**: 486-96.
6. Fatterpekar GM, Galheigo D, Narayana A, Johnson G, Knopp E. Treatment-related change versus tumor recurrence in high-grade gliomas: a diagnostic conundrum—use of dynamic susceptibility contrast-enhanced (DSC) perfusion MRI. *AJR Am J Roentgenol* 2012; **198**: 19-26.

7. Patronas NJ, Di Chiro G, Brooks RA, DeLaPaz RL, Kornblith PL, Smith BH, et al. Work in progress: [18F] fluorodeoxyglucose and positron emission tomography in the evaluation of radiation necrosis of the brain. *Radiology* 1982; **144**: 885-9.
8. Di Chiro G, Oldfield E, Wright DC, De Michele D, Katz DA, Patronas NJ, et al. Cerebral necrosis after radiotherapy and/or intraarterial chemotherapy for brain tumors: PET and neuropathologic studies. *AJR Am J Roentgenol* 1988; **150**: 189-97.
9. Wong TZ, van der Westhuizen GJ, Coleman RE. Positron emission tomography imaging of brain tumors. *Neuroimaging Clin N Am* 2002; **12**: 615-26.
10. Olivero WC, Dulebohn SC, Lister JR. The use of PET in evaluating patients with primary brain tumors: Is it useful? *J Neurol Neurosurg Psychiatry* 1995; **58**: 250-2.
11. Ramirez de Molina A, Rodriguez-Gonzalez A, Gutierrez R, Martinez-Pineiro L, Sanchez J, Bonilla F. Overexpression of choline kinase is a frequent feature in human tumor derived cell lines and in lung, prostate, and colorectal human cancers. *Biochem Biophys Res Commun* 2000; **296**: 580-3.
12. Shinoura N, Nishijima M, Hara T, Haisa T, Yamamoto H, Fujii K. Brain tumors: detection with C-11 choline PET. *Radiology* 1997; **202**: 497-503.
13. Sollini M, Sghedoni R, Erba PA, Cavuto S, Froio A, De Berti G, et al. Diagnostic performances of [18F]fluorocholine positron emission tomography in brain tumors. *Q J Nucl Med Mol Imaging* 2015; Sep 1 [Epub ahead of print]; PMID: 26329494.
14. Friedland RP, Mathis CA, Budinger TF. Labelled choline and phosphorycholine: Body distribution and brain autoradiography. *J Nucl Med* 1983; **24**: 812-5.
15. Wyss MT, Weber B, Honer M, Späth N, Ametamey SM, Westera G, et al. ¹⁸F-choline in experimental soft tissue infection assessed with autoradiography and high-resolution PET. *Eur J Nucl Med Mol Imaging* 2004; **3**: 312-6.
16. Oxender DL, Christensen HN. Distinct mediating systems for the transport of neutral amino acids by the Ehrlich cell. *J Biol Chem* 1963; **238**: 3686-99.
17. Kaim AH, Weber B, Kurrer MO, Westera G, Schweitzer A, Gottschalk J, et al. ¹⁸F-FDG and ¹⁸F-FET uptake in experimental soft tissue infection. *Eur J Nucl Med Mol Imaging* 2002; **29**: 648-54.
18. Buck D, Förschler A, Lapa C, Schuster T, Vollmar P, Korn T, et al. ¹⁸F-FDG PET detects inflammatory infiltrates in spinal cord experimental autoimmune encephalomyelitis lesions. *J Nucl Med* 2012; **53**: 1269-76.
19. Messing-Jünger AM, Floeth FW, Pauleit D, Reifenberger G, Willing R, Gärtner J, et al. Multimodal target point assessment for stereo-tactic biopsy in children with diffuse bithalamic astrocytomas. *Child's Nerv Syst* 2002; **18**: 445-9.
20. Pauleit D, Floeth F, Tellmann L, Hamacher K, Hautzel H, Müller HW, et al. Comparison of O-(2-[18F]-fluoroethyl)-L-tyrosine PET and 3-123I-iodo-alpha-methyl-L-tyrosine SPECT in brain tumors. *J Nucl Med* 2004; **45**: 374-81.
21. Pöppel G, Goldbrunner R, Gildehaus FJ, Kreth FW, Tanner P, Holtmannspötter M, et al. O-(2-[18F]fluoroethyl)-L-tyrosine PET for monitoring the effects of convection-enhanced delivery of paclitaxel in patients with recurrent glioblastoma. *Eur J Nucl Med Mol Imaging* 2005; **32**: 1018-25.
22. Pöppel G, Götz C, Rächinger W, Schnell O, Gildehaus FJ, Tonn JC, et al. Serial O-(2-[18F]fluoroethyl)-L-tyrosine PET for monitoring the effects of intracavitary radioimmunotherapy in patients with malignant glioma. *Eur J Nucl Med Mol Imaging* 2006; **33**: 792-800.
23. Piroth MD, Pinkawa M, Holy R, Klotz J, Nussen S, Stoffels G, et al. Prognostic value of early [18F]fluoroethyltyrosine positron emission tomography after radiochemotherapy in glioblastoma multiforme. *Int J Radiat Oncol Biol Phys* 2011; **30**: 176-84.
24. Wyss M, Hofer S, Bruehlmeier M, Hefti M, Uhlmann C, Bäertschi E, et al. Early metabolic responses in temozolomide treated low-grade glioma patients. *J Neurooncol* 2009; **95**: 87-93.
25. Yao KC, Komata T, Kondo Y, Kanzawa T, Kondo S, Germano IM. Molecular response of human glioblastoma multiforme cells to ionizing radiation: cell cycle arrest, modulation of the expression of cyclin-dependent kinase inhibitors, and autophagy. *J Neurosurg* 2003; **98**: 378-84.
26. Stein GH. T98G: an anchorage-independent human tumor cell line that exhibits stationary phase G1 arrest in vitro. *J Cell Physiol* 1979; **99**: 43-54.
27. Buroni FE, Pasi F, Persico MG, Lodola L, Aprile C, Nano R. Evidence of ¹⁸F-FCH uptake in human T98G glioblastoma cell line. *Anticancer Res* 2015; **35**: 6443-8.
28. Wyss MT, Spaeth N, Biollaz G, Pahnke J, Alessi P, Trachsel E, Treyer V, et al. Uptake of ¹⁸F-Fluorocholine, ¹⁸F-FET, and ¹⁸F-FDG in C6 gliomas and correlation with 131I-SIP(L19), a marker of angiogenesis. *J Nucl Med* 2007; **48**: 608-14.
29. Spaeth N, Wyss MT, Pahnke J, Biollaz G, Lutz A, Goepfert K, et al. Uptake of ¹⁸F-fluorocholine, ¹⁸F-fluoro-ethyl-L-tyrosine and ¹⁸F-fluoro-2-deoxyglucose in F98 gliomas in the rat. *Eur J Nucl Med Mol Imaging* 2006; **33**: 673-82.
30. Bolcaen J, Descamps B, Deblaere K, Boterberg T, De Vos Pharm F, Kalala JP, et al. (18F)F-fluoromethylcholine (FCho), (18F)F-fluoroethyltyrosine (FET), and (18F)F-fluorodeoxyglucose (FDG) for the discrimination between high-grade glioma and radiation necrosis in rats: a PET study. *Nucl Med Biol* 2015; **42**: 38-45.
31. Wang L, Lieberman BP, Ploessl K, Kung HF. Synthesis and evaluation of ¹⁸F labelled FET prodrugs for tumor imaging. *Nucl Med Biol* 2014; **41**: 58-67.
32. Wang HE, Wu SY, Chang CW, Liu RS, Hwang LC, Lee TW, et al. Evaluation of F-18-labeled amino acid derivatives and [18F]FDG as PET probes in a brain tumor-bearing animal model. *Nucl Med Biol* 2005; **32**: 367-75.
33. Habermeyer A, Graf J, Sandhöfer BF, Boissel JP, Roesch F, Closs EI. System L amino acid transporter LAT1 accumulates O-(2-fluoroethyl)-L-tyrosine (FET). *Amino Acids* 2015; **47**: 335-44.
34. Heiss P, Mayer S, Herz M, Wester HJ, Schwaiger M, Senekowitsch-Schmidtker R. Investigation of transport mechanism and uptake kinetics of O-(2-[18F]fluoroethyl)-L-tyrosine in vitro and in vivo. *J Nucl Med* 1999; **40**: 1367-73.
35. Bansal A, Shuyan W, Hara T, Harris RA, Degrado TR. Biodisposition and metabolism of [(18F)]fluorocholine in 9L glioma cells and 9L glioma-bearing fisher rats. *Eur J Nucl Med Mol Imaging* 2008; **35**: 1192-203.
36. Stöber B, Tanase U, Herz M, Seidl C, Schwaiger M, Senekowitsch-Schmidtker R. Differentiation of tumour and inflammation: characterisation of [methyl-3H]methionine (MET) and O-(2-[18F]fluoroethyl)-L-tyrosine (FET) uptake in human tumour and inflammatory cells. *Eur J Nucl Med Mol Imaging* 2006; **33**: 932-9.
37. van Waarde A, Elsinga PH. Proliferation markers for the differential diagnosis of tumor and inflammation. *Curr Pharm Des.* 2008; **14**: 3326-39.
38. Langen KJ, Hamacher K, Weckesser M, Floeth F, Stoffels G, Bauer D, et al. O-(2-[18F]fluoroethyl)-L-tyrosine: uptake mechanisms and clinical applications. *Nucl Med Biol* 2006; **33**: 287-94.
39. Spaeth N, Wyss MT, Weber B, Scheidegger S, Lutz A, Verwey J, et al. Uptake of ¹⁸F-fluorocholine, ¹⁸F-fluoroethyl-L-tyrosine, and ¹⁸F-FDG in acute cerebral radiation injury in the rat: implications for separation of radiation necrosis from tumor recurrence. *J Nucl Med* 2004; **45**: 1931-8.
40. Piroth MD, Prasath J, Willuweit A, Stoffels G, Sellhaus B, van Oosterhout A, et al. Uptake of O-(2-[18F]fluoroethyl)-L-tyrosine in reactive astrocytosis in the vicinity of cerebral gliomas. *Nucl Med Biol* 2013; **40**: 795-800.

Imaging of human glioblastoma cells and their interactions with mesenchymal stem cells in the zebrafish (*Danio rerio*) embryonic brain

Milos Vittori¹, Barbara Breznik^{1,2}, Tajda Gredar³, Katja Hrovat^{1,3}, Lilijana Bizjak Mali³, Tamara T. Lah^{1,4}

¹ Department of Genetic Toxicology and Cancer Biology, National Institute of Biology, Ljubljana, Slovenia

² Jozef Stefan International Postgraduate School, Ljubljana, Slovenia

³ Department of Biology, Biotechnical Faculty, University of Ljubljana, Ljubljana, Slovenia

⁴ Department of Chemistry and Biochemistry, Faculty of Chemistry and Chemical Technology, University of Ljubljana, Ljubljana, Slovenia

Radiol Oncol 2016; 50(2): 159-167.

Received 3 December 2015

Accepted 7 February 2016

Correspondence to: Miloš Vittori, Department of Genetic Toxicology and Cancer Biology, National Institute of Biology, Večna pot 111, SI-1000 Ljubljana, Slovenia. Phone: +386 59 232 884; Fax: +386 59 232 715; E-mail: milos.vittori@gmail.com

Disclosure: No potential conflicts of interest were disclosed.

Background. An attractive approach in the study of human cancers is the use of transparent zebrafish (*Danio rerio*) embryos, which enable the visualization of cancer progression in a living animal.

Materials and methods. We implanted mixtures of fluorescently labeled glioblastoma (GBM) cells and bone-marrow-derived mesenchymal stem cells (MSCs) into zebrafish embryos to study the cellular pathways of their invasion and the interactions between these cells *in vivo*.

Results. By developing and applying a carbocyanine-dye-compatible clearing protocol for observation of cells in deep tissues, we showed that U87 and U373 GBM cells rapidly aggregated into tumor masses in the ventricles and midbrain hemispheres of the zebrafish embryo brain, and invaded the central nervous system, often using the ventricular system and the central canal of the spinal cord. However, the GBM cells did not leave the central nervous system. With co-injection of differentially labeled cultured GBM cells and MSCs, the implanted cells formed mixed tumor masses in the brain. We observed tight associations between GBM cells and MSCs, and possible cell-fusion events. GBM cells and MSCs used similar invasion routes in the central nervous system.

Conclusions. This simple model can be used to study the molecular pathways of cellular processes in GBM cell invasion, and their interactions with various types of stromal cells in double or triple cell co-cultures, to design anti-GBM cell therapies that use MSCs as vectors.

Key words: brain tumors; tumor microenvironment; animal models; xenotransplantation

Introduction

Glioblastoma multiforme (GBM) is the most aggressive type of glioma and also the most frequent and fatal among brain tumors.¹ An essential hallmark of GBM is its diffuse invasion into the brain parenchyma, which prevents successful surgical removal.² Understanding the mechanisms and the pathways of GBM cell invasion is therefore of crucial importance for the treatment of the ag-

gressive spread of GBM.¹⁻³ The process of GBM cell infiltration into the brain parenchyma⁴ differs from carcinoma cells invading the more compact extracellular matrix and the basal membranes of blood vessels.^{5,6} The recently recognized important role of the tumor microenvironment in cancer cell invasion⁷ has become an important topic and the subject of intensive research.⁸⁻¹⁰ The effects of the microenvironment also include the impact of the different types of cells comprising the stroma

within a tumor mass. Infiltrating and tumor-associated mesenchymal stem cells (MSCs) may significantly affect tumor progression and resistance to treatment, as reviewed in.^{8,11} MSCs are known to be recruited by tumor-secreted signaling molecules *via* the blood circulation, and to become part of the tumor-supporting stroma, where they have a role that remains poorly understood.^{10,12} Several studies have addressed this issue *in vitro* and *in vivo*, also by using genetically modified MSCs.^{13,14} Previously, we studied the molecular mechanisms that support the observed phenotype changes in GBM cells and MSCs upon co-culture *in vitro*, including decreased U87 GBM cell proliferation and invasion, and increased U373 GBM cell invasion *in vitro*.^{15,16} By investigating the GBM-MSC interactions in a mouse model, Behnan *et al.*¹⁷ recently showed that cells with an MSC-like phenotype can infiltrate the stroma of the mouse GBM and have important roles in tumor cell growth. Moreover, their data demonstrated an alteration in GBM cell marker expression upon the encounter with MSCs *in vivo*. In the present study, we aimed to use an alternative and simpler *in vivo* GBM xenotransplantation model in zebrafish embryos¹⁸, to study human GBM cell invasion and their interactions with MSCs at the cellular level.

The zebrafish (*Danio rerio*) is the major vertebrate model in developmental biology and genetics.¹⁹ There are several technologies available in the zebrafish that have made it a unique model in cancer research.²⁰ In particular, cancers can be studied throughout the life cycle of zebrafish, with each zebrafish developmental stage offering its own experimental advantages. This makes zebrafish a powerful complement to other more traditional model systems.²¹ As well as their high fecundity and ease of maintenance, the major advantage of zebrafish is the transparency of their embryos and larvae, which allows *in vivo* visualization of cellular processes related to cancer growth and progression at single-cell resolution.^{20,22,23} Xenotransplantation of either dye-labeled or fluorescent-protein-expressing human cells in zebrafish embryos is becoming an increasingly used tool to study cancers of the central nervous system (CNS).^{18,24-26}

The aim of the present study was to investigate the interactions of GBM cells with the brain matrix components and MSCs in the zebrafish embryonic brain by co-implantation of fluorescently labeled GBM cells and MSCs. To deepen our understanding of GBM cell behavior within the brain of zebrafish embryos, we combined *in vivo* imaging of GBM progression with imaging of fluorescently

counterstained whole-mount preparations that allowed the visualization of the anatomical context of the implanted cells. As chemical fixation leads to loss of transparency of the embryonic tissues, it necessitated the clearing of the embryos, which was achieved with the use of clearing agents.²⁷⁻³⁹ To this end, we optimized and applied protocols to clear fixed tissues while preserving the fluorescent protein signal over a period of several weeks.

Materials and methods

Ethical statement

The experimental procedures were approved by the Republic of Slovenia National Medical Ethics Committee, approval No. 92/06/12. All of the procedures were performed according to the relevant regulations.

Zebrafish husbandry

Wild-type AB zebrafish (*Danio rerio*) were maintained under conditions according to the Organisation for Economic Cooperation and Development guidelines.⁴⁰ The zebrafish embryos were collected and incubated in dilution water (ISO 7346-3:1996) with 0.005% phenylthiourea, to inhibit pigment formation after 36 h of age.

Human cells

The U373 and U87-MG human GBM cell lines were from American Type Culture Collection (USA), and the BM-MSC2 human bone-marrow-derived MSC cell line was from Lonza Bioscience (USA). The cells were cultured in Dulbecco's modified Eagle's medium (Sigma-Aldrich, USA) supplemented with 10% fetal bovine serum (Gibco, USA), 100 U/mL penicillin (Sigma-Aldrich), 100 mg/mL streptomycin (Sigma-Aldrich), 2 mM L-glutamine (Sigma-Aldrich), 1 mM Na-pyruvate (Gibco), and non-essential amino acids (Sigma-Aldrich).

Xenotransplantation procedures

The U373 GBM cells were transfected with the pEGFP-N1 plasmid to stably express enhanced green fluorescent protein (GFP). The U87 GBM cells were transfected for the expression of the red fluorescent protein DsRed, as described previously.¹⁶ Cells were transfected using the Superfect Transfection Reagent (Qiagen, Germany) by 3 h pre-incubation at 37°C, 5% CO₂. The transfection

TABLE 1. Compositions of the selected optical clearing agents

Optical clearing agent	Composition	Reference
SeeDB	80% (w/w) fructose, 0.5% (w/w) α -thioglycerol in water	Ke <i>et al.</i> ³⁴
sRIMS	70% (w/v) sorbitol, 0.01% (w/v) sodium azide, 0.1% (w/v) Tween 20 in 0.02 M phosphate buffer (pH 7.5)	Yang <i>et al.</i> ³⁹
ScaleA2	4 M urea, 0.1% (w/v) Triton X-100, 10% (w/w) glycerol in water	Hama <i>et al.</i> ³³
ScaleU2	4 M urea, 0.1% (w/v) Triton X-100, 30% (w/w) glycerol in water	Hama <i>et al.</i> ³³

mix was then removed and upon washing with phosphate-buffered saline (PBS), fresh culture medium was added to the cells. Transfected cells were selected for by adding 0.8 mg/ml Geneticin (G418, Gibco, USA) to the medium. The uniformity of emitted fluorescence was confirmed with flow cytometry. The stability of fluorescent protein expression was verified with repeated flow cytometry analyses after 10 and 20 passages and proved to be stable (>99% of fluorescent protein-expressing cells). Prior to implantation, MSCs were labeled with Vybrant DiI or DiO (Molecular Probes, USA) for co-implantation with the U373 and U87 cells, respectively, according to the manufacturer instructions. For injection into the embryos, suspensions of GBM cells prepared in PBS were mixed with labeled MSCs in a 1:1 ratio. Embryos at 52 h after fertilization were injected either with 50 to 100 GBM cells or 100 to 200 cells of the GBM/MSM mixture (*i.e.*, maintaining 50-100 GBM cells), using a borosilicate glass capillary and a MICROINJECTOR system (Tritech Research, USA). After cell implantation, the embryos were incubated at 31°C in 48-well plates for 3 days.

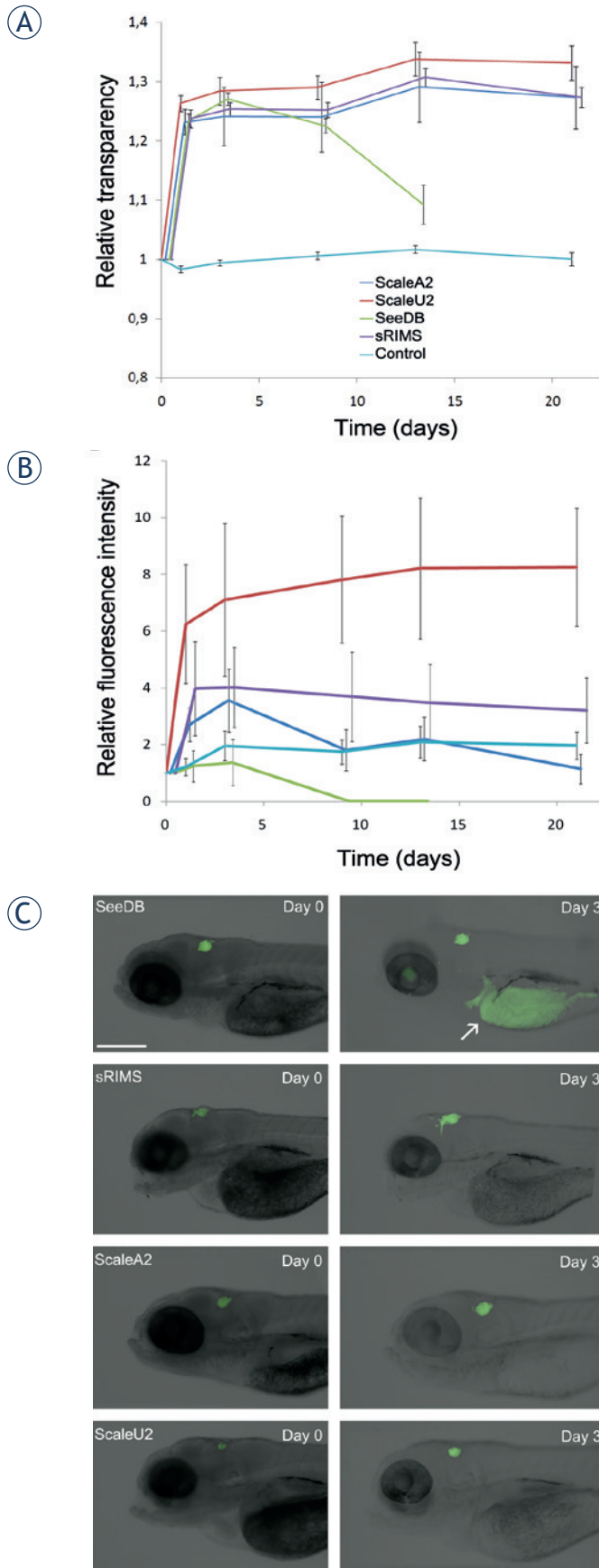
Clearing agents

The clearing agents used were SeeDB, a near-saturated solution of fructose with α -thioglycerol³⁴, sRIMS, a buffered solution of sorbitol³⁹, and two aqueous solutions of urea and glycerol known as ScaleA2 and ScaleU2.³³ An overview of the compositions of these clearing agents is shown in Table 1.

Analysis of clearing efficiency and fluorescence preservation

At 3 days after fertilization (for measurements of transparency and size) and 5 days after fertilization (for fluorescence imaging of implanted cells), the zebrafish embryos were fixed in 4% paraformaldehyde at 4°C overnight, after which time the fixative was washed off with PBS. The fixed embryos were

then embedded in 2% low-melting-point agarose in PBS in 50-mm Petri dishes. For the optical clearing agent SeeDB, the embryos were transferred to SeeDB through a graded series of sucrose, as described by Ke *et al.*³⁴, and maintained at room temperature. For sRIMS and Scale, the embryos were immersed in the clearing agents and kept at 4°C in the dark. In all cases, the clearing agents were replaced every 3 days. The control embryos were incubated in parallel in PBS. For analysis of the whole-embryo clearing, transmitted light images were obtained at constant (maximum) illumination at 32 \times magnification. For imaging and quantification of GFP fluorescence, the images were captured at 80 \times magnification using the GFP filter set. Micrographs were obtained using a fluorescence stereomicroscope (Leica MZ FLIII). The imaging was carried out over a period of 21 days. The analysis of fluorescence preservation was performed on embryos with implanted U373 cells. Fluorescence intensity, embryo transparency, and embryo size were quantified with the image analysis software ImageJ.⁴¹ For determination of embryo transmittance, the parameter 'Integrated density' was measured. The relative integrated densities and areas were determined by dividing the values of these parameters at the given time points with their values at the beginning of the observation on day 0. As integrated density represents the product of pixel intensities and area, the changes in embryo size that were caused by some of the clearing agents were accounted for by dividing the integrated density of the structure analyzed with its area, thus obtaining the relative embryo transparency. Fluorescence intensity was analyzed by thresholding the fluorescent images with a constant threshold and measuring the integrated density of the selection. For the analysis of changes in embryo size and transparency, 8 embryos per treatment were measured. For the analysis of GFP fluorescence intensity changes, 24 embryos per treatment were measured. Measurements were compared with ANOVA in GraphPad Prism.



Confocal microscopy

The nuclei of the embryos that had been fixed, embedded in agarose, and cleared as described above were counterstained by addition of 0.004% methyl green to the individual clearing agent.⁴² Confocal z-stacks of the embryos were obtained using a spectral confocal laser scanning microscope (Leica TCS SPE) at 10× magnification after 7 days of treatment.

Results

Clearing efficiencies of the different clearing agents

To evaluate the applicability of the different optical clearing agents (Table 1) to zebrafish embryo imaging, we treated embryos fixed at 3 days after fertilization with SeeDB, sRIMS, ScaleA2, and ScaleU2 for 3 weeks, with regular imaging. The tissues were cleared best by ScaleU2 and ScaleA2 with no statistically significant difference between them at any time point. These agents performed significantly better than SeeDB on all treatment days. The least effective agent was sRIMS (Figure 1A). After approximately 1 week of incubation, fructose began to crystallize from the SeeDB solution, preventing further analyses. With regard to the preservation of GFP fluorescence, ScaleU2 was the optimal clear-

FIGURE 1. (A) Clearing of zebrafish embryos. Embryos were fixed 3 days after fertilization, exposed to the different clearing agents SeeDB, sRIMS, ScaleA2, and ScaleU2 for 21 days, and imaged regularly. Time courses of changes in relative transparency are shown, which represents the value of integrated density relative to day 0 divided by the embryo area relative to day 0. Differences between treatments are statistically significant in all cases except between ScaleA2 and Scale B2 (on all days) and between ScaleA2 and sRIMS on day 21. Green, SeeDB; purple, sRIMS; dark blue, ScaleA2; red, ScaleU2; light blue, PBS control. Data for the different clearing agents are displaced horizontally for improved clarity. Means \pm SE of eight embryos per treatment are shown. **(B)** Preservation of GFP fluorescence during clearing. Changes in the detected GFP fluorescence intensity of glioblastoma cells implanted in the brain of zebrafish embryos during treatment with different clearing agents of SeeDB, sRIMS, ScaleA2, and ScaleU2, measured over 21 days of the treatment. The integrated density of GFP-expressing cells relative to day 0 was measured. Fluorescence intensity was significantly increased compared to control in the case of ScaleU2 on all days except on day 3, but not in the case of other clearing agents. Means \pm SE of 24 embryos per treatment are shown. **(C)** Fluorescence of U373-GFP cells in the brain of zebrafish embryos. Representative images show embryos treated with the different clearing agents obtained at the beginning of observation (Day 0, left) and after 3 days of clearing (Day 3, right). The appearance of autofluorescence of the yolk (arrow) is evident in the case of SeeDB. Scale bar: 400 μ m.

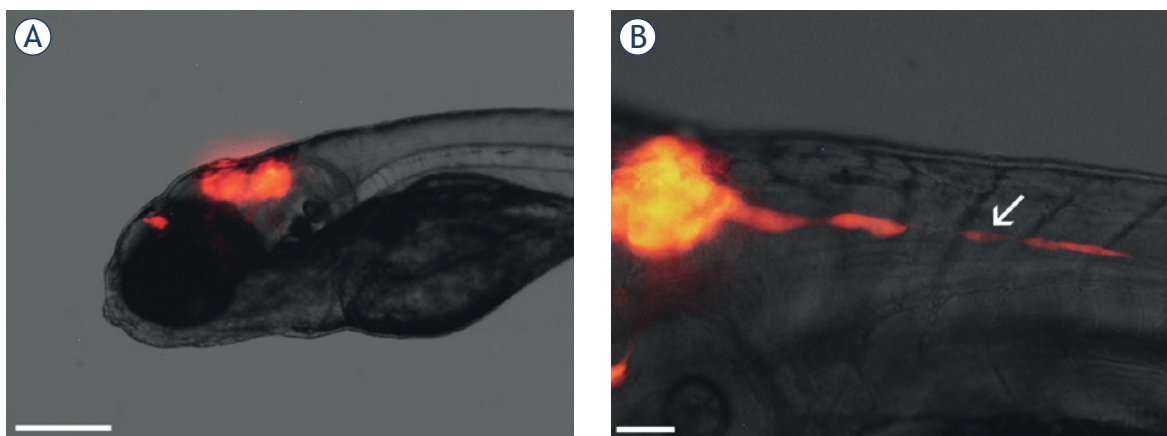


FIGURE 2. *In vivo* imaging of glioblastoma cells in the brain of zebrafish embryos. **(A)** Embryo 3 days after the implantation of U87-DsRed cells in the brain (visible as red fluorescence). Compact tumors have formed in the midbrain and forebrain. **(B)** An embryo with implanted U87-DsRed cells 2 days after implantation, with a string of U87-DsRed cells rapidly invading from the tumor in the brain in the posterior direction (arrow). Scale bars: 300 μm **(A)**; 50 μm **(B)**.

ing agent, resulting in a several-fold increase in fluorescence intensity during the first 3 days of incubation and no demonstrable reduction in its intensity during 3 weeks of observation (Figure 1B). These changes were statistically significant when compared with the control. Complete loss of fluorescence occurred in the case of SeeDB within a week and no statistically significant increases in intensity compared to the control were demonstrated in the cases of ScaleA2 and sRIMS. The loss of GFP fluorescence in SeeDB was accompanied by the appearance of strong autofluorescence of the yolk and eye (Figure 1C).

Localization of implanted glioblastoma cells and pathways of GBM cell invasion in the zebrafish embryonic brain

After selecting ScaleU2 as the optimal clearing agent for the visualization of the fluorescent-protein-labeled cells, it was applied to visualize tumor progression in the whole-mount preparations of the zebrafish embryos. We implanted U373-GFP cells into the brain of embryos 2 days after fertilization, and monitored these over the following 3 days.

By imaging the GBM cells in zebrafish embryos *in vivo*, we demonstrated that implanted cells aggregated and formed tumors in the zebrafish brain (Figure 2A). In some embryos, individual cells moved posteriorly in the embryo at great speed, as they progressed at several hundreds of micrometers per day (Figure 2B). This rapid invasion outside of the brain in the posterior direction was ob-

served more frequently for the U87 cells ($35 \pm 5\%$ of the embryos, as 3 experimental repeats, and 20 embryos per repeat) than for the U373 cells ($20 \pm 5\%$ of the embryos, as 3 experimental repeats, and 20 embryos per repeat).

Tumors were seen to form predominantly in the midbrain hemispheres and in the ventricles of the midbrain and hindbrain (Figure 3A–C). Individual cells, or small strands of cells, invaded the ventricular system and the brain tissue using pseudopodal movement (Figure 3A,B). In particular, cells present in the midbrain hemispheres formed elongated pseudopodia and invaded the neighboring brain areas dorsally, most likely along axonal tracts that connect the hemispheres (Figure 3A). Whole-mount imaging of embryos with cells invading posteriorly in the body revealed that the rapidly invading cells invaded the spinal cord *via* the central canal (Figure 3D,E). We did not observe GBM cells outside of the brain and spinal cord, indicating that GBM cell invasion in zebrafish embryos was limited to the CNS, and that the cells did not spread *via* the circulatory system.

Imaging of xenotransplanted GBM and MSC co-cultures

To study the interactions between the GBM cells and MSCs *in vivo*, we implanted co-cultures of U373-GFP cells and carbocyanine-dye-labeled human MSCs into the brain of zebrafish embryos 2 days after fertilization. As labeling with carbocyanine dyes relies on the hydrophobic nature of these dyes, they can be washed out with organic sol-

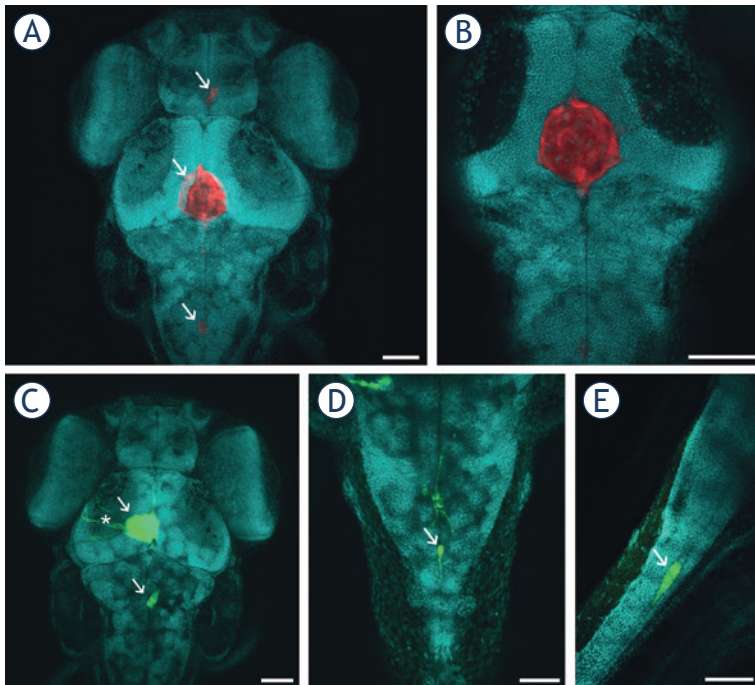


FIGURE 3. Visualization of GBM cells in cleared zebrafish embryos, counterstained with methyl green (presented in blue). Embryos with U373-GFP and U87-DsRed cells implanted in the brain were cleared with ScaleU2, counterstained with methyl green, and imaged with confocal microscopy. **(A)** U87-DsRed cells (arrows) in the brain of a zebrafish embryo 3 days after implantation. **(B)** An optical section through the tumor in **(A)**, demonstrating that the tumor is a compact mass of U87 cells in the midbrain ventricle. **(C)** U373-GFP cells (arrows) in the brain of a zebrafish embryo 3 days after implantation. Elongated U373-GFP cells are visible invading from the tumor (asterisk). **(D)** A U373-GFP cell invading along the central canal of the spinal cord (arrow), in dorsal view. **(E)** A U373-GFP cell invading along the central canal of the spinal cord (arrow), in lateral view. Scale bars: 70 μm (**A**, **B**, **C**); 50 μm (**D**, **E**).

vents and detergents. Thus, we prepared ScaleU2 without Triton X-100, with which we successfully visualized dye-labeled cells in whole-mount preparations. In implanted mixtures of GBM cells and MSCs, the MSCs preferentially associated with the implanted GBM cells instead of being interspersed individually or as separate clusters in the brain (Figure 4A–C). The MSCs often used similar invasion routes as the GBM cells, as they moved along the ventricles and the central canal of the spinal cord (Figure 4B,C).

Confocal imaging of U373 and MSC co-cultures *in situ* revealed that the GBM cells and MSCs formed mixed tumor masses that consisted of both of these cell types in similar locations as for the GBM cells alone; *i.e.*, in the ventricles and midbrain hemispheres (Figure 4A,B). These two cell types were interspersed in these tumors, and interacted closely with each other (Figure 4D). In some cases, cells simultaneously emitting the fluorescence of

proteins and the carbocyanine dye were observed, which indicated possible cell fusion between the GBM cells and MSCs (Figure 5).

Discussion

The major advantage of the zebrafish model is the transparency of their embryos and larvae, which allows *in vivo* visualization of cellular processes related to cancer progression at single-cell resolution. We identified ScaleU2 as the optimal clearing agent for zebrafish embryos among the agents tested. Furthermore, we were able to modify it to be compatible with the labeling of cells with carbocyanine dyes. The superiority of ScaleU2 in fluorescence preservation appears to result from its high glycerol concentration, and thus might be linked to the protein-stabilizing effects of glycerol in aqueous solution.^{43,44}

The proposed protocols were used to study the invasion of the U87 and U373 human GBM cell lines alone and in co-cultures with bone-marrow-derived MSCs in the zebrafish embryo. By combining the *in vivo* imaging with confocal microscopy of fluorescently counterstained whole-mount preparations, we demonstrated that GBM cells aggregate in the brain of zebrafish embryos and form tumors predominantly in the ventricles. This indicates that GBM cells have tropism towards each other upon implantation to form tumors, which are preferentially formed in the ventricles and dorsal areas of the midbrain. The tendency of the GBM cells to aggregate in these areas might be linked to the ease of dislodging the embryonic brain tissues in anatomical structures such as the ventricles, which are fluid-filled spaces where the brain cells are not in direct contact. The localization of GBM cells to the ventricular system has previously not been reported. Eden *et al.*⁴⁵ recently reported that mouse xenografts in the brain of juvenile (30-day-old) zebrafish reproduced the histology and gene expression profiles of the murine tumors of their origin within the tissues of the brain. Thus, the observed localization of the GBM cells to the ventricular system might be limited to embryos and larval stages.

We were able to identify the central canal of the spinal cord as the major route of GBM invasion in zebrafish embryos that has not been reported before. Furthermore, GBM cells did not leave the central nervous system, which is similar to their behavior in humans.⁴⁶ In a previous study on murine tumor xenografts in the zebrafish brain, tumor masses developed 1 day to 2 days after the im-

plantation in the spinal cord. Histological analysis confirmed that these masses were independent, distant tumors, rather than direct extensions of the main tumor mass, thus demonstrating that the implanted GBM cells disseminated in the CNS of the zebrafish.⁴⁵ This is in agreement with our observations of single-cell invasion along the central canal of the spinal cord, which may result in separate tumor formation within the spinal cord. The underlying molecular mechanisms of this rapid invasion remain to be established. The process might be facilitated by the low resistance of the central canal to cell invasion, as the GBM cells are believed to generally invade through structures that have low resistance to cell movement.^{5,6,46}

One of the preferential pathways of GBM invasion in the human brain is the white matter, where GBM cells invade along axons.⁴⁶ It is likely that this preference is recapitulated in zebrafish embryos, as we observed pseudopodal invasion in the midbrain area that is rich in axonal connections between the two hemispheres (Figure 3C). This is reminiscent of tumor invasion via the *corpus callosum* in human patients.²

Pseudopodia and cell elongation characterize the mesenchymal type of cell invasion, which is typical for gliomas and depends on cell-matrix adhesion.^{5,6} The observed strand migration in the spinal cord as well as the midbrain (Figure 2B,4B) is linked to proteolytic matrix remodeling and is characteristic of cancer cells belonging to the mesenchymal type.⁵ A mesenchymal molecular fingerprint has recently been established for U373 GBM cells.⁴⁷ This invasion pattern has also previously been observed for U87 cells in mouse models, together with elevated cathepsin B expression at the tumor periphery.⁴⁸ In a study on zebrafish larvae, invasion of U87 GBM cells along the abluminal surface of blood vessels has also been demonstrated.²⁵ As the basal lamina of blood vessels is a known invasion pathway in the human brain⁴⁶, this further strengthens the view that the invasion of GBM cells in the zebrafish model resembles this process in mammals.

Confocal imaging of GBM and MSC co-cultures *in situ* revealed that both of these types of cells form mixed tumor masses at similar locations as for the GBM cells alone; *i.e.*, in the ventricles and midbrain hemisphere. The GBM and MSC cells used similar invasion routes along the ventricles and the central canal of the spinal cord, but did not invade other tissues. The association of GBM cells and MSCs into such mixed tumors in the brain of these zebrafish embryos suggests a strong intercellular interaction

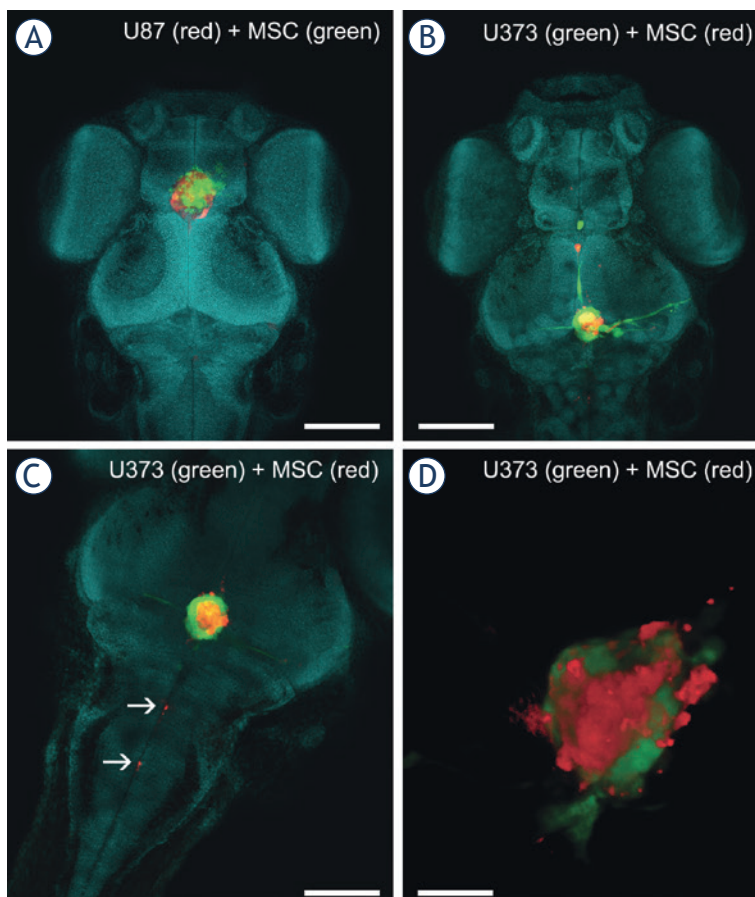


FIGURE 4. Imaging of co-cultures of GBM cells and MSCs in the brain of zebrafish embryos. A mixture of fluorescent-protein-expressing GBM cells and carbocyanine-dye-labeled MSCs was implanted into the brain of the zebrafish embryos. Three days after implantation, the embryos were fixed, cleared in ScaleU2 without the addition of Triton X-100, and imaged with confocal microscopy. **(A)** The head of a zebrafish embryo with a co-culture of U87-DsRed cells (red) and DiO-labeled MSCs (green) implanted in the brain. **(B)** The head of a zebrafish embryo with a co-culture of U373-GFP cells (green) and DiI-labeled MSCs (red) implanted in the brain. **(C)** Invasion of DiI-labeled MSCs (red) along the central canal of the spinal cord. **(D)** Three-dimensional rendering of a mixed mass of U373 cells (green) and MSCs (red) in a brain obtained from a cleared embryo. Nuclei are stained with methyl green (presented in blue). Scale bars: 250 μ m (A, B); 100 μ m (C); 50 μ m (D).

between them, which would appear to also have a role in the human GBM microenvironment. Indeed, MSC tropism towards GBM cells has previously been described¹⁰, and a set of cytokines has been shown to mediate the interactions between these cells *in vitro*.^{49,50} Among these, the monocyte chemoattractant protein (MCP-1) has been suggested as the major trigger of various molecular pathways that can enhance MSC proliferation and invasion, whereas a different set of genes has been shown to impair U87 cell invasion and proliferation, and to even induce their senescence.⁴⁹ When mixtures of U87 or U373 GBM cells and MSCs were implanted

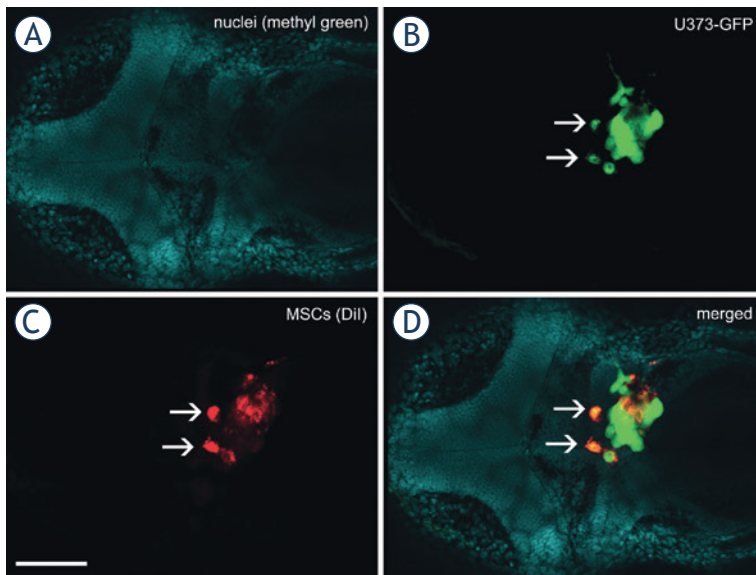


FIGURE 5. Fusion between GBM cells and MSCs in the zebrafish brain. A mixture of U373-GFP cells and Dil-labeled MSCs was implanted in the brain of the embryos, which were fixed, cleared and imaged 3 days after implantation of the cells. Two cells (arrows) emit green GFP fluorescence as well as red Dil fluorescence, which strongly indicates that the U373-GFP cells and MSCs have fused after implantation. **(A)** Nuclei of embryonic tissues labeled with methyl green. **(B)** Green fluorescent protein fluorescence of U373 cells. **(C)** Red fluorescence of Dil, used to label the MSCs. **(D)** Merged image of all of the fluorescent channels. Scale bar: 200 μ m.

into the zebrafish embryos, these established very close contacts and apparently also formed a structural syncytium *in vivo*. This finding confirms our previous *in-vitro* studies of direct co-cultures using U373 GBM cells and MSCs. These studies showed the formation of gap junctions between these cell types (*i.e.*, formation of a functional syncytium), as demonstrated by fluorescein transmission and connexin 43 expression. Furthermore, there was membrane fusion between these cells (*i.e.*, formation of a structural syncytium), as demonstrated by the co-localization of different carbocyanine dyes.¹⁵ Direct membrane fusion between the GBM cells and MSCs affects gene expression and the cell phenotype, which might lead to enhanced invasion of hybrid cells, which is of relevance to tumor progression.¹⁵

Taken together, our enhanced clearing methodology has enabled us to study GBM cell localization in the brain of zebrafish embryos and to observe their interaction with MSCs at single-cell resolution. This allowed us to identify the invasion patterns of GBM cells in the zebrafish brain and identify the central canal of the spinal cord as a major invasion route. As the frequency of this single-cell invasion of the spinal cord is also quantifiable,

the observation of this process in high-throughput screening can now be developed as a fast and objective methodology. Thus it can not only be used to study basic mechanisms in terms of the differences among heterogeneous GBM populations, but also for diagnostic purposes with patient biopsies. This study is also the first to address co-culture implantation in the zebrafish brain model in order to define the interactions between GBM cells and MSCs. We demonstrated that these two cell types invade the surrounding brain tissue along similar invasion roots as the GBM cells alone, whereby they often moved along the central canal of the spinal cord, but did not leave the CNS.

In perspective, the zebrafish xenotransplantation model of GBM has many benefits in terms of cost, simplicity, possibility for single-cell visualization *in vivo*, and high throughput.¹⁸ As demonstrated by the present study, this simple model can be used to study cell processes involved in GBM cell invasion and the interactions of GBM cells with many other cells of the stroma in double or triple cell co-cultures.

Acknowledgments

The authors wish to thank Prof. Dr. Cornelis J.F. van Noorden (Academic Medical Centre, Amsterdam) for his introduction to the CLARITY technique. We also thank Dr. David Dobnik (National Institute of Biology, Ljubljana) for his help with confocal microscopy. This work was funded by the INTERREG EC Project 2011, Ref. No. 42 (GLIOMA) and the Reserch Programme P1-0245, awarded by the Slovenian Research Agency.

References

- Ohgaki H, Kleihues P. The definition of primary and secondary glioblastoma. *Clin Cancer Res* 2013; **19**: 764-72.
- Claes A, Idema A, Wesseling P. Diffuse glioma growth: a guerilla war. *Acta Neuropathol* 2007; **114**: 443-58.
- Gupta MK, Jayaram S, Reddy DN, Polisetty RV, Sirdeshmukh R. Transcriptomic and proteomic data integration and two-dimensional molecular maps with regulatory and functional linkages: application to cell proliferation and invasion networks in glioblastoma. *J Proteome Res* 2015; **14**: 5017-27.
- Klekner Á, Hutóczki G, Virga J, Reményi-Puskár J, Tóth J, Scholtz B, et al. Expression pattern of invasion-related molecules in the peritumoral brain. *Clin Neurol Neurosurg* 2015; **139**: 138-43.
- Friedl P, Wolf K. Tumour-cell invasion and migration: diversity and escape mechanisms. *Nat Rev Cancer* 2003; **3**: 362-74.
- Friedl P, Wolf K. Plasticity of cell migration: a multiscale tuning model. *J Cell Biol* 2010; **188**: 11-9.
- Hanahan D, Weinberg RA. Hallmarks of cancer: the next generation. *Cell* 2011; **144**: 646-74.

8. Grisendi G, Bussolari R, Veronesi E, Piccinno S, Burns JS, De Santis G, et al. Understanding tumor-stroma interplays for targeted therapies by armed mesenchymal stromal progenitors: the Mesenkillers. *Am J Cancer Res* 2011; **1**: 787-805.
9. Kološa K, Motaln H, Herold-Mende C, Koršič M, Lah TT. Paracrine effects of mesenchymal stem cells induce senescence and differentiation of glioblastoma stem-like cells. *Cell Transplant* 2015; **24**: 631-44.
10. Motaln H, Lah TT. Cytokines play a key role in communication between mesenchymal stem cells and brain cancer cells. *Protein Pept Lett* 2015; **22**: 322-31.
11. Barcellos-de-Souza P, Gori V, Bambi F, Chiarugi P. Tumor microenvironment: bone marrow-mesenchymal stem cells as key players. *Biochim Biophys Acta* 2013; **1836**: 321-35.
12. Arango-Rodriguez ML, Ezquer F, Ezquer M, Conget P. Could cancer and infection be adverse effects of mesenchymal stromal cell therapy? *World J Stem Cells* 2015; **7**: 408-17.
13. Fei S, Qi X, Kedong S, Guangchun J, Jian L, Wei Q. The antitumor effect of mesenchymal stem cells transduced with a lentiviral vector expressing cytosine deaminase in a rat glioma model. *J Cancer Res Clin Oncol* 2012; **138**: 347-57.
14. Kim SM, Woo JS, Jeong CH, Ryu CH, Lim JY, Jeun SS. Effective combination therapy for malignant glioma with TRAIL-secreting mesenchymal stem cells and lipoxigenase inhibitor MK886. *Cancer Res* 2012; **72**: 4807-17.
15. Schichor C, Albrecht V, Korte B, Buchner A, Riesenberger R, Mysliwicz J, et al. Mesenchymal stem cells and glioma cells form a structural as well as a functional syncytium in vitro. *Exp Neurol* 2012; **234**: 208-19.
16. Pilat MM, Oliveira M, Motaln H, Breznik B, Glaser T, Lah TT, et al. Glioblastoma-mesenchymal stem cell communication modulates expression and activities of kinin receptors: possible involvement of bradykinin on information flow. *Cytometry A* 2016; DOI: 10.1002/cyto.a.22800
17. Behnan J, Isakson P, Joel M, Cilio C, Langmoen I, Vik-Mo EO, et al. Recruited brain tumor-derived mesenchymal stem cells contribute to brain tumor progression. *Stem Cells* 2014; **32**: 1110-23.
18. Vittori M, Motaln H, Lah TT. The study of glioma by xenotransplantation in zebrafish early life stages. *J Histochem Cytochem* 2015; **63**: 749-61.
19. Grunwald DJ, Eisen JS. Headwaters of the zebrafish – emergence of a new model vertebrate. *Nat Rev Genet* 2002; **3**: 717-24.
20. Feng Y, Martin P. Imaging innate immune responses at tumour initiation: new insights from fish and flies. *Nat Rev Cancer* 2015; **15**: 556-62.
21. White R, Rose K, Zon L. Zebrafish cancer: the state of the art and the path forward. *Nat Rev Cancer* 2013; **13**: 624-36.
22. Zon LI, Peterson RT. *In vivo* drug discovery in the zebrafish. *Nat Rev Drug Discov* 2005; **4**: 35-44.
23. Keller PJ, Schmidt AD, Wittbrodt J, Stelzer EH. Reconstruction of zebrafish early embryonic development by scanned light sheet microscopy. *Science* 2008; **322**: 1065-9.
24. Geiger GA, Fu W, Kao GD. Temozolomide-mediated radiosensitization of human glioma cells in a zebrafish embryonic system. *Cancer Res* 2008; **68**: 3396-404.
25. Lal S, La Du J, Tanguay RL, Greenwood JA. Calpain 2 is required for the invasion of glioblastoma cells in the zebrafish brain microenvironment. *J Neurosci Res* 2012; **90**: 769-81.
26. Konantz M, Balci TB, Hartwig UF, Delleire G, André MC, Berman JN, et al. Zebrafish xenografts as a tool for *in vivo* studies on human cancer. *Ann N Y Acad Sci* 2012; **1266**: 124-37.
27. Sakhalkar HS, Dewhirst M, Oliver T, Cao Y, Oldham M. Functional imaging in bulk tissue specimens using optical emission tomography: fluorescence preservation during optical clearing. *Phys Med Biol* 2007; **52**: 2035-54.
28. Dodt HU, Leischner U, Schierloh A, Jährling N, Mauch CP, Deininger K, et al. Ultramicroscopy: three-dimensional visualization of neuronal networks in the whole mouse brain. *Nat Methods* 2007; **4**: 331-6.
29. Zukor KA, Kent DT, Odelberg SJ. Fluorescent whole-mount method for visualizing three-dimensional relationships in intact and regenerating adult newt spinal cords. *Dev Dyn* 2010; **239**: 3048-57.
30. Oldham M, Sakhalkar H, Oliver T, Allan Johnson G, Dewhirst M. Optical clearing of unsectioned specimens for three-dimensional imaging via optical transmission and emission tomography. *J Biomed Opt* 2008; **13**: 021113.
31. Ertürk A, Becker K, Jährling N, Mauch CP, Hojer CD, Egen JG, et al. Three-dimensional imaging of solvent-cleared organs using 3DISCO. *Nat Protoc* 2012; **7**: 1983-95.
32. Becker K, Jährling N, Saghafi S, Weiler R, Dodt H-U. Chemical clearing and dehydration of GFP expressing mouse brains. *PLoS ONE* 2012; **7**: e33916.
33. Hama H, Kurokawa H, Kawano H, Ando R, Shimogori T, Noda H, et al. Scale: a chemical approach for fluorescence imaging and reconstruction of transparent mouse brain. *Nat Neurosci* 2011; **14**: 1481-8.
34. Ke MT, Fujimoto S, Imai T. SeeDB: a simple and morphology-preserving optical clearing agent for neuronal circuit reconstruction. *Nat Neurosci* 2013; **16**: 1154-61.
35. Susaki EA, Tainaka K, Perrin D, Kishino F, Tawara T, Watanabe TM, et al. Whole-brain imaging with single-cell resolution using chemical cocktails and computational analysis. *Cell* 2014; **157**: 726-39.
36. Tainaka K, Kubota SI, Suyama TQ, Susaki EA, Perrin D, Ukai-Tadenuma M, et al. Whole-body imaging with single-cell resolution by tissue decolorization. *Cell* 2014; **159**: 911-24.
37. Kuwajima T, Sitko AA, Bhansali P, Jurgens C, Guido W, Mason C. Clear⁺: a detergent- and solvent-free clearing method for neuronal and non-neuronal tissue. *Development* 2013; **140**: 1364-8.
38. Chung K, Wallace J, Kim SY, Kalyanasundaram S, Andalman AS, Davidson TJ, et al. Structural and molecular interrogation of intact biological systems. *Nature* 2013; **497**: 332-7.
39. Yang B, Treweek JB, Kulkarni RP, Deverman BE, Chen CK, Lubeck E, et al. Single-cell phenotyping within transparent intact tissue through whole-body clearing. *Cell* 2014; **158**: 945-58.
40. Organisation for Economic Cooperation and Development. *OECD Guidelines For Testing of Chemicals*. Test No. 236. Fish Embryo Acute Toxicity (FET) Test. Paris: OECD Publishing; 2013.
41. Abramoff MD, Magalhães PJ, Ram SJ. Image processing with ImageJ. *Biophotonics Intern* 2004; **11**: 36-42.
42. Prieto D, Aparicio G, Morande PE, Zolessi FR. A fast, low-cost, and highly efficient fluorescent DNA labeling method using methyl green. *Histochem Cell Biol* 2014; **142**: 335-45.
43. Gekko K, Timasheff SN. Mechanism of protein stabilization by glycerol: preferential hydration in glycerol-water mixtures. *Biochemistry* 1981; **20**: 4667-76.
44. Street TO, Bolen DW, Rose GD. A molecular mechanism for osmolyte-induced protein stability. *Proc Natl Acad Sci U S A* 2006; **103**: 13997-4002.
45. Eden C, Ju B, Murugesan M, Phoenix T, Nimmervoll B, Tong Y, et al. Orthotopic models of pediatric brain tumors in zebrafish. *Oncogene* 2015; **34**: 1736-42.
46. Gritsenko PG, Iliina O, Friedl P. Interstitial guidance of cancer invasion. *J Pathol* 2012; **226**: 185-99.
47. Motaln H, Koren A, Gruden K, Ramšak Ž, Schichor C, Lah TT. Heterogeneous glioblastoma cell cross-talk promotes phenotype alterations and enhanced drug resistance. *Oncotarget* 2015; **38**: 40998-1017.
48. Gole B, Huszthy PC, Popović M, Jeruc J, Ardebili YS, Bjerkvig R, Lah TT. The regulation of cysteine cathepsins and cystatins in human gliomas. *Int J Cancer* 2012; **131**: 1779-89.
49. Motaln H, Gruden K, Hren M, Schichor C, Primon M, Rotter A, et al. Human mesenchymal stem cells exploit the immune response mediating chemokines to impact the phenotype of glioblastoma. *Cell Transplant* 2012; **21**: 1529-45.
50. Tajnšek U, Motaln H, Levičar N, Rotter A, Lah TT. The duality of stem cell: double edged sword in tumour evolution and treatment. In: Resende RR, Ulrich H, editor. *Trends in Stem Cell Proliferation and Cancer Research*. Dordrecht: Springer Netherlands; 2013. p. 391-434.

Identification of differentially expressed genes associated with the enhancement of X-ray susceptibility by RITA in a hypopharyngeal squamous cell carcinoma cell line (FaDu)

Jinwei Luan, Xianglan Li, Rutao Guo, Shanshan Liu, Hongyu Luo, Qingshan You

Department of Radiation Oncology, The Third Affiliated Hospital of Harbin Medical University, Harbin, China

Radiol Oncol 2016; 50(2): 168-174.

Received 22 April 2015

Accepted 3 January 2016

Correspondence to: Qingshan You, M.D., Department of Radiation Oncology, The Third Affiliated Hospital of Harbin Medical University, Num.150, Haping Road, Harbin, China, 150081. Phone and Fax: +860 451 8629 8532; E-mail: haveqingsh@163.com

Disclosure: No potential conflicts of interest were disclosed.

Background. Next generation sequencing and bio-informatic analyses were conducted to investigate the mechanism of reactivation of p53 and induction of tumor cell apoptosis (RITA)-enhancing X-ray susceptibility in FaDu cells.

Materials and methods. The cDNA was isolated from FaDu cells treated with 0 X-ray, 8 Gy X-ray, or 8 Gy X-ray + RITA. Then, cDNA libraries were created and sequenced using next generation sequencing, and each assay was repeated twice. Subsequently, differentially expressed genes (DEGs) were identified using Cuffdiff in Cufflinks and their functions were predicted by pathway enrichment analyses. Genes that were constantly up- or down-regulated in 8 Gy X-ray-treated FaDu cells and 8 Gy X-ray + RITA-treated FaDu cells were obtained as RITA genes. Afterward, the protein-protein interaction (PPI) relationships were obtained from the STRING database and a PPI network was constructed using Cytoscape. Furthermore, ClueGO was used for pathway enrichment analysis of genes in the PPI network.

Results. Total 2,040 and 297 DEGs were identified in FaDu cells treated with 8 Gy X-ray or 8 Gy X-ray + RITA, respectively. *PARP3* and *NEIL1* were enriched in base excision repair, and *CDK1* was enriched in p53 signaling pathway. *RFC2* and *EZH2* were identified as RITA genes. In the PPI network, many interaction relationships were identified (e.g., *RFC2*-*CDK1*, *EZH2*-*CDK1* and *PARP3*-*EZH2*). ClueGO analysis showed that *RFC2* and *EZH2* were related to cell cycle.

Conclusions. *RFC2*, *EZH2*, *CDK1*, *PARP3* and *NEIL1* may be associated, and together enhance the susceptibility of FaDu cells treated with RITA to the deleterious effects of X-ray.

Key words: hypopharyngeal squamous cell carcinoma; next generation sequencing; RITA; X-ray

Introduction

Head and neck squamous cell carcinoma (HNSCC), which arises in the head and neck region that composes pharynx, larynx, nasal cavity, oral cavity, paranasal sinuses and salivary glands, has an estimated 500,000 new cases and becomes the sixth most common cancer in 2010 worldwide.¹ As one type of HNSCC, hypopharyngeal squamous cell carcinoma (HSCC) has a poor prognosis, and the overall survival rate for HSCC patients is only 15–45%.^{2,3} The patients

diagnosed with HSCC are often at a late stage and distant metastasis occur after conventional treatments.² Thus, the poor survival of patients with HSCC may be due to lacking of early detection and highly metastatic behavior.⁴ Radiotherapy is the principal treatment of loco-regionally advanced squamous-cell carcinoma of the head and neck region (including oral cavity, oropharynx, hypopharynx, and larynx).^{5,6} Recently, instead of radiotherapy, chemoradiotherapy has become the standard treatment for patients with locally advanced disease.⁷ Many small molecules have

been identified to enhance the radiation response. For example, panitumumab has been discovered to have an enhanced effect on radiation in the preclinical setting of upper aerodigestive tract cancer.⁸ Moreover, it has been found that the p53-reactivating small-molecule RITA (reactivation of p53 and induction of tumor cell apoptosis), alone or in combination with cisplatin, can induce the reactivation of p53 in many HNSCC cell lines.^{9,10} However, this effect is not universal. The HNSCC cell line JHU-028 can express wild type (wt) p53, but the cells do not undergo apoptosis in response to RITA treatment.¹⁰

Previously, we used RITA combined with X-ray to investigate the effect of RITA on X-ray susceptibility for the treatment of HSCC cell line FaDu (which is HPV-negative cell line) and found that RITA could enhance the radiation response of HSCC (data not shown). In this study, using RNA sequencing data from the HSCC cell line FaDu, we aimed to screen differentially expressed genes (DEGs) between 8 Gy X-ray-treated FaDu cells and 0 Gy X-ray-treated FaDu cells, as well as those between 8 Gy X-ray + RITA treated FaDu cells and 8 Gy X-ray treated FaDu cells. The underlying functions of the DEGs were predicted by Gene Ontology (GO), Kyoto Encyclopedia of Genes and Genomes (KEGG) and BioCarta enrichment analysis. Moreover, the genes related to RITA were further analyzed. Additionally, a protein-protein interaction (PPI) network was constructed to identify key genes involved in enhanced X-ray susceptibility of FaDu cells treated with RITA.

Materials and methods

Cell culture and processing

The HSCC cell line FaDu was purchased from American Type Culture Collection (ATCC, Manassas, VA, USA). The FaDu cells were cultured in media made from Dulbecco modified Eagle medium (DMEM, GIBCO, Gaithersburg, USA), 10% fetal bovine serum (FBS, GIBCO) and 1% mycillin double antibody (GIBCO) at 37°C in a humidified, 5% CO₂ incubator (Thermo, Pittsburgh, USA). When the confluency of FaDu cells covered 80%-90% of the petri dish, they were digested with pancreatin (GIBCO), centrifuged, and the supernatant was discarded. Next, the FaDu cells were resuspended in a frozen stock solution composed of 10% dimethyl sulfoxide (DMSO, GIBCO), 40% FBS and 50% DMEM, and preserved in a program frozen box.

After digestion, FaDu cells were centrifuged and counted, and then inoculated in 96-well plates (ABI, Foster City, USA) (6×10⁴ cells/well) and cultured overnight. Subsequently, RITA (10 μM) (Selleck, Houston, USA) was added to each well of the experimental group, and DMSO (0.1%) was added to that the wells of the control group. The cells were preprocessed for 24 h at 37°C in a humidified, 5% CO₂ incubator. The plates were then sealed by parafilm and placed in a radiometer, and the cells in the experimental group were irradiated with a radiation dose of 8 Gy and a radiation speed of 1 Gy/min. After irradiation, the parafilm was removed and the plates were placed at 37°C in a humidified, 5% CO₂ incubator for 48 h.

RNA isolation and sequencing preparation

The total RNA was extracted from the cells using the SV total RNA Isolation System (Invitrogen, Shanghai, CHN) according to the manufacturer's instructions. The integrity of the total RNA was verified by 2% Agarose Gel Electrophoresis. The purity of RNA was determined by the A260/A280 ratio as determined by a spectrophotometer (Merinton, Beijing, CHN).

Construction of cDNA library

The cDNA libraries were constructed using a NEBNext® Ultra™ RNA Library Prep Kit for Illumina® (NEB E7530) (Vazyme, Nanjing, CHN), according to the manufacturer's instructions. Through heating, mRNA was broken into short fragments (200 nt). Using these short fragments as templates, random hexamer-primer (Sangon, Shanghai, CHN) was used to synthesize the first-strand of cDNA. Next, the second-strand of cDNA was synthesized. The short fragments were connected to sequencing adapters after poly (A) sequences were added. Afterwards, the UNG enzyme (Prospect Biosystems, Newark, USA) was used to degrade the second-strand cDNA, and the product was purified using a MiniElute PCR Purification Kit (Qiagen, Dusseldorf, GER) before PCR amplification. Finally, the library could be sequenced using an Illumina Hiseq 2500 v4 100PE (Illumina, San Diego, USA), and raw reads were generated. Reads with adaptor sequences, with unknown nucleotide content higher than 10% and/or those with low quality bases accounting for higher than 50% of the total nucleotides were filtered out.

Sequence alignment and identification of differentially expressed genes

The high quality reads were mapped to the human genome (version: hg19) using Tophat (version: 2.0.12), and BAM files were obtained.¹¹ The parameters were set to defaults. Cuffdiff in Cufflinks¹² was used to identify DEGs. The Benjamini & Hochberg method¹³ was applied to correct for multiple tests. The adjusted p-value (that is false discovery rate, FDR) < 0.05 and |log fold change (FC)| ≥ 1 were used as the cut-off criteria.

Functional enrichments

The KEGG pathway database can be used to identify the relationships and interactions between genes in a given system.¹⁴ KEGG was used for pathway enrichment analysis, and a p-value < 0.05 was considered a significantly enriched pathway.

The genes related to RITA (RITA genes) screening

To further investigate the effect of RITA on FaDu cells, we identified common DEGs in 0 Gy X-ray treated FaDu cells vs 8 Gy X-ray treated FaDu cells, and 8 Gy X-ray treated FaDu cells vs 8 Gy X-ray + RITA treated FaDu cells (Figure 1). A previous study showed that X-rays could reduce cell viability and that treatment with RITA could enhance the susceptibility of FaDu cells to the deleterious effects of X-rays.¹⁰ Therefore, the genes that were consistently up- or down-regulated in 8 Gy X-ray treated FaDu cells vs 0 Gy X-ray treated FaDu cells and 8 Gy X-ray + RITA treated FaDu cells vs 8 Gy X-ray treated FaDu cells were characterized as the RITA genes.

PPI network construction

The online tool STRING¹⁵ was utilized to analyze the interactions between the proteins encoded by the common DEGs. A required confidence (com-

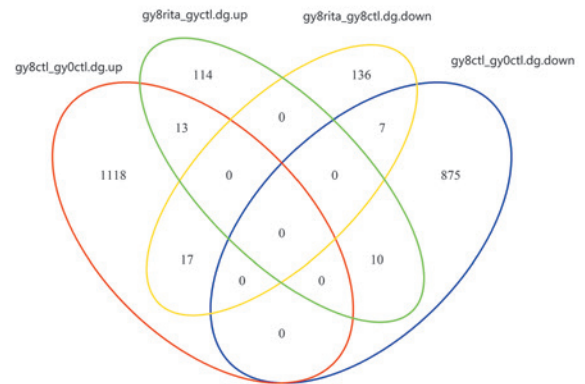


FIGURE 1. Venn diagram of DEGs between 0 Gy X-ray-treated FaDu cells and 8 Gy X-ray-treated FaDu cells, as well as the DEGs between 8 Gy X-ray-treated FaDu cells and 8 Gy X-ray + RITA-treated FaDu cells.

binated score) > 0.4 was used as the cut-off criterion. Subsequently, Cytoscape software¹⁶ was used to visualize the PPI network.

ClueGO analysis

ClueGO¹⁷ in Cytoscape was used to conduct GO, KEGG and BioCarta enrichment analyses. Further, ClueGO divided terms into different functional groups based on the common genes involved in different terms. In our study, ClueGO was used for KEGG pathway enrichment analysis. A p-value < 0.05 was used as the cut-off criterion.

Results

Alignment analysis

The total reads were above 82% and the mapped reads were above 70% in all of the data sets. The detailed sequencing information is shown in Table 1.

DEG analysis

Compared with 0 Gy X-ray-treated FaDu cells, a total of 2,040 DEGs (1,148 up-regulated and 892

TABLE 1. Summary statistics of paired-end (PE) RNA-Seq reads in six cell lines

Sample	Total PE reads	Total high quality PE reads	Total mapped PE reads	Total uniquely mapped PE reads
Sample_L141211001	10467886	8650424 (82.3%)	6846290 (79.1%)	6749179
Sample_L141211002	11510210	9627883 (83.6%)	7197526 (74.7%)	7097908
Sample_L141211003	11119410	9365349 (84.2%)	6910499 (73.7%)	6825529
Sample_L141211004	11271934	9510517 (84.3%)	6752339 (70.9%)	6669811
Sample_L141211005	10854414	9110446 (83.9%)	7129465 (78.2%)	7043831
Sample_L141211006	10532245	8802840 (83.5%)	6752224 (76.7%)	6671073

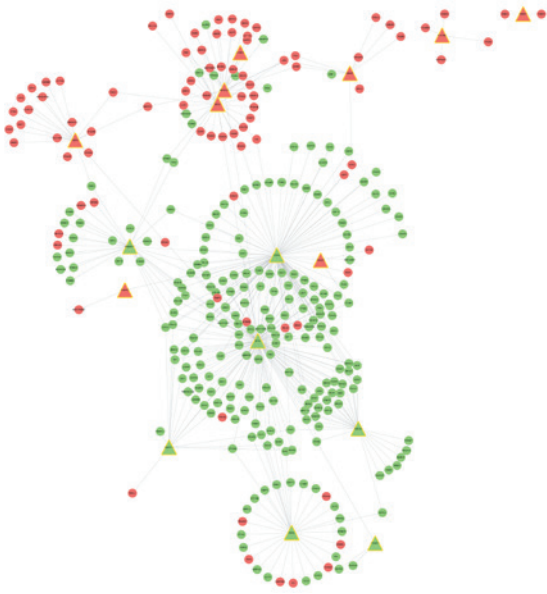


FIGURE 2. The PPI network for the RITA genes and their related DEGs. The red hubs represent the up-regulated DEGs; the green hubs represent the down-regulated DEGs; the triangle hubs represent the RITA genes; the lines represent the interactions between the genes.

down-regulated DEGs) were identified in the 8 Gy X-ray-treated FaDu cells. Moreover, 297 DEGs (137 up-regulated and 160 down-regulated DEGs) were identified in the 8 Gy X-ray + RITA-treated FaDu cells compared with the 8 Gy X-ray-treated FaDu cells.

Pathway enrichment analysis

The results of KEGG pathway enrichment for the DEGs are listed in Table 2. Replication factor C subunit 2 (*RFC2*) was significantly enriched in DNA replication ($p = 5.85E-19$) and nucleotide excision repair ($p = 2.25E-04$). Poly (ADP-ribose) polymerase 3 (*PARP3*) and nei endonuclease VIII-like 1 (*NEIL1*) were significantly enriched in the pathway of base excision repair ($p = 2.00E-08$). Moreover, cyclin-dependent kinase 1 (*CDK1*) was significantly enriched in the p53 signaling pathway ($p = 1.85E-02$).

RITA genes screening

A total of 20 consistently dysregulated genes in the 8 Gy X-ray-treated FaDu cells vs 0 Gy X-ray-

TABLE 2. The top ten up- and down-regulated DEGs between 0 Gy X-ray treated FaDu cells and 8 Gy X-ray treated FaDu cells, as well as 8 Gy X-ray treated FaDu cells and 8 Gy X-ray + RITA treated FaDu cells

	Gene symbols	log2 fold change	P-value	Gene symbols	log2 fold change	P-value
Up-regulated	<i>BMF</i>	-1.79769e+308	1.23E-11	<i>BMF</i>	-1.79769e+308	1.23E-11
	<i>SDCBP</i>	-1.79769e+308	0.00097112	<i>SDCBP</i>	-1.79769e+308	0.00097112
	<i>IL32</i>	-1.79769e+308	0.0110064	<i>IL32</i>	-1.79769e+308	0.0110064
	<i>MAD1L1</i>	-1.79769e+308	9.77E-05	<i>MAD1L1</i>	-1.79769e+308	9.77E-05
	<i>SIRT3</i>	-1.79769e+308	0.00289562	<i>SIRT3</i>	-1.79769e+308	0.00289562
	<i>KAZN</i>	-1.79769e+308	7.93E-10	<i>KAZN</i>	-1.79769e+308	7.93E-10
	<i>TSPAN4</i>	-1.79769e+308	0.0136997	<i>TSPAN4</i>	-1.79769e+308	0.0136997
	<i>PPAN-P2RY11</i>	-1.79769e+308	4.71E-08	<i>PPAN-P2RY11</i>	-1.79769e+308	4.71E-08
	<i>CDC14B</i>	-1.79769e+308	1.49E-06	<i>CDC14B</i>	-1.79769e+308	1.49E-06
	<i>CXCL16</i>	-1.79769e+308	0.000434357	<i>CXCL16</i>	-1.79769e+308	0.000434357
Down-regulated	<i>C3orf14</i>	-5.88442	0.006353	<i>KCTD2</i>	-3.8901	1.23E-06
	<i>TTC28-AS1</i>	-3.10554	1.30E-09	<i>TSPAN4</i>	-3.68234	0.0124825
	<i>KRT4</i>	-2.86398	0	<i>FGFR3</i>	-3.47603	0.0322468
	<i>ALPP</i>	-2.68741	1.30E-13	<i>PLEKHM1.1</i>	-3.41618	0.0191408
	<i>MND1</i>	-2.64752	0.022297	<i>CHFR</i>	-3.39824	0.0369514
	<i>DHRS2</i>	-2.38983	4.17E-11	<i>KREMEN2</i>	-3.32824	0.033903
	<i>FGF3</i>	-2.33156	2.25E-12	<i>SMAP2</i>	-3.3199	0.0215792
	<i>TERC</i>	-2.268	0.027132	<i>EPS15L1</i>	-3.30518	0.00562372
	<i>UTP20</i>	-2.23728	0	<i>MORF4L2</i>	-3.0731	0.0300806
	<i>GAL</i>	-2.22661	0	<i>PIGQ</i>	-2.94079	0.0327601

DEGs = differentially expressed genes

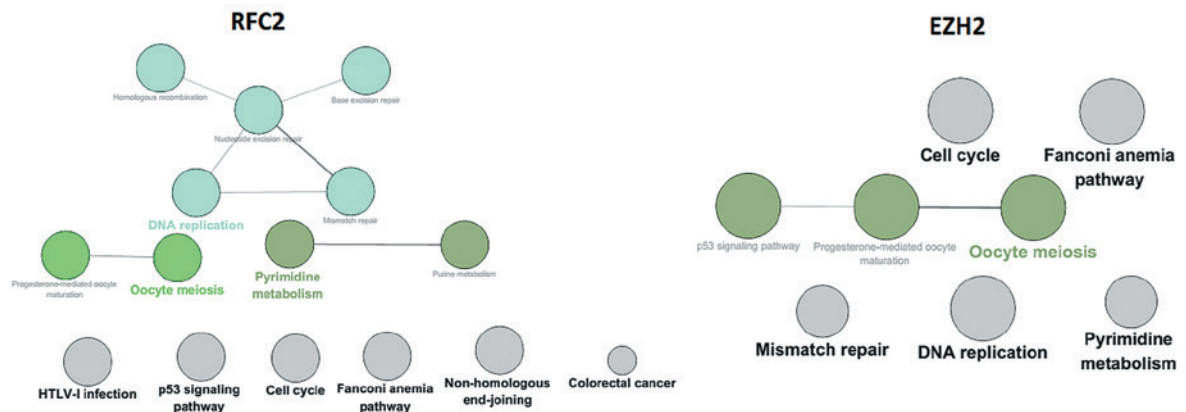


FIGURE 3. Functional annotation for *RFC2* and *EZH2* clusters. Node color represents the functional groups; node size reflects the p-value, with the smaller the node size indicating larger p-values, while the larger node size represents smaller p-values.

treated FaDu cells and in the 8 Gy X-ray + RITA-treated FaDu cells vs 8 Gy X-ray-treated FaDu cells were identified, including 13 consistently up-regulated (B cell lymphomas 6, *BCL6*; integrin, beta 2-antisense RNA 1, *ITGB2-AS1*; L1 cell adhesion molecule, *L1CAM*; LIM and calponin homology domains 1, *LIMCH1*; latent transforming growth factor- β binding protein 3, *LTBP3*; v-MAF avian musculoaponeurotic fibrosarcoma oncogene family, *MAFF*; neutrophil cytosolic factor 2, *NCF2*; nuclear factor of activated T-cells, cytoplasmic, calcineurin-dependent 1, *NFATC1*; *PARP3*; RAB43, member RAS oncogene family, *RAB43*; regulator of cell cycle, *RGCC*; Src homology 2 domain containing F, *SHF*; and troponin T type 1, *TNNT1*) and 7 consistently down-regulated DEGs (adenylosuccinate lyase, *ADSL*; enhancer of zeste homolog 2, *EZH2*; nudix-type motif 1, *NUDT1*; proteasome 26S subunit, non-ATPase 11, *PSMD11*; *RFC2*; Treacher Collins-Franceschetti syndrome 1, *TCOF1*; and X-ray repair cross-complementing group 3, *XRCC3*) (Figure 1).

PPI network and module analysis

The PPI network for RITA genes and the DEGs related to RITA had 448 interactions (Figure 2). In the PPI network, the RITA genes of *RFC2* (degree = 126) and *EZH2* (degree = 115) had relatively higher degrees. Additionally, *RFC2* and *EZH2* could interact with *CDK1*. The results of the pathway enrichment analysis for *RFC2*, *EZH2* and their interaction genes are shown in Figure 3. *RFC2* and *EZH2* were enriched in the cell cycle pathways, oocyte meiosis, and DNA replication.

Discussion

In the present study, a total of 2,040 DEGs, including 1,148 up-regulated and 892 down-regulated DEGs, were identified in 8 Gy X-ray-treated FaDu cells, compared with 0 Gy X-ray-treated FaDu cells. Moreover, 297 DEGs, including 137 up-regulated and 160 down-regulated DEGs, were identified in 8 Gy X-ray + RITA-treated FaDu cells, compared with 8 Gy X-ray-treated FaDu cells. Among these DEGs, *EZH2* and *RFC2*, which were consistently down-regulated in 8 Gy X-ray-treated FaDu cells vs 0 Gy X-ray-treated FaDu cells and 8 Gy X-ray + RITA-treated FaDu cells vs 8 Gy X-ray-treated FaDu cells, were characterized as the RITA genes. A previous study has reported that enhancers of *EZH2*, which is the enzymatic component of the polycomb repressive complex 2, can regulate cell proliferation and differentiation during embryonic development.¹⁸ Moreover, it has also been demonstrated that targeting *EZH2* can suppress cancer progression and recurrence by reversing oncogenic properties and stemness of tumor cells.¹⁹ *RFC2*, belonging to the replication factor C family, has been implicated in nasopharyngeal carcinoma.²⁰ In our study, ClueGO analysis showed that *RFC2* and *EZH2* were related to the cell cycle. Cell cycle regulation by p53 is widely accepted as the major mechanism for tumor formation.²¹ Therefore, we speculated that *RFC2* and *EZH2* may regulate the cancer cell proliferation of HSCC cells through the cell cycle pathway. According to the PPI network, both *RFC2* and *EZH2* could interact with *CDK1*, and the KEGG pathway enrichments showed that *CDK1* was significantly enriched in the p53 sign-

TABLE 3. The KEGG pathway enrichment for the DEGs between 0 GY X-ray treated FaDu cells and 8 GY X-ray treated FaDu cells, as well as 8 GY X-ray treated FaDu cells and 8 GY X-ray + RITA treated FaDu cells.

Term	Count	P value	Gene symbols
gy8ctl vs. gy0ctl			
hsa03030: DNA replication	28	5.85E-19	POLA1, POLA2, RPA3, RPA1, PRIM1, RPA2, POLE4, MCM7, POLE3, FEN1
hsa04110: Cell cycle	43	1.91E-11	E2F1, E2F2, DBF4, PRKDC, PKMYT1, CHEK1, CDC45, MCM7, CDKN2B, CDKN2C ...
hsa03430: Mismatch repair	16	1.15E-09	EXO1, SSBP1, MSH2, LIG1, MLH1, RPA3, RFC5, POLD3, RPA1, RPA2 ...
hsa00240: Pyrimidine metabolism	32	2.00E-08	POLR2G, DTYMK, POLA1, CAD, POLA2, CMPK2, TK1, PRIM1, TYMS, POLE4 ...
hsa03410: Base excision repair	16	2.06E-06	HMGB1, UNG, NEIL3, LIG1, POLE, NEIL1, POLD3, POLD4, POLE4, POLE3 ...
hsa03440: Homologous recombination	14	3.36E-06	RAD51C, XRCC3, NBN, BLM, SSBP1, MRE11A, EME1, RPA3, RAD51, POLD3 ...
hsa03420: Nucleotide excision repair	15	2.25E-04	LIG1, POLE, RPA3, RFC5, POLD3, RPA1, RPA2, POLD4, RFC3, POLE4 ...
hsa00230: Purine metabolism	33	3.73E-04	XDH, POLR2G, POLA1, POLA2, PFAS, PRIM1, POLE4, POLE3, PDE4A, ENTPD8 ...
hsa05200: Pathways in cancer	52	0.010417112	FGF19, E2F1, HSP90AB1, E2F2, PTGS2, PDGFB, PGF, STAT5A, ARNT2, FGF11 ...
hsa05219: Bladder cancer	11	0.016627297	E2F1, E2F2, TYMP, CDKN1A, PGF, VEGFA, RB1, DAPK2, CDK4, MMP2, DAPK1
hsa04115: p53 signaling pathway	15	0.018499656	CDK1, CYCS, CHEK1, ATR, CDK4, CCNG2, GTSE1, CCNB1, CDKN1A, CCNB2 ...
hsa04512: ECM-receptor interaction	17	0.024887625	HSPG2, SDC4, COL5A1, CHAD, HMMR, VWF, LAMB3, LAMB2, ITGB8, ITGA5 ...
hsa03020: RNA polymerase	8	0.03298698	POLR3G, POLR2G, POLR3K, POLR1E, POLR1A, POLR1C, POLR1B, POLR3B
hsa00970: Aminoacyl-tRNA biosynthesis	10	0.036943456	IARS, NARS2, LARS, FARSB, EPRS, WARS2, DARS2, AARS2, KARS, EARS2
hsa03040: Spliceosome	22	0.044130211	NCBP1, MAGOH, TRA2B, LSM6, TRA2A, SNRPD1, HSPA1A, PRPF4, RBMX, HNRNPA1 ...
hsa05222: Small cell lung cancer	16	0.048720159	E2F1, TRAF1, E2F2, CKS1B, PTGS2, PIK3CD, CYCS, SKP2, RB1, BIRC3 ...
gy8rita vs. gy8ctl			
hsa03410: Base excision repair	4	0.014381142	NEIL1, LIG3, PARP3, SMUG1
hsa05212: Pancreatic cancer	5	0.021107952	AKT1, PGF, PIK3CB, ERBB2, RALGDS
hsa05213: Endometrial cancer	4	0.040674333	AKT1, PIK3CB, ERBB2, CTNNA1
hsa04150: mTOR signaling pathway	4	0.040674333	AKT1, PGF, PIK3CB, EIF4E2

DEGs = differentially expressed genes

aling pathway. *p53* can negatively regulate the transcription of a large number of genes (including *BCL-2* and *MCL1*) that suppress apoptosis.²² Additionally, a former study has also demonstrated that the reactivation of *p53* can induce apoptosis in HNSCC, which includes HSCC.²³ Consequently, we proposed that *CDK1* could be correlated with HSCC by regulation of apoptosis of the cancer cells through the *p53* signaling pathway. In addition, *CDK1* might also function in HSCC through interacting with *RFC2* and *EZH2*.

Additionally, the RITA gene *PARP3* was significantly enriched in base excision repair. Base excision repair is a cellular mechanism that repairs damaged DNA throughout the cell cycle. It has been reported that the DNA repair capacity is crucial for preventing genomic instability and, in turn, may be associated with heightened risk of cancer.²⁴ Furthermore, reduced expression of nucleotide excision repair core genes such as Cockayne's

syndrome complementary group B/excision repair cross-complementing 6 (*CSB/ERCC6*), excision repair cross-complementing 1 (*ERCC1*), Xeroderma pigmentosum group G/excision repair cross-complementing 5 (*XPG/ERCC5*) and Xeroderma pigmentosum group B/excision repair cross-complementing 3 (*XPB/ERCC3*) can increase the risk for development of HNSCC for more than two-fold.²⁵ The ADP ribosyl transferase *PARP3* gene has been identified as a vital player in the stabilization of mitotic spindles and in telomere integrity. Notably, *PARP3* associates and regulates the mitotic components NuMA and tankyrase 1; therefore, *PARP3* can be a potential biomarker in cancer therapy.²⁶ In the PPI network, *PARP3* is capable of interacting with *EZH2*. Accordingly, it came to the speculation that *PARP3*, as well as its interaction with *EZH2*, could play a role in HSCC by regulating DNA damage through the base excision repair pathway. Moreover, *NEIL1* was also enriched in base exci-

sion repair. A former study showed that the functional variants of the NEIL1 protein can lead to risk and progression of squamous cell carcinomas of the oral cavity and oropharynx.²⁷ Therefore, *PARP3* and *NEIL1* could be involved in development of HSCC through the base excision repair pathway.

RFC2, *EZH2*, *CDK1*, *PARP3* and *NEIL1* may be related to an enhancement of the susceptibility of FaDu cells to X-rays with co-treatment of RITA. However, further research is needed to illustrate their mechanisms.

References

- Torre LA, Bray F, Siegel RL, Ferlay J, Lortet-Tieulent J, Jemal A. Global cancer statistics, 2012. *CA Cancer J Clin* 2015; **65**: 87-108.
- Chaturvedi AK, Engels EA, Pfeiffer RM, Hernandez BY, Xiao W, Kim E, et al. Human papillomavirus and rising oropharyngeal cancer incidence in the United States. *J Clin Oncol* 2011; **29**: 4294-301.
- Van Monsjou HS, Balm AJ, Van den Brekel MM, Wreesmann VB. Oropharyngeal squamous cell carcinoma: a unique disease on the rise? *Oral Oncol* 2010; **46**: 780-5.
- Garden AS, Asper JA, Morrison WH, Schechter NR, Glisson BS, Kies MS, et al. Is concurrent chemoradiation the treatment of choice for all patients with Stage III or IV head and neck carcinoma? *Cancer* 2004; **100**: 1171-8.
- Kramer S, Gelber RD, Snow JB, Marcial VA, Lowry LD, Davis LW, et al. Combined radiation therapy and surgery in the management of advanced head and neck cancer: final report of study 73-03 of the Radiation Therapy Oncology Group. *Head Neck Surg* 1987; **10**: 19-30.
- Kato K, Muro K, Minashi K, Ohtsu A, Ishikura S, Boku N, et al. Phase II study of chemoradiotherapy with 5-fluorouracil and cisplatin for stage II-III esophageal squamous cell carcinoma: JCOG Trial (JCOG 9906). *Int J Radiat Oncol Biol Phys* 2011; **81**: 684-90.
- Kruser TJ, Armstrong EA, Ghia AJ, Huang S, Wheeler DL, Radinsky R, et al. Augmentation of radiation response by panitumumab in models of upper aerodigestive tract cancer. *Int J Radiat Oncol Biol Phys* 2008; **72**: 534-42.
- Roh J-L, Ko JH, Moon SJ, Ryu CH, Choi JY, Koch WM. The p53-reactivating small-molecule RITA enhances cisplatin-induced cytotoxicity and apoptosis in head and neck cancer. *Cancer Lett* 2012; **325**: 35-41.
- Roh J-L, Kang SK, Minn I, Califano JA, Sidransky D, Koch WM. p53-Reactivating small molecules induce apoptosis and enhance chemotherapeutic cytotoxicity in head and neck squamous cell carcinoma. *Oral Oncol* 2011; **47**: 8-15.
- Kim D, Pertege G, Trapnell C, Pimentel H, Kelley R, Salzberg SL. TopHat2: accurate alignment of transcriptomes in the presence of insertions, deletions and gene fusions. *Genome Biol* 2013; **14**: R36.
- Trapnell C, Williams BA, Pertea G, Mortazavi A, Kwan G, van Baren MJ, et al. Transcript assembly and quantification by RNA-Seq reveals unannotated transcripts and isoform switching during cell differentiation. *Nat Biotechnol* 2010; **28**: 511-15.
- Benjamini Y, Hochberg Y. Controlling the false discovery rate: a practical and powerful approach to multiple testing. *J R Stat Soc Series B Stat Methodol* 1995; **57**: 289-300.
- Kanehisa M, Goto S. KEGG: kyoto encyclopedia of genes and genomes. *Nucleic Acids Res* 2000; **28**: 27-30.
- Franceschini A, Szklarczyk D, Frankild S, Kuhn M, Simonovic M, Roth A, et al. STRING v9. 1: protein-protein interaction networks, with increased coverage and integration. *Nucleic Acids Res* 2013; **41**: D808-D15.
- Saito R, Smoot ME, Ono K, Ruscheinski J, Wang P-L, Lotia S, et al. A travel guide to Cytoscape plugins. *Nat Methods* 2012; **9**: 1069-76.
- Bindea G, Mlecnik B, Hackl H, Charoentong P, Tosolini M, Kirilovsky A, et al. ClueGO: a Cytoscape plug-in to decipher functionally grouped gene ontology and pathway annotation networks. *Bioinformatics* 2009; **25**: 1091-93.
- Qi W, Chan H, Teng L, Li L, Chuai S, Zhang R et al. Selective inhibition of Ezh2 by a small molecule inhibitor blocks tumor cells proliferation. *Proc Natl Acad Sci* 2012; **109**: 21360-65.
- Chang C, Hung M. The role of EZH2 in tumour progression. *Br J Cancer* 2012; **106**: 243-47.
- Xiong S, Wang Q, Zheng L, Gao F, Li J. Identification of candidate molecular markers of nasopharyngeal carcinoma by tissue microarray and in situ hybridization. *Med Oncol* 2011; **28**: 341-48.
- Li T, Kon N, Jiang L, Tan M, Ludwig T, Zhao Y, et al. Tumor suppression in the absence of p53-mediated cell-cycle arrest, apoptosis, and senescence. *Cell* 2012; **149**: 1269-83.
- Mirzayans R, Andrais B, Scott A, Murray D. New insights into p53 signaling and cancer cell response to DNA damage: implications for cancer therapy. *Biomed Res Int* 2012: 170325. doi: 10.1155/2012/170325.
- Chuang H-C, Yang LP, Fitzgerald AL, Osman A, Woo SH, Myers JN, et al. The p53-Reactivating Small Molecule RITA Induces Senescence in Head and Neck Cancer Cells. *PLoS One* 2014; **9**: e104821.
- de Boer JG. Polymorphisms in DNA repair and environmental interactions. *Mutat Res* 2002; **509**: 201-10.
- Song X, Sturgis EM, Jin L, Wang Z, Wei Q, Li G. Variants in nucleotide excision repair core genes and susceptibility to recurrence of squamous cell carcinoma of the oropharynx. *Int J Cancer* 2013; **133**: 695-704.
- Boehler C, Gauthier LR, Mortusewicz O, Biard DS, Saliou J-M, Bresson A, et al. Poly (ADP-ribose) polymerase 3 (PARP3), a newcomer in cellular response to DNA damage and mitotic progression. *Proc Natl Acad Sci* 2011; **108**: 2783-88.
- Zhai X, Zhao H, Liu Z, Wang L-E, El-Naggar AK, Sturgis EM, et al. Functional variants of the NEIL1 and NEIL2 genes and risk and progression of squamous cell carcinoma of the oral cavity and oropharynx. *Clin Cancer Res* 2008; **14**: 4345-52.

Diffusion tensor MR microscopy of tissues with low diffusional anisotropy

Franci Bajd^{1,2}, Carlos Mattea¹, Siegfried Stapf¹, Igor Sersa²

¹ TU Ilmenau, Institute of Physics, Fachgebiet Technische Physik II, Ilmenau, Germany

² Jožef Stefan Institute, Ljubljana, Slovenia

Radiol Oncol 2016; 50(2): 175-187.

Received 27 August 2015

Accepted 8 February 2016

Correspondence to: Igor Sersa, Ph.D., Jožef Stefan Institute, Jamova 39, SI-1000 Ljubljana, Slovenia. Fax: + 386 1 477 3191;

E-mail: igor.sersa@ijs.si

Disclosure: No potential conflicts of interest were disclosed.

Background. Diffusion tensor imaging exploits preferential diffusional motion of water molecules residing within tissue compartments for assessment of tissue structural anisotropy. However, instrumentation and post-processing errors play an important role in determination of diffusion tensor elements. In the study, several experimental factors affecting accuracy of diffusion tensor determination were analyzed.

Materials and methods. Effects of signal-to-noise ratio and configuration of the applied diffusion-sensitizing gradients on fractional anisotropy bias were analyzed by means of numerical simulations. In addition, diffusion tensor magnetic resonance microscopy experiments were performed on a tap water phantom and bovine articular cartilage-on-bone samples to verify the simulation results.

Results. In both, the simulations and the experiments, the multivariate linear regression of the diffusion-tensor analysis yielded overestimated fractional anisotropy with low SNRs and with low numbers of applied diffusion-sensitizing gradients.

Conclusions. An increase of the apparent fractional anisotropy due to unfavorable experimental conditions can be overcome by applying a larger number of diffusion sensitizing gradients with small values of the condition number of the transformation matrix. This is in particular relevant in magnetic resonance microscopy, where imaging gradients are high and the signal-to-noise ratio is low.

Key words: microscopy; diffusion tensor imaging; anisotropy; signal-to-noise ratio; cartilage

Introduction

Diffusion tensor imaging (DTI) is a widely used magnetic-resonance imaging (MRI) technique, which enables noninvasive assessment of structural integrity of fibrous tissues with a high degree of anisotropy, such as brain white matter and myocardium.^{1,2} Specifically, the technique could be exploited for a dynamical follow-up of minor anisotropy alternations due to tissue structural changes arising during progressive disease development, such as schizophrenia³, multiple sclerosis⁴ and myocardium infarct.⁵ The method is gaining clinical interest also in applications to tissues with less expressive anisotropy or highly localized compartments with increased level of fiber alignment,

such as articular cartilage^{6,7}, which is a relatively thin tissue with a thickness of up to few millimeters and has a depth-dependent collagen fiber architecture. In DTI, the basic assumption is that diffusive motion of spin bearing particles within the tissue is determined by an alignment of tissue fibers; hence their diffusional anisotropy directly corresponds to anisotropy of the restrictive fibers. The method basically consists of an imaging part, usually employing spin-echo based MRI pulse sequences⁸, to which a pair of diffusion sensitizing gradients (DSG) is added in order to encode magnetic resonance (MR) signal of spin bearing particles with diffusive motion, resulting into a diffusion-attenuated MR signal. In order to obtain sufficient information on anisotropy of diffusive

motion, DSG must be applied in at least six non-coplanar directions to determine six independent elements of the laboratory-frame diffusion tensor.⁹ In the DT-MRI analysis, diffusion anisotropy is calculated by transforming the laboratory-frame diffusion tensor into the principal frame of reference using diagonalization.¹⁰

Determination of diffusion anisotropy can be biased due to instrumentation imperfections⁹, such as non-optimally calibrated DSG, and due to post-processing errors.^{11,12} It was shown, that a number and directionality of the applied DSG configuration play an important role in a noise propagation in DTI post-processing analysis.¹² Specifically, noise propagation in DTI, resulting to noise-induced rotational variance of diffusion tensor ellipsoid, can be reduced by decreasing a condition number (CN) of the b-matrix¹² as well as by increasing the signal-to-noise ratio (SNR).¹¹ Therefore, attempts were made to find a robust measure for diffusion anisotropy, such as the lattice index.¹³ Among all the proposed measures fractional anisotropy (FA) became commonly accepted. Accuracy in determination of diffusion tensor is of a great importance in biomedical imaging as falsely measured tissue anisotropy could lead to clinical misinterpretations and inappropriate treatment decisions.¹⁴

Reliability of the DTI method can be efficiently tested either by using perfectly aligned fiber phantoms with an a priori known anisotropy, yielding anisotropic diffusion along the preferential fiber orientation^{15,16}, or by using completely isotropic materials. In both cases, overestimated apparent anisotropy could arise as an undesirable consequence of the DTI analysis. A fundamental question is, how the DTI factors, specifically SNR and a choice of a DSG configuration, influence accuracy of a diffusion tensor determination. This issue is specifically important in diffusion tensor magnetic resonance microscopy (DT-MRM), in which SNR is usually low due a high diffusion weighting and due to a small voxel size, respectively. The effect of low SNR is more pronounced in some biomaterials with anisotropic diffusion that exhibit short T_2 relaxation time, as for example articular cartilage.^{17,18}

The main motivation for this study is analysis of factors influencing diffusion anisotropy in DT-MRM signal post-processing. The study is organized into two parts. In the first part, the effect of noise propagation from synthetic raw DTI data to the diffusion tensor eigenvalues is examined theoretically for different DSG configurations: selected commonly used, random and isotropic DSG configurations. In the second part, the theoretical

results are verified experimentally. DT-MRM was performed for two different materials, tap water with isotropic diffusion and bovine articular cartilage-on-bone samples before and after compression. The study is in particular focused to unfavorable experimental conditions that often arise in DT-MRM and could result in biased diffusional anisotropy.

Materials and methods

Theoretical background and simulations

Single-voxel DTI data of an isotropic medium with a diffusion constant equal to D_0 were generated as a N_{DSG} -dimensional column vector (N_{DSG} being the number of DSG directions) containing normalized magnitude MR signal intensities

$$I \equiv \mathcal{S}(\text{DA}, \text{SNR}) = \text{DA}(G_0) \cdot \text{NF}(\text{SNR}), \quad n = 1, \dots, N_{\text{DSG}}, \quad [1]$$

where $\text{DA}(G_0) = e^{-\gamma^2 G_0^2 \delta^2 (\Delta - \delta/3) D_0}$ is referred to as *diffusion attenuation*¹⁹ and $\text{NF}(\text{SNR}) = \left(1 + \frac{2.0\zeta_n - 1.0}{\text{SNR}}\right)$

is a *noise factor*. Here, γ is gyromagnetic ratio, G_0

is DSG amplitude, δ is duration of an individual DSG pulse, Δ is time-separation between the two DSG pulses and SNR is signal-to-noise ratio in the pulsed field gradient (PFG) pulse sequence. The noise was introduced to the generated DTI data by a N_{DSG} -dimensional noise vector ζ , of which components $\zeta_n \in [0, 1]$ are uniformly distributed random numbers, which are included in the noise factor. Seventeen commonly used DSG directions¹², presented in Table 1, as well as different random and isotropic DSG directions with $6 \leq N_{\text{DSG}} \leq 300$ were considered. With random DSG configurations, directions of diffusion sensitizing gradients were modeled as

$$G_n = G_0 (\xi_{x,n}, \xi_{y,n}, \xi_{z,n}), \quad n = 1, \dots, N_{\text{DSG}} \quad [2]$$

where $\xi_{x,n} \in [0, 1]$, $\xi_{y,n} \in [0, 1]$ and $\xi_{z,n} \in [0, 1]$ are three evenly distributed random numbers with $\sqrt{\xi_{x,n}^2 + \xi_{y,n}^2 + \xi_{z,n}^2} = 1$. Isotropic DSG configurations were obtained from the corresponding random DSG configurations (for each N_{DSG}) by numerically minimizing their average Coulomb-like interaction energy (*i.e.*, the Thompson's problem²⁰)

$$E_{N_{\text{DSG}}} = \frac{1}{N_{\text{DSG}}} \sum_{n < m}^{N_{\text{DSG}}} \frac{1}{|G_n - G_m|}, \quad [3]$$

using Monte Carlo simulation approach.²¹ For each DSG, its transformation matrix b_n was calculated using definition

$$b_n(t) = \int_0^t \mathbf{k}_n(t') \otimes \mathbf{k}_n(t') dt', \quad [4]$$

where

$$\mathbf{k}_n(t') = \gamma \int_0^{t'} \mathbf{G}_{n,eff}(t'') dt'' \quad [5]$$

and the effective gradient for a spin echo-like DTI pulse sequence including a pair of DSG gradients is equal to

$$\mathbf{G}_{n,eff}(t'') = \begin{cases} \mathbf{G}_n, & 0 \leq t'' \leq \delta \\ -\mathbf{G}_n, & \Delta \leq t'' \leq \Delta + \delta \end{cases} \quad [6]$$

The 3 x 3 b -value matrix \mathcal{b}_n defined in Eq. 4 has only six different elements that can be arranged into a 1 x 6 row vector with elements $\mathcal{b}_n = (b_{n,xx}, b_{n,yy}, b_{n,zz}, 2b_{n,xy}, 2b_{n,xz}, 2b_{n,yz})$. The row vectors can be further arranged into a $N_{DSG} \times 6$ DTI transformation matrix \mathcal{b} . A condition number of the matrix \mathcal{b} was calculated as $CN = \|\mathcal{b}\| \|\mathcal{b}^{-1}\|$. The components of the diffusion tensor in the laboratory frame of reference, $\mathcal{D} = (D_{xx}, D_{yy}, D_{zz}, D_{xy}, D_{xz}, D_{yz})$, were calculated by solving an over-determined system of equations, $\mathcal{b}\mathcal{D} = -\ln\{\mathbf{I}\}$, in a form of

$$\mathcal{D} = -(\mathcal{b}^T \mathcal{b})^{-1} \mathcal{b}^T \ln\{\mathbf{I}\}. \quad [7]$$

The laboratory-frame diffusion tensor,

$$D_{LAB} = \begin{pmatrix} D_{xx} & D_{xy} & D_{xz} \\ D_{xy} & D_{yy} & D_{yz} \\ D_{xz} & D_{yz} & D_{zz} \end{pmatrix}, \quad [8]$$

was then diagonalized to the principal-axis-frame diffusion tensor

$$D_{PRINC} = \begin{pmatrix} D_1 & 0 & 0 \\ 0 & D_2 & 0 \\ 0 & 0 & D_3 \end{pmatrix}. \quad [9]$$

The diffusion tensor eigenvalues D_1 , D_2 and D_3 were used to calculate the average diffusion coefficient, $ADC = \frac{1}{3}(D_1 + D_2 + D_3) = Tr[D_{PRINC}] = Tr[D_{LAB}]$, and the fractional anisotropy, defined as¹⁰

$$FA = \sqrt{\frac{3(D_1 - ADC)^2 + (D_2 - ADC)^2 + (D_3 - ADC)^2}{2(D_1^2 + D_2^2 + D_3^2)}}. \quad [10]$$

For each DSG configuration, either taken from the Table 1¹² or calculated as random or isotropic directions, diffusion tensor eigenvalues as well as

TABLE 1. A list of the analyzed commonly used diffusion sensitizing gradients (DSG) configurations in DTI, adopted from¹², along with the corresponding values of N_{DSG} , condition number(CN) and P .

#	Scheme name	N_{DSG} [1]	CN [1]	P [%]
1	Tetrahedral	6	9.148	16.53
2	Cond 6	6	5.984	14.19
3	Decahedral	10	2.748	10.70
4	Jones noniso	7	2.560	12.13
5	Dual-gradient	6	2.000	11.44
6	Jones 10	10	1.624	9.67
7	Jones 20	20	1.615	8.10
8	Jones 30	30	1.594	7.16
9	Papadakis	12	1.587	9.29
10	Jones 6	6	1.583	11.04
11	Muthupallai	6	1.581	11.11
12	Tetraortho	7	1.527	10.68
13	DSM 6	6	1.323	11.41
14	DSM 10	10	1.324	10.02
15	DSM 20	20	1.668	8.43
16	DSM 30	30	1.430	7.45
17	DSM 40	40	1.401	6.87

CN = condition number

the corresponding ADC and FA were calculated as a function of DA ($0 \leq DA \leq 1$) and SNR ($1 \leq SNR \leq 100$) for $N_\varsigma = 100$ different noise vectors ς mimicking N_ς different experiments of which results were then averaged in order to reduce their randomness:

$$\bar{D}_1(DA, SNR) = \frac{1}{N_\varsigma} \sum_{\{\varsigma\}} D_1(DA, SNR, \varsigma), \quad [11]$$

$$\bar{D}_2(DA, SNR) = \frac{1}{N_\varsigma} \sum_{\{\varsigma\}} D_2(DA, SNR, \varsigma),$$

$$\bar{D}_3(DA, SNR) = \frac{1}{N_\varsigma} \sum_{\{\varsigma\}} D_3(DA, SNR, \varsigma),$$

$$\overline{ADC}(DA, SNR) = \frac{1}{N_\varsigma} \sum_{\{\varsigma\}} ADC(DA, SNR, \varsigma),$$

$$\overline{FA}(DA, SNR) = \frac{1}{N_\varsigma} \sum_{\{\varsigma\}} FA(DA, SNR, \varsigma).$$

The diffusion tensor quantities were then averaged over the characteristic window of the DA – SNR domain ($0.4 \leq DA \leq 0.6, 20 \leq SNR \leq 60$) to obtain their representative characteristic scalar values denoted as D_1, D_2, D_3, ADC and FA. For random

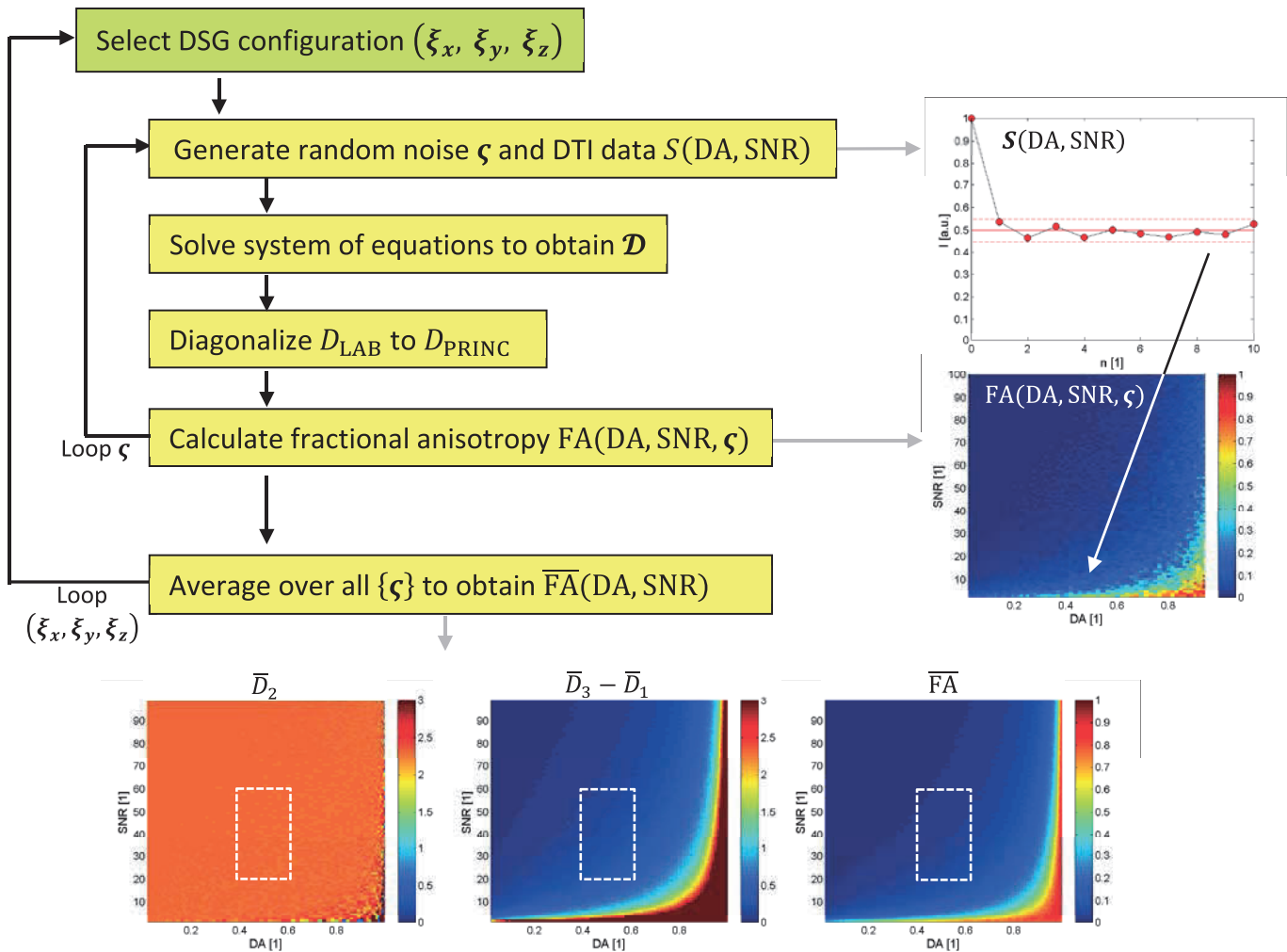


FIGURE 1. A simulation flowchart for analysis of selected commonly used and random/isotropic diffusion sensitizing gradients (DSG) configurations.

DSG configurations, a relation between CN and FA was modeled with a power-law function

$$FA = \alpha_{FA} CN^{\kappa_{FA}}, \quad [12]$$

where α_{FA} and κ_{FA} are two fitting parameters. In the simulations, water-like isotropic medium with $D_0 = 2.3 \cdot 10^{-9} \text{ m}^2 / \text{s}$ was considered.

Simulations were performed using an in-house written program, developed within the Matlab programming environment (MathWorks Inc., Natick, MA, USA). Flowcharts presenting the simulation algorithm for the simulations including DSG configurations from Table 1 and random or isotropic DSG configurations are shown in Figure 1.

Additional numerical simulations were performed in order to investigate the effect of noise propagation in tissues with low diffusional anisotropy. In these simulations, diffusion tensor in

the principal frame of reference was considered as a prolate spheroid, which was, for the sake of convenience, oriented with the largest dimension along the z-axis of the laboratory frame of reference (z_{LAB}). In this direction, non-restricted diffusion was assumed, *i.e.*, the corresponding eigenvalue was equal to D_0 while diffusion was reduced to αD_0 ($0 \leq \alpha \leq 1$) in the other two orthogonal directions. The principal-frame diffusion tensor was hence modeled as

$$D_{PRINC} = D_0 \begin{pmatrix} \alpha & 0 & 0 \\ 0 & \alpha & 0 \\ 0 & 0 & 1 \end{pmatrix}. \quad [13]$$

The primary eigenvector (corresponding to the largest eigenvalue) was equal to $p_3 = (0, 0, 1)$, while the other two eigenvectors were chosen as $p_1 = (1, 1, 0) / \sqrt{2}$ and $p_2 = (1, -1, 0) / \sqrt{2}$. The eigenvec-

tors determined the change-of-basis transformation matrix between the principal and the laboratory frame of reference:

$$P = (\mathbf{p}_1^T, \mathbf{p}_2^T, \mathbf{p}_3^T) = \begin{pmatrix} 1/\sqrt{2} & 1/\sqrt{2} & 0 \\ 1/\sqrt{2} & -1/\sqrt{2} & 0 \\ 0 & 0 & 1 \end{pmatrix}. \quad [14]$$

The transformation of the diffusion tensor into the laboratory frame of reference was calculated as $D_{\text{LAB}} = P D_{\text{PRINC}} P^{-1}$. In the case of the above-defined prolate spheroid, components of the diffusion tensor in the laboratory frame of refer-

ence were expressed by $D_{\text{LAB}}^{ij} = D_0 \sum_{k=1}^3 \tilde{\alpha}^k P^{ik} (P^{-1})^{kj}$,

where $\tilde{\alpha} = (\alpha, \alpha, 1)$. Normally distributed (Gaussian) noise was added to the MR signal intensities. For a given preset FA value and for a given DSG configuration, the results of simulations are presented by a difference between the calculated fractional anisotropy FA' and the preset fractional anisotropy FA, i.e., by FA' - FA. In addition, an orientation difference between the preset and the calculated primary eigenvector, i.e., $\Delta\theta = \arccos(\mathbf{p}_3' \cdot \mathbf{p}_3)$, is presented as well.

DT-MRM of tap water

DT-MRM experiments of a tap water phantom with a cone shape were performed on a horizontal-bore 2.35-T MRI scanner (Oxford Instruments, Abingdon, United Kingdom), equipped with microimaging accessories (Bruker, Ettlingen, Germany) and controlled by a Tecmag Apollo spectrometer (Tecmag, Houston TX, USA). The gradient system had top gradients of 0.25 T/m and slew rate of 1200 mT/m/ms. For acquisition of one-dimensional DTI profiles along cone axis, a spin-echo based 1D DT-MRM sequence was employed. For the sequence, the following imaging parameters were used: 256 acquisition points, field of view 40 mm, spatial resolution of 156 μm , dwell time 10 μs , number of averages 4 (with the half-Cyclops phase cycling scheme), echo and repetition time TE/TR = 30/1030 ms. Square-shaped DSG pulses with $G_0 = 0.157 \text{ T/m}$ and $\delta/\Delta = 3.0/20$ ms were used, yielding the corresponding diffusion attenuation equal to DA = 0.50. 1D DT-MRM was examined for isotropic DSG configurations with $N_{\text{DSG}} = 6-100$. The contribution of imaging gradients to the DTI transformation matrix was minimized using non-selective (hard) excitation RF pulses and by performing imaging in just one

dimension. As the read gradients in 1D DT-MRM were applied only during or close to MR signal acquisition, their contribution to the transformation matrix was minor and was therefore neglected. Prior to the experiments, Stejskal-Tanner plots were measured for each gradient channel. The gradient channels were then calibrated to yield a diffusion constant of water at room temperature.

DT-MRM of articular cartilage

Bovine cartilage-on-bone samples, containing an intact cartilage tissue and the underlying part of a subchondral bone, were carefully dissected from fresh stifle joints of bovine femur bones (provided by a local meat provider) using a commercially available bow saw and a dentist driller set (Meisinger, Neuss, Germany). Samples were cut into cylindrically shaped pieces with a diameter of 6 mm and with an average height of 8 mm, fitting to an NMR tube with an inner diameter of 7 mm. After dissection, the samples were washed in physiological phosphate buffer saline (PBS) and sealed into plastic bags for deep-freezing storage.²² Prior to DT-MRM experiments, each sample was allowed to spontaneously defreeze at temperature of 8°C. Then, the sample was inserted into an NMR tube and immersed into Fluorinert FC-70 (Sigma-Aldrich, Germany), which was used to prevent samples from desiccation. Compression of articular cartilage was obtained by loading a plastic indenter, positioned above the articular surface, with weight-induced pressure of $p = 0.56 \text{ MPa}$ at the indenter-cartilage interface. After the application of an external pressure, each sample was allowed for spontaneous equilibration for 2 hours.¹⁷

DT-MRM experiments on articular cartilage-on-bone samples were performed on a 7-Tesla vertical-bore superconducting magnet equipped with microimaging accessories and controlled by the Avance spectrometer (Bruker, Ettlingen, Germany). The gradient system had maximum gradients of 1 T/m and slew rate of 4000 mT/m/ms. Due to relatively fast transversal relaxation processes in cartilage tissue, DT-MRM was performed using a stimulated-echo pulse sequence. The following imaging parameters were used: imaging matrix 256 \times 128 (or 128 \times 64), field of view 20 \times 10 mm, isotropic in-plane resolution of 78 μm (or 156 μm), slice thickness 2 mm, dwell time 10 μs (or 20 μs), number of averages 32, echo and repetition time TE/TR = 40/2000 ms. A DSG configuration with $N_{\text{DSG}} = 6$ and CN = 2.618 was used.¹⁸ Square-shaped DSG pulses with $G_0 = 0.19 \text{ T/m}$ and $\delta/\Delta = 2.1/30$ ms were used,

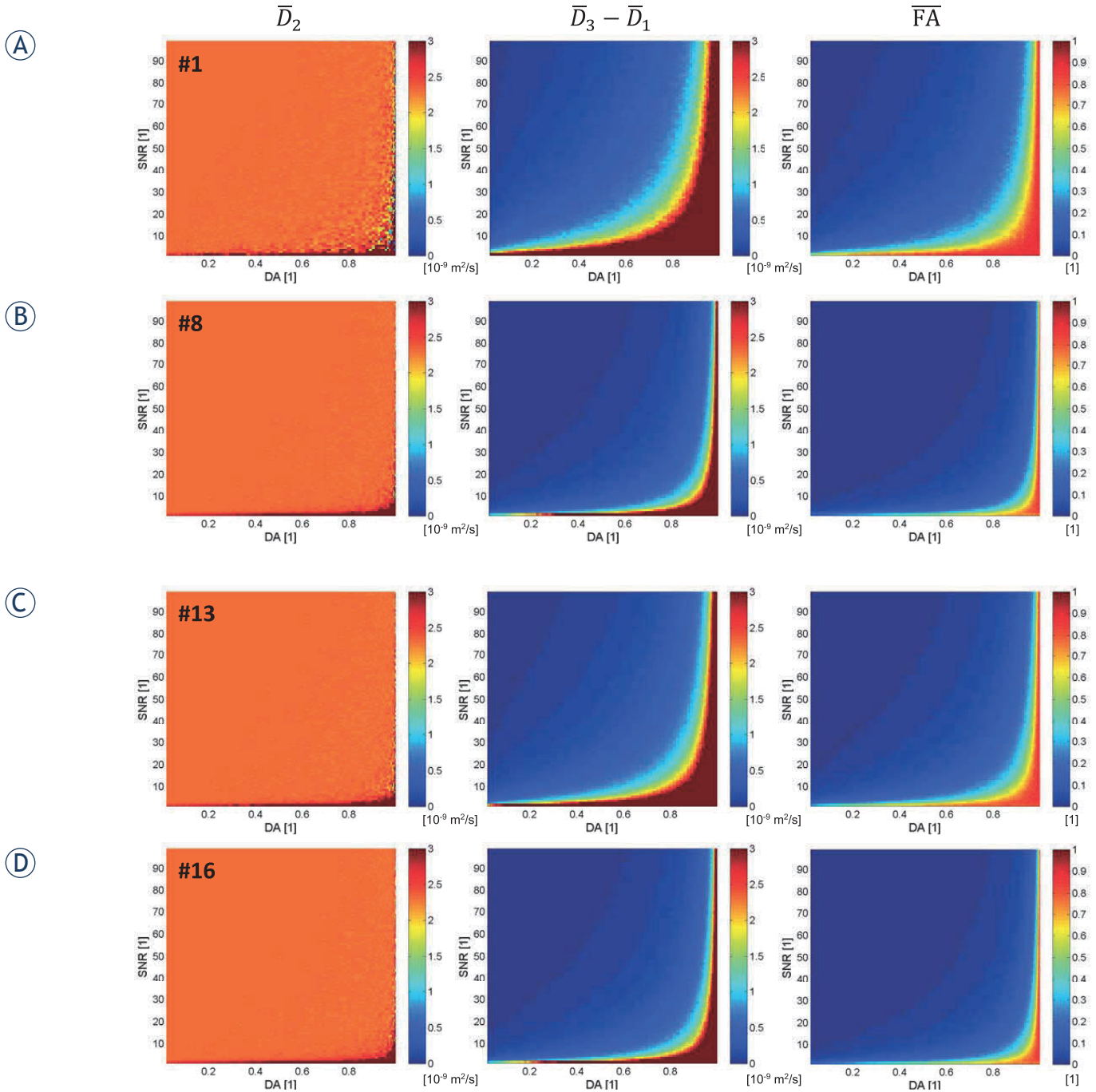


FIGURE 2. Simulated two dimensional maps of \bar{D}_2 (DA, signal-to-noise ratio [SNR]), \bar{D}_3 (DA, SNR) - \bar{D}_1 (DA, SNR) and fractional anisotropy (\overline{FA}) (DA, SNR) for four representative, commonly used diffusion sensitizing gradients (DSG) configurations from Table 1 (#1, #8, #13 and #16).

yielding the corresponding diffusion attenuation equal to $DA = 0.47$. Again, the imaging gradients (read-dephase and phase gradients) were applied immediately before MR signal acquisition in order to minimize their contribution to the transformation matrix \hat{b} . All gradients, the imaging gradients and DSG, were considered in the numerical calculation of the transformation matrix elements (according to

Eq. 4). All DT-MRM analyses were performed within the Matlab programming environment.

Results

Simulated 2D maps over the DA -SNR domain of the second largest eigenvalue \bar{D}_2 (DA, SNR), of the

difference among the smallest and the largest eigenvalue $\overline{D}_3(\text{DA,SNR}) - \overline{D}_1(\text{DA,SNR})$ and of the corresponding fractional anisotropy $\overline{\text{FA}}(\text{DA,SNR})$ for four representative DSG configurations, *i.e.*, the DSG configurations #1, #8, #13 and #16 from Table 1, are presented in Figure 2. Two of the selected DSG configurations correspond to the commonly used DSG configurations (#1 with $N_{\text{DSG}} = 6$ and #8 with $N_{\text{DSG}} = 30$ in Figure 3A,B, respectively), while the other two correspond to the DSG configurations, optimized in¹² with respect to the condition number CN (again with $N_{\text{DSG}} = 6$ and $N_{\text{DSG}} = 30$). It can be seen that the largest deviations of the studied diffusion tensor quantities from their ideal values (\overline{D}_2 from D_0 , $\overline{D}_3 - \overline{D}_1$ from 0 and $\overline{\text{FA}}$ from 0) are found at high values of DA and low values of SNR. From the result in Table 1, it is evident that region proportions P of poorly determined DT eigenvalues, *i.e.*, dark red regions in maps in Figure 2 defined by the condition $\overline{D}_3 - \overline{D}_1 > 1.3D_0 = 3 \cdot 10^{-9} \text{ m}^2/\text{s}$ decrease with a decreasing CN. The results in Table 1 also indicate that for all DSG configurations, the proportion P could be additionally decreased by increasing N_{DSG} .

Figure 3 shows DA – SNR domain-averaged values of diffusion tensor eigenvalues D_1, D_2 and D_3 (Figure 3A,B) along with the corresponding average diffusion coefficient ADC (Figure 3C,D) and fractional anisotropy FA (Figure 3E,F) as a function of CN for random DSG configurations with different $N_{\text{DSG}} = 6, 8, 10, 12, 14, 20, 30, 40, 60, 80, 100, 200$. The results are shown in two formats, *i.e.*, the calculated quantities in a log format with a broad range of condition numbers $1 < \text{CN} < 10^4$ are shown in Figure 3A,C,E, while the same quantities in a linear format with the range of $1 < \text{CN} < 10$ (zoomed gray regions of the corresponding log graphs) are shown in Figure 3B,D,F. From the graphs in Figure 4 it can be seen that random DSG configurations with low N_{DSG} and high CN overestimate the largest diffusion tensor eigenvalue and underestimate the smallest eigenvalue, while the remaining eigenvalue remains independent on CN and the equality $D_2 = D_0$ holds for a broad range of CN. Therefore, the difference $D_3 - D_1$ remains non-zero (of the order of $\lesssim 0.05D_0$) also for the smallest D_2 values. Interestingly, as the difference is symmetric with respect to D_0 , its undesired contribution is canceled in the calculation of ADC, of which values are hence only weakly scattered around D_0 in a broad range of CN. On the contrary, the symmetric difference $D_3 - D_1$ is not canceled in the calculation of FA, which thus contributes to an existence of the apparent fractional anisotropy of a generic iso-

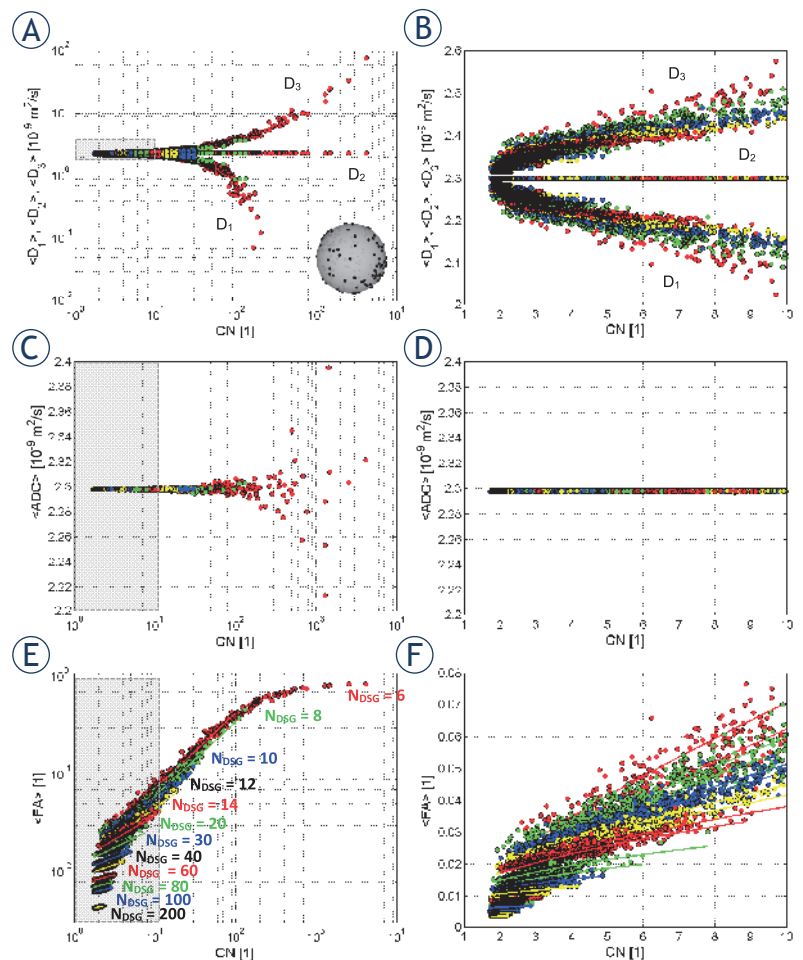


FIGURE 3. Panels on the left show simulated average values of diffusion tensor eigenvalues D_1, D_2 and D_3 (A), of average diffusion constant ADC (C) and of fractional anisotropy FA (E) as a function of condition number $1 < \text{CN} < 10^4$ for random diffusion sensitizing gradients (DSG) configurations. Panels on the right (B,D,F) display the zoomed left-side panels for condition numbers in the range $1 < \text{CN} < 10$. Solid-line curves (E,F) correspond to best fits of the model function [Eq. 12] to the simulated data. The graphical insert in panel (A) illustrates the selected random DSG configuration with $N_{\text{DSG}} = 220$.

tropic medium. With FA in the range of $1 < \text{CN} < 10$, the values of FA span range between 0.01 and 0.08. In Figure 4, the minimal $\text{CN} = 1.786$ was obtained with $N_{\text{DSG}} = 30$. Clearly, apparent fractional anisotropy is highly dependent on the condition number. Solid curves in Figure 3E,F represent best fits of the model function in Eq. 12 to the simulated FA vs. CN data calculated for each N_{DSG} independently. As can be seen from the graphs in Figure 3E,F, the model fits well to the data for $\text{CN} < 100$, while for $\text{CN} \gtrsim 100$ the model is less accurate due to saturation of $\text{FA} \rightarrow 1$.

Figure 4 shows maximal, average and minimal values of FA (Figure 4A) as well as the optimally fitting parameters of Eq. 12, *i.e.*, α_{FA} and κ_{FA} along

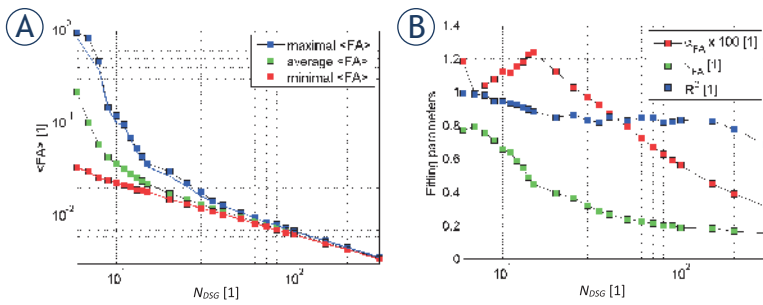


FIGURE 4. Characteristic values of the simulated correlations between FA and condition number (CN) for random diffusion sensitizing gradients (DSG) configurations as a function of N_{DSG} : maximal, average and minimal values of FA (A), best fit parameters α_{FA} , κ_{FA} and fit quality R^2 (B). The arrow designates a crossover, at which apparent fractional anisotropy drops below fractional anisotropy FA ~ 0.01 . The graphical insert in panel A illustrates the selected random DSG configuration with $N_{\text{DSG}} = 220$.

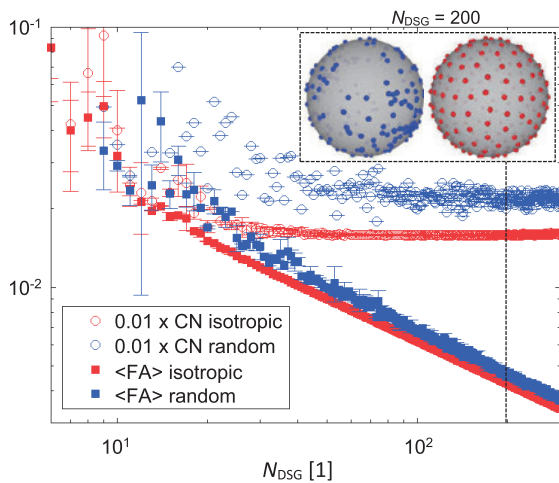


FIGURE 5. Simulated average fractional anisotropy FA (solid symbols) and the corresponding condition number CN (void symbols) as a function of N_{DSG} for random (blue symbols) and isotropic (red symbols) diffusion sensitizing gradients (DSG) configurations. The graphical insert illustrates a distribution of DSG directions in a random and an isotropic DSG configuration with $N_{\text{DSG}} = 200$.

with the corresponding values of R^2 as a function of N_{DSG} for random DSG directions (Figure 4B). The data shown in Figure 4 are taken from Figure 3E,F. From Figure 4A it can be seen that the maximal and minimal FA as well as the difference between them decrease with an increasing N_{DSG} . At $N_{\text{DSG}} \sim 40$, both, the maximal and minimal FA drop to approximately 0.01. In addition, as can be seen from Figure 4B, best fit parameters are monotonically decreasing for $N_{\text{DSG}} > 15$. However, fit quality decreases with larger N_{DSG} from $R^2 = 1$ at $N_{\text{DSG}} = 6$ to $R^2 = 0.7$ at $N_{\text{DSG}} = 300$.

Average fractional anisotropy FA (solid symbols) and the corresponding condition number

CN (void symbols) as a function of N_{DSG} for both random (blue symbols) and the corresponding isotropic (red symbols) DSG configurations, are shown in Figure 5. The data shown in Figure 5 were obtained by averaging the corresponding quantities that were calculated with two different random seeds. As can be clearly seen from the blue curves, the condition number is for random DSG configurations in the range of $2 < \text{CN} < 10$ with a plateau value of ~ 2 , while average fractional anisotropy is a monotonically decreasing function of N_{DSG} . Both CN and average fractional anisotropy values are more scattered at smaller N_{DSG} and less scattered at larger N_{DSG} . With isotropic DSG configurations (red curves), however, both average fractional anisotropy and condition number at a given N_{DSG} are comparatively smaller than with the corresponding random DSG configurations. Moreover, the condition number decreases with an increasing N_{DSG} to approximately $N_{\text{DSG}} \sim 30$, where it attains a constant plateau value of 1.59 ± 0.01 , while the average fractional anisotropy monotonically decreases with an increasing N_{DSG} . A significant drop of the average fractional anisotropy from $\text{FA} = 0.083 \pm 0.031$ at $N_{\text{DSG}} = 6$ to $\text{FA} = 0.011 \pm 0.000$ at $N_{\text{DSG}} = 30$ is noticed for both isotropic as well as random DSG configurations.

Figure 6 depicts results of numerical simulations that were performed with three different preset fractional anisotropies (FA = 0.0, 0.1, 0.3) and with two different SNRs (SNR = 5, 30). In the simulations random and isotropic DSG configurations with $N_{\text{DSG}} = 6-100$ were considered, while diffusion attenuation was held constant by setting $G_0 = 0.3$ T/m and $\delta/\Delta = 2/15$ ms. For each DSG configuration, the results are displayed as an average of $N_c = 100$ simulation runs of different noise vectors. As can be seen, the curves of $\text{FA}' - \text{FA}$ and the curves of $\Delta\theta$ are decreasing with an increasing N_{DSG} and SNR; both curve types are decreasing also with an increasing preset FA. Interestingly, the difference of $\text{FA}' - \text{FA}$ is largest with small $N_{\text{DSG}} \leq 10$ with both random and isotropic DSG configurations (irrespective of the preset FA value and SNR).

Experimental results of a tap water phantom, examined by 1D DT-MRM are shown in Figure 7 with stack plots of 1D profiles of diffusion tensor quantities (ADC, FA, D_1 , D_2 and D_3) as a function of N_{DSG} . The 1D profiles were measured with isotropic DSG configurations (the same configurations as in Figure 6) along the axis of the cone-shaped phantom. As can be seen from the 2D MR image (without slice selection) of the phantom and the corresponding 1D intensity profile along the phantom

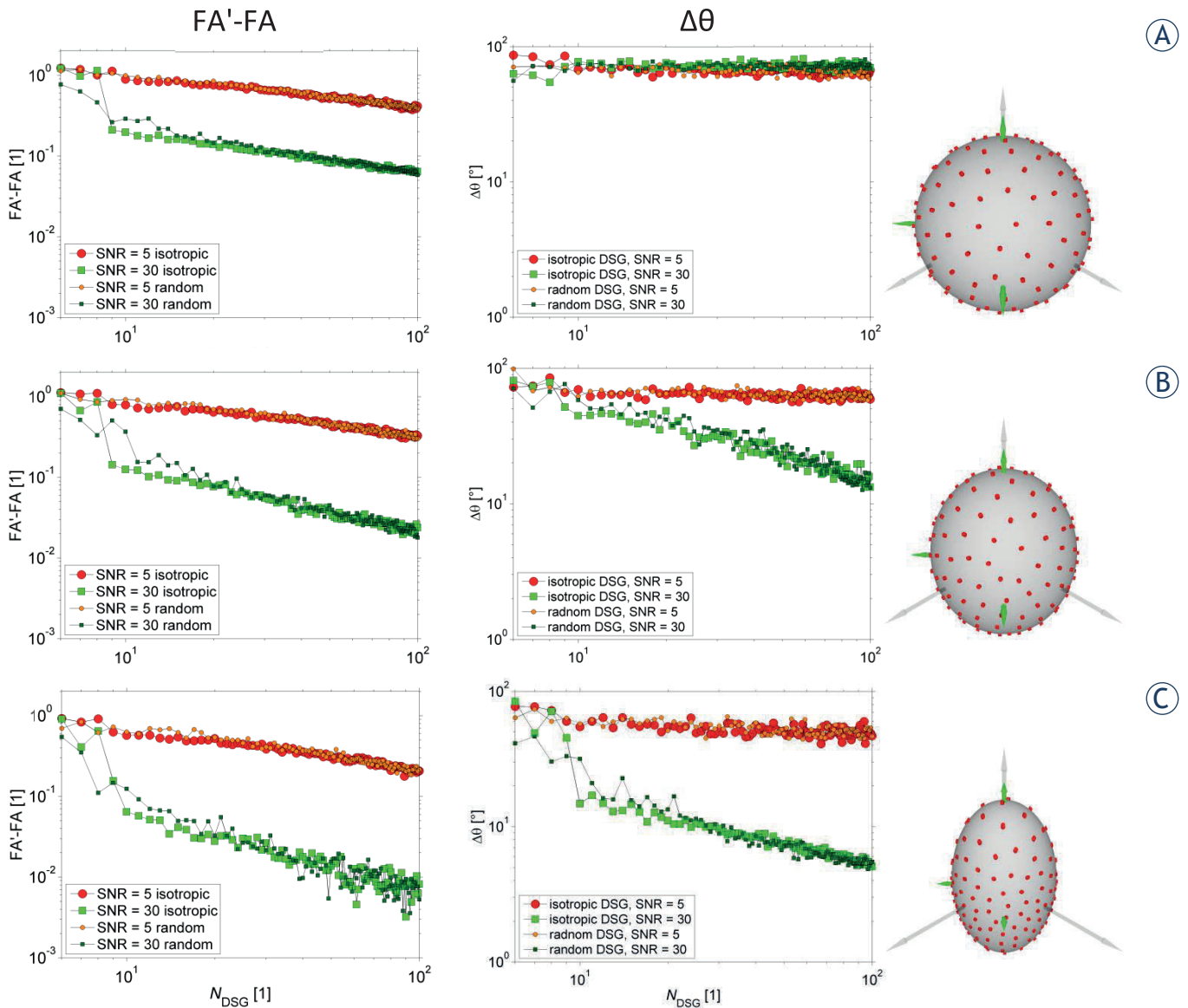


FIGURE 6. The results of numerical simulations with three different fractional anisotropy (FA) values: 0, 0.1, and 0.3 for isotropic (FA = 0) vs. anisotropic (FA = 0.1, 0.3) case.

axis, SNR decreases monotonically towards the tip of the cone-shaped phantom. From the stack plots it can be seen that diffusion tensor quantities are biased in the phantom regions with poor SNR. The results can be improved by increasing N_{DSG} . This can be well seen in the stack plot of FA, where FA is the lowest in the encircled region (FA < 0.03) corresponding to $N_{\text{DSG}} \gtrsim 20$ and the central phantom region with high SNR.

Figure 8 shows the experimental DT-MRM results of two bovine cartilage-on-bone samples, *i.e.*, maps of D_1 , D_2 and D_3 as well as the corresponding maps of ADC and FA, obtained before and after its compression with $p = 0.56$ MPa. The maps were cal-

culated from the corresponding magnitude MR images obtained with an isotropic in-plane resolution of either $78 \mu\text{m}$ (Figure 8A) or $156 \mu\text{m}$ (Figure 8B). In Figure 8 with the compressed sample, three various regions of interest (ROI₁-ROI₃) are delineated, from which SNR was determined. While ROI₁ designates the indenter region (providing no MR signal) for background noise determination, ROI₂ and ROI₃ designate two regions of weakly and fully compressed cartilage, respectively. The corresponding SNR values were in the higher-resolution MR images equal to SNR₂ = 29 and SNR₃ = 4, while they were equal to SNR₂ = 33 and SNR₃ = 6 in the lower-resolution MR images. Average values

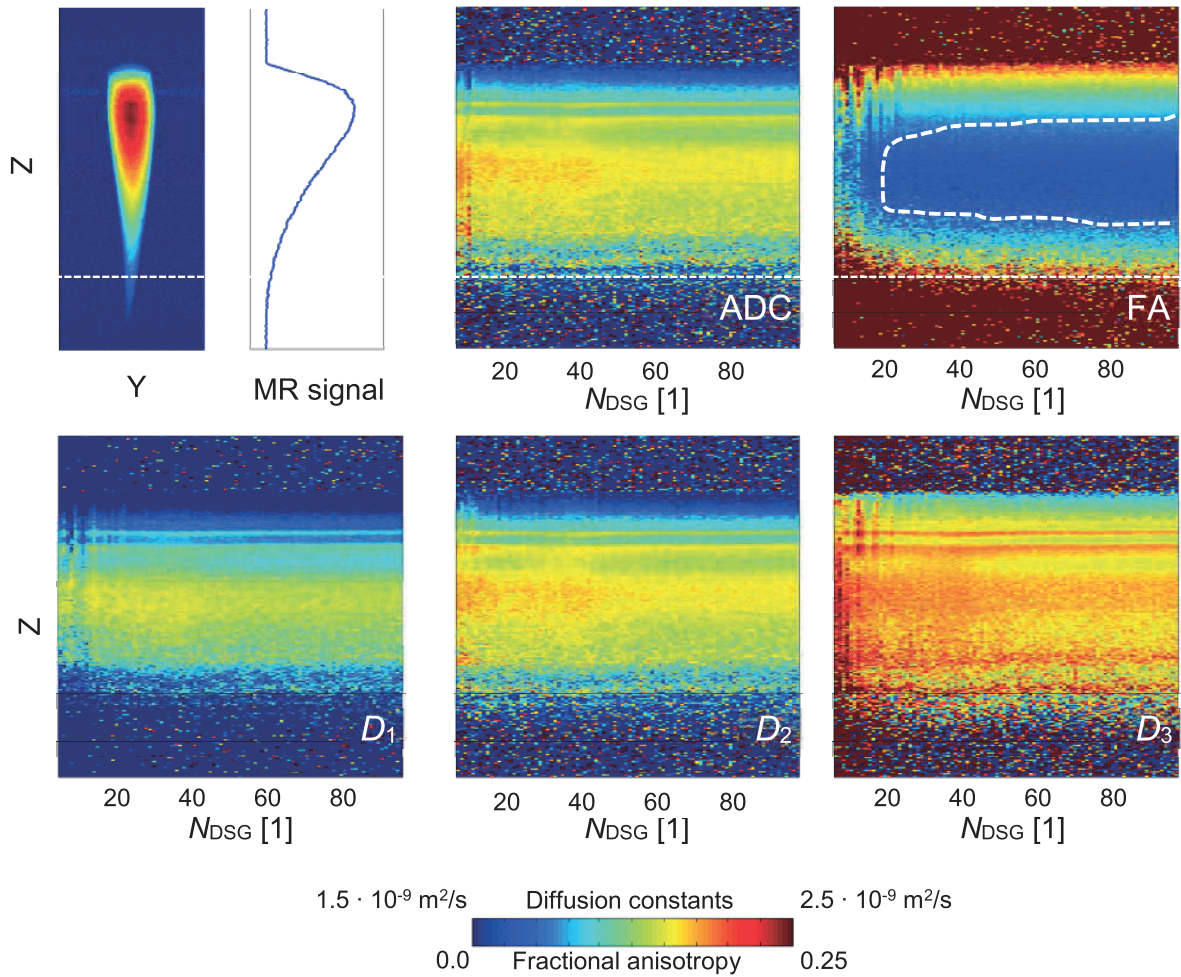


FIGURE 7. Experimental 1D DT-MRM results of the cone-shaped water phantom: 2D MR image of the phantom with the corresponding signal-to-noise ratio (SNR) 1D profile along the phantom axis (top left) and stack plots of the diffusion tensor quantities (D_1 , D_2 , D_3 , average diffusion coefficient [ADC] and FA) as 1D profiles as a function of N_{DSG} . Isotropic diffusion sensitizing gradients (DSG) configurations were used. The white dotted curve depicts the region with noticeably reduced fractional anisotropy.

TABLE 2. Average values of average diffusion coefficient (ADC) and fractional anisotropy (FA) in three different regions of an uncompressed and compressed cartilage sample obtained with two different spatial resolutions

	Higher resolution (78 μm)		Lower resolution (156 μm)	
	ADC [10^{-9} m ² /s]	FA [1]	ADC [10^{-9} m ² /s]	FA [1]
Uncompressed cartilage	0.99±0.13	0.27±0.13	1.12±0.14	0.14±0.08
Compression zone	0.63±0.42	0.87±0.27	1.01±0.82	0.82±0.23
Liquid droplet	1.35±0.11	0.24±0.06	1.34±0.19	0.11±0.04

ADC = average diffusion coefficient; FA = fractional anisotropy

of ADC and FA in three different regions (uncompressed cartilage, compression zone, liquid expelled from the cartilage tissue) of uncompressed and compressed cartilage obtained with two different spatial resolutions are given in Table 2.

Discussion

The aim of this study is to analyze the effect of the signal-to-noise ratio and DSG configuration on noise propagation in the DT-MRM post-processing analysis for the isotropic (FA = 0) as well as for anisotropic case (FA > 0). The principal findings of the study are: i) noise propagation in the DT-MRM analysis is manifested in an increased deviation of diffusion tensor eigenvalues; ii) deviations of diffusion tensor eigenvalues result to an overestimation of fractional anisotropy, while the average diffusion coefficient remains unchanged; iii) fractional anisotropy bias could be reduced by increasing SNR and by optimizing a DSG configuration to a small condition number at a large number of DSG directions.

The analysis of numerical simulations is based on correlating the diffusion tensor quantities of

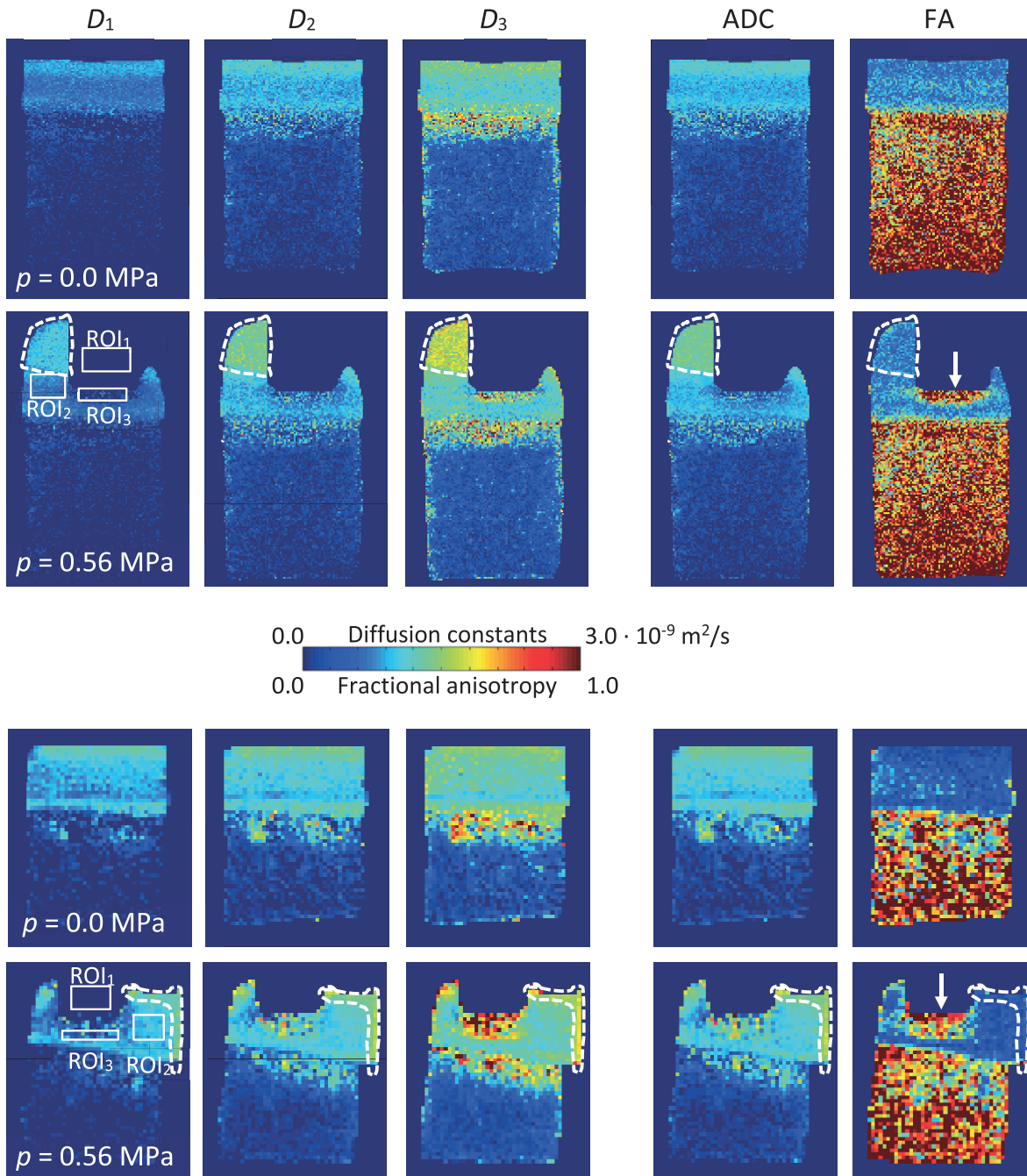


FIGURE 8. Experimental DT-MRM results of articular cartilage-on-bone samples in a form of 2D maps of D_1 , D_2 , D_3 , average diffusion coefficient (ADC) and fractional anisotropy (FA). The maps were obtained with a spatial resolution of either 78 μm (A) or 156 μm (B). Solid white boxes indicate three different ROI regions for signal-to-noise ratio (SNR) determination, while dashed white lines encircle droplets of liquid expelled from the cartilage tissue. White arrows denote the compression zone.

isotropic medium with the condition number of the transformation matrix and the number of DSG directions. It was evidently shown (Figures 3-5) that the extent of the fractional anisotropy overestimation is dependent of the both parameters. Interestingly, noise propagation with random DSG

configurations appears in a form of a symmetric deviation of the largest and the smallest diffusion tensor eigenvalue from the expected value of D_0 (Figure 3B), while the second diffusion tensor eigenvalue remains practically unchanged over the entire range of condition numbers. The deviation

contributes to an apparent fractional anisotropy considerably, while the deviation is canceled in the calculation of the average diffusion coefficient.

With random DSG configurations, an average fractional anisotropy FA highly correlates with a condition number, which is consistent with *et al.*¹² The minimal values of FA were obtained with the smallest values of the condition number ($1 < CN < 2$ in Figure 3F) corresponding to nearly isotropic DSG configurations, which is in agreement with the results of the study by Batchelor *et al.*²³ This is evident from comparison of minimal FA as a function of N_{DSG} with random DSG configurations (Figure 4A) and of FA as a function of N_{DSG} with isotropic DSG configurations (Figure 5). However, high values of FA correspond to DSG configurations with one or more preferential directions around which DSG directions are clustered. From the results of simulations, it is also evident that the apparent fractional anisotropy decreases with a large number of DSG directions. Namely, the difference between the maximal and the minimal fractional anisotropy in Figure 4A monotonically decreases with an increasing number of DSG directions. The decrease is also associated with a reduction of the corresponding best fit parameters and the fit quality R^2 (Figure 4B).

Fractional anisotropy overestimation in isotropic water phantom was studied by DT-MRM only in 1D due to a required large set of isotropic DSG configurations with different N_{DSG} . The experiments were performed in 1D to reduce the total acquisition time and for the phantom cone-shaped water-filled sample was used to obtain continuously decreasing SNR along the phantom axis. In 2D DT-MRM of articular cartilage, SNR was reduced additionally due to a faster transversal relaxation and a reduced voxel size, which resulted into an overestimation of fractional anisotropy. The measured values listed in Table 2 are somewhat larger than those in literature.¹⁷ The reported fractional anisotropy values in the uncompressed cartilage are equal to FA ~ 0.08 in the tangential zone close to the articular surface, FA ~ 0.05 in the intermediate zone with disordered collagen fibers and FA ~ 0.14 in the radial zone close to the cartilage-bone interface, while after compression fractional anisotropy in the compression zone increases to FA ~ 0.14 and remained unaltered in other zones. A discrepancy between the measured and the reported values can be attributed mostly to the unfavorable SNR conditions. SNR was the lowest in the compression zone, on account of water redistribution from the zone

to the articular surface.²⁴ However, the measured fractional anisotropy values in the subchondral bone region were close to unity, which is in an agreement with another high-field DT-MRM study of articular cartilage.²⁵

In comparison to conventional MRI, in MRM, noise has additional origins. Firstly, SNR is usually low due to a much smaller voxel size. Secondly, in MRM imaging gradients are due to an increased spatial resolution large, which in turn contribute to their interaction with DSG. Interaction between DSG and possible background gradients is possible as well. If the contributions are neither compensated by flipping the signs of DSG on alternate averages⁹ nor properly considered in the calculation of transformation matrix elements according to Eq. 4, variations of the diffusion attenuated MR signal within an individual voxel could be misinterpreted as a noise which could lead to an overestimated fractional anisotropy. SNR can be improved by optimizing magnetization recovery during each repetition time. The echo time, however, should be set as a compromise between two competing effects, diffusion weighting that increases with the echo time and transversal relaxation that decreases with it.

A limitation of the study is that the simulations of anisotropic diffusion were performed only with two different SNR values. However, the selected SNRs were taken from DT-MRM experiment on articular cartilage presented in this study. Another limitation of the study is that the experiments on the water phantom were performed only in one dimension to save experimental time and to thus enable testing of more DSG configurations. The one dimensional DT-MRM approach would be difficult to apply with cartilage samples due to the tissue heterogeneity, which was even more pronounced after the cartilage compression.

Conclusions

In this study a possible overestimation of fractional anisotropy in DT-MRM was analyzed. It was shown by means of numerical simulations and DT-MRM experiments on the isotropic water phantom and low-anisotropy bovine cartilage-on-bone samples that noise propagation from raw data to diffusion tensor eigenvalues can be efficiently reduced by applying DSG configurations with small condition numbers and large numbers of DSG directions.

References

1. Assaf Y, Pasternak O. Diffusion tensor imaging (DTI)-based white matter mapping in brain research: A review. *J Mol Neurosci* 2008; **34**: 51-61.
2. Axel L, Wedeen VJ, Ennis DB. Probing dynamic myocardial microstructure with cardiac magnetic resonance diffusion tensor imaging. *J Cardiovas Magn Res* 2014; **16**: 89.
3. Kubicki M, Westin CF, McCarley RW, Shenton ME. The application of DTI to investigate white matter abnormalities in schizophrenia. *Ann Ny Acad Sci* 2005; **1064**: 134-48.
4. Roosendaal SD, Geurts JJ, Vrenken H, Hulst HE, Cover KS, Castelijns JA, et al. Regional DTI differences in multiple sclerosis patients. *NeuroImage* 2009; **44**: 1397-403.
5. Wu EX, Wu Y, Nicholls JM, Wang J, Liao S, Zhu S, et al. MR diffusion tensor imaging study of postinfarct myocardium structural remodeling in a porcine model. *Magn Reson Med* 2007; **58**: 687-95.
6. Filidoro L, Dietrich O, Weber J, Rauch E, Oerther T, Wick M, et al. High-resolution diffusion tensor imaging of human patellar cartilage: Feasibility and preliminary findings. *Magn Reson Med* 2005; **53**: 993-8.
7. Pierce DM, Trobin W, Raya JG, Trattng S, Bischof H, Glaser C, et al. DT-MRI based computation of collagen fiber deformation in human articular cartilage: a feasibility study. *Ann Biomedical Eng* 2010; **38**: 2447-63.
8. Basser PJ, Mattiello J, LeBihan D. Estimation of the effective self-diffusion tensor from the NMR spin echo. *J Magn Reson Series B* 1994; **103**: 247-54.
9. Basser PJ, Jones DK. Diffusion-tensor MRI: theory, experimental design and data analysis - a technical review. *NMR Biomed* 2002; **15**: 456-67.
10. Callaghan PT. Translational dynamics and magnetic resonance. New York: Oxford University Press; 2011.
11. Bastin ME, Armitage PA, Marshall I. A theoretical study of the effect of experimental noise on the measurement of anisotropy in diffusion imaging. *Magn Reson Imaging* 1998; **16**: 773-85.
12. Skare S, Hedehus M, Moseley ME, Li TQ. Condition number as a measure of noise performance of diffusion tensor data acquisition schemes with MRI. *J Magn Reson* 2000; **147**: 340-52.
13. Pierpaoli C, Basser PJ. Toward a quantitative assessment of diffusion anisotropy. *Magn Reson Med* 1996; **36**: 893-906.
14. Jones DK, Knosche TR, Turner R. White matter integrity, fiber count, and other fallacies: the do's and don'ts of diffusion MRI. *NeuroImage* 2013; **73**: 239-54.
15. Farrher E, Kaffanke J, Celik AA, Stöcker T, Grinberg F, Shah NJ. Novel multisection design of anisotropic diffusion phantoms. *Magn Reson Imaging* 2012; **30**: 518-26.
16. Hellerbach A, Schuster V, Jansen A, Sommer J. MRI phantoms - are there alternatives to agar? *PLoS one* 2013; **8**: e70343.
17. de Visser SK, Crawford RW, Pope JM. Structural adaptations in compressed articular cartilage measured by diffusion tensor imaging. *Osteoarthritis Cartilage* 2008; **16**: 83-9.
18. Deng X, Farley M, Nieminen MT, Gray M, Burstein D. Diffusion tensor imaging of native and degenerated human articular cartilage. *Magn Reson Imaging* 2007; **25**: 168-71.
19. Kuchel PW, Pages G, Nagashima K, Velan S, Vijayaragavan V, Nagarajan V, et al. Stejskal-tanner equation derived in full. *Concept Magn Reson A* 2012; **40A**: 205-14.
20. Altschuler EL, Williams TJ, Ratner ER, Tipton R, Stong R, Dowla F, et al. Possible global minimum lattice configurations for Thomson's problem of charges on a sphere. *Phys Rev Lett* 1997; **78**(14): 2681-2685.
21. Press WH. *Numerical recipes in C : the art of scientific computing*. 2nd ed. Cambridge Cambridgeshire ; New York: Cambridge University Press; 1992.
22. Rössler E, Mattea C, Stapf S. NMR dispersion investigations of enzymatically degraded bovine articular cartilage. *Magn Reson Med* 2015; **73**: 2005-14.
23. Batchelor PG, Atkinson D, Hill DLG, Calamante F, Connelly A. Anisotropic noise propagation in diffusion tensor MRI sampling schemes. *Magn Reson Med* 2003; **49**: 1143-51.
24. Greene GW, Zappone B, Banquy X, Lee DW, Söderman O, Topgaard D, et al. Hyaluronic acid-collagen network interactions during the dynamic compression and recovery of cartilage. *Soft Matter* 2012; **8**: 9906-14.
25. Raya JG, Melkus G, Dietrich O, et al. Multiparametric characterization of healthy and diseased articular cartilage at 17.6T: Early results. *Proc Intl Soc Mag Reson Med* 2008; **16**: 330.

The prognostic value of whole blood *SOX2*, *NANOG* and *OCT4* mRNA expression in advanced small-cell lung cancer

Eva Sodja¹, Matija Rijavec¹, Ana Koren¹, Aleksander Sadikov², Peter Korošec¹, Tanja Cufer¹

¹ University Clinic Golnik, Golnik, Slovenia

² University of Ljubljana, Faculty of Computer and Information Science, Ljubljana, Slovenia

Radiol Oncol 2016; 50(2): 188-196.

Received 25 February 2015

Accepted 11 June 2015

Correspondence to: Eva Sodja, University Clinic Golnik, Golnik 36, 4204 Golnik, Slovenia. Phone: +386 4 25 69 433; Fax: +386 4 25 69 162; E-mail:eva.sodja@klinika-golnik.si

Disclosure: No potential conflicts of interest were disclosed.

Background. The data on expression and clinical impact of cancer stem cell markers *SOX2*, *NANOG* and *OCT4* in lung cancer is still lacking. The aim of our study was to compare *SOX2*, *NANOG* and *OCT4* mRNA expression levels in whole blood between advanced small-cell lung cancer (SCLC) patients and healthy controls, and to correlate mRNA expression with progression-free survival (PFS) after first-line chemotherapy and overall survival (OS) in advanced SCLC patients.

Patients and methods. 50 advanced SCLC patients treated with standard chemotherapy and followed at University Clinic Golnik, Slovenia, between 2009 and 2013 were prospectively included. *SOX2*, *NANOG* and *OCT4* mRNA expression levels were determined using TaqMan qPCR in whole blood collected prior to chemotherapy. Whole blood of 34 matched healthy individuals with no cancerous disease was also tested.

Results. *SOX2* mRNA expression was significantly higher in whole blood of SCLC patients compared to healthy controls ($p = 0.006$). Significant correlation between *SOX2* mRNA expression levels and the number of distant metastatic sites was established ($p = 0.027$). In survival analysis, patients with high *SOX2* expression had shorter OS ($p = 0.017$) and PFS ($p = 0.046$). In multivariate Cox analysis, an independent value of high *SOX2* expression for shorter OS ($p = 0.002$), but not PFS was confirmed. No significant differences were observed for *NANOG* or *OCT4* expression levels when comparing SCLC patients and healthy controls neither when analysing survival outcomes in SCLC patients.

Conclusions. *SOX2* mRNA expression in whole blood might be a promising non-invasive marker for molecular screening of SCLC and important prognostic marker in advanced chemotherapy-treated SCLC patients, altogether indicating important role of cancer stem-like cell (CSC) regulators in cancer spread. Further evaluation of *SOX2* as a possible screening/prognostic marker and a therapeutic target of SCLC is warranted.

Key words: small-cell lung cancer; cancer stem cell markers; *SOX2*; *OCT4*; *NANOG*; mRNA expression; prognosis

Introduction

Lung cancer is the leading cause of cancer-related deaths worldwide, with small-cell lung cancer (SCLC) representing approximately 15% of all lung cancer cases.^{1,2} SCLC represents one of the most aggressive human cancers, with early metastatic dissemination, initiated by cancer cell intravasation into blood, migration and consequent colonisation

of sites distant to primary tumour. Despite some advances in therapeutic approaches, most of the advanced SCLC patients still die within the first year after diagnosis.^{3,4}

SCLC is initially chemosensitive disease, with high response rates achieved with first-line chemotherapy regimens. However, majority of SCLC patients relapse within a few months and achieve only modest response rates to second-line chemo-

therapy, leading to poor survival rates. Platinum-based chemotherapeutic regimens with cisplatin or carboplatin still represent the only effective systemic therapy for SCLC patients. Unfortunately, still, no effective targeted therapy is available in clinical practice to treat SCLC.

Classical clinico-pathological characteristics (*e.g.* age, gender, performance status, stage, burden of metastatic disease) are still the only ones to predict survival outcome of SCLC patients.⁵⁻⁷ Despite an increased effort in identifying additional prognostic and predictive molecular markers, none of the so far studied molecular markers proved to have prognostic or predictive value in advanced SCLC.^{6,7}

In the last several years, growing body of evidence indicates that cancer stem-like cells (CSCs) behave as crucial actors in cancer development, progression and metastasis.^{8,9} CSCs have been identified in many human cancer types, including breast cancer¹⁰, prostate cancer¹¹, pancreatic cancer¹² and lung cancer.¹³ For detection and identification of lung CSCs several key regulators have been proposed, normally essential for maintenance of pluripotent state of embryonic stem cells and self-renewal of tissue-specific adult stem cells; these regulators include SRY (sex determining region Y)-box 2 (SOX2)¹⁴, homeobox protein NANOG (named after Celtic word *Tír na nÓg* meaning the land of the young)¹⁵ and octamer-binding transcription factor 4 (OCT4).¹⁶ Cancer stem cells seem to be enriched in tumours resistant to conventional systemic therapy and radiotherapy.¹⁷⁻¹⁹ Recent reports also suggest that SOX2, NANOG and OCT4 are potential diagnostic and prognostic markers in lung cancer.²⁰⁻²⁷ Moreover, as indicated by a recent publications^{28,29}, SOX2 is a commonly activated tumour oncogene that activates ACT²⁸ and EGFR²⁹ signalling pathways in human cancers, altogether indicating its complex biological role in cell faith.

Recent studies mainly conducted in early stage non-small cell lung cancer (NSCLC) after radical surgical therapy correlated SOX2 genomic amplification and/or consequent protein overexpression in primary tumour tissue with better prognosis^{21,27,30-33}; these results were also supported by a meta-analysis, which confirmed significant interaction between high SOX2 expression and improved survival in early NSCLC, regardless of histopathological subtype.²² On the contrary in study evaluating the prognostic value of SOX2 protein expression in primary tumour tissue of early stage SCLC, high SOX2 protein expression was independent prognostic marker for poor survival outcome in SCLC patients.²³ So far, only one

study quantified the levels of serum SOX2 DNA in patients with different histopathological types and stages of lung cancer.²⁰ In this particular study, serum SOX2 DNA level in lung cancer patients was higher compared to the level in healthy group, and it was closely associated with TNM stage, histopathological type, and tumour size; unfortunately, the association with course of disease and disease prognosis was not assessed in the frame of the later study.

The prognostic value of NANOG and OCT4 has only been evaluated in several retrospective studies with small number of NSCLC patients included.^{24-26,34-36} Elevated protein expression of both markers, NANOG^{24,25,34,35} or OCT4^{24,26,36} in primary tumour was correlated with poor survival outcomes in early NSCLC patients treated with radical surgery. According to our knowledge there are no published data on prognostic or predictive value of NANOG or OCT4 expression in either blood or tumour tissue in SCLC patients.

Up to date, various studies have demonstrated that circulating cell-free tumour nucleic acids may reflect the same genetic characteristics as the primary tumour and are therefore attractive for non-invasive biomarkers determination especially during the course of diseases and in patients with no tumour tissue available.³⁷ In lung cancer, previously mentioned study proposed circulating SOX2 DNA levels quantified by fluorescent qPCR as a novel, screening biomarker for lung cancer.²⁰ So far, the prognostic value of SOX2, NANOG or OCT4 mRNA expression in whole blood samples of SCLC patients has not been evaluated yet. Several genetic (*e.g.* mutations, genomic amplifications) and epigenetic mechanisms, can either decrease or increase the transcription of a particular mRNA^{38,39}; measuring the mRNA expression is therefore an attractive approach in cases where there is no known genetic mechanism affecting gene expression.

The aim of our study was to evaluate the level of SOX2, NANOG and OCT4 mRNA expression in whole blood samples of advanced SCLC patients compared to healthy controls, and to correlate biomarkers expression with overall survival (OS) and progression-free survival (PFS) after first line chemotherapy in advanced SCLC patients.

Patients and methods

The present study was conducted and is reported following recommendations for tumour marker prognostic studies (REMARK).⁴⁰

Patients, healthy volunteers and collection of whole blood samples

50 consecutive patients with pathologically confirmed advanced SCLC, treated with first-line platinum or anthracycline-based chemotherapy and followed at University Clinic Golnik, Slovenia, between December 2009 and June 2013 were prospectively enrolled. For comparison, 50 volunteers with no clinical evidence of cancer disease were also included. Matching criteria were age and gender. 16 volunteers with other chronic pulmonary diseases (chronic obstructive pulmonary disease, asthma) were excluded from this study.

For *SOX2*, *NANOG* and *OCT4* mRNA expression, whole blood samples (2.5 ml; PAXgene Blood RNA Tubes, which contain proprietary solution that reduces RNA degradation and gene induction; Qiagen) were collected from advanced SCLC patients before the onset of chemotherapy and from healthy controls at health check examinees by peripheral venous puncture. All blood samples were obtained after the first 5 ml of blood were discarded to avoid contamination of the blood sample with skin epithelial cells and stored at -30°C until RNA isolation.

Patients included in this study were treated and followed according to the standard clinical practices in use at the time. All patients received first-line systemic therapy with cisplatin-etoposide or carboplatin-etoposide (PE) or cyclophosphamide-epirubicin-vincristine (CEV) chemotherapy. The dosing schedules, dose modifications and supportive therapy were offered according to the standard practice. The second-line chemotherapy including CEV or PE was offered at clinician's discretion. Response to chemotherapy was evaluated according to the RECIST1.1 criteria⁴¹ at regular time intervals (every 2-3 months) using chest radiography or computerised tomography (CT) scans. Number of distant metastatic sites was defined as the number of the organs or organic systems involved in cancer disease.

mRNA expression analysis

Total RNA was isolated from whole blood using PAXgene Blood miRNA Kit (Qiagen) using the fully automated QIAcube system (Qiagen) to standardize the RNA isolation procedure. Total RNA quantity and purity were assessed using NanoDrop 2000 (ThermoScientific). After isolation and purification of total RNA from blood samples additional step including digestion of genomic DNA with DNaseI (ThermoScientific) was included. Reverse

transcription reactions were performed using the High Capacity cDNA Reverse Transcription Kit (Applied Biosystems).

All reagents for RT-PCR were supplied by Applied Biosystems (USA). The expression of stem cell markers was detected by TaqMan RT-qPCR (ABI PRISM 7500 FAST Real-Time PCR System) using gene-specific primers-probe sets (*SOX2*: Hs01053049_s1, *OCT4*: Hs00999632_g1, *NANOG*: Hs02387400_g1) and TaqMan Universal PCR Master Mix II. All measurements were performed in triplicate and relative mRNA expression was determined by the $\Delta\Delta\text{Ct}$ method. GAPDH was used as endogenous control and pooled RNA from blood samples of healthy controls was used as a calibrator. All samples with threshold cycle ≥ 38.0 were considered as negative for *SOX2*, *NANOG* or *OCT4* mRNA expression.

Statistics

Median relative expression values of each analysed stem cell marker were compared between advanced SCLC patients and healthy controls using the Mann-Whitney U-test. The relationship between *SOX2*, *NANOG* or *OCT4* mRNA expression and patient characteristics was evaluated using the Mann-Whitney U-test or Fisher's exact test, as appropriate.

Overall survival was defined as the period of time in months from the date of diagnosis to the date of death or last follow-up; the secondary endpoint PFS was defined as the period of time in months from the start of the first-line chemotherapy to the date of progression or death whichever occurred first. Survival probabilities, OS and PFS, were calculated by the Kaplan-Meier method and log-rank test was used to compare different categories, where optimal cut-off value between low and high expression level was set at the median mRNA expression level for each of the three markers analysed in SCLC patients. The independent prognostic value of each individual marker was tested in Cox regression model adjusted for gender, age, PS and the number of distant metastatic sites. A *p*-value below 0.05 was considered statistically significant. All statistical analyses were carried out using SPSS (version 21, SPSS, Inc., Chicago, IL, USA). All reported *p*-values are two-tailed.

The study was approved by the Slovenian National Medical Ethics Committee (approval number 135/07/09) before the enrolment of the SCLC patients and healthy controls. The informed consent was obtained before the start of the study from all subjects.

Results

Patient and treatment characteristics

Demographic and treatment characteristics of 50 advanced SCLC patients and 34 healthy volunteers are listed in Table 1. At the time of diagnosis, median age of patients was 65 years (range 46-88 years), majority of the patients were male (35/50; 69%), and in good PS (PS ≤ 1 in 38/50; 76%). As first-line chemotherapy, the majority of patients received platinum-based chemotherapy (42/50; 84%). The second line chemotherapy was offered to 14/50 (28%) patients.

Evaluation of SOX2, OCT4 and NANOG mRNA expression

SOX2 relative mRNA expression levels were detected in 46/50 (92%) blood samples of advanced SCLC patients and in 25/34 (73%) blood samples of healthy controls. SOX2 mRNA expression levels were significantly higher in whole blood samples of SCLC patients when compared to healthy controls (median: 0.8 (range: 0.0-11.1) vs. 0.6 (range: 0.0-1.8), respectively, $p = 0.006$; Figure 1). On the other hand, NANOG and OCT4 relative mRNA expression levels were detected in all blood samples of SCLC patients and healthy controls. In addition, no significant differences were observed in NANOG (median: 1.5 (range: 0.4-4.8) vs. 1.2 (range: 0.4-4.4), respectively; $p = 0.199$, Figure 1) and OCT4 (median: 1.5 (range: 0.4-3.3) vs. 1.2 (range: 0.3-3.4), respectively; $p = 0.224$; Figure 1) median mRNA levels between SCLC patients and healthy group.

As already mentioned in the methods section, cut-off value between low and high mRNA expression was set at the median expression level for the three markers analysed in SCLC patients. The associations between SOX2, NANOG or OCT4 mRNA expression and clinical variables are shown in Table 2. High SOX2 mRNA expression was correlated with the higher number of distant metastatic sites ($p = 0.027$). There were no other significant correlations between SOX2, NANOG or OCT4 mRNA expression and other clinical variables, such as gender and age.

Survival analysis

After the median follow-up of 8.5 months (range: 0.5-32.5 months) median PFS was 6.2 months and median OS was 8.4 months in 50 SCLC patients included into analysis.

TABLE 1. Characteristics of small-cell lung cancer (SCLC) patients and healthy volunteers

Characteristic	SCLC patients (N = 50)	Healthy volunteers (N = 34)
Age in years: median (range)	65 (46-88)	62 (47-78)
Gender, N (%)		
Male	34 (68)	24 (71)
Female	16 (32)	10 (29)
PS ^a , N (%)		
0-1	38 (76)	
≥ 2	12 (24)	
Number of distant metastatic sites, N (%)		
< 3	34 (68)	
≥ 3	16 (32)	
Type of first-line chemotherapy, N (%)		
PE	42 (84)	
CEV	8 (16)	

^aEast Cooperative Oncology Group performance status; CEV = cyclophosphamide-epirubicin-vincristine; N = number of SCLC patients/healthy volunteers; PE = platinum (cisplatin or carboplatin)-etoposide

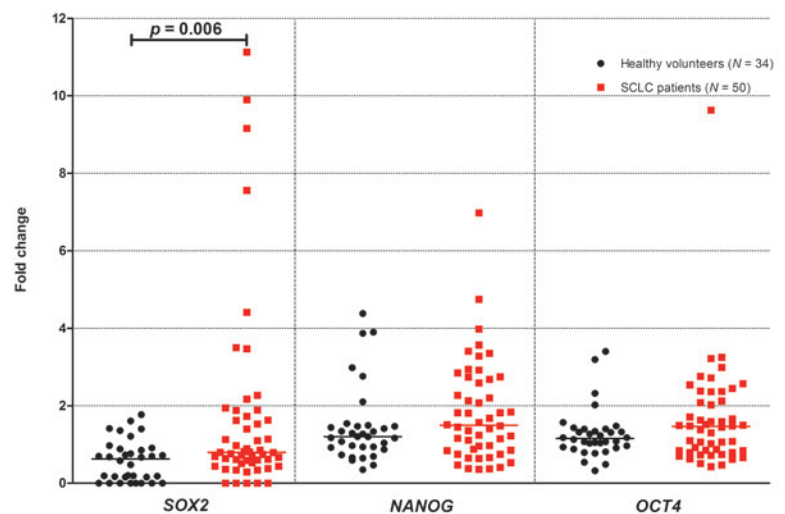


FIGURE 1. SOX2, NANOG and OCT4 mRNA expression levels in whole blood of healthy volunteers and small-cell lung cancer (SCLC) patients.

N: number of SCLC patients/healthy volunteers; p: p-value

The level of SOX2 mRNA expression, significantly influenced both PFS after first-line chemotherapy ($p = 0.046$; Table 3, Figure 2A) and OS ($p = 0.017$; Table 3, Figure 3A) in our patients, with high SOX2 being associated with poor PFS and OS. Furthermore, in multivariate analysis independent prognostic value of SOX2 expression was confirmed for OS ($p = 0.002$; Table 3). On the other hand, no significant correlation between NANOG

TABLE 2. Association between SOX2, NANOG and OCT4 mRNA expression and patients' characteristics

Characteristic	SOX2 high ^b	SOX2 low ^b	p-value	NANOG high ^b	NANOG low ^b	p-value	OCT4 high ^b	OCT4 low ^b	p-value
Age in years: median (range)	63 (46–78)	66 (47–88)	0.301 ^c	65 (47–79)	65 (46–88)	0.648 ^c	64 (47–77)	66 (46–88)	0.466 ^c
Gender, N (%)			0.756 ^d			0.762 ^d			
Male	12 (35)	22 (65)		18 (53)	16 (47)		16 (47)	18 (53)	0.762 ^d
Female	7 (44)	9 (56)		7 (44)	9 (56)		9 (56)	7 (44)	
PS ^a , N (%)			0.332 ^d			0.742 ^d			1.000 ^d
0–1	16 (42)	22 (58)		20 (53)	18 (47)		19 (50)	19 (50)	
≥ 2	3 (25)	9 (75)		5 (42)	7 (58)		6 (50)	6 (50)	
Number of distant metastatic sites, N (%)			0.027^d			0.762 ^d			1.000 ^d
< 3	9 (26)	25 (74)		18 (53)	16 (47)		17 (50)	17 (50)	
≥ 3	10 (62)	6 (38)		7 (44)	9 (56)		8 (50)	8 (50)	

N = number of patients; ^a East Cooperative Oncology Group performance status; ^b median mRNA expression levels for each of the three markers analysed were used to stratify patients as either SOX2/NANOG/OCT4 low or high; ^c Mann-Whitney U-test; ^d Fisher's exact test

or OCT4 expression and survival outcomes was observed in univariate (Table 3, Figures 2-3) or multivariate analysis (Table 3).

Discussion

The present study aimed to compare SOX2, NANOG and OCT4 mRNA expression in whole blood between advanced SCLC patients and healthy controls, and to assess the prognostic impact of mRNA expression in 50 advanced SCLC patients treated with first-line chemotherapy, either platinum or anthracycline-based. Only SOX2 mRNA levels were significantly higher in advanced SCLC patients when compared to healthy controls.

Moreover, elevated SOX2 expression levels had an independent prognostic value for better OS in advanced chemotherapy-treated SCLC.

Our results indicate significantly higher SOX2 mRNA expression in whole blood of SCLC patients when compared to healthy controls, and are consistent with the only study which observed significantly higher serum SOX2 DNA levels in 94 patients with different histopathological types and stages of lung cancer in comparison to benign lung disease group or healthy group.²⁰ Moreover, we observed a significant positive correlation between high SOX2 mRNA expression in whole blood and the higher number of distant metastatic sites ($p = 0.027$), suggesting that SOX2 expression might mirror an important oncogenic and metastatic po-

TABLE 3. Progression-free survival (PFS) after first-line chemotherapy and overall survival (OS) according to SOX2, NANOG and OCT4 mRNA expression

mRNA expression	Median PFS (months)	p-value HR (95% CI)		Median OS (months)	p-value HR (95% CI)	
		UV	MV		UV	MV
All patients (N = 50)	6.2			8.4		
SOX2 low	7.4	0.046	0.377	9.9	0.017	0.002
SOX2 high	5.6	1.988 (1.011-3.922)	1.054 (0.938-1.183)	7.5	2.370 (1.164-4.831)	3.205 (1.536-6.711)
NANOG low	5.7	0.221	0.299	7.4	0.347	0.376
NANOG high	6.5	0.693 (0.384-1.247)	0.864 (0.656-1.139)	8.7	0.750 (0.412-1.366)	0.884 (0.674-1.161)
OCT4 low	5.6	0.156	0.227	7.8	0.251	0.416
OCT4 high	7.3	0.652 (0.362-1.178)	0.780 (0.521-1.167)	9.9	0.810 (0.446-1.471)	0.891 (0.673-1.178)

95% CI = 95% confidence interval; HR = hazard ratio; MV = multivariate analysis adjusted for age, gender, N = number of patients; PS and the number of distant metastatic sites; relative expression values for each of the three markers analysed were used in MV; UV = univariate analysis; Log-rank test was used to analyse different categories dichotomised according to the median mRNA expression levels for each of the three markers analysed

tential in SCLC. Furthermore, correlation between high SOX2 mRNA expression and both poorer PFS after first-line chemotherapy ($p = 0.046$) and poorer OS ($p = 0.017$) was observed; association between high SOX2 expression and poor OS ($p = 0.002$) persisted also in multivariate analysis. Our findings obtained in whole blood of SCLC patients, seem to be consistent with the only study evaluating the prognostic value of SOX2 protein expression in SCLC primary tumours obtained after surgery, where high SOX2 protein expression in the primary tumour proved to be an independent prognostic marker for worse OS and shorter recurrence-free survival in patients with early stage SCLC who underwent surgery.²³

In contrast to SCLC, high SOX2 protein expression and SOX2 gene amplification in primary tumours seem to be associated with better prognosis in NSCLC.²² These contradictory results might be due to different methodologies of biomarker determination (e.g. fluorescent in situ hybridization or quantitative PCR for detection of SOX2 genomic amplification, immunohistochemistry for SOX2 protein expression), small number of patients included in our study or may even suggest cancer-specific role of SOX2 in different histopathological types of lung cancer.

Detection of mRNA expression levels of selected biomarkers in whole blood is relatively new concept in lung cancer or any other human cancer that could be developed as an ancillary tool for disease screening and monitoring. Furthermore, it might represent an attractive approach for evaluating gene expression with no known underlying genetic mechanism affecting its expression. Moreover, detection of tumour specific DNA alterations⁴² and differential mRNA expression⁴³⁻⁴⁶ in primary tumours and/or circulating nucleic acids by high-throughput technologies (next-generation sequencing, microarrays) may provide a substantial advance in monitoring disease burden and treatment response in all human cancers.

The cut-off point for SOX2 positivity was set at the median value of SOX2 mRNA expression. Of note, there are no clinically validated cut-off values for SOX2 mRNA expression available in lung cancer, because this is the first study evaluating SOX2 mRNA expression in lung cancer. Studies conducted in other human cancers, including prostate cancer, rectal cancer, and hepatocellular cancer, so far used different, not yet validated thresholds based on the cohort of the included patients.⁴⁷⁻⁴⁹

Our results indicate no difference in NANOG and OCT4 mRNA expression levels in whole

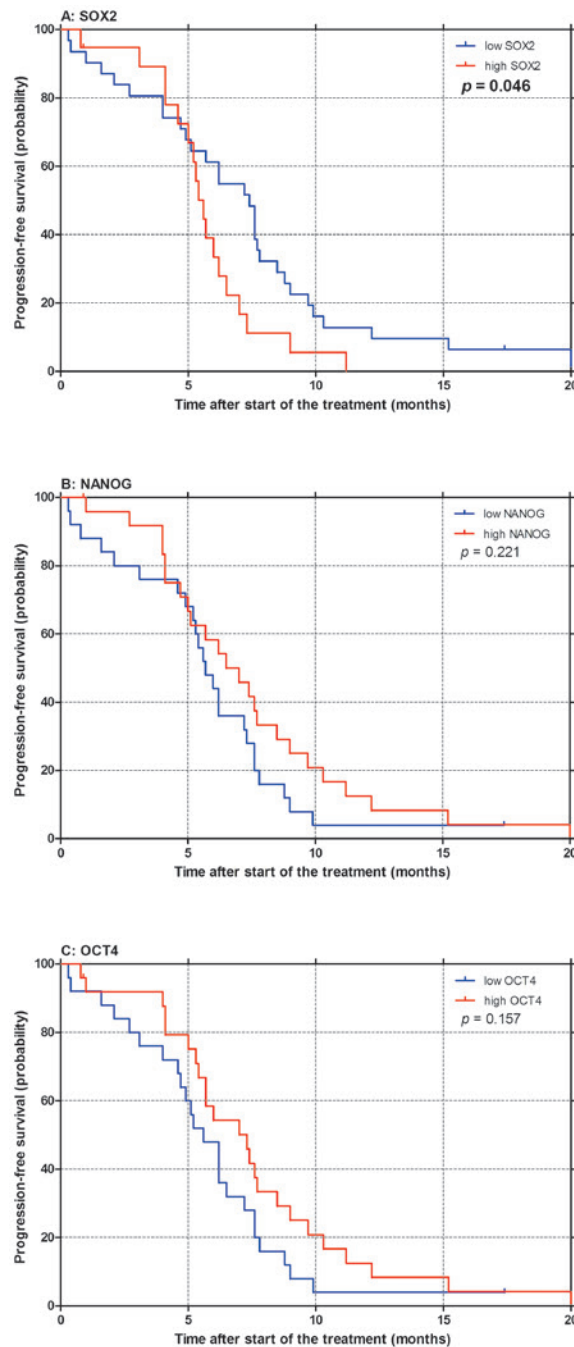


FIGURE 2. Progression-free survival (PFS) after first-line chemotherapy according to SOX2 (A), NANOG (B) and OCT4 (C) mRNA expression in small-cell lung cancer patients. p : p -value

blood when comparing SCLC patients and control group. Moreover, no correlation between NANOG and OCT4 expression in whole blood and survival outcomes was observed in our study. To our best knowledge, the diagnostic and prognostic value of NANOG and OCT4 mRNA expression in tumour tissue or whole blood has not yet been evaluated

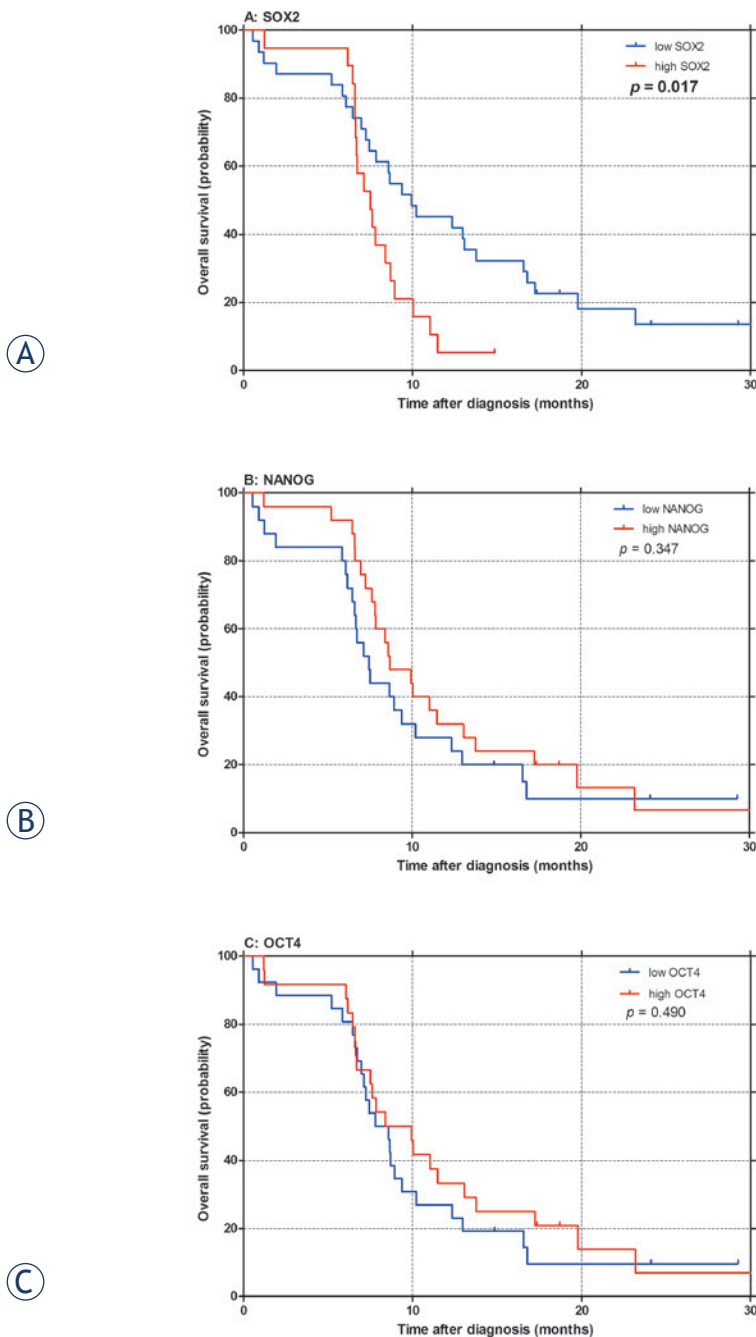


FIGURE 3. Overall survival (OS) according to SOX2 (A), NANOG (B) and OCT4 (C) mRNA expression in small-cell lung cancer patients. *p*: *p*-value.

in SCLC. However, several retrospective studies with small number of NSCLC patients included associated high NANOG or high OCT4 protein expression in primary tumour with poor survival outcome of NSCLC patients treated mainly with curative surgical resection.^{24-26,34-36} Again, these differences might be due to different methodologies of biomarker determination, low number of pa-

tients or specific role of these two markers in histopathological types of lung cancer.

The present study has several potential limitations, such as the small sample size that has an impact on statistical power of survival analysis and could therefore greatly limit the accuracy of the results. Furthermore, there are still methodological issues of biomarkers determination that should be appropriately resolved. The methods currently used for the evaluation of SOX2, NANOG or OCT4 expression in lung cancer patients differ greatly among the published reports. Studies conducted in lung cancer mainly used immunohistochemistry (IHC) for SOX2, NANOG and OCT4 protein expression and fluorescence in situ hybridisation (FISH) or quantitative PCR (qPCR) for SOX2 gene amplification detection.^{21-26,31-33} Besides, there are no clinically validated cut-off values for SOX2, NANOG and OCT4 mRNA expression available in the published literature and major differences still exists regarding the cut-off values of defining the specimens as positive/high for SOX2, NANOG or OCT4 expression determined either by IHC, FISH or qPCR.^{21-26,31-33} Furthermore, transcription of NANOG and OCT4 pseudogenes was reported in some tumour tissues and their detection by qPCR could give false-positive results.^{50,51} Unfortunately, direct comparison of SOX2, NANOG and OCT4 mRNA expression between whole blood and primary tumour tissue was not assessed in the frame of our study due to low number of patients with available tumour tissue. Further studies evaluating the correlation between gene expression profiles in whole blood and primary tumour tissue would be of valuable to assess the potential similarity of gene expression characteristics between blood circulation and primary lung tumour.

In conclusion, our prospective observational study found significantly higher mRNA expression levels of SOX2 in whole blood samples of advanced SCLC patients when compared to healthy controls. Equally importantly, a possible prognostic value of SOX2 mRNA expression for overall survival of SCLC patients was observed. No such correlations were found for NANOG or OCT4 expression. Our findings support the emerging oncogenic and metastatic role of SOX2 in SCLC with potential applications as a prognostic CSC marker and therapeutic target in lung cancer. In addition, recently published study highlights a new role of SOX2 biomarker in the regulation of EGFR oncogenic signalling pathway²⁹, for which EGFR oncogene-directed therapies already exist and a number of other therapies are in development.

Nevertheless, possible diagnostic and prognostic value of SOX2 still requires further evaluation in the frame of large-scale prospective trials. However, before embarking on large prospective clinical trials a proper standardization and validation of methodological approaches used for evaluation of selected biomarkers is necessary.

References

- Siegel R, Ma J, Zou Z, Jemal A. Cancer statistics 2014. *CA Cancer J Clin* 2014; **64**: 9-29.
- Ferlay J, Steliarova-Foucher E, Lortet-Tieulent J, Rosso S, Coebergh JWW, Comber H, et al. Cancer incidence and mortality patterns in Europe: Estimates for 40 countries in 2012. *Eur J Cancer* 2013; **49**: 1374-403.
- Planchard D, Le Péchoux C. Small cell lung cancer: new clinical recommendations and current status of biomarker assessment. *Eur J Cancer* 2011; **47**(Suppl 3): S272-83.
- Kalemkerian GP. Advances in the treatment of small-cell lung cancer. *Semin Respir Crit Care Med* 2011; **32**: 94-101.
- Foster NR, Mandrekar SJ, Schild SE, Nelson GD, Rowland KM Jr, Deming RL, et al. Prognostic factors differ by tumor stage for small cell lung cancer: a pooled analysis of North Central Cancer Treatment Group trials. *Cancer* 2009; **115**: 2721-31.
- Knez L, Sodja E, Kern I, Košnik M, Cufer T. Predictive value of multidrug resistance proteins, topoisomerases II and ERCC1 in small cell lung cancer: a systematic review. *Lung Cancer* 2011; **72**: 271-9.
- Sodja E, Knez L, Kern I, Ovčariček T, Sadikov A, Cufer T. Impact of ERCC1 expression on treatment outcome in small-cell lung cancer patients treated with platinum-based chemotherapy. *Eur J Cancer* 2012; **48**: 3378-85.
- Berns A. Stem cells for lung cancer? *Cell* 2005; **121**: 811-3.
- Pine SR, Marshall B, Varticovski L. Lung cancer stem cells. *Dis Markers* 2008; **24**: 257-66.
- Ponti D, Costa A, Zaffaroni N, Pratesi G, Petrangolini G, Coradini D, et al. Isolation and in vitro propagation of tumorigenic breast cancer cells with stem/progenitor cell properties. *Cancer Res* 2005; **65**: 5506-11.
- Patrawala L, Calhoun T, Schneider-Broussard R, Li H, Bhatia B, Tang S, et al. Highly purified CD44+ prostate cancer cells from xenograft human tumors are enriched in tumorigenic and metastatic progenitor cells. *Oncogene* 2006; **25**: 1696-708.
- Li C, Heidt DG, Dalerba P, Burnat CF, Zhang L, Adsay V, et al. Identification of pancreatic cancer stem cells. *Cancer Res* 2007; **67**: 1030-7.
- Eramo A, Lotti F, Sette G, Pilozi E, Biffoni M, Di Virgilio A, et al. Identification and expansion of the tumorigenic lung cancer stem cell population. *Cell Death Differ* 2008; **15**: 504-14.
- Lu Y, Futtner C, Rock JR, Xu X, Whitworth W, Hogan BLM, et al. Evidence that SOX2 overexpression is oncogenic in the lung. *PLoS One* 2010; **5**: e11022.
- Gialmanidis IP, Bravou V, Petrou I, Kourea H, Mathioudakis A, Lilis I, et al. Expression of Bmi1, FoxF1, Nanog, and γ -catenin in relation to hedgehog signaling pathway in human non-small-cell lung cancer. *Lung* 2013; **191**: 511-21.
- Chen YC, Hsu HS, Chen YW, Tsai TH, How CK, Wang CY, et al. Oct-4 expression maintained cancer stem-like properties in lung cancer-derived CD133-positive cells. *PLoS One* 2008; **3**: e2637.
- Sullivan JP, Minna JD, Shay JW. Evidence for self-renewing lung cancer stem cells and their implications in tumor initiation, progression, and targeted therapy. *Cancer Metastasis Rev* 2010; **29**: 61-72.
- Bertolini G, Roz L, Perego P, Tortoeto M, Fontanella E, Gatti L, et al. Highly tumorigenic lung cancer CD133+ cells display stem-like features and are spared by cisplatin treatment. *Proc Natl Acad Sci* 2009; **106**: 16281-6.
- Stewart DJ. Tumor and host factors that may limit efficacy of chemotherapy in non-small cell and small cell lung cancer. *Crit Rev Oncol Hematol* 2010; **75**: 173-234.
- Wu Y, Du X, Xue C, Li D, Zheng Q, Li X, et al. Quantification of serum SOX2 DNA with FQ-PCR potentially provides a diagnostic biomarker for lung cancer. *Med Oncol* 2013; **30**: 737.
- Velcheti V, Schalper K, Yao X, Cheng H, Kocoglu M, Dhodapkar K, et al. High SOX2 levels predict better outcome in non-small cell lung carcinomas. *PLoS One* 2013; **8**: e61427.
- Chen Y, Huang Y, Huang Y, Chen J, Wang S, Zhou J. The prognostic value of SOX2 expression in non-small cell lung cancer: a meta-analysis. *PLoS One* 2013; **8**: e71140.
- Yang F, Gao Y, Geng J, Qu D, Han Q, Qi J, et al. Elevated expression of SOX2 and FGFR1 in correlation with poor prognosis in patients with small cell lung cancer. *Int J Clin Exp Pathol* 2013; **6**: 2846-54.
- Chiou SH, Wang ML, Chou YT, Chen CJ, Hong CF, Hsieh WJ, et al. Coexpression of oct4 and nanog enhances malignancy in lung adenocarcinoma by inducing cancer stem cell-like properties and epithelial-mesenchymal transdifferentiation. *Cancer Res* 2010; **70**: 10433-44.
- Li XQ, Yang XL, Zhang G, Wu SP, Deng XB, Xiao SJ, et al. Nuclear β -catenin accumulation is associated with increased expression of Nanog protein and predicts poor prognosis of non-small cell lung cancer. *J Transl Med* 2013; **11**: 114.
- Li XL, Jia LL, Shi MM, Li X, Li ZH, Li HF, et al. Downregulation of KPNA2 in non-small-cell lung cancer is associated with Oct4 expression. *J Transl Med* 2013; **11**: 232.
- Wilbertz T, Wagner P, Petersen K, Stiedl AC, Scheble VJ, Maier S, et al. SOX2 gene amplification and protein overexpression are associated with better outcome in squamous cell lung cancer. *Mod Pathol* 2011; **24**: 944-53.
- Tian Y, Jia X, Wang S, Li Y, Zhao P, Cai D, et al. SOX2 oncogenes amplified and operate to activate AKT signaling in gastric cancer and predict immunotherapy responsiveness. *J Cancer Res Clin Oncol* 2014; **140**: 1117-24.
- Chou YT, Lee CC, Hsiao SH, Lin SE, Lin SC, Chung CH, et al. The emerging role of SOX2 in cell proliferation and survival and its crosstalk with oncogenic signaling in lung cancer. *Stem Cells* 2013; **31**: 2607-19.
- Hussenet T, Dali S, Exinger J, Monga B, Jost B, Dembelé D, et al. SOX2 is an oncogene activated by recurrent 3q26.3 amplifications in human lung squamous cell carcinomas. *PLoS One* 2010; **5**: e8960.
- Toschi L, Finocchiaro G, Nguyen TT, Skokan MC, Giordano L, Gianoncelli L, et al. Increased SOX2 gene copy number is associated with FGFR1 and PIK3CA gene gain in non-small cell lung cancer and predicts improved survival in early stage disease. *PLoS One* 2014; **9**: e95303.
- Cai YR, Zhang HQ, Zhang ZD, Mu J, Li ZH. Detection of MET and SOX2 amplification by quantitative real-time PCR in non-small cell lung carcinoma. *Oncol Lett* 2011; **2**: 257-64.
- Sasaki H, Yokota K, Hikosaka Y, Moriyama S, Yano M, Fujii Y. Increased Sox2 copy number in lung squamous cell carcinomas. *Exp Ther Med* 2012; **3**: 44-8.
- Chen WJ, Ho CC, Chang YL, Chen HY, Lin CA, Ling TY, et al. Pulmonary adenocarcinoma in malignant pleural effusion enriches cancer stem cell properties during metastatic cascade. *PLoS One* 2013; **8**: e54659.
- Du Y, Ma C, Wang Z, Liu Z, Liu H, Wang T. Nanog, a novel prognostic marker for lung cancer. *Surg Oncol* 2013; **22**: 224-9.
- Li X, Wang J, Xu Z, Ahmad A, Li E, Wang Y, et al. Expression of sox2 and oct4 and their clinical significance in human non-small-cell lung cancer. *Int J Mol Sci* 2012; **13**: 7663-75.
- Schwarzenbach H, Hoon DS, Pantel K. Cell-free nucleic acids as biomarkers in cancer patients. *Nat Rev Cancer* 2011; **11**: 426-37.
- Croce CM. Oncogenes and cancer. *N Engl J Med* 2008; **358**: 502-11.
- Jones PA, Baylin SB. The epigenomics of cancer. *Cell* 2007; **128**: 683-92.
- Altman DG, McShane LM, Sauerbrei W, Taube SE. Reporting Recommendations for Tumor Marker Prognostic Studies (REMARK): Explanation and Elaboration. *PLoS Med* 2012; **9**: e1001216.
- Eisenhauer EA, Therasse P, Bogaerts J, Schwartz LH, Sargent D, Ford R, et al. New response evaluation criteria in solid tumours: revised RECIST guideline (version 1.1). *Eur J Cancer* 2009; **45**: 228-47.

42. Sequist LV, Heist RS, Shaw AT, Fidias P, Rosovsky R, Temel JS, et al. Implementing multiplexed genotyping of non-small-cell lung cancers into routine clinical practice. *Ann Oncol* 2011; **22**: 2616-24.
43. Li Y, Elashoff D, Oh M, Sinha U, St John MA, Zhou X, et al. Serum circulating human mRNA profiling and its utility for oral cancer detection. *J Clin Oncol* 2006; **24**: 1754-60.
44. Beane J, Spira A, Lenburg ME. Clinical impact of high-throughput gene expression studies in lung cancer. *J Thorac Oncol* 2009; **4**: 109-18.
45. Garber ME, Troyanskaya OG, Schluens K, Petersen S, Thaesler Z, Pacyna-Gengelbach M, et al. Diversity of gene expression in adenocarcinoma of the lung. *Proc Natl Acad Sci U S A* 2001; **98**: 13784-9.
46. Bhattacharjee A, Richards WG, Staunton J, Li C, Monti S, Vasa P, et al. Classification of human lung carcinomas by mRNA expression profiling reveals distinct adenocarcinoma subclasses. *Proc Natl Acad Sci U S A* 2001; **98**: 13790-5.
47. Saigusa S, Tanaka K, Toyama Y, Yokoe T, Okugawa Y, Ioue Y, et al. Correlation of CD133, OCT4, and SOX2 in rectal cancer and their association with distant recurrence after chemoradiotherapy. *Ann Surg Oncol* 2009; **16**: 3488-98.
48. Fujimura T, Takahashi S, Urano T, Takayama K, Sugihara T, Obinata D, et al. Expression of androgen and estrogen signaling components and stem cell markers to predict cancer progression and cancer-specific survival in patients with metastatic prostate cancer. *Clin Cancer Res* 2014; **20**: 4625-35.
49. Huang P, Qiu J, Li B, Hong J, Lu C, Wang L, et al. Role of Sox2 and Oct4 in predicting survival of hepatocellular carcinoma patients after hepatectomy. *Clin Biochem* 2011; **44**: 582-9.
50. Zhao S, Yuan Q, Hao H, Guo Y, Liu S, Zhang Y, et al. Expression of OCT4 pseudogenes in human tumours: lessons from glioma and breast carcinoma. *J Pathol* 2011; **223**: 672-82.
51. Uchino K, Hirano G, Hirahashi M, Isobe T, Shirakawa T, Kusaba H, et al. Human Nanog pseudogene8 promotes the proliferation of gastrointestinal cancer cells. *Exp Cell Res* 2012; **318**: 1799-807.

Tenckhoff tunneled peritoneal catheter placement in the palliative treatment of malignant ascites: technical results and overall clinical outcome

Geert Maleux¹, Inge Indesteege¹, Annouschka Laenen², Chris Verslype³, Ignace Vergote⁴, Hans Prenen³

¹ Department of Radiology, University Hospitals Leuven, Belgium

² Department of Biostatistics and and Statistical Bioinformatics, KU Leuven and Universiteit Hasselt, Belgium

³ Department of Digestive Oncology, University Hospitals Leuven, Belgium

⁴ Department of Gynaecology, University Hospitals Leuven, Belgium

Radiol Oncol 2016; 50(2): 197-203.

Received 13 October 2015

Accepted 20 December 2015

Correspondence to: Geert Maleux, M.D., Ph.D., Department of Radiology, University Hospitals Leuven, Herestraat 49, B-3000 Leuven; Belgium. Phone: +32 16 34 37 82; Fax: +32 16 34 37 65; E-mail: geert.maleux@uzleuven.be

Disclosure: The authors have no conflicts of interest to disclose.

Background. To assess the technical and clinical outcome of percutaneous insertion of tunneled peritoneal catheters in the palliative treatment of refractory malignant ascites and to determine the safety and feasibility of intraperitoneal administration of cytotoxic drugs through the tunneled catheter.

Materials and methods. Consecutive patients palliatively treated with a tunneled peritoneal catheter to drain the malignant ascites were identified. Patients' medical history, procedural and clinical follow-up data, including complications and estimated survival, were reviewed. Additionally, a sub analysis of the patients with widespread ovarian cancer and refractory ascites treated with or without intraperitoneal administration of cytotoxic drugs was made.

Results. In all 94 patients it was technically feasible to insert the peritoneal drainage catheter and to drain a median of 3260 cc (range 100 cc – 8500 cc) of malignant ascitic fluid. Post procedural complications included catheter infection (n = 2; 2%), fluid leakage around the entry site (n = 4; 4%), catheter occlusion (n = 2; 2%), sleeve formation around the catheter tip (n = 1; 1%) and accidental loss of the catheter (n = 1; 1%). There was no increase in catheter infection rate in patients treated with or without intraperitoneal administration of cytotoxic drugs. Median overall survival after catheter insertion is 1.7 months.

Conclusions. Percutaneous insertion of a tunneled Tenckhoff catheter for the palliative drainage of malignant ascites and intraperitoneal infusion of cytotoxic drugs is feasible and associated with a very low complication rate, including catheter infection. These tunneled peritoneal lines are beneficial for symptomatic palliative treatment of refractory ascites and allow safe intraperitoneal chemotherapy.

Key words: peritoneal catheter; malignant ascites; palliation

Introduction

Malignant ascites is a manifestation of terminal metastatic disease with a life expectancy ranging from 1 to 4 months; the ascitic fluid production is usually associated with peritoneal tumours, lymphangitic carcinomatosis, lymphatic obstruction,

encasement of the portal vein by a tumour causing prehepatic portal hypertension, or a combination of these pathophysiological mechanisms.¹⁻³ Clinically, these patients suffer from abdominal distension, early satiety, shortness of breath, fatigue or gastrointestinal symptoms such as nausea and vomiting. Medical treatment, including diuret-

ics, have little or no effect on malignant fluid accumulation and the standard treatment for these patients was repeated paracentesis, despite the risks of infection, haemorrhage or bowel wall injury and the need for frequent trips to the hospital.⁴ In the past decade, alternative drainage options intended to avoid repetitive punctures, have been tested and used. These drainage techniques include internal drainage like peritoneo-venous⁵, peritoneo-gastric⁶ and peritoneo-cystic⁷ shunting and external drainage techniques requiring the placement of an indwelling, tunneled peritoneal drainage or port-catheter.^{2,3,5,8-13} An important disadvantage of external drainage is albumin loss, which may need to be considered in deciding between external drainage and internal shunts. Most of the experience with indwelling drainage catheters has been described with the PleurX catheter; this monocuffed catheter was initially designed for drainage of malignant pleural effusions but it can also be used for drainage of malignant peritoneal fluid.^{3,9-11} Additionally, if this type of indwelling tunneled catheter is used, it is recommended to use vacuum bottles for adequate drainage.

In this study we retrospectively analysed the technical feasibility and safety of the insertion of a Tenckhoff peritoneal tunnelled catheter. Additionally, the overall clinical outcomes in this patient population were analysed and finally we evaluated the feasibility and safety of intraperitoneal chemotherapy delivery through the Tenckhoff catheter in patients with widespread ovarian cancer and refractory ascites using catumaxomab.

Materials and Methods

Patients and study design

A retrospective analysis was carried out on consecutive patients in whom a Tenckhoff tunnelled peritoneal catheter was inserted percutaneously for the management of refractory malignant ascites in the authors' institution between March 2006 and January 2013. The inclusion criteria for catheter placement were symptomatic, malignant ascites refractory to conservative and medical management in patients with widespread metastatic disease; haemostatic parameters allowing small skin incisions and subcutaneous tunnelling; absence of compartmentalization of the malignant ascitic fluid. Active infection is considered as an exclusion criterion for catheter insertion. Refractory malignant ascites is defined as ascites in patients with widespread metastatic disease in whom the

ascites cannot be mobilized by conservative or medical therapies. Patients' history, procedural and post-procedural data were documented based on the patients' hospital electronic medical records and after telephone calls with the patients' general practitioners.

The patients gave informed consent before the start of the interventional procedure and institutional review board approval was obtained for this retrospective study analysis.

Interventional procedure of Tenckhoff catheter placement

Patients were referred to the interventional radiology department after discussion between the attending interventional radiologist and medical or surgical oncologist. Patient preparation included a bedside ultrasound for evaluation of the amount of ascites and more specifically for evaluation of a window of ascitic fluid at the intraperitoneal puncture site. The preferred intraperitoneal puncture site was near the midline, inferior and to the right of the umbilicus; if no ascitic fluid window was identified in that area, a left-sided infra-umbilical puncture site was prepared with a tunnel area to the left flank. Laboratory analysis included acceptable haematological parameters for tunneled catheter insertion, including a platelet count of at least 50,000/L, a haemoglobin level > 8 g/dL and an International Normalized Ratio (INR) of less than 1.5. Tenckhoff tunneled peritoneal drainage catheter insertion was performed under sterile conditions in the interventional radiology suite.

After standard surgical preparation, local anaesthesia of the puncture site and the subcutaneous tunnel area was administered with 30 mL of lidocaine hydrochloride (Linisol 2%, B. Braun, Diegem, Belgium). No other sedation or prophylactic antibiotic medication was administered; a 2 cm skin incision was made near the midline, inferior and to the right (or left) of the umbilicus and ultrasound-guided puncture of the malignant ascitic fluid was carried out using an 18 gauge (G) sheathed needle (Surflo I.V. Catheter, Terumo Europe, Leuven, Belgium) (Figure 1A). A 0.035 inch hydrophilic guide wire (HydroSteer, St-Jude Medical, St-Paul, MN, USA) was introduced into the peritoneal cavity using a 0.035 inch 4 French (F) Cobra catheter (Slip-cath, Cook Medical, Bjaeverskov, Denmark) positioned in the pelvis (Figure 1B). This was then exchanged for a 0.035 inch stiff guide wire (Amplatz, Cook Medical, Bjaeverskov, Denmark) (Figure 1C). Over the stiff guide wire the punc-

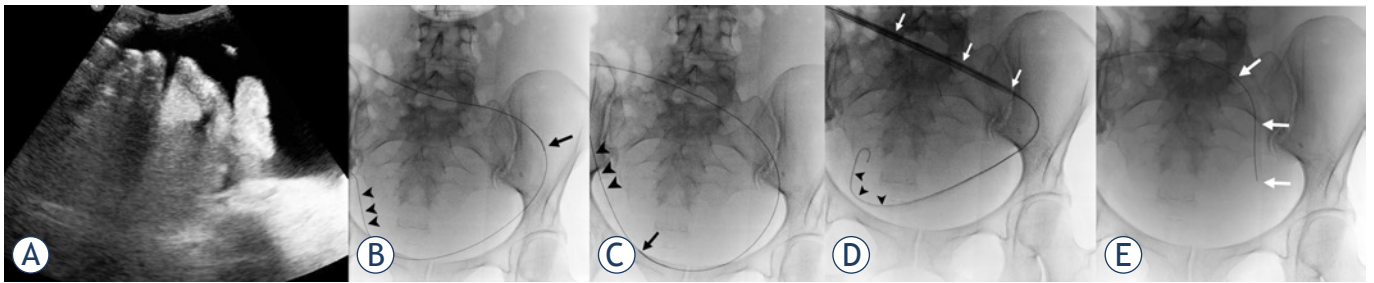


FIGURE 1. (A) Ultrasound-guided puncture of the ascitic fluid. The tip of the puncture needle (white arrow) is located within the fluid, far from intestinal or other abdominal structures. (B) Using a 4F Cobra catheter (black arrow), the hydrophilic guide wire (arrowheads) is navigated to the lower portion of the pelvis. (C) The hydrophilic guide wire is exchanged for a stiff Amplatz wire (arrowheads) on the Cobra catheter (arrow). (D) The 15F peel-away sheath (white arrows) is introduced into the peritoneal cavity over the stiff Amplatz wire (arrowheads). (E) The Tenckhoff catheter (white arrows) is introduced through the 15F peel-away sheath into the peritoneal cavity.

ture tract was dilated using a 8F dilator (Cook Medical, Bjaeverskov, Denmark) and finally a 15F peel-away introducer (PTFE-peel-Apart, BARD Benelux, Olen, Belgium) was inserted (Figure 1D). The Tenckhoff peritoneal drainage catheter (Argyle peritoneal dialysis catheter, Covidien, Mansfield, MA, USA) with the Cobra catheter inside was introduced over the stiff guide wire into the peritoneal cavity and positioned in a curved position in the lower pelvic region (Figure 1E). The Tenckhoff catheter is made of translucent silicone rubber tubing containing a radio-opaque stripe. The total length of the 15F catheter is 47 cm and the inner diameter is 2.6 mm. The intraperitoneal part of the catheter contains small fenestrations over a length of 15 cm (Figure 2). The cuffed end of the Tenckhoff catheter is tunnelled to the right (or left) flank using a metallic tunnelling device (Argyle Faller Tunneling device, Covidien, Mansfield, MA, USA) and exteriorized 7 cm lateral to the peritoneal entry site. Finally, the small cutaneous incisions are sutured and the external part of the tunnelled catheter is connected to a drainage bag (3L Empty Bag System II, Baxter Healthcare, Zurich, Switzerland) using a sterile connecting device (Connection Shield System II with Povidone-Iodine Solution, Baxter Healthcare, Zurich, Switzerland) to begin drainage.

The intraperitoneal chemotherapy infusion technique was performed using a catumaxomab-based regimen as described by Baumann *et al.*¹⁴ Briefly, catumaxomab (Removab®, Neovii Biotech, Waltham, MA, USA) 10 µg, 20 µg, 50 µg and 150 µg in 250 mL of 0.9% NaCl physiologic solution was injected intraperitoneally through the Tenckhoff catheter, respectively at day 1, 4, 8 and 11 of the treatment.

Patients were followed up until the end of the study (March 2013) or the patient's death.

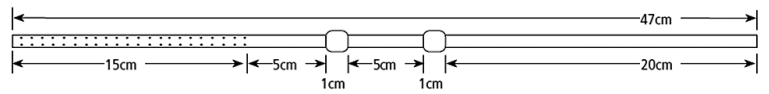


FIGURE 2. Schematic drawing of the Tenckhoff catheter: the intraperitoneal portion contains small fenestrations over a length of 15 cm. Two cuffs with a length of 1 cm are positioned in the subcutaneous tissues.

Statistical analysis

Overall survival probabilities are estimated by the Kaplan-Meier method. The Wilcoxon test is used for testing survival differences between ovarian cancer patients with or without intraperitoneal chemotherapy treatment (IPCT). The prognostic value of primary pathology for survival is analysed using Cox proportional hazards models. Fisher's exact test is used for the association between intraperitoneal chemotherapy treatment and catheter infection.

All tests are two-sided. A 5% significance level is assumed for all tests. All analyses have been carried out using SAS software, version 9.3 of the SAS System for Windows (SAS Institute Inc., Cary, NC, USA).

Results

Patient demographics

In 94 patients (27 men; 28.7% and 67 women; 71.3%) with a mean age of 60.1 years (median 59.4 years; standard deviation 12.4 years) a tunnelled peritoneal Tenckhoff catheter was inserted for drainage of malignant ascites. Malignant ascites was associated with different types of metastatic cancer disease as summarized in Table 1. The category 'rest' included lung carcinoma (n = 2), multiple myeloma (n = 2) and myxoid liposarcoma (n = 1).

TABLE 1. Type of primary cancer

Primary malignant disease	Statistic	All
Gynaecological cancer	n/N (%)	41/94 (43.6%)
Ovarian cancer	n/N	38/94
Endometrial cancer	n/N	3/94
Hepatobiliary cancer	n/N (%)	24/94 (25.5%)
Pancreatic cancer	n/N	11/94
Cholangiocarcinoma	n/N	12/94
Hepatocellular carcinoma	n/N	1/94
Gastrointestinal cancer	n/N (%)	11/94 (11.7%)
Colorectal cancer	n/N	6/94
Gastric cancer	n/N	3/94
Small bowel neuroendocrine cancer	n/N	2/94
Breast cancer	n/N (%)	13/94 (13.8%)
Rest	n/N (%)	5/94 (5.3%)

TABLE 2. Paracenteses prior to Tenckhoff catheter placement

Number of paracenteses	Statistic	All
0	n/N (%)	19/94 (20.2%)
1	n/N (%)	20/94 (21.3%)
2	n/N (%)	16/94 (17.0%)
3	n/N (%)	15/94 (16.0%)
4 or > 4	n/N (%)	24/94 (25.5%)

TABLE 3. Kaplan-Meier estimates for overall survival since Tenckhoff insertion at specific follow-up times (+95% confidence interval)

Months since Tenckhoff insertion	% Survival	Lower limit	Upper limit
3	30.0	20.9	39.6
6	18.0	10.8	26.8
12	7.7	3.2	14.5
18	2.6	0.3	9.9
24	2.6	0.3	9.9

The number of paracenteses prior to Tenckhoff catheter insertion is indicated in Table 2; overall, patients underwent a mean of 3.4 paracenteses (median: 2.0; standard deviation: 5.6; range: 0–44 paracenteses). In 15 out of 94 patients (16%) intraperitoneal chemotherapy treatment (IPCT) with catumaxomab was given; these 15 patients suffered from widespread metastatic ovarian cancer associated with refractory malignant ascites.

Technical outcome

In all patients (100%), the Tenckhoff tunnelled peritoneal drainage catheter was successfully inserted; in 90 patients (96%), the Tenckhoff catheter was tunnelled subcutaneously into the right flank, in the remaining 4 patients (4%) the peritoneal access was made in the left para and infraumbilical region and the catheter was tunnelled into the left flank. Once the Tenckhoff catheter was in place, a median of 3,260 cc (range 100 cc – 8,500 cc) of malignant ascitic fluid was drained.

Clinical outcome

Clinical follow-up was available for 90 patients; 4 patients (4.2%) were lost to follow-up.

Two patients (2.1%) presented with a clinical suspicion of catheter infection, including fever, painful cutaneous and subcutaneous tunnel infection, but without clear signs of peritonitis, 36 & 40 days respectively after initial catheter placement. One of these two patients was also treated with intraperitoneal chemotherapy infusions. Other minor complications included ascitic fluid leakage around the entry point of the catheter in the right flank (n = 4; 4%), catheter occlusion (n = 2; 2%) and sleeve formation around the tip of the catheter resulting in insufficient drainage (n = 1; 1%). Management of these complications included extra skin sutures around the catheter entry point (n = 4), catheter removal (n = 1) or catheter flushing (n = 2) respectively.

In another three patients (3%), initially presenting with malignant ascites related to breast carcinoma (n = 1), endometrial carcinoma (n = 1) and ovarian carcinoma (n = 1), the Tenckhoff catheter was removed after 111, 134 and 39 days respectively, owing to regression of ascitic fluid production. Another patient accidentally lost the catheter 11 days after initial placement.

Five out of 90 patients (5.3%) were still alive at the end of the study (March 2013); the remaining 85 patients (90.4%) died before March 2013. The time interval until end of follow-up or the patient's death was a mean of 3.41 months (median 1.7 months; standard deviation: 4.73; min: 0.03, max 25.7 months).

Kaplan-Meier estimates for overall survival after Tenckhoff insertion is summarized in Figure 3 and Table 3, showing an estimated survival at 3 and 6 months of nearly 30% and 18% respectively. Further, a more detailed analysis of survival after Tenckhoff catheter insertion is made based on the underlying

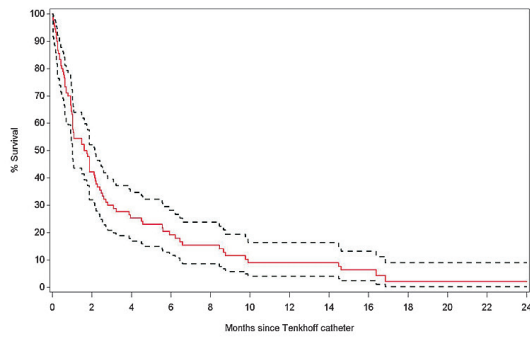


FIGURE 3. Overall survival after Tenckhoff catheter insertion with 95% confidence limits.

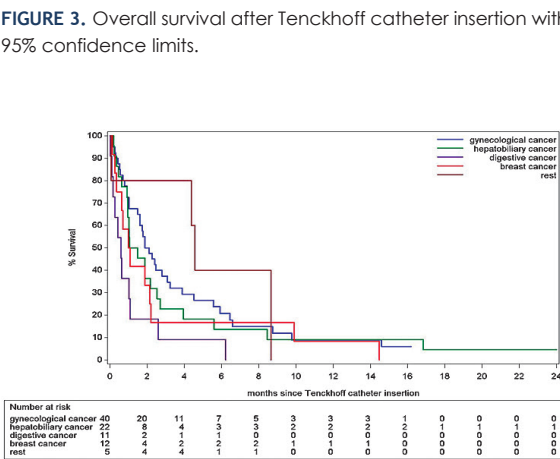


FIGURE 4. Overall estimated survival for different cancer types after Tenckhoff catheter insertion.

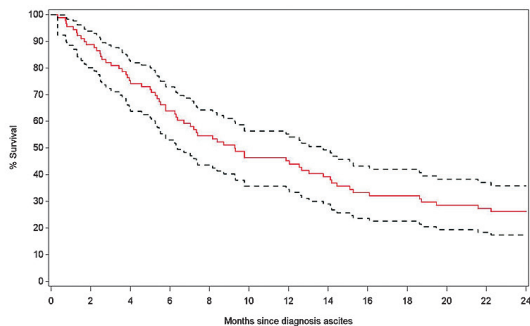


FIGURE 5. Overall estimated survival since clinical diagnosis of malignant ascites with 95% confidence limits.

type of cancer. We analysed five categories of underlying aetiologies: gynaecological cancers (n = 40) including ovarian and endometrial cancers; hepatobiliary cancers (n = 22) including pancreatic cancer, cholangiocarcinoma and hepatocellular carcinoma;

TABLE 4. Kaplan-Meier estimates for overall survival since clinical diagnosis of ascites at specific follow-up times (+ 95% confidence interval)

Months since clinical diagnosis of ascites	% Survival	Lower limit	Upper limit
3	82.2%	72.6%	88.7%
6	63.2%	53.3%	72.2 %
12	44.7 %	34.1%	54.7%
18	30.6%	21.2%	40.4%
24	24.7%	16.2%	34.1%

TABLE 5. Analysis of overall survival since clinical diagnosis of malignant ascites for different groups of cancers

	Hazard ratio	Lower limit	Upper limit	P-value
Gynaecological cancers (reference)	-	-	-	0.06
Hepatobiliary cancers	1.17	0.68	2.02	0.575
Gastrointestinal cancers	2.58	1.30	5.13	0.007
Breast cancer	1.42	0.73	2.74	0.299
Rest	0.71	0.25	1.99	0.511

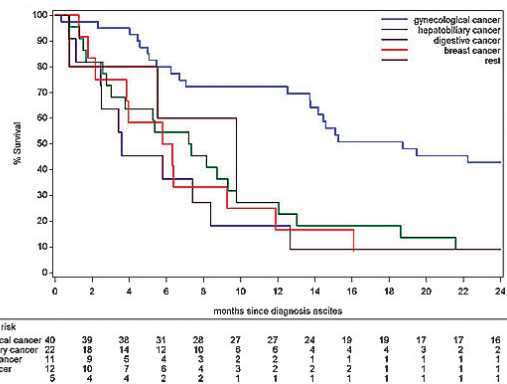


FIGURE 6. Overall estimated survival for different types of cancer since clinical diagnosis of malignant ascites.

gastrointestinal cancers (n = 11) including colorectal cancer, gastric cancer and neuroendocrine tumours; breast carcinoma (n = 11) and rest (n = 5) including lung carcinoma (n = 2), multiple myeloma (n = 2) and myxoid liposarcoma (n = 1); the survival of these different groups is summarized in Figure 4. Analysis suggests a difference in risk for early death after Tenckhoff catheter insertion according to the underlying cancer: patients with widespread gastrointestinal cancers and refractory malignant ascites have a higher risk for early death compared to the reference group of patients with widespread metastatic gynaecological cancers.

TABLE 6. Survival analysis in patients with metastatic ovarian cancer and malignant ascites treated with or without intraperitoneal infusion of catumaxomab after Tenckhoff catheter insertion

IPCT	Median survival in months	95% confidence interval	
		Lower limit	Upper limit
With IPCT	3.22	1.61	6.58
Without IPCT	1.61	0.69	2.40

IPCT = intraperitoneal chemotherapy treatment

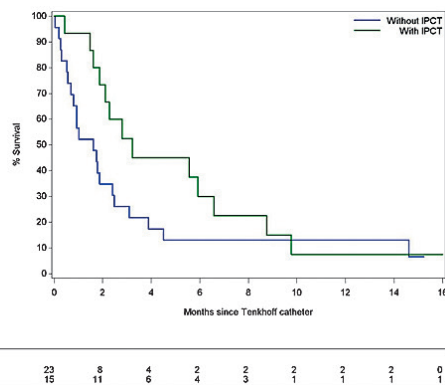


FIGURE 7. Overall estimated survival in patients with metastatic ovarian cancer associated with malignant ascites is better if intraperitoneal infusion of catumaxomab through the Tenckhoff catheter is carried out ($p = 0.02$).

Overall survival after clinical diagnosis of malignant ascites demonstrates a 3 and 6 month estimated survival of 82.0% and 63.9% respectively, as shown in Table 4 and Figure 5. An analysis of the potential outcome differences between the five categories of cancer mentioned above was carried out and summarized in Table 5 and Figure 6. The risk analysis for early death after clinical diagnosis of malignant ascites also demonstrates a significant difference in survival for patients with malignant gynaecological cancer compared to patients with gastrointestinal cancers ($p = 0.007$).

Tunnelled Tenckhoff catheters were inserted in a total of 38 patients presenting with metastatic ovarian cancer and malignant ascites. In 23 of these patients the Tenckhoff catheter was inserted solely for repeated drainage purposes. In the remaining 15 patients the Tenckhoff catheter was inserted for the purpose of drainage of malignant ascites and for the purpose of intraperitoneal infusion of a catumaxomab-based solution. Overall survival of the two sub-groups of patients (Table 6 and Figure 7) revealed better survival in the group with intraperitoneal infusion of catumaxomab ($p = 0.02$).

Discussion

This study demonstrates a very high technical success rate (100%) for tunnelled, peritoneal Tenckhoff catheter insertion in patients suffering from refractory malignant ascites, which is in line with experiences in other centres using the same^{2,15} or other types of tunnelled peritoneal catheters such as the PleurX-catheter^{3,8-11} or Medcomp catheter.¹⁶ Furthermore, subcutaneous insertion of port catheters has a 100% success rate^{12,13}, although there are only a few reports covering a small number of included patients. The major difference between the PleurX catheter and the Tenckhoff or Medcomp catheter is the number of cuffs: the PleurX catheter has one cuff whereas the other two have two cuffs; the number of infection events with these different types of tunnelled catheters does not, however, seem to be different: we encountered two patients (2%) with clinical signs of infection which is almost identical to the series with the PleurX catheter.^{9,11}

The technique of tunnelled catheter insertion is essentially the same for the different types of peritoneal tunnelled catheters: percutaneous access to the peritoneal cavity is gained under ultrasound guidance using Seldinger technique and insertion of the catheter through a peel-away sheath can be performed blindly or under fluoroscopic guidance. When using these techniques, however, the position of the tip of the tunnelled catheter is not always predictable. Instead, we used a catheter-based technique (Cobra catheter and hydrophilic guide wire) to position the tip and the fenestrated area of the Tenckhoff catheter in the dependent portion of the peritoneal cavity (lower pelvic region) which might result in better drainage of the ascitic fluid later on, especially when the patient is in a sitting or supine position, although catheter tip migration after insertion is still possible especially in case of recurrent ascitic fluid accumulation associated with bowel and body movements in general.

Other post-procedural complications apart from infection are almost always minor complications and may include fluid leakage around the catheter entry point, catheter occlusion or accidental loss despite the presence of two cuffs. This very low rate of serious complications may suggest earlier referral for Tenckhoff catheter placement for the palliative drainage of malignant ascites resulting in patients' improved quality of life.

Importantly, this study also suggests the usefulness of the Tenckhoff catheter for intraperitoneal administration of chemotherapeutic agents such as catumaxomab without a significant increase in

adverse, infectious events, although the number of patients treated with intraperitoneal chemotherapy infusion was small (n = 15).

The life expectancy of patients with refractory malignant ascites is very poor, with a range from 1 to 4 months, which is in line with the overall results of this study, showing a median overall survival of 1.7 months. This short life expectancy mainly depends on the natural history of the underlying widespread malignancy and subsequently patients with a longer life expectancy associated with refractory malignant ascites, such as patients with gynaecological tumours, may also benefit from the tunnelled Tenckhoff catheter for a longer period compared to patients with more aggressive tumours such as gastrointestinal malignancies.

Finally, a sub-analysis of patients with refractory ascites and widespread malignant ovarian tumours reveals improved survival if catumaxomab is administered intraperitoneally (p = 0.02). This conclusion should be interpreted with caution, however, because this is a retrospective, single-centre, non-randomized analysis including a small number of patients. Additionally, a multi-centre, randomized open-label phase IIa study was only able to demonstrate a slightly better therapeutic index in a high-dose catumaxomab regimen as compared to a low-dose regimen¹⁴ and other researchers found a non-significant survival benefit (110 days versus 81 days) if intraperitoneal administration of catumaxomab took place in patients with recurrent ovarian cancer.¹⁷

In conclusion, this study demonstrates that percutaneous image-guided insertion of a tunnelled Tenckhoff catheter in the peritoneal cavity is safe and effective for drainage of refractory malignant ascites, with a very low complication rate including catheter infection. The catheter is also an efficient and safe tool for intraperitoneal administration of cytotoxic drugs with no increase in peritonitis or other infectious adverse events. Finally, owing to the natural course of the underlying malignant tumor, patients with widespread metastatic gynaecological cancers and refractory ascites may benefit for a longer period from this interventional procedure than patients with other cancers and associated malignant ascites.

References

- Mullard A, Bishop J, Jibani M. Intractable malignant ascites: An alternative management option. *J Palliative Med* 2011; **2**: 251-3.
- O'Neill M, Weissleder R, Gervais D, Hahn P, Mueller P. Tunnelled peritoneal catheter placement under sonographic and fluoroscopic guidance in the palliative treatment of malignant ascites. *Am J Roentgenol* 2001; **177**: 615-8.
- Richard H, Coldwell D, Boyd-Kranis R, Murthy R, Van Echo D. Pleurx tunneled catheter in the management of malignant ascites. *J Vasc Intervent Radiol* 2001; **12**: 373-5.
- Belfort M, Stevens P, DeHaek K, Soeters R, Krige J. A new approach to the management of malignant ascites; a permanently implanted abdominal drain. *Eur J Surg Oncol* 1990; **16**: 47-53.
- Arai Y, Inaba Y, Sone M, Saitoh H, Takeuchi Y, Shioyama Y, et al. Phase I/II study of transjugular transhepatic peritoneovenous venous shunt, a new procedure to manage refractory ascites in cancer patients: Japan Interventional Radiology in Oncology Study Group 0201. *Am J Roentgenol* 2011; **196**: W621-W626.
- Lorentzen T, Sengeløv L, Nolsøe CP, Khattar SC, Karstrup S, von der Maase H. Ultrasonically guided insertion of a peritoneo-gastric shunt in patients with malignant ascites. *Acta Radiol* 1995; **36**:481-4.
- Stehman F, Ehrlich C. Peritoneo-cystic shunt for malignant ascites. *Gynecol Oncol* 1984; **18**: 402-7.
- Rosenberg S, Courtney A, Nemcek A, Omary R. Comparison of percutaneous management techniques for recurrent malignant ascites. *J Vasc Intervent Radiol* 2004; **15**: 1129-31.
- Tapping C, Ling L, Razack A. PleurX drain use in the management of malignant ascites: safety, complications, long-term patency and factors predictive of success. *Br J Radiol* 2012; **85**: 623-8.
- Lungren M, Kim C, Stewart J, Smith T, Miller M. Tunnelled peritoneal drainage catheter placement for refractory ascites: Single-center experience in 188 patients. *J Vasc Intervent Radiol* 2014; **24**: 1303-8.
- Courtney A, Nemcek A, Rosenberg S, Tutton S, Darcy M, Gordon G. Prospective evaluation of the PleurX catheter when used to treat malignant ascites associated with malignancy. *J Vasc Intervent Radiol* 2008; **19**: 1723-31.
- Savin M, Kirsch M, Romano W, Wang S, Arpasi P, Mazon C. Peritoneal ports for treatment of intractable ascites. *J Vasc Intervent Radiol* 2005; **16**: 363-8.
- Ozkan O, Akinci D, Gocmen R, Gil B, Ozmen M, Akhan O. Percutaneous placement of peritoneal port-catheter in patients with malignant ascites. *Cardiovasc Intervent Radiol* 2007; **30**: 232-6.
- Baumann K, Pfisterer J, Wimberger P, Burchardi N, Kurzeder C, du Bois A, et al. Intraperitoneal treatment with the trifunctional bispecific antibody Catumaxomab in patients with platinum-resistant epithelial ovarian cancer: A phase IIa study of the AGO Study Group. *Gynecol Oncol* 2011; **123**: 27-32.
- Barnett T, Rubins J. Placement of a permanent tunnelled peritoneal drainage catheter for palliation of malignant ascites: A simplified percutaneous approach. *J Vasc Intervent Radiol* 2002; **13**: 379-83.
- Akinci D, Erol B, Ciftci T, Akhan O. Radiologically placed tunnelled peritoneal catheter in palliation of malignant ascites. *Eur J Radiol* 2008; **80**: 265-8.
- Heiss M, Murawa P, Koralewski P, Kutarska E, Kolesnik O, Ivanchenko V, et al. The trifunctional antibody catumaxomab for the treatment of malignant ascites due to epithelial cancer: results of a prospective randomized phase II/III trial. *Int J Cancer* 2010; **127**: 2209-21.

CA19-9 serum levels predict micrometastases in patients with gastric cancer

Tomaz Jagric¹, Stojan Potrc², Katarina Mis³, Mojca Plankl², Tomaz Mars³

¹ Department of Abdominal and General Surgery, University Medical Centre Maribor, Maribor, Slovenia

² Institute of Pathophysiology, Faculty of Medicine, University of Ljubljana, Ljubljana, Slovenia

Radiol Oncol 2016; 50(2): 204-211.

Received 4 October 2014

Accepted 9 May 2015

Correspondence to: Tomaz Jagric, M.D., Ph.D., Department of Abdominal and General Surgery, University Medical Centre Maribor, Ljubljanska 5, Maribor 2000, Slovenia. Phone: +386 41 424 225; E-mail: tomaz.jagric@gmail.com

Disclosure: No potential conflicts of interest were disclosed.

Background. We explored the prognostic value of the up-regulated carbohydrate antigen (CA19-9) in node-negative patients with gastric cancer as a surrogate marker for micrometastases.

Patients and methods. Micrometastases were determined using reverse transcription quantitative polymerase chain reaction (RT-qPCR) for a subgroup of 30 node-negative patients. This group was used to determine the cut-off for preoperative CA19-9 serum levels as a surrogate marker for micrometastases. Then 187 node-negative T1 to T4 patients were selected to validate the predictive value of this CA19-9 threshold.

Results. Patients with micrometastases had significantly higher preoperative CA19-9 serum levels compared to patients without micrometastases ($p = 0.046$). CA19-9 serum levels were significantly correlated with tumour site, tumour diameter, and perineural invasion. Although not reaching significance, subgroup analysis showed better five-year survival rates for patients with CA19-9 serum levels below the threshold, compared to patients with CA19-9 serum levels above the cut-off. The cumulative survival for T2 to T4 node-negative patients was significantly better with CA19-9 serum levels below the cut-off ($p = 0.04$).

Conclusions. Preoperative CA19-9 serum levels can be used to predict higher risk for haematogenous spread and micrometastases in node-negative patients. However, CA19-9 serum levels lack the necessary sensitivity and specificity to reliably predict micrometastases.

Key words: gastric cancer; micrometastases; CA19-9

Introduction

In addition to local extent tumours, preoperative nodal staging is of the utmost importance when deciding upon lymphadenectomies in gastric cancer. Unfortunately, contemporary imaging modalities struggle with the modest sensitivities and specificities when it comes to nodal staging.¹ To make matters even more challenging, the first metastases in early gastric cancer are usually in the form of small tumour-cell deposits, and the metastatic lymph nodes are often not enlarged.² The average size of lymph nodes with micrometastases has been reported to be < 5 mm, which is below the size that can be reliably detected with preoperative imaging.²

Although the importance of micrometastases has been widely debated, there is some consensus on the prognostic relevance of micrometastases in lymph nodes.³⁻⁵ Due to their impact on long-term prognosis; many studies have searched for simple and reliable ways to detect micrometastases in patients with gastric cancer. To date, the only way to determine the presence of micrometastases is the additional analysis of lymph nodes using immunohistochemical or molecular methods.⁶⁻⁹ However, such elaborate and expensive methods used to detect micrometastases cannot be applied to clinical practice in their present form. Additional markers that can indicate the presence of such micrometastases will thus be of immense value.

Serum tumour markers have long been used for early detection and follow-up in patients with gastric cancer.¹⁰⁻¹⁵ Elevated serum levels of carbohydrate antigen 19-9 (CA19-9; or the sialyl-Lewis A determinant) have been the focus of investigations because of the reported association of CA19-9 with lymph-node metastases.¹⁴ CA19-9 is a tumour-associated carbohydrate determinant. Epigenetic silencing of the sialyltransferase gene early in tumour development leads to reduction in the production of the normally present disialyl-Lewis A determinant. This incomplete synthesis in tumour cells thus results in accumulation of the sialyl-Lewis A determinant (i.e., CA19-9). CA19-9 is a ligand for E-selectin, which is expressed on the surface of endothelial cells. These changes allow tumour cells to invade lymphovascular structures in the setting of low oxygen tissue tension during accelerated growth.¹⁶ Patients who show high expressing levels of the CA19-9 antigen have been shown to be at greater risk of developing lymph-node and haematogenous metastases.^{14,16} The use of CA19-9 to indicate lymph-node metastases is, however, still controversial.^{10,12,13,17} The low sensitivity and specificity of CA19-9 does not allow for its use in the prediction of lymph-node metastases. Furthermore, CA19-9 serum levels are usually low in early gastric cancer, which precludes its use for the detection of early lymph-node metastases, or even micrometastasis.

In our previous report, we demonstrated significant differences in the subclinical expression of serum levels of CA19-9 in patients with micrometastases, compared to patients with negative lymph nodes.¹⁸ This led us to further explore these differences in patients with node-negative gastric cancer. To confirm the correlation of preoperative CA19-9 serum levels with micrometastases in the lymph nodes, we measured the preoperative CA19-9 serum levels in patients with and without lymph-node micrometastases. We then investigated the correlation between micrometastases and preoperative CA19-9 serum levels to determine the cut-off level for micrometastases detection, along with the respective sensitivities and specificities. Finally, the prognostic value of this cut-off for CA19-9 serum levels was investigated for a group of patients with node-negative gastric cancer.

Patients and methods

Between 1992 and 2013, a total of 1,129 patients underwent surgery for gastric cancer at the University

Clinical Centre Maribor, Slovenia. From these, only node-negative patients with complete clinicopathological records and preoperative CA19-9 serum levels were included in this study.

The inclusion criteria were for histologically confirmed node-negative adenocarcinoma of the stomach, D2 lymphadenectomy (as defined by the 3rd English edition of the Japanese Gastric Cancer Association guidelines¹⁸), and complete record of preoperative tumour marker levels. All surgical specimens underwent pathological examination according to the guidelines for gastric cancer of the International Union Against Cancer. Patients with missing values were excluded from further analysis. Thus, 187 patients were included in the final study group, with their preoperative CA19-9 cut-off levels tested for clinical significance.

First, in a test group of 30 patients, we prospectively performed with reverse transcription quantitative polymerase chain reaction (RT-qPCR) analysis of sentinel lymph nodes for micrometastases, as described in our earlier reports.^{19,20} The preoperative differences in CA19-9 serum levels in these patients were used to determine the cut-off value of the preoperative CA19-9 serum levels for further analysis.

The study group of 187 patients was then used to determine the correlations between the preoperative CA19-9 serum levels with tumour characteristics, its predictive significance, and the cut-off value. The mean follow-up was 37 ± 49 months (range, 2 days to 241 months). The patients were divided into two groups according to the derived cut-off value for the CA19-9 serum levels.

Blood samples were obtained by peripheral venous puncture before surgery. CA19-9 serum levels were determined using commercial enzyme immunoassay kits (CA19-9; Dainabot, Tokyo, Japan). The cut-off value was determined through receiver operating characteristics (ROC) analysis of the expression profiles from the RT-qPCR analysis for micrometastases.

The sentinel lymph nodes were extracted as described in our previous reports.^{19,21} In brief, preoperative risk assessment for the metastatic involvement of lymph nodes was carried out according to the Maruyama computer program, preoperative staging, and intraoperative dye navigation (Patente Blue V Dye; Guerbet Patent Blue V Sodium 2.5%; Guerbet, Roissy, France). The sentinel lymph nodes were harvested for RT-qPCR analysis. The total RNA was extracted using RNeasy Mini Plus kits (Qiagen, Hilden, Germany), and reverse transcribed with High Capacity cDNA Reverse

TABLE 1. Patient demographic and tumor characteristics according to their positive and negative Ca19-9 serum levels around the cut-off of 3.5 IU/ml

Characteristic	Ca19-9 negative	Ca19-9 positive
Gender [male (%)]	63	57
Age (years \pm SD)	64 \pm 12.2	64 \pm 11.9
ASA (%)		
I	41.8	37.1
II	37.3	37.1
III	20.9	25.7
Lymphadenectomy (%)		
D1	19.2	23.9
D2	80.8	76.1
Tumour site (%)		
Lesser curvature	33.3	38.6
Greater curvature	38.9	40.4
Anterior wall	25.0	15.8
Posterior wall	1.4	2.6
Circumferential	1.4	2.6
Differentiation (%)		
Well	27.4	21.0
Moderate	25.8	33.0
Poor	46.8	46.0
Lauren (%)		
Intestinal	63.9	47.2
Diffuse	19.7	31.5
Mixed	16.4	21.3
Lymphangial invasion [yes (%)]	52.9	54.7
Vascular invasion[yes (%)]	7.3	11.1
Perineural invasion[yes (%)]	15.7	14.4
T stage (%)		
1	31.5	43.8
2	38.4	28.9
3	26.0	18.4
4	4.1	8.8
UICC (%)		
Ia	31.5	45.6
Ib	38.4	28.9
IIa	26.0	16.7
IIb	1.4	5.3
IIIb	2.7	3.5
Tumour diameter (mm \pm SD)	52 \pm 33.8	50 \pm 32.4
Number of extracted lymph nodes (n \pm SD)	21 \pm 11.2	20 \pm 10.7

ASA = American Society of Anesthesiologists physical status classification system; UICC = Union for International Cancer Control

Transcription kits (Applied Biosystems, Carlsbad, CA, USA). Q-PCR was performed on an ABI Prism SDS 7500 PCR machine (Applied Biosystems), using TaqMan chemistry in a 96-well format. TaqMan Universal PCR Master Mix (Applied Biosystems) and the following Gene Expression Assays (Applied Biosystems) were used: for CEACAM5 Hs 00237075_m1; for KRT20 Hs00300643_m1; and for GAPDH 4333764. Thirty-five cycles were selected as the Ct threshold values for CEACAM5 and CK-20 expression, as determined in our sensitivity and specificity studies.¹⁹

All continuous data are expressed as means \pm standard deviations, and the categorical data are expressed in percentages. Continuous variables were compared with Student's t tests, and χ -squared tests were used for the comparison of discrete variables. Linear correlations were accessed by calculation of Pearson's correlation coefficients. The ROC curves were used to identify potential cut-off values for the CA19-9 serum levels, along with the sensitivities and specificities. The Kaplan-Maier method was used for the survival analysis. Survival time was calculated from surgery to death or the date of the last follow-up visit. The overall survival differences between the groups were determined using log-rank tests. Cox regression models were used to determine the factors related to the overall survival of node-negative patients. The final model was calculated with backward stepwise selection. A *p* value < 0.05 was defined as the limit of significance. SPSS v.20 for Windows 8 was used for the statistical analyses. The probability of lymph-node involvement was estimated with WinEstimate (version 2.5; München, Germany).

Results

Micrometastases were detected in eight patients (26.7%) from the 30 histologically node-negative patients. These patients with micrometastases had significantly higher preoperative CA19-9 serum levels (15.8 \pm 13 IU/ml) than those without micrometastases (6.9 \pm 9 IU/ml; *p* = 0.046). With the ROC analysis, the cut-off value for CA19-9 serum levels of 3.5 IU/ml was selected as a predictor for micrometastases deposits in lymph nodes. With this threshold value, patients with micrometastases were determined with a sensitivity of 87.5% and a specificity of 50% (AUC, 0.724; *p* = 0.064).

The mean CA19-9 serum level of the patients with node-negative gastric cancer was 27.8 \pm 185 IU/ml. Out of the 187 patients, 114 (61%) were

above the threshold CA19-9 serum level of 3.5 IU/ml. There was significant linear correlation between the preoperative CA19-9 serum levels and tumour sites ($p = 0.035$), tumour diameters ($p = 0.012$), and perineural infiltration ($p = 0.007$). There were significant differences in the preoperative CA19-9 serum levels between patients with different tumour sites, as seen by one-way analysis of variance (ANOVA) tests. The patients with Bormann type IV tumour (i.e., whole stomach involvement) had the highest preoperative CA19-9 serum levels (i.e., lesser curvature: 15.9 ± 48 IU/ml; greater curvature: 15.1 ± 52 IU/ml; anterior wall: 11.7 ± 20 IU/ml; whole circumference: 633.7 ± 1227 IU/ml; posterior wall:

TABLE 2. Median survival rates of patients with T1 to T4 N0 tumours according to their positive and negative Ca19-9 serum levels around the cut-off of 3.5 IU/ml

Tumour stage	Ca19-9 cut-off	Median survival (months \pm SD)
T1N0	Negative	121 \pm 15.7
	Positive	126 \pm 12.2
T2N0	Negative	121 \pm 13.9
	Positive	89 \pm 13.1
T3N0	Negative	103 \pm 18
	Positive	65 \pm 12.4
T4N0	Negative	47 \pm 18.9
	Positive	18 \pm 2.2

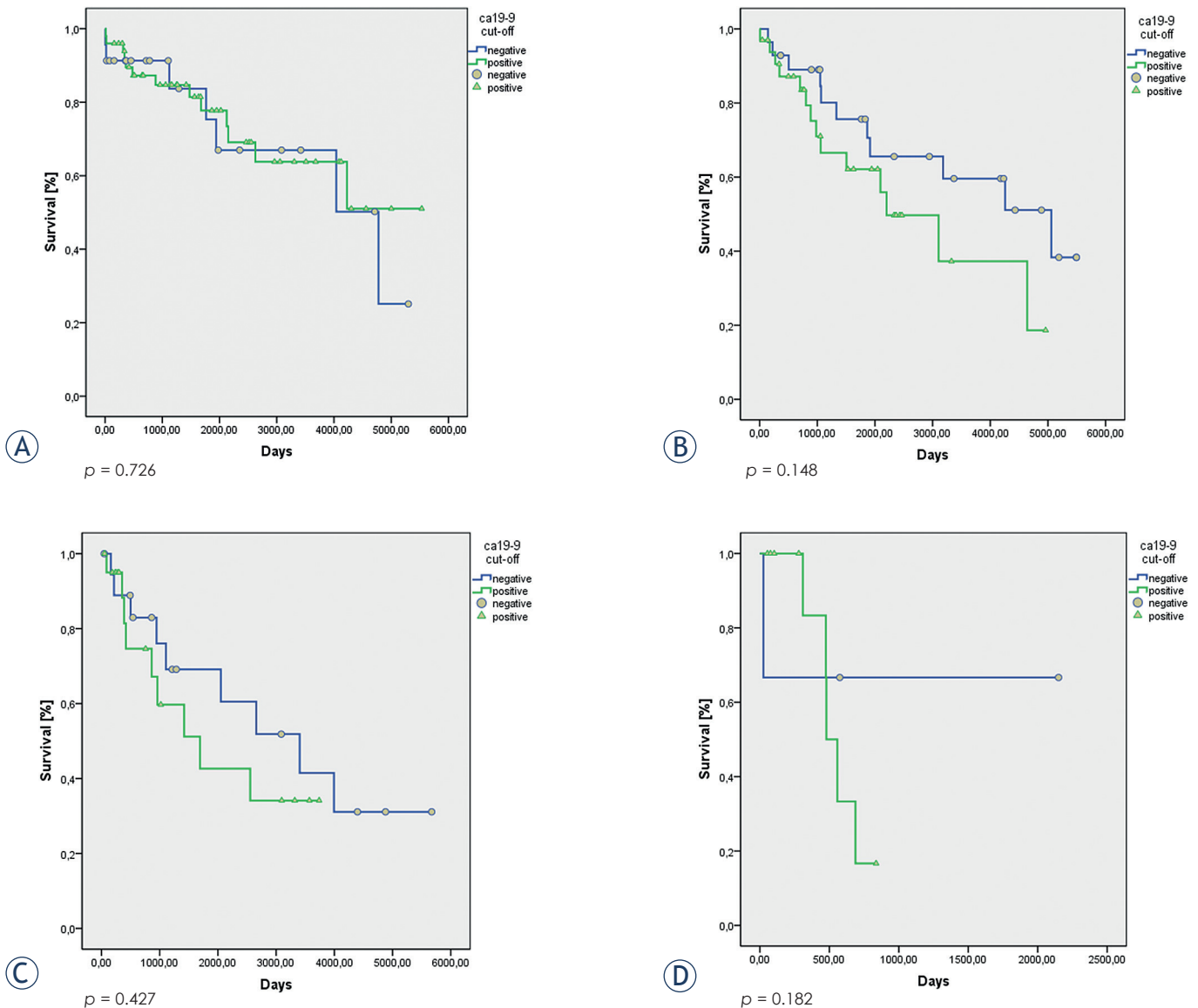
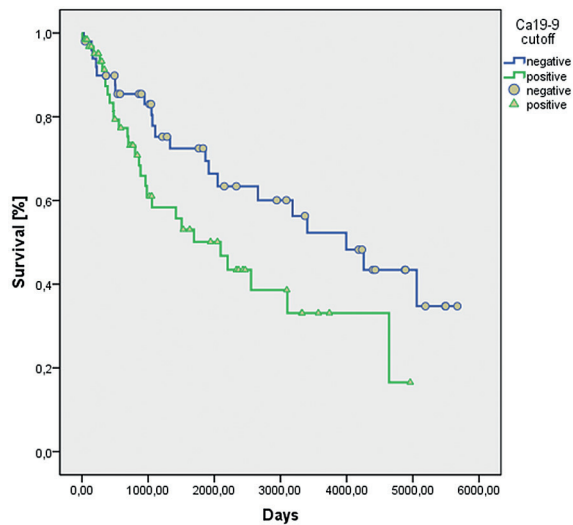


FIGURE 1. Survival of patients with T1 N0 (A), T2 N0 (B), T3 N0 (C) and T4 N0 (D) gastric cancer according to their positive and negative Ca19-9 serum levels around the cut-off of 3.5 IU/ml.

TABLE 3. Results of the multivariate regression model analysis

Factor	Hazard ratio	95% confidence interval		p
		Lower	Upper	
Perineural invasion	1.337	0.612	2.921	NS
Tumour site	1.151	0.881	1.502	NS
T stage	1.755	1.321	2.330	0.0001
Extracted lymph nodes	0.972	0.948	0.997	0.026
Preoperative Ca19-9 serum level	1	1.000	1.001	NS
Ca19-9 cut-off (3.5 IU/ml)	1.045	0.528	2.068	NS

NS = not significant



p = 0.04

FIGURE 2. Survival of patients with T2 to T4 N0 gastric cancer according to their positive and negative Ca19-9 serum levels around the cut-off of 3.5 IU/ml.

9.7 ± 7 IU/ml; $p < 0.0001$). The preoperative CA19-9 serum levels of the patients with a tumour involving the entire stomach were significantly greater than those where the tumour was confined to one location, irrespective of the TNM stage ($p < 0.0001$). Also, the patients with perineural infiltration had significantly higher preoperative CA19-9 serum levels (143.4 ± 526 IU/ml vs. 14.5 ± 43 IU/ml; $p = 0.007$). There were no statistically significant correlations between the cut-off value for the CA19-9 serum levels and the clinicopathological characteristics of the patients.

These clinicopathological characteristics of the patients with CA19-9 serum levels above and below the cut-off of 3.5 IU/ml are shown in Table 1. Between these groups, there were no significant differences in age, gender, grade, Lauren histologi-

cal type, TNM stage, tumour diameter, lymphangial infiltration, vascular infiltration, perineural invasion, extranodal infiltration, or extent of lymphadenectomy distribution.

The cumulative 5 year survival of the node-negative patient group was 67.4% ± 4%, with a median survival of 130.9 months. The cumulative 5 year overall survival rates by T stage for T1, T2, T3, T4a and T4b were 77% ± 6%, 69% ± 7%, 56% ± 9%, 25% ± 22% and 31% ± 24%, respectively.

There were no significant differences in the cumulative 5 year overall survival rates between groups with different cut-off values of the CA19-9 serum levels (CA19-9 negative group: 73% ± 6%; CA19-9 positive group: 63% ± 5%; $p = 0.305$). However, if we excluded the patients with stages T1a and T1b from the analysis, a significant difference was seen between the overall survival of the patients with CA19-9 serum levels above and below our cut-off of 3.5 IU/ml (CA19-9 negative group: 72% ± 7%; CA19-9 positive group: 50% ± 8%; $p = 0.04$). Subgroup analysis failed to show significant differences in the 5 year overall survival rates for the individual stages of T1 to T4 between these CA19-9 negative and positive groups. Even so, the patients with stages T2 to T4 with CA19-9 serum levels above the set cut-off of 3.5 IU/ml had consistently worse overall survival rates than the patients below this cut-off value (Table 2, Figures 1, 2).

The factors identified as significant predictors through univariate analysis were: preoperative CA19-9 serum level, tumour site, tumour diameter, T stage, number of extracted lymph nodes and the CA19-9 cut-off value. These were included in the Cox proportional hazard regression model. The multivariate analysis identified the significant prognostic factors in node-negative patients as T stage (hazard ratio, 1.755; 95% confidence interval, 1.321–2.33; $p < 0.001$) and number of extracted lymph nodes (hazard ratio, 0.972; 95% confidence interval, 0.948–0.997; $p = 0.026$) (Table 3).

The procedures described in this study were in accordance with the Helsinki declaration. All patients gave their written informed consent before being included in the present study. This study was approved by the National Ethics Committee (No. 153/02/0).

Discussion

According to previous reports, micrometastases in the lymph nodes have significant impact on patient survival.^{5,22-24} As the incidence of micrometastases

is said to be even as high as 30% in node-negative patients²⁵⁻²⁷, it appears that these patients should be correctly staged at least intraoperatively. While it might be possible to reliably detect micrometastases with immunohistochemical or molecular techniques⁶⁻⁹, these techniques are time and labour intensive, and the results are usually available only after the operation. To identify a preoperative tool for micrometastases prediction, we explored the prognostic value of CA19-9 serum levels in node-negative patients.

Since the introduction of CA19-9 serum levels in clinical practice, numerous publications have confirmed that elevated CA19-9 serum levels are a predictor for lymph-node metastases and indicate worse prognosis for patients with advanced gastric cancer.¹⁰⁻¹⁵ To the best of our knowledge, the preoperative CA19-9 serum levels have never been used to predict micrometastases in patients with gastric cancer. As the up-regulated sialyl-Lewis A determinant (i.e., the CA19-9 antigen) in tumour cells has been shown to predispose patients with adenocarcinoma and squamous cell carcinoma to haematogenous metastases¹⁶, it can be seen that patients with elevated CA19-9 serum levels are at greater risk for micrometastatic lymph-node involvement. The aim of our study was to determine whether there is a correlation between early elevation of CA19-9 serum levels and the presence of micrometastases in patients with gastric cancer. We therefore studied the correlations of CA19-9 serum levels with the pathological properties of these tumours and the impact on the long-term survival of patients with node-negative gastric cancer.

As previously reported by our group, a significant difference was noted in the preoperative subclinical (< 37 IU/ml) CA19-9 serum levels in patients with node-negative gastric cancer with micrometastases, compared to patients without micrometastases.¹⁸ Patients with micrometastases were seen to have preoperative CA19-9 serum levels that were almost twice as high as those for patients without micrometastases. This observation led us to believe that CA19-9 serum levels can be used as a predictor for micrometastatic lymph-node involvement in patients with node-negative gastric cancer.

Cut-off values for CA19-9 serum levels as a marker for micrometastases were determined on a subgroup of 30 patients where their sentinel lymph nodes were subjected to RT-qPCR analysis in addition to routine histology.¹⁹⁻²¹ For further analysis, the patients in the study group were divided into two groups according to the derived cut-off value

of CA19-9 serum level of 3.5 IU/ml. This cut-off value was used as a surrogate marker for micrometastases. Based on this cut-off, 61% of node-negative patients were shown to have elevated CA19-9 serum levels. Assuming that these patients were at high risk of harbouring micrometastases, the incidence of micrometastases was significantly higher than the 30% usually reported.²⁴⁻²⁷ In contrast with the present study, T4 patients are usually excluded from micrometastases studies, due to the high proportion of early tumour recurrence in the peritoneal cavity.^{28,29} The T4 patients included in the present study with a probability of lymph-node deposits of > 80%, explain a much higher micrometastatic involvement in the patient cohort in the present study compared to other reports.

To determine whether CA19-9 serum levels were elevated in patients with micrometastases, a group of node-negative patients was retrospectively analysed. We selected patients from our database with TNM stages T1 to T4N0. As it would have been too time consuming to retrospectively look for micrometastases in the paraffin blocks of the lymph nodes of 187 patients, we instead searched for correlations of CA19-9 serum levels with the pathological features usually associated with node-negative patients with micrometastases, as indirect markers for the presence of micrometastases. In the present study, a significant correlation was observed between the preoperative CA19-9 serum levels and tumour size, perineural invasion, and type Borman IV tumours. All of these pathological features are signs of more aggressive and invasive tumour behavior³⁰⁻³⁵, and patients with tumours that show such features were found to be at greater risk for haematogenic spread and micrometastases in the lymph nodes.

To determine whether the cut-off value of the CA19-9 serum levels has a similar prognostic impact on node-negative patients as described for micrometastases, we compared the survival of the node-negative patients stratified into two groups according to the derived CA19-9 cut-off level. While there was no difference in the cumulative survival rate, a significant difference was found when the T1N0 patients were excluded. Patients with a tumour limited to the mucosa (T1a) have an excellent long-term survival rate, and when a D2 lymphadenectomy is performed, only a modest survival benefit is achieved compared to patients without micrometastases.^{28,29,36} Reports of the impact of micrometastases on survival are usually restricted to stages T1b, T2 and T3.^{28,29,36,37} These findings coincide with our data here that indicate a sur-

vival benefit for the T2 to T4N0 patients with lower CA19-9 serum levels, and hence a lower probability of micrometastases. Assuming that preoperative CA19-9 serum levels are indeed a marker for micrometastases in node-negative patients, we can see that the stratification of patients according to our CA19-9 cut-off level had the same impact on survival as would be expected in patients with micrometastases. However, although this cut-off of CA19-9 serum levels of 3.5 IU/ml was identified as a significant predictor with univariate analysis, it failed to reach the limit of significance with multivariate analysis. Thus, multivariate analysis identified only T stage and the number of extracted lymph nodes as significant prognostic factors for overall survival.

Although tumour markers have been extensively used for the follow-up of oncological patients, their preoperative prognostic value remains to be determined. Based on our data, we show here that tumours with elevations in CA19-9 serum levels above 3.5 IU/ml share similar pathological properties as seen in patients with micrometastases. This would identify the patients with higher likelihood for haematogenic dissemination. Whether CA19-9 serum levels can serve as a surrogate marker for micrometastases in patients with gastric cancer remains a matter of debate, but we have shown here that our CA19-9 cut-off of 3.5 IU/ml has prognostic significance in some node-negative patients, and in the future, this might be one of the preoperative screening tests that can be used to guide surgical and multimodal treatments of patients with node-negative gastric cancer.

References

1. Kwee RM, Kwee TC. Imaging in assessing lymph node status in gastric cancer. *Gastric Cancer* 2009; **12**: 6-22.
2. Arai K, Iwasaki Y, Takahashi T. Clinicopathological analysis of early gastric cancer with solitary lymph node metastasis. *Brit J Surg* 2002; **89**: 1435-7.
3. Yasuda K, Adachi Y, Shiraiishi N, Inomata M, Takeuchi H, Kitano S. Prognostic effect of lymph node micrometastasis in patients with histologically node-negative gastric cancer. *Ann Surg Oncol* 2002; **9**: 771-4.
4. Huang J, Xu Y, Li M, Sun Z, Zhu Z, Song Y, et al. The prognostic impact of occult lymph node metastasis in node-negative gastric cancer: A systemic review and meta-analysis. *Ann Surg Oncol* 2013; **20**: 3927-34.
5. Cai J, Ikeguchi M, Kaibara N, Sakatani T. Clinicopathological value of immunohistochemical detection of occult involvement in pT3N0 gastric cancer. *Gastric Cancer* 1999; **2**: 95-100.
6. Yanagita S, Natsugoe S, Uenosono Y, Arigami T, Arima H, Kozono T, et al. Detection of micrometastases in sentinel node navigation surgery for gastric cancer. *Surg Oncol* 2008; **17**: 203-10.
7. Kubota K, Nakanishi H, Hiki N, Shimizu N, Tsuji E, Yamaguchi H, et al. Quantitative detection of micrometastases in the lymph nodes of gastric cancer patients with Real-time RT-PCR: A comparative study with immunohistochemistry. *Int J Cancer* 2003; **105**: 136-43.
8. Osaka H, Yashiro M, Sawada T, Katsuragi K, Hirakawa K. Is a lymph node detected by the dye-guided method a true sentinel node in gastric cancer? *Clin Cancer Res* 2004; **10**: 6912-8.
9. Shimizu Y, Takeuchi H, Sakakura Y, Saikawa Y, Nakahara T, Mukai M, et al. Molecular detection of sentinel node micrometastases in patients with clinical N0 gastric carcinoma with real-time multiplex reverse transcription-polymerase chain reaction assay. *Ann Surg Oncol* 2012; **19**: 469-77.
10. Ishigami S, Natsugoe S, Hokita S, Che X, Tokuda K, Nakajo A, et al. Clinical importance of preoperative carcinoembryonic antigen and carbohydrate antigen 19-9 levels in gastric cancer. *J Clin Gastroenterol* 2001; **32**: 41-4.
11. Dilege E, Mihmanli M, Demir U, Özer K, Bostancu Ö, Kaya C, et al. Prognostic value of preoperative CEA and CA 19-9 levels in resectable gastric cancer. *Hepatogastroenterology* 2010; **57**: 674-7.
12. Kodera Y, Yamamura Y, Torii A, Uesaka K, Hirai T, Yasui K, et al. The prognostic value of preoperative serum level of CEA and CA19-9 in patients with gastric cancer. *Am J Gastroent* 1996; **91**: 49-53.
13. Mihmanli M, Dilege E, Demir U, Coskun H, Eroglu T, Uysalol MD. The use of tumor markers as predictors of prognosis in gastric cancer. *Hepatogastroenterology* 2004; **51**: 1544-7.
14. Tsirlis TD, Kostakis A, Papastratis G, Masselou K, Vlachos I, Papachristodoulou A, et al. Predictive significance of preoperative serum VEGF-C and VEGF-D, independently and combined with Ca19-9, for the presence of malignancy and lymph node metastasis in patients with gastric cancer. *J Surg Oncol* 2010; **102**: 699-703.
15. Mattar R, Alves de Andrade CR, DiFavero GM, Gama-Rodrigues JJ, Laudanna AA. Preoperative serum levels of CA 72-5, CEA, CA 19-9 and Alpha-fetoprotein in patients with gastric cancer. *Rev Hosp Clin Fac Med S Paulo* 2002; **57**: 89-92.
16. Kannagi R. Carbohydrate antigen Sialyl Lewis x – Its pathophysiological significance and induction mechanism in cancer progression. *Chang Gung Med J* 2007; **30**: 189-209.
17. Duraker N, Celik AN. The prognostic significance of preoperative serum CA 19-9 in patients with resectable gastric carcinoma: Comparison with CEA. *J Surg Oncol* 2001; **76**: 266-71.
18. Japanese Gastric Cancer Association. Japanese gastric cancer treatment guidelines 2010 (ver. 3). *Gastric Cancer* 2011; **14**: 113-23.
19. Jagrio T, Potrc S, Ivanecz A, Horvat M, Plankl M, Mars T. Evaluation of focused sentinel lymph node RT-qPCR screening for micrometastases with the use of the Maruyama computer program. *Eur Surg* 2013; **45**: 270-6.
20. Jagrio T, Plankl M, Ivanecz A, Horvat M, Gajzer B, Grubic Z, et al. The prognostic value of micrometastases found intraoperatively in the first draining lymph node in gastric cancer patients. *Zdrav Vestn* 2012; **81**: 775-83.
21. Jagrio T, Ivanecz A, Horvat M, Plankl M, Kavalar R, Potrc S, et al. Evaluation of a focused sentinel lymph node protocol in node-negative gastric cancer patients. *Hepatogastroenterol* 2013; **60**: 1231-6.
22. Ishigami S, Natsugoe S, Tokuda K, Nakajo A, Higashi H, Watanabe T, et al. Clinical impact of micrometastasis of lymph node in gastric cancer. *Am Surg* 2003; **69**: 573-7.
23. Nakajo A, Natsugoe S, Ishigami S, Matsumoto M, Nakashima S, Hokita S, et al. Detection and prediction of micrometastasis in the lymph nodes of patients with pN0 gastric cancer. *Ann Surg Oncol* 2000; **8**: 158-62.
24. Sievert JR, Kestlmaier R, Busch R, Böttcher K, Roder JD, Müller J, et al. Benefits of D2 lymph node dissection for patients with gastric cancer and pN0 and pN1 lymph node metastases. *Brit J Surg* 1996; **83**: 1144-7.
25. Saito H, Osaki T, Murakami D, Sakamoto T, Kanaji S, Ohro S, et al. Recurrence in early gastric cancer – Presence of micrometastases in lymph node negative early gastric cancer patient with recurrence. *Hepatogastroenterol* 2007; **54**: 620-4.
26. Otsuji E, Toma A, Kobayashi S, Okamoto K, Hagiwara A, Yamagishi H. Outcome of prophylactic Radical lymphadenectomy with gastrectomy in patients with early gastric carcinoma without lymph node metastases. *Cancer* 2000; **89**: 1425-30.
27. Nakajo A, Natsugoe S, Ishigami S, Matsumoto M, Nakashima S, Hokita S, et al. Detection and prediction of micrometastases in the lymph nodes of patients with pN0 gastric cancer. *Ann Surg Oncol* 2001; **8**: 158-62.

28. Fukagawa T, Sasako M, Ito S, Nakanishi H, Iinuma H, Natsugoe S. The prognostic significance of isolated tumor cells in the lymph nodes of gastric cancer patients. *Gastric Cancer* 2010; **13**: 191-6.
29. Fukagawa T, Sasako M, Mann GB, Sano T, Katai H, Maruyama K, et al. Immunohistochemically detected micrometastases of the lymph nodes in patients with gastric carcinoma. *Cancer* 2001; **92**: 753-60.
30. Cao L, Hu X, Zhang Y, Huang G. Adverse prognosis of clustered-cell versus single-cell micrometastases in pN0 early gastric cancer. *J Surg Oncol* 2011; **103**: 53-6.
31. Kim JJ, Song KY, Hur H, Hur JJ, Park SM, Park CH. Lymph node micrometastasis in node negative early gastric cancer. *Eur J Surg Oncol* 2009; **35**: 409-14.
32. Chou HH, Kuo CJ, Hsu JT, Chen TH, Lin CJ, Tseng JH, et al. Clinicopathologic study of node-negative advanced gastric cancer and analysis of factors predicting its recurrence and prognosis. *Am J Surgery* 2013; **101**: 623-30.
33. Iwasaki Y, Sasako M, Yamamoto S, Nakamura K, Sano T, Katai H, et al. Phase II study of preoperative chemotherapy with S-1 and Cisplatin followed by gastrectomy for clinically resectable type 4 and large type 3 gastric cancers (JCOG0210). *J Surg Oncol* 2013; **107**: 741-5.
34. Kodera Y, Nakanishi H, Ito S, Mochizuki Y, Yamamura Y, Fujiwara M, et al. Detection of disseminated cancer cells in linitis plastica-type gastric carcinoma. *Jpn J Clin Oncol* 2004; **34**: 525-31.
35. Endo K, Sakurai M, Kusumoto E, Uehara H, Yamaguchi S, Tsutsumi N, et al. Biological significance of localized type IV scirrhous gastric carcinoma. *Oncol Letters* 2012; **3**: 94-9.
36. Miwa K, Miyazaki I, Sahara H, Fujimura T, Yonemura Y, Noguchi M, et al. Rationale for extensive lymphadenectomy in early gastric carcinoma. *Brit J Cancer* 1995; **72**: 1518-24.
37. Maehara Z, Oshiro T, Endo K, Baba H, Oda S, Ichiyoshi Y, et al. Clinical significance of occult micrometastasis lymph nodes from patients with early gastric cancer who died of recurrence. *Surgery* 1996, **119**: 397-402.

Hepatic splenosis mimicking liver metastases in a patient with history of childhood immature teratoma

Sara Jereb¹, Blaz Trotovsek², Breda Skrbinc³

¹ Infectious Diseases Department, University Medical Centre Ljubljana, Ljubljana, Slovenia

² Department of Abdominal Surgery, University Medical Centre Ljubljana, Ljubljana, Slovenia

³ Department of Medical Oncology, Institute of Oncology Ljubljana, Ljubljana, Slovenia

Radiol Oncol 2016; 50(2): 212-217.

Received 20 July 2014

Accepted 28 August 2014

Correspondence to: Sara Jereb, M.D., Infectious Diseases Department, University Medical Centre Ljubljana, Japljeva 2, 1000 Ljubljana, Slovenia. E-mail: sara.jereb@gmail.com

Disclosure: No potential conflicts of interest were disclosed.

Background. Hepatic splenosis is rare condition, preceded by splenectomy or spleen trauma, the term refers to nodular implantation of normal splenic tissue in the liver. In patients with history of malignancy in particular, it can be mistaken for metastases and can lead to unnecessary diagnostic procedures or inappropriate treatment.

Case report. Twenty-two-year old male was treated for immature teratoma linked to undescended right testicle after birth. On regular follow-up examinations no signs of disease relapse or long-term consequences were observed. He was presented with incidental finding of mature cystic teratoma after elective surgery for what appeared to be left-sided inguinal hernia. The tumour was most likely a metastasis of childhood teratoma. Origin within remaining left testicle was not found. Upon further imaging diagnostics, several intrahepatic lesions were revealed. Based on radiologic appearance they were suspicious to be metastases. The patient underwent two ultrasound guided fine-needle aspiration biopsies. Cytologic diagnosis was inconclusive. Histology of laparoscopically obtained tissue disclosed presence of normal splenic tissue and led to diagnosis of hepatic splenosis.

Conclusions. Though hepatic splenosis is rare, it needs to be included in differential diagnosis of nodular hepatic lesions. Accurate interpretation of those lesions is crucial for appropriate management of the patient. If diagnosis eludes after cytologic diagnostics alone, laparoscopic excision of nodular lesion is warranted before considering more extensive liver resection.

Key words: hepatic splenosis; teratoma; metastases; laparoscopy

Introduction

Ectopic spleen tissue takes two forms, it is either congenital and presents as accessory spleens or an acquired condition, called splenosis. Splenosis occurs as un-encapsulated splenic tissue localized outside the spleen. It is a benign condition, most commonly linked to splenic trauma or splenectomy. Post traumatic splenosis is believed to be a rare state; however, it is more likely only to be under-recognized. Patients are in fact most often asymptomatic and the majority of cases are diagnosed by coincidence.¹

As a rule, there are multiple splenic tissue implants embedded in serous surfaces of abdominal cavity such as mesentery, omentum, surfaces of the colon or diaphragm. After penetrating abdominal trauma, extraperitoneal splenosis has also been reported in subcutaneous tissue, pleural cavity or pericardium.²⁻⁵

Rarely, splenic tissue can implant in parenchyma of a visceral organ such as liver. In that case, the condition is defined as hepatic splenosis. Mechanism of splenic tissue spread is not completely understood. One of the hypotheses postulates invagination of splenic implants into

sub-capsular area of the liver after spleen trauma. Alternatively, deep-seated hepatic splenic nodules would result from the microembolisation via the splenic vein. Nodular lesions in liver parenchyma are non-specific on imaging and can mimic malignant as well as benign lesions.⁶ Exploratory laparoscopy is the least invasive method for reaching definitive diagnosis and is the most suitable, especially in patients with history of malignant disease where liver metastases are suspected.

Case report

A 22-year old Caucasian male was presented after operative procedure due to left-sided inguinal hernia, during which a cystic mass inside of hernial sac was revealed. Histology of the tumour disclosed it to be mature cystic teratoma.

The patient was treated for immature teratoma with a prevalence of neuroepithelial components and with high mitotic activity 22 years prior and the tumour most likely originated from retained right testicle. Surgical procedure was performed on day 6 after birth. The tumour had perforated and was macroscopically removed. He received 3 cycles of chemotherapy with vincristine, actinomycin D, cyclophosphamide and cisplatin in the adjuvant setting. On follow-up examinations there were no signs of relapse. At the age of 4 he underwent splenectomy after a motor vehicle accident. For the past year he had been treated for Henoch-Schönlein purpura with renal impairment, he was receiving methylprednisolone.

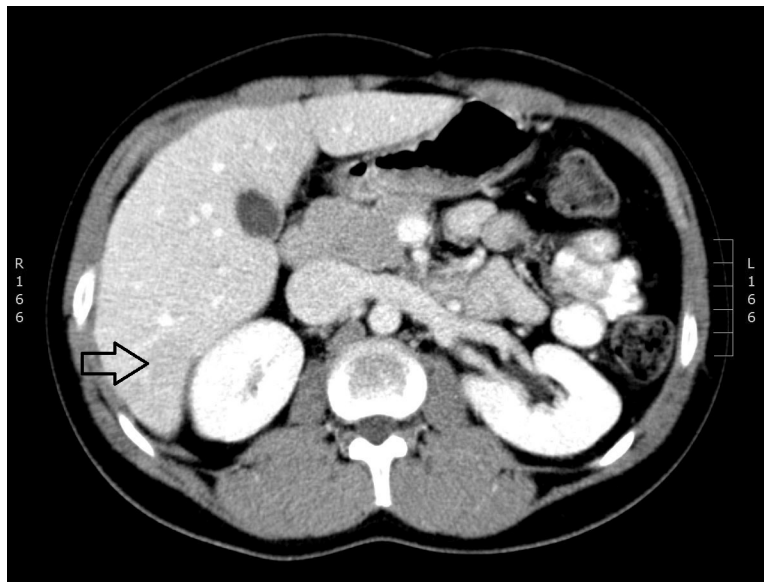


FIGURE 1. CT; portal phase of contrast enhancement - subtle hypodense lesions in 6th liver segment.

After the operative procedure for hernia, patient's alpha-fetoprotein (AFP), Beta unit of human Chorionic Gonadotropin (Beta hCG) and Lactate dehydrogenase (LDH) levels were within normal ranges: AFP 2.2 kU/L (< 5.8), Beta hCG < 0.1 U/L (< 2.0), LDH 2.25 ukat/L (< 4.13). Additional laboratory testing revealed thrombocyte count $491 \times 10^9/L$ (140–340), neutrophil count 77.7% (40–75%), lymphocyte count 17.3% (20–40%), eosinophil count 0.7% (1–6%), and sedimentation rate 29 mm/h (< 19). Electrolyte concentrations, liver function

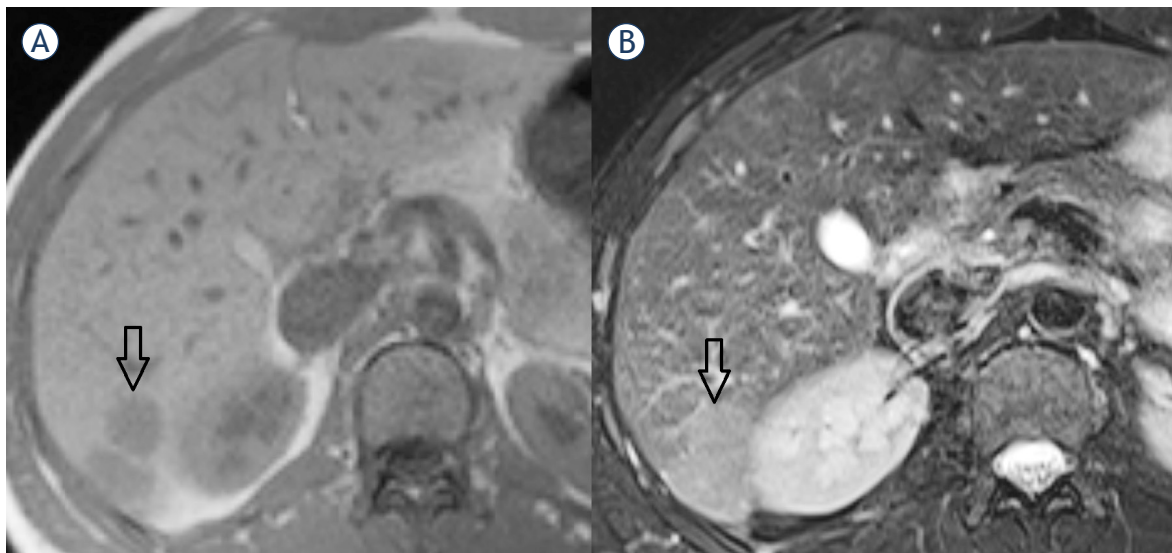


FIGURE 2. MRI; (A) hypointense hepatic lesion in T1 weighted image (WI); (B) T2 fast spin echo (FSE) WI: slightly high signal intensity of hepatic lesion.

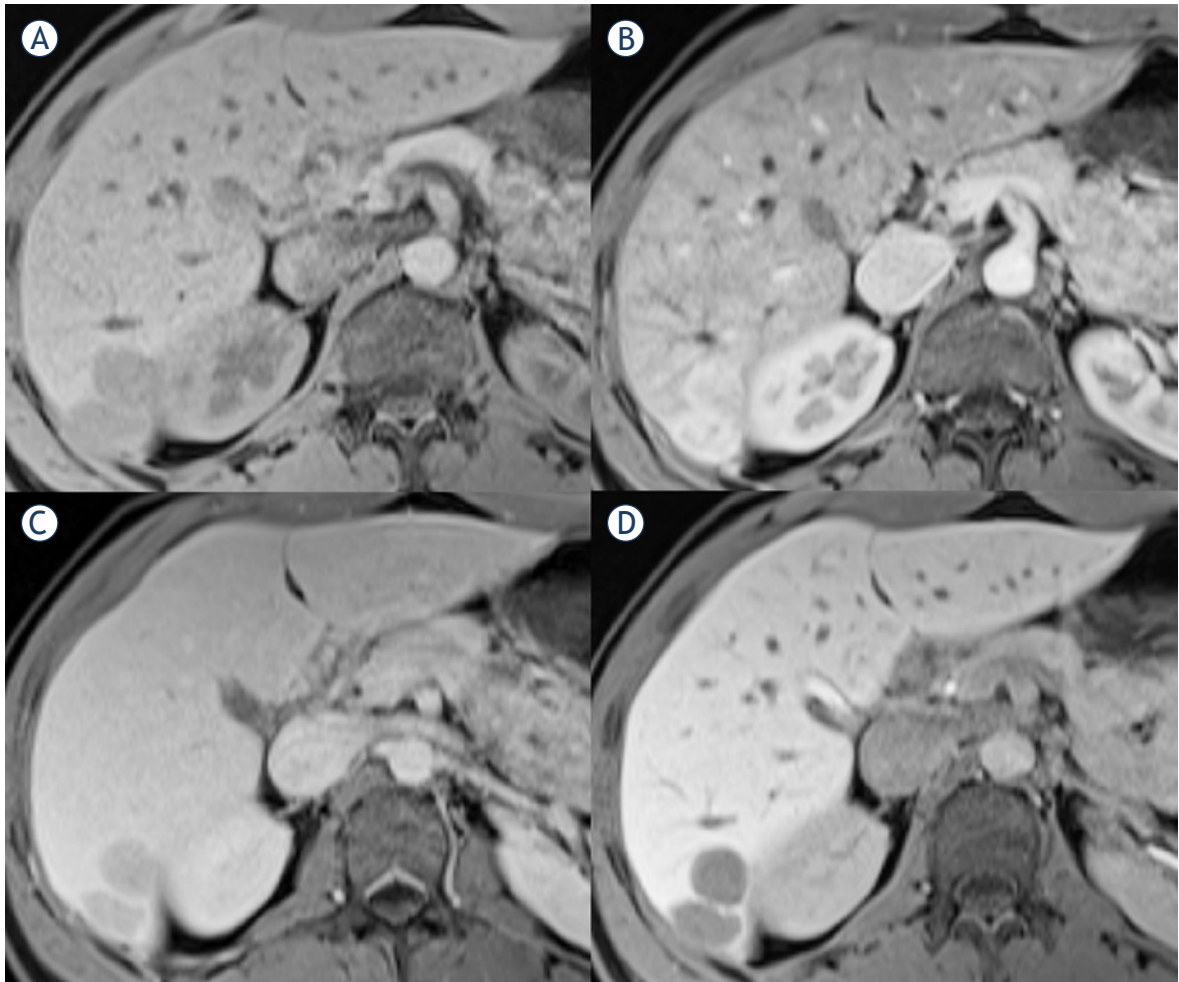


FIGURE 3. MRI; hepatic lesions in T1 volume interpolated breathhold examination (VIBE) fat saturated (FS); (A) pre-contrast; (B) arterial phase; (C) portal phase; (D) delayed phase (20 minutes) of enhancement.

tests, LDH and thyroid hormones were within normal limits.

Imaging diagnostics were performed for disease staging. Scrotal ultrasound revealed small left-sided hydrocele, and no suspicious lesions in left testicle. Left epididymis seemed appropriate. Computed tomography (CT) scan of thoracic organs demonstrated no signs of disease progression. However, on abdominal CT scan two poorly demarcated areas in the 6th liver segment and under the capsule were seen in portal phase of contrast enhancement (Figure 1). There was also small perihepatic oval shaped peritoneal solid lesion of same appearance. Liver size was normal.

With a view to define perihepatic lesions, magnet resonance imaging (MRI) with hepatospecific contrast medium (Gd-EOB-DTPA disodium, i.e. Primovist, Bayer Pharma AG) was performed. Five

round lesions ranging from 0.7 to 2.6 cm in diameter were visible in 2nd, 6th segment and on the border of 6th and 7th segment. They were subcapsularly in liver parenchyma and on the surface of the liver. Lesions were hypointense in T1 weighted images (WI), slightly hyperintense in T2 WI, after administration of hepatospecific contrast medium enhanced during arterial phase, after that they remained hypointense in the late phase images (Figures 2–4). Lesions were suspected to be metastases.

The patient underwent two ultrasound guided fine-needle aspiration biopsies. Sonographically lesions were barely seen, mildly hyperechoic (Figure 5). Obtained samples were unfit to warrant a cytologic diagnosis.

In order to verify suspicious lesions, laparoscopic excision was carried out and intraoperative frozen section analysis evinced spleen tissue.

Histology of the obtained sample confirmed hepatic splenosis.

Tumour, a coincidental finding at operative procedure in left inguinal region, was most likely a metastasis of childhood germ cell tumour. There were no signs of disease spread. Treatment of asymptomatic hepatic splenosis was not indicated.

Discussion

Hepatic splenosis is heterotopic autotransplantation of splenic tissue, as a rule it is a consequence of spleen trauma or splenectomy carried out from other reasons. Ectopic splenic tissue in abdominal cavity is present in more than 60% of patients after traumatic splenic rupture; however, isolated hepatic localization is described only in individual cases.⁶⁻¹⁰ The diagnosis is usually an incidental finding following diagnostics in the scope of another disease, as patients are most often asymptomatic. Mescoli *et al.* report an average time of 29 years between splenectomy and the liver nodules detection.⁶ The patient in our report underwent splenectomy 18 years before the hepatic splenosis was established. He was subjected to regular follow-up after the treatment for childhood immature teratoma, and intermittent abdominal sonography revealed no lesions in hepatic parenchyma.

However, none of the imaging techniques is specific enough to identify hepatic splenosis; ultrasound sensitivity is very poor, CT imaging is

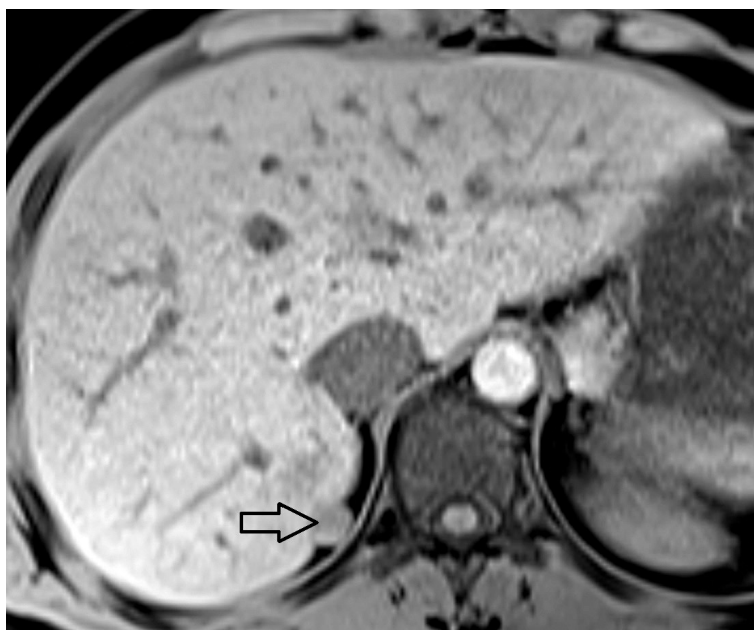


FIGURE 4. Perihepatic lesion in pre-contrast T1 volume interpolated breathhold examination (VIBE) fat saturated (FS).

moderately sensitive and MRI has high sensitivity. Hypervascular nodular hepatic lesions are most commonly haemangioma, hepatic metastases, hepatic adenoma, focal nodular hyperplasia, hepatocellular carcinoma.¹¹ Strictly peripheral lesions in hepatic parenchyma with peritoneal deposits in spleenless patient should warrant differential

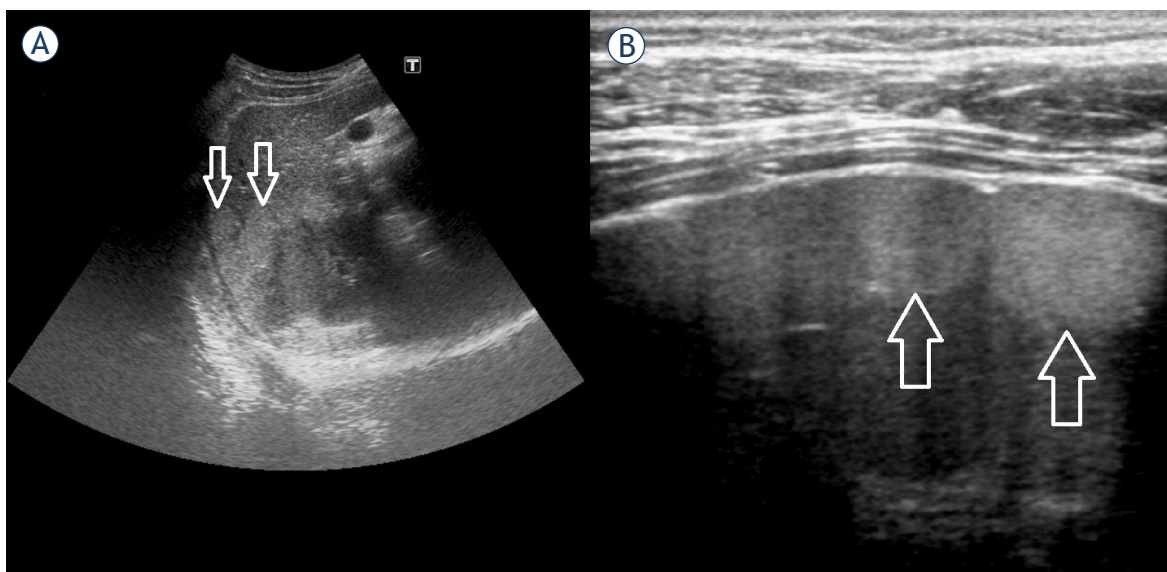


FIGURE 5. US; mildly hyperechoic subcapsular hepatic lesions; (A) abdominal probe; (B) high frequency linear probe.

diagnosis of splenosis. With respect to childhood tumour, hepatic metastases and/or peritoneal dissemination seemed a plausible differential diagnostic option in presented case. The patient was subjected to operative treatment for abdominal tumour few days after birth. Tumour was linked to undescended right testicle and was histologically diagnosed to be immature teratoma. Data shows a link between intraabdominal teratoma and cryptorchidism in children, also, tumour localization at the *annulus inguinalis profundus* is believed to cause testicular retention.¹² Mature teratoma presenting in our patient's adulthood was considered to be a metastasis of primary childhood tumour and less likely metastatic germ cell tumour originating in left testicle. It is known that contralateral testicular tumour is more often found in patients with history of teratoma and *in situ* disgenesis is present in 9% of the patients.¹³ However, clinical examination, biochemistry and imaging excluded left testicle pathology with high probability.

Considering differential diagnosis, nodular hepatic and perihepatic lesions could reflect metastases of immature childhood teratoma as well as mature adulthood teratoma. Immature teratomas are known to metastasize to the solid organs, including liver. Metastatic foci can contain histologically more mature elements than found in primary tumour. One of the reasons is retroconversion of metastases to differentiated mature teratoma under the influence of chemotherapy.¹⁴ Mature teratomas are usually asymptomatic and slow growing, 1.8 mm per year on average. That explains the long-time interval between primary tumor management after birth and finding the mature teratoma at the age of 22 in our case. Also, slow growth could explain presence of nodular hepatic lesions, assessed as possible metastases. On the other hand, the origin of metastases could be the adulthood teratoma, as malignant alteration and metastasizing occur in 1 to 2% of mature teratomas.¹⁵

Differential diagnosis of hepatic splenosis is wide and indirect diagnostic procedures are unreliable as opposed to histologic evaluation. Hematological evaluation can be useful in assessing any persistence of functioning splenic tissue and the absence of Howell-Jolly bodies, Heinz bodies or pitted cells on blood smears may be helpful in diagnosing splenosis. However, sensitivity of the test is low, especially when there is only small amount of ectopic splenic tissue.

There are no typical radiological features of intrahepatic splenosis. Sonographic appearance is

completely unspecific, similar to the current case. Hypoechoic, homogeneous, solid and well circumscribed implants are described in literature, however, in our case lesions were sonographically mildly hyperechoic.¹⁰ In contrast-enhanced CT scans, intrahepatic splenosis is generally revealed as round, oval, or lobular, well circumscribed, non-calcified and homogeneously enhancing. Before injection of contrast medium the implants are usually hypodense or isodense to the liver. In the literature, there are few published descriptions of hepatic splenosis on MRI.^{10,16-21}

On MRI, the characteristics of splenosis are limited to anecdotal cases that have found such lesions as homogeneous, of low signal intensity in T1 WI and moderately hyperintense in T2 WI. Sometimes hypointense thin layer of capsule around the lesion is found in T1 and T2 WI. In arterial or/and portal phase of enhancement lesions are mostly hypervascular and hypointense in delayed images.¹⁷

According to published reports intrahepatic splenosis is most commonly manifested as nodular, solitary lesions, and ranging from 2 to 6 cm in size.^{6,8,10} Described characteristics are true in our case with the exception of the number of lesions. In contrast with presented case Mescoli *et al.* reported that solitary splenic nodules were found in 24 out of 27 patients with the hepatic splenosis. In only one patient more than three nodular lesions were found.⁶ Difference may stem from an underestimation of the results based on radiological investigations. In our case five intrahepatic implants were identified with MRI and two with CT, what is in concordance with multiple studies, which have shown that MRI is superior to CT in sensitivity and accuracy of detecting hepatic lesions.²² Upon ultrasonography the lesions were particularly indistinguishable and mildly hyperechoic. In the literature, all the lesions were described as hypoechoic.

Splenosis is thought to be uncommon, but the incidence is probably underreported since the majority of patients are asymptomatic. Distinguishing the aetiology of hepatic nodular lesions is important because it significantly alters therapeutic procedures. Typical imaging modalities such as US, CT or MRI will not differentiate splenosis from other entities and a histologic specimen needs to be obtained to reach definitive diagnosis. Unfortunately, result of fine-needle aspiration biopsy can be inconclusive as it was in presented case. On the other hand, laparotomy is an excessive operational procedure with potential complications in patients with hepatic splenosis. We presented a case in

which hepatic splenosis has been confirmed by explorative laparoscopy. A laparoscopic approach is minimally invasive for the visualization of suspected intrahepatic masses, and allows access for potential liver biopsy or resection. Similar experiences have been described, but in only few published reports.^{9,23}

Conclusions

Due to the significant impact on treatment decisions intrahepatic splenosis must be considered in the diagnostic spectrum of nodular liver lesions, especially in patients with prior splenic trauma or surgery.

References

- Fleming CR, Dickson ER, Harrison EG Jr. Splenosis: autotransplantation of splenic tissue. *Am J Med* 1976; **61**: 414-19.
- Brewster DC. Splenosis. Report of two cases and review of the literature. *Am J Surg* 1973; **126**: 14-9.
- Bock DB, King BF, Hezmall HP, Oesterling JE. Splenosis presenting as a left renal mass indistinguishable from renal cell carcinoma. *J Urol* 1991; **146**: 152-4.
- Grantham JR, Clore FC. Subcutaneous splenosis. *AJR Am J Roentgenol* 1990; **154**: 655.
- Normand JP, Rioux M, Dumont M, Bouchard G, Letourneau L. Thoracic splenosis after blunt trauma: frequency and imaging findings. *AJR Am J Roentgenol* 1993; **161**: 739-41.
- Mescoli C, Castoro C, Sergio A, Ruol A, Farinati F, Rugge M. Hepatic spleen nodules (HSN). *Scand J Gastroenterol* 2010; **45**: 628-32.
- Livingston CD, Levine BA, Lecklitner ML, Sirinek KR. Incidence and function of residual splenic tissue following splenectomy for trauma in adults. *Arch Surg* 1983; **118**: 617-20.
- D'Angelica M, Fong Y, Blumgart LH. Isolated hepatic splenosis: first reported case. *HPB Surg* 1998; **11**: 39-42.
- Abu Hilal M, Harb A, Zeidan B, Steadman B, Primrose JN, Pearce NW. Hepatic splenosis mimicking HCC in a patient with hepatitis C liver cirrhosis and mildly raised alpha feto protein; the important role of explorative laparoscopy. *World J Surg Oncol* 2009; **7**: 1.
- Kang KC, Cho GS, Chung GA, Kang GH, Kim YJ, Lee MS, et al. Intrahepatic splenosis mimicking liver metastasis in a patient with gastric cancer. *J Gastric Cancer* 2011; **11**: 64-8.
- Toshikuni N, Shiroeda H, Ozaki K, Matsue Y, Minato T, Nomura T, et al. Advanced ultrasonography technologies to assess the effects of radiofrequency ablation on hepatocellular carcinoma. *Radiol Oncol* 2013; **47**: 224-9.
- Doi O, Itoh F, Aoyama K. Mature teratoma arising in intraabdominal undescended testis in an infant with previous inguinal exploration: case report and review of intraabdominal testicular tumors in children. *J Pediatr Surg* 2002; **37**: 1236-8.
- Faure-Contier C, Rocourt N, Sudour-Bonnange H, Vérité C, Martelli H, Patte C, et al. Pediatric germ cell tumours. *Bull Cancer* 2013; **100**: 381-91.
- Kurata A, Hirano K, Nagane M, Fujioka Y. Immature teratoma of the ovary with distant metastases: favorable prognosis and insights into chemotherapeutic retroconversion. *Int J Gynecol Pathol* 2010; **29**: 438-44.
- Outwater EK, Siegelman ES, Hunt JL. Ovarian teratomas: tumor types and imaging characteristics. *Radiographics* 2001; **21**: 475-90.
- Gruen DR, Gollub MJ. Intrahepatic splenosis mimicking hepatic adenoma. *AJR Am J Roentgenol* 1997; **168**: 725-6.
- Tsitouridis I, Michaelides M, Sotiriadis C, Arvaniti M. CT and MRI of intraperitoneal splenosis. *Diagn Interv Radiol* 2010; **16**: 145-9.
- Menth M, Herrmann K, Haug A, Raziorrouh B, Zachoval R, Jung CM, et al. Intra-hepatic splenosis as an unexpected cause of a focal liver lesion in a patient with hepatitis C and liver cirrhosis: a case report. *Cases J* 2009; **2**: 8335.
- Choi GH, Ju MK, Kim JY, Kang CM, Kim KS, Choi JS, et al. Hepatic splenosis preoperatively diagnosed as hepatocellular carcinoma in a patient with chronic hepatitis B: a case report. *J Korean Med Sci* 2008; **23**: 336-41.
- Nakajima T, Fujiwara A, Yamaguchi M, Makiyama A, Wakae T, Fujita K, et al. Intrahepatic splenosis with severe iron deposition presenting with atypical magnetic resonance images. *Intern Med* 2008; **47**: 743-6.
- Imbriaco M, Camera L, Mancinuria A, Salvatore M. A case of multiple intra-abdominal splenosis with computed tomography and magnetic resonance imaging correlative findings. *World J Gastroenterol* 2008; **14**: 1453-5.
- Marcan M, Pavliha D, Music MM, Fuckan I, Magjarevic R, Miklavcic D. Segmentation of hepatic vessels from MRI images for planning of electroporation-based treatments in the liver. *Radiol Oncol* 2014; **48**: 267-81.
- Liu K, Liang Y, Liang X, Yu H, Wang Y, Cai X. Laparoscopic resection of isolated hepatic splenosis mimicking liver tumors: case report with a literature review. *Surg Laparosc Endosc Percutan Tech* 2012; **22**(5): e307-11.

Treatment of nasopharyngeal carcinoma using simultaneous modulated accelerated radiation therapy via helical tomotherapy: a phase II study

Lei Du^{1,2}, Xin Xin Zhang³, Lin Chun Feng¹, Jing Chen¹, Jun Yang⁴, Hai Xia Liu¹, Shou Ping Xu¹, Chuan Bin Xie¹, Lin Ma¹

¹ Department of Radiation Oncology, Chinese PLA General Hospital, Beijing, China

² Department of Radiation Oncology, Hainan Branch of Chinese PLA General Hospital, Haitang Bay, Sanya, China

³ Department of Otorhinolaryngology, Chinese PLA General Hospital, Beijing, China

⁴ Department of Oncology, the First Affiliated Hospital of Xinxiang Medical University, Xinxiang, Henan, China

Radiol Oncol 2016; 50(2): 218-225.

Received 31 August 2015

Accepted 9 December 2015

Correspondence to: Lin Ma, M.D., Department of Radiation Oncology, Chinese PLA General Hospital, 28 Fuxing Road, Beijing 100853, China. E-mail: malinpharm@sina.com

Disclosure: No potential conflicts of interest were disclosed.

The first and second authors contributed equally to this article

Background. The aim of the study was to evaluate short-term safety and efficacy of simultaneous modulated accelerated radiation therapy (SMART) delivered via helical tomotherapy in patients with nasopharyngeal carcinoma (NPC).

Methods. Between August 2011 and September 2013, 132 newly diagnosed NPC patients were enrolled for a prospective phase II study. The prescription doses delivered to the gross tumor volume (pGTV_{rx}) and positive lymph nodes (pGTV_{nd}), the high risk planning target volume (PTV1), and the low risk planning target volume (PTV2), were 67.5 Gy (2.25 Gy/F), 60 Gy (2.0 Gy/F), and 54 Gy (1.8 Gy/F), in 30 fractions, respectively. Acute toxicities were evaluated according to the established RTOG/EORTC criteria. This group of patients was compared with the 190 patients in the retrospective P70 study, who were treated between September 2004 and August 2009 with helical tomotherapy, with a dose of 70-74 Gy/33F/6.5W delivered to pGTV_{rx} and pGTV_{nd}.

Results. The median follow-up was 23.7 (12-38) months. Acute radiation related side-effects were mainly problems graded as 1 or 2. Only a small number of patients suffered from grade 4 leucopenia (4.5%) or thrombocytopenia (2.3%). The local relapse-free survival (LRFS), nodal relapse-free survival (NRFS), local-nodal relapse-free survival (LNRFS), distant metastasis-free survival (DMFS) and overall survival (OS) were 96.7%, 95.5%, 92.2%, 92.7% and 93.2%, at 2 years, respectively, with no significant difference compared with the P70 study.

Conclusions. SMART delivered via the helical tomotherapy technique appears to be associated with an acceptable acute toxicity profile and favorable short-term outcomes for patients with NPC. Long-term toxicities and patient outcomes are under investigation.

Key words: nasopharyngeal carcinoma; simultaneous modulated accelerated radiation therapy; helical tomotherapy; acute toxicities, clinical outcome

Introduction

Nasopharyngeal carcinoma (NPC) is a kind of head and neck cancer with a good prognosis, and can be cured by radiation therapy especially inten-

sity-modulated radiation therapy (IMRT) alone or in combination with chemotherapy and/or anti-epithelial growth factor receptor (anti-EGFR) monoclonal antibody (Mab) treatment.¹ The curative effect and radiation injury are closely related to radi-

ation techniques. Simultaneous modulated accelerated radiation therapy (SMART) has been clinically confirmed as safe and effective, and widely used in the treatment of NPC.² This technique can simultaneously deliver different doses to different targets, and improve local control through increasing the fraction dose and shortening the overall treatment time (OTT), so as to reduce post-procedure accelerated repopulation of tumor cells.

Helical tomotherapy (HT) is believed to excel in realizing the function of SMART. Providing better dose conformity and uniformity, HT could improve local control with less radiation damage. The first HT unit in China was installed in September 2007 at our center; and by December 2014, nearly 500 NPC patients had received treatment. The prescription dose of 70 Gy was given to the target volume in 33 fractions (2.12 Gy per fraction) in a previous study (P70 study) conducted by our team, and the clinical efficacy was satisfactory with an acceptable safety profile. The local relapse-free survival (LRFS), nodal relapse-free survival (NRFS), local-nodal relapse-free survival (LNRFs), distant metastasis-free survival (DMFS) and overall survival (OS) were 96.1%, 98.2%, 94.2%, 95.5% and 91.4%, at 2 years, respectively.³ The present phase II study (P67.5) was based on P70, starting from September 2011. In P67.5 we shortened the treatment time to 6 weeks by designing a hypofractionated regimen with a total dose of 67.5 Gy (2.25 Gy/F). By comparison with the P70 study, we evaluated the feasibility and short-term outcomes of this new hypofractionated regimen.

Methods

Eligibility criteria

P67.5 is a single-center, prospective, phase II clinical study, with a registration code of ChiCTR-ONC-14004895. The research ethics board of the Chinese PLA General Hospital approved the study with an official number of S2014-048-01, and all eligible patients provided informed consent in written form.

Inclusion criteria were as follows: histologically proven type I and II NPC according to World Health Organization (WHO) criteria; stage I–IVa according to the Union for International Cancer Control (UICC) 2002 Staging System; aged between 15 and 75 years; Karnofsky performance status score \geq 70; white blood cell count \geq 3,500/ μ L, platelet count \geq 100,000/ μ L, serum creatinine concentration $<$ 133 μ mol/L, and liver transaminase level $<$ 2.0 times of

the upper normal value. Exclusion criteria were as follows: distant metastasis; concomitant diseases (heart disease, tuberculosis, *etc.*) that interfere with the completion of treatment, increase incidence of adverse reactions or influence the prognosis; withdrawal during the treatment or violation of the protocol due to any factors; diagnosed with or treated for other malignances.

Patient characteristics

Between August 2011 and September 2013, 132 newly diagnosed non-metastatic NPC patients were included in the study. There were 95 males and 37 females. The median age was 47 years old. All patients underwent nasopharyngeal and skull base magnetic resonance imaging (MRI), chest computed tomography (CT), endoscopic evaluation, complete blood counts, hepatic and renal function tests, neck and abdomen ultrasound, and bone scans. Positron emission tomography (PET) was optional. Clinical stage was practiced according to the UICC 2002 staging system (Table 1).

We compared the preliminary results of the P67.5 study with the retrospective P70 study, in which a dose of 70–74 Gy (2.12–2.24 Gy per fraction) was delivered to the primary tumor (pGT-Vnx) and metastatic nodes (pGTVnd), 60–62.7 Gy (1.82–1.89 Gy per fraction) to the high risk planning target volume (PTV1) and 52–56 Gy (1.63–1.70 Gy per fraction) to the low risk planning target volume (PTV2), in 33 fractions.³ Table 2 summarizes patients' characteristics in the two studies.

Radiation therapy

Patients were placed in the supine position and the head and neck immobilized with a thermoplastic mask. Plain and enhanced CT images with 3-mm slice thickness were taken for treatment planning then transmitted to the Pinnacle³ 8.0 workstation and fused. Enhanced CT, MRI or PET images were

TABLE 1. Distributions of patients in P67.5/P70 study according to the Union for International Cancer Control (UICC) 2002 staging system

Stage	N0	N1	N2	N3	Total
T1	6/16	13/27	11/15	3/3	33/61
T2	3/13	15/24	23/22	3/2	44/61
T3	2/8	15/11	18/18	3/3	38/40
T4	2/3	3/10	11/11	1/4	17/28
Total	13/40	46/72	63/66	10/12	132/190

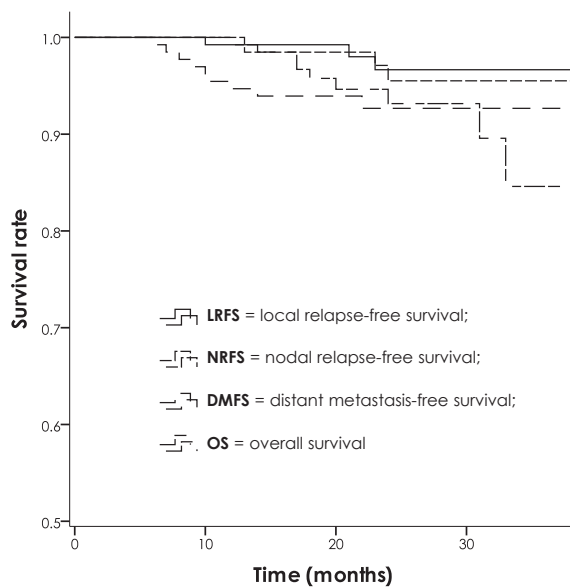


FIGURE 1. Different survival rates for patients in the P67.5 study.

TABLE 2. Patients' characteristics

Characteristics	P67.5 study		P70 study		p
	n.	%.	n.	%	
Age (median)	15–75	(47)	10–81	(44)	0.527
Gender					
Male	95	72.0	144	75.8	0.441
Female	37	28.0	46	24.2	
Region					
Northern China	110	83.3	159	83.7	0.933
Southern China	22	16.7	31	16.3	
KPS					
90-100	105	79.5	133	70.0	0.055
70-80	27	20.5	57	30.0	
Pathology					
WHO type I	2	1.5	3	1.6	0.964
WHO type II	130	98.5	187	98.4	
UICC 2002 Stage					
I	6	4.5	16	8.4	0.045
II	31	23.5	64	33.7	
III	68	51.5	71	37.4	
IVa-b	27	20.5	39	20.5	

KPS = Karnofsky performance status; UICC = Union for International Cancer Control; WHO = World Health Organization

used as a guide for target contours. Target naming and delineation were consistent with the P70 study³, and CT images together with the contour objects created by the physicians were transferred to Hi Art TomoTherapy 2.2.4.1 workstation. Physicists in the same group designed and verified the treatment plans. The three main parameters of field width, pitch, and modulation factor were set to the same values as in the P70 study.

During HT treatment, all patients underwent megavoltage computed tomography (MVCT) imaging everyday to rectify setup errors. The range of the CT scans typically included the central area of the whole target volume, ensuring that crystals were avoided. Automated and manual registration of the MVCT images with the planning CT images was based on bone and tissue anatomy.

The planned D95 was 67.5 Gy for pGTVnx and pGTVnd, 60 Gy for PTV1 and 54 Gy for PTV2, in 30 fractions. No more than 5% of the PTV received more than 110% of the prescribed dose. The dose-volume constraints for OARs (organs at risk) were the same as the P70 study.³

Biological effective dose (BED) is calculated with linear quadratic (LQ) radiobiological model: $BED = nd \times [1 + d/(\alpha/\beta)]$.⁴ In the formula, “n” represents the number of fractions and “d” fraction dose. The α/β value of tumor tissue or early response normal tissues is 10 Gy and that of late response normal tissues is 3 Gy or 5 Gy. If the impact of overall treatment time (OTT) and tumor proliferation is considered, the adjusted formula is $BED = nd \times [1 + d/(\alpha/\beta)] - \gamma/\alpha \times (T - Tk)$.⁵ The “ γ/α ” equals 0.6. “T” and “Tk” represent OTT (including weekends) and 7 days, respectively.

Chemotherapy and anti-EGFR monoclonal antibody (Mab) treatment

In this study, patients at stage III or IV (including stage II with lymph node metastasis) generally underwent neoadjuvant chemotherapy plus concurrent chemotherapy. Two cycles of neoadjuvant chemotherapy were routinely used, some patients with stage III and IV or whose tumor volume reduced less than 30% had additional 1-2 cycles. One hundred and one patients underwent 1–4 cycles of neoadjuvant chemotherapy with DP (docetaxel 75 mg/m², d1, and cisplatin 75 mg/m², d1, every 3 weeks) according to the primary tumor size or chemotherapy response. In accordance with the physical condition, clinical staging, treatment tolerance, 115 cases underwent two patterns of concurrent chemotherapy: 1) cisplatin 80 mg/m², d1,

every 3 weeks; 2) cisplatin 60 mg/m² and docetaxel 60 mg/m², d1, every 3 weeks. Concurrent anti-EGFR Mab treatment (cetuximab with a loading dose of 400 mg/m² and then 250 mg/m² or nimotuzumab 200 mg every week) was used in 45 patients. Adjuvant DP chemotherapy as used in the neoadjuvant setting was administered in 68 patients (range 1–4 cycles, median 1.93 cycles).

Statistical analysis and follow-up

Acute side-effects were evaluated weekly and peak toxicities were recorded. Acute and late side-effects were identified according to the established RTOG/EORTC criteria.⁶ The preliminary response was evaluated 1–3 months after the end of radiation therapy based on the Response Evaluation Criteria in Solid Tumors (RECIST) Version 1.1.⁷ Patients received follow-up examinations including nasopharyngeal and skull base MRI, nasopharyngoscopy, neck ultrasound, *etc.*, to evaluate the therapeutic effects every 3 months during the first year, and then every 6 months afterwards. By the end of October 2014, the median follow-up period was 23.7 (12–38) months with a follow-up rate of 100%. Survival analysis was performed with Kaplan-Meier method and Log-rank test was used to evaluate the differences between the 2 studies. Comparison of rates and means between the two groups was performed by Pearson χ^2 test and t test, respectively. A two-sided value of $p < 0.05$ was considered significant. The analyses were executed with SPSS 19.0 (Statistical Product and Service Solutions Inc., Chicago, IL).

Results

BED and dosimetric analyses

The prescription dose in the study for tumor targets was 67.5 Gy (2.25 Gy \times 30F) with a BED of 82.7 Gy. If the impact of OTT was considered, the adjusted BED would be 62.9 Gy, 0.9 Gy higher than that of the P70 study, and would theoretically result in better tumor control. For normal tissues, radiation doses to both early and late response tissues were lower in this study than in the P70 study (Table 3).

The mean dose (Dmean) to pGTVnx, pGTVnd, PTV1 and PTV2 was 70.2 Gy, 70.1 Gy, 64.9 Gy and 56.7 Gy, respectively (Table 3). Except the Dmean of inner ears and Dmean of both parotid glands, the dose delivered to OARs which generally met the established constraints were significantly lower in the P67.5 study than in the P70 study (Table 4).

TABLE 3. BED of the two SMART regimens (Gy)

	BED (P67.5)	BED (P70)
Tumor OTT disregarded ($\alpha/\beta = 10\text{Gy}$)	82.7	84.8
Tumor OTT taken into account ($\alpha/\beta = 10\text{Gy}$)	62.9	62.0
Normal tissue ($\alpha/\beta = 5\text{Gy}$)	97.9	99.7
Normal tissue ($\alpha/\beta = 3\text{Gy}$)	118.1	119.5

BED = biological effective dose; OTT = overall treatment time; SMART = simultaneous modulated accelerated radiation therapy

TABLE 4. Dosimetric data of organs at risk

	Mean value (Range)		P
	P67.5 study	P70 study	
Beam-on time (s)	413.8 (336.0–521.7)	455.8 (358.0–696.0)	0.674
Couch travel (cm)	21.4 (18.0–27.0)	22.6 (17.0–28.7)	0.000
pGTVnx Dmean	70.2 (69.2–72.6)	72.3 (70.4–75.6)	0.000
pGTVnd Dmean	70.1 (69.2–72.7)	72.3 (70.1–75.6)	0.000
PTV1 Dmean	64.9 (63.1–67.3)	64.6 (62.1–70.5)	0.083
PTV2 Dmean	56.7 (55.7–59.8)	57.4 (54.7–61.7)	0.000
Brainstem Dmax	51.1 (35.9–69.1)	54.5 (41.6–71.9)	0.000
Spinal cord Dmax	40.6 (35.2–51.1)	41.5 (33.7–51.8)	0.003
Optic nerve Dmax			
Left	29.0 (3.9–70.5)	38.3 (9.7–72.2)	0.000
Right	28.3 (4.6–70.8)	39.3 (9.2–72.9)	0.000
Eyeball Dmax			
Left	19.4 (4.0–38.9)	29.6 (10.0–65.4)	0.000
Right	19.1 (5.3–38.8)	29.6 (11.2–57.7)	0.000
Lens Dmax			
Left	3.2 (2.0–5.3)	4.1 (2.2–8.1)	0.000
Right	3.2 (2.2–8.3)	4.1 (2.2–8.3)	0.000
TMJ Dmean			
Left	33.7 (22.6–60.4)	38.7 (22.9–58.5)	0.000
Right	33.1 (22.5–64.7)	38.2 (21.1–51.8)	0.000
Inner ear Dmean			
Left	45.4 (27.4–67.1)	43.1 (12.3–58.0)	0.055
Right	44.7 (26.3–61.7)	44.4 (11.6–65.2)	0.815
Parotid gland Dmean			
Left	30.8 (25.2–39.9)	31.2 (23.8–55.1)	0.334
Right	30.7 (22.9–65.2)	31.0 (22.0–47.9)	0.636
Oral cavity Dmean	34.2 (26.6–42.0)	38.8 (11.5–50.2)	0.000
L-E-T Dmean	32.7 (24.2–38.8)	38.7 (19.1–49.6)	0.000

Dmean = mean dose (Gy); Dmax = maximum dose (Gy); L-E-T = Larynx-esophagus-trachea; pGTVnd = positive lymph nodes; pGTVnx = prescription doses delivered to the gross tumor volume; TMJ = Temporomandibular joint;

TABLE 5. Acute toxicities of normal organs [n (%)]

Toxicity	Grade 0		Grade 1		Grade 2		Grade 3		Grade 4		p
	P67.5	P70	P67.5	P70	P67.5	P70	P67.5	P70	P67.5	P70	
Skin reaction	6 (4.5)	7 (3.7)	92 (69.7)	137 (72.1)	27 (20.5)	37 (19.5)	7 (5.3)	9 (4.7)	0 (0.0)	0 (0.0)	0.961
Mucositis	2 (1.5)	4 (2.1)	54 (40.9)	72 (37.9)	64 (48.5)	108 (56.8)	12 (9.1)	6 (3.2)	0 (0.0)	0 (0.0)	0.100
Xerostomia	4 (3.0)	9 (4.7)	33 (25.0)	100 (52.6)	95 (72.0)	81 (42.6)	0 (0.0)	0 (0.0)	0 (0.0)	0 (0.0)	0.000
Pharyngitis-esophagitis	0 (0.0)	7 (3.7)	51 (38.6)	83 (43.7)	79 (59.9)	99 (52.1)	2 (1.5)	1 (0.5)	0 (0.0)	0 (0.0)	0.072
Leucopenia	29 (22.0)	86 (45.3)	32 (24.2)	42 (22.1)	39 (29.6)	50 (26.3)	26 (19.7)	10 (5.3)	6 (4.5)	2 (1.0)	0.000
Anemia	66 (55.0)	175 (92.1)	44 (33.4)	14 (7.4)	18 (13.6)	1 (0.5)	4 (3.0)	0 (0)	0 (0.0)	0 (0)	0.000
Thrombocytopenia	103 (78.0)	180 (94.7)	16 (12.1)	7 (3.7)	5 (3.8)	2 (1.1)	5 (3.8)	1 (0.5)	3 (2.3)	0 (0)	0.000

Acute and late side-effects

All patients completed radiation therapy but one who underwent 27 fractions because of severe gastrointestinal side-effects. One hundred and twenty-four cases finished their radiation therapy in 6 weeks, and radiation therapy was interrupted for 10.9 days on average in 7 patients because of grade 3 acute pharyngitis-esophagitis or hematologic toxicity. Acute radiation related side-effects were mainly problems graded as 1 or 2 with skin, oral mucosa, salivary glands, and pharynx-esophagus. Grade 3 skin toxicities were noted in 7 cases, mucositis in 12 and pharyngitis-esophagitis in 2. Some patients who received neoadjuvant and/or concurrent chemotherapy suffered from different degrees of hematologic toxicities. Distribution of acute side-effects is shown in Table 5. The differences were statistically significant between the incidences of xerostomia and hematologic toxicities of the two studies. At the end of radiation therapy, there was an average weight loss by 10.6%, ranging from 0% to 21.4%.

Late toxicities generally appeared 3 months after radiation therapy and the most common one was xerostomia. Although patients generally had less dry feeling as time passed by and 24 patients had no signs of late xerostomia at all, there were 102 and 6 cases suffering from grade 1 and 2 xerostomia during the follow-up, respectively. The sense of taste diminished in 6 patients and was lost completely in 1 patient. Forty-one patients had audition test abnormal on one side, 30 of whom had no obvious clinical symptoms; however, 12 and 5 cases appeared to have grade 1 and 2 hearing loss, respectively. Fifteen cases developed otitis media that needed surgical treatment. Seventeen patients

had a difficulty in opening mouth, and 3 of them had a mouth opening less than a one-finger width. Increased tooth sensitivity occurred in 30 patients; gingival recession in 16 patients; tooth fracture or loss in 10 patients. One 39-year-old female had a menstrual disorder and one female patient had hypothyroidism requiring medical treatment.

Short-term outcomes and patterns of failure

At a median time of 1.5 months (at least one month and no more than 3 months) after the end of radiation therapy, evaluation of primary tumors showed that 49 patients had complete responses (CR), 71 partial responses (PR), and 12 stable disease (SD); evaluation of involved nodes in 113 patients showed 42 CR, 62 PR, and 9 SD, with an effective rate of 100%.

Sixteen patients suffered from treatment failure during the follow-up, including 3 local recurrences (2 intra-target recurrences and 1 marginal recurrence), 4 regional recurrences and 9 distant metastases. In the patients with local recurrence, the T3N2M0 case received re-irradiation alone, the T3N0M0 case underwent re-irradiation with concurrent chemotherapy, and the T3N1M0 case refused salvage treatment. All these three patients died of bleeding with a mean survival time of 7.7 (3–10) months from recurrence to death. Among the regional recurrence patients, 3 had a neck node recurrence and 1 had an ipsilateral parotid metastasis; these patients underwent re-irradiation, chemotherapy, concurrent chemo-radiotherapy and brachytherapy respectively and were all alive throughout the follow-up. Distant metastasis was the most common failure pattern and the most

common distant organs involved were liver (4 cases), lung (2 cases), bone (2 cases), and liver-lung (1 case). Seven of the 9 cases received chemotherapy, of whom 2 had also concurrent Anti-EGFR Mab treatment (4 cases died, 3 cases alive); and the other 2 cases had no salvage treatment and died in 4 and 7 months, respectively (Table 6). The local relapse-free survival (LRFS), nodal relapse-free survival (NRFS), local-nodal relapse-free survival (LNRFS), distant metastasis-free survival (DMFS) and overall survival (OS) were 96.7%, 95.5%, 92.2%, 92.7% and 93.2%, at 2 years, respectively, with no significant difference compared with the P70 study.

Discussion

It is generally believed that, in order to obtain a satisfactory local control, the prescribed dose of radiation therapy (RT) in NPC should exceed 64 Gy⁸, but it does not mean higher doses lead to higher local control rate (LCR). In contrast, clinical and radiobiological evidence has proved OTT as an important factor impacting curative effect of RT. Some tumor cells exhibited accelerated repopulation during the late period of RT. As the treatment continued, the probability of proliferation of tumor stem cells increased and the total dose should compensate for the “wasted dose” in every extra day because of accelerated repopulation of stem cells (0.6 Gy/d, equal to γ/α value).^{5,9-11} At the same time, a higher prescribed dose would cause higher irradiation to OARs and increase the risk of radiation related injury.

When we prescribe the specific dose in radical RT for NPC with conventional fractionation, in addition to considering tumor extension or size, we must also pay attention to the impact of fraction size and OTT, so that the proper fraction dose can be chosen to avoid not only increased injury of late response normal tissues but also extended OTT. That was why a dose of more than 70 Gy was not recommended in conventionally fractionated RT for NPC. The limitation of conventionally fractionated RT in NPC seemed to have been solved by hyperfractionated radiation therapy which was however difficult to carry out in the past due to technical limitations of the two-dimensional conventional or three-dimensional conformal radiation therapy. After 20 years of continuous development and improvement, IMRT could solve the above problem through SMART which could deliver different doses to different targets according to the radiosensitivity (α/β value) of OARs and

TABLE 6. Patients with treatment failure

TNM stage	Failure time (month)	Failure site	Salvage treatment	Living status	Follow-up* (month)
1. T1N2M0	6	Bone	CT	Dead	17
2. T3N3bM0	7	Liver	CT	Dead	14
3. T2N2M0	8	Lung	CT+AT	Living	14
4. T1N2M0	9	Bone	CT+AT	Dead	12
5. T3N2M0	10	Lung	-	Dead	17
6. T1N2M0	10	Liver	CT	Living	16
7. T3N2M0	10	Local	RT	Dead	20
8. T3N1M0	12	Liver	CT	Dead	31
9. T3N2M0	13	Nodal	RT	Living	37
10. T1N3bM0	13	Nodal	BT	Living	26
11. T4N0M0	14	Liver	-	Dead	18
12. T3N1M0	21	Local	-	Dead	24
13. T3N1M0	22	Liver & Lung	CT	Living	33
14. T3N0M0	23	Local	CRT	Dead	33
15. T3N2M0	23	Nodal	CT	Living	27
16. T2N2M0	24	Nodal	CRT	Living	37

AT = anti-EGFR Mab therapy; BT = brachytherapy; CRT = concurrent chemoradiotherapy; CT = chemotherapy; RT = radiation therapy;

* The time from diagnosis.

boost doses to tumor targets within a limited time, so as to improve the efficacy with less normal tissue damage, and increase the gain ratio of RT.

A number of clinical studies of SMART in NPC have been reported, but prospective studies were lacking. Table 7 listed the results of some prospective studies with fractionation patterns, LCR, *etc.* It could be seen that fraction dose ranged from 2.12 to 2.4 Gy, and the total BED based on prescription doses all exceeded 80 Gy. An adjusted BED was obtained between 60 and 70 Gy. The 2–4 year LCR was beyond 90% except the 88% reported by Lee *et al.*, probably because of a small sample size and a high proportion (95% of patients) of advanced disease.¹² The RTOG 0225 study was a classic multi-center study which led the 70 Gy/33F SMART regimen to be used as the standard RT of NPC with a LCR of 92.6% at 2 years.¹⁴ Our center began to conduct P70 study with the same fractionated regimen in September 2007 when the HT system was first introduced into China; and achieved good outcomes with the 2-year LRFS of 96.1%.³ In the present study which was based on the P70 study, the fraction dose increased from 2.17 Gy to 2.25 Gy and the adjusted BED to tumor targets got higher, while BED to normal tissues was reduced. Xiao *et al.*¹⁵ conducted a

TABLE 7. Summary of reported prospective studies on simultaneous modulated accelerated radiation therapy (SMART) for nasopharyngeal carcinoma (NPC)

Author	N	T3-4 tumor n (%)	Positive node n (%)	Fractionation patterns for GTV					LCR (%)
				Fraction	Prescription dose (Gy)	Fraction dose (Gy)	BED* (Gy) OT disregarded	BED* (Gy)	
Lee SW (2005) ¹²	20	8 (40)	18 (90)	30	72	2.4	89.3	69.5	88.0 (2-y)
Lin SJ (2009) ¹³	323	260 (80.5)	293 (90.7)	30 / 31	66 / 69.8	2.2 / 2.25	80.5 / 85.4	60.7 / 63.8	95.0 (3-y LRFS)
RTOG0225 (2009) ¹⁴	68	23 (33.8)	50 (73.5)	33	70	2.12	84.8	62.0	92.6 (2-y)
Xiao WW (2011) ¹⁵	81	81 (100)	56 (69.1)	30	68	2.27	83.4	63.6	94.9 (3-y)
Bakst RL (2011) ¹⁶	25	16 (64)	20 (80)	30	70.2	2.34	86.6	66.8	91.0 (3-y)
Wang RS (2013) ¹⁷	300	214 (71.3)	277 (92.3)	30-32	68-72	2.25-2.27	83.4-88.2	63.6-66.0	94.0 (4-y)
Author (2014) ³	190	68 (35.8)	150 (78.9)	33	70	2.12	84.8	62.0	96.1 (2-y LRFS)
Current study	132	55 (41.7)	119 (90.2)	30	67.5	2.25	82.7	62.9	96.7 (2-y LRFS)

*: $\alpha/\beta = 10\text{Gy}$; OT = overall treatment time; LCR = local control rate; LRFS = local relapse-free survival; y = year

phase II study in T3-4 patients using a 68 Gy/33F regimen similar to ours and the 3-year LCR reached 94.9%. In the study of Wang *et al.*¹⁷, the 68 Gy/33F regimen was still applied although up to 83% of the patients had locally advanced disease; LCR remained to be 94%. In this study, the 2-year LRFS and NRFS achieved 96.7% and 95.5%, respectively, without difference compared with the P70 study, in which LRFS and NRFS being 96.1% and 98.2% ($\chi^2 = 0.469$, $p = 0.494$; $\chi^2 = 1.145$, $p = 0.285$).

As the prescription dose and fraction dose increase, the incidence of serious adverse reactions would become significantly higher. Kwong *et al.*¹⁸ set the prescribed dose as 76 Gy/35F with a BED of up to 92.5 Gy. Though higher prescription dose ensured the LCR (95.7% at 3 years), 78% and 46% of patients suffered from grade 3 mucositis and skin reactions, respectively. In the study of Bakst *et al.*¹⁶, the total dose was 70 Gy but the fraction dose increased up to 2.34 Gy, so about 12% of patients had temporal lobe necrosis of varying degrees, especially in patients with T4 whose pGTV included part of brain tissue. This situation did not appear in earlier study of the same authors in which 70 Gy/33F regimen was used.¹⁹ It could be seen that blind pursuit of high-dose or high fraction dose does not further improve LCR but might lead to more severe radiation related damage.

In recent years, the hot issues about IMRT for NPC have focused on how to minimize the dose

delivered to OARs and it might be realized in two main ways: 1) to improve the accuracy of radiation therapy; 2) to lower the total dose. Helical tomotherapy (HT) is a unique IMRT modality that combines elements of diagnostic radiology and radiation therapy in a single unit. In addition to the ability to deliver a highly conformal dose distribution, HT is equipped with xenon detectors designed to obtain MVCT images utilized for pre-treatment set-up verification, and some studies have confirmed the advantage of HT compared with step-and-shoot IMRT in dose distribution and OAR protection.²⁰⁻²²

In this study, the Dmean of pGTVnx and pGTVnd decreased by 2.1 Gy and 2.2 Gy, respectively, compared to the P70 study, which was equivalent to a 2.5 Gy reduction of prescription dose. The doses were statistically reduced almost in all OARs except in the inner ear of which the Dmean was a bit higher and in the parotid gland with a decline of the Dmean by only 0.3 Gy. The Dmax of both eyeballs and optic nerves decreased by about 34% and 25%, respectively; the Dmean of the temporomandibular joint fell by more than 5 Gy and the reduction in oral cavity was about 4.6 Gy. At the same time, the Dmean of the parotid gland remained at a high level and was far above the constraint of 28 Gy; and the incidence of grade 2 xerostomia was significantly higher than the P70 study ($\chi^2 = 27.225$, $p = 0.000$). After data analysis, we noticed that acute toxic-

ties were evaluated by different doctors in the two studies and acute xerostomia was underestimated in the P70 study. Leung *et al.*²³ summarized their 5-year experience in NPC treatment with HT and the Dmean of the ipsilateral and contralateral parotid gland was 22.1 Gy and 20.7 Gy, respectively, significantly lower than ours. The possible reason is delineation of the deep lobe of the parotid gland which was not spared from CTV1 in our studies. Because of the advantages of TH, the incidence of acute and late side-effects were low and acute toxicities in skin, oral mucosa, pharynx-esophagus and salivary glands were mainly graded as level 1-2 in this study. Moreover, as a proportion of locally advanced cases received neoadjuvant chemotherapy and/or concurrent chemo-radiotherapy, a higher incidence of grade 3-4 neutropenia can be accounted for.

In addition, the shortening of the treatment course from 33 fractions in 6.5 weeks to 30 fractions in 6 weeks reduced treatment costs for patients as well as improving equipment turnover.

Conclusions

A 67.5 Gy/30F SMART regimen delivered via the HT technique appears to be associated with acceptable toxicities and favorable short-term outcomes for patients with NPC. Long-term toxicities and outcomes are under investigation.

References

- Al-Sarraf M, Le Blanc M, Giri PG, Fu KK, Cooper J, Vuong T, et al. Chemoradiotherapy versus radiotherapy in patients with advanced nasopharyngeal cancer: phase III randomized intergroup study 0099. *J Clin Oncol* 1998; **16**: 1310-7.
- Lee N, Xia P, Quivey JM, Sultanem K, Poon I, Akazawa C, et al. Intensity-modulated radiotherapy in the treatment of nasopharyngeal carcinoma: an update of the UCSF experience. *Int J Radiat Oncol Biol Phys* 2002; **53**: 12-22.
- Du L, Zhang XX, Ma L, Feng LC, Li F, Zhou GX, et al. Clinical study of nasopharyngeal carcinoma treated by helical tomotherapy in China: 5-year outcomes. *Biomed Res Int* 2014, Article ID: 980767. doi: 10.1155/2014/980767.
- Fowler JF. A review: the linear quadratic formula and progress in fractionated radiotherapy. *Br J Radiol* 1989; **62**: 679-94.
- Fowler JF. 21 years of biologically effective dose. *Br J Radiol* 2010; **83**: 554-68.
- Cox JD, Stetz J, Pajak TF. Toxicity criteria of the Radiation Therapy Oncology Group (RTOG) and the European Organization for Research and Treatment of Cancer (EORTC). *Int J Radiat Oncol Biol Phys* 1995; **31**: 1341-6.
- Eisenhauer EA, Therasse P, Bogaerts J, Schwartz LH, Sargent D, Ford R, et al. New response evaluation criteria in solid tumours: revised RECIST guideline (version 1.1). *Eur J Cancer* 2009; **45**: 228-47.
- Lee AW, Law SC, Foo W, Poon YF, Chan DK, O SK, et al. Nasopharyngeal carcinoma: local control by megavoltage irradiation. *Br J Radiol* 1993; **66**: 528-36.
- Withers HR, Taylor JM, Maciejewski B. The hazard of accelerated tumor clonogen repopulation during radiotherapy. *Acta Oncol* 1988; **27**: 131-46.
- Withers HR. Biologic basis for altered fractionation schemes. *Cancer* 1985; **55**(9 Suppl): 2086-95.
- Ho KF, Fowler JF, Sykes AJ, Yap BK, Lee LW, Slevin NJ. IMRT dose fractionation for head and neck cancer: variation in current approaches will make standardisation different. *Acta Oncol* 2009; **48**: 431-9.
- Lee SW, Back GM, Yi BY, Choi EK, Ahn SD, Shin SS, et al. Preliminary results of a phase I/II study of simultaneous modulated accelerated radiotherapy for nondisseminated nasopharyngeal carcinoma. *Int J Radiat Oncol Biol Phys* 2006; **65**: 152-60.
- Lin SJ, Pan JJ, Han L, Zhang X, Liao X, Lu JJ. Nasopharyngeal carcinoma treated with reduced-volume intensity-modulated radiation therapy: report on the 3-year outcome of a prospective series. *Int J Radiat Oncol Biol Phys* 2009; **75**: 1071-8.
- Lee N, Harris J, Garden AS, Straube W, Glisson B, Xia P, et al. Intensity-modulated radiation therapy with or without chemotherapy for nasopharyngeal carcinoma: Radiation Therapy Oncology Group phase II trial 0225. *J Clin Oncol* 2009; **27**: 3684-90.
- Xiao WW, Huang SM, Han F, Wu SX, Lu LX, Lin CG, et al. Local control, survival, and late toxicities of locally advanced nasopharyngeal carcinoma treated by simultaneous modulated accelerated radiotherapy combined with cisplatin concurrent chemotherapy: long-term results of a phase 2 study. *Cancer* 2011; **117**: 1874-83.
- Bakst RL, Lee N, Pfister DG, Zelefsky MJ, Hunt MA, Kraus DH, et al. Hypofractionated dose-painting intensity modulated radiation therapy with chemotherapy for nasopharyngeal carcinoma: a prospective trial. *Int J Radiat Oncol Biol Phys* 2011; **80**: 148-53.
- Wang RS, Wu F, Lu HM, Wei B, Feng G, Li G, et al. Definitive intensity-modulated radiation therapy for nasopharyngeal carcinoma: long-term outcome of a multicenter prospective study. *J Cancer Res Clin Oncol* 2013; **139**: 139-45.
- Kwong DL, Sham JS, Leung LH, Cheng AC, Ng WM, Kwong PW, et al. Preliminary results of radiation dose escalation for locally advanced nasopharyngeal carcinoma. *Int J Radiat Oncol Biol Phys* 2006; **64**: 374-81.
- Wolden SL, Chen WC, Pfister DG, Kraus DH, Berry SL, Zelefsky MJ. Intensity-modulated radiation therapy (IMRT) for nasopharynx cancer: update of the Memorial Sloan-Kettering experience. *Int J Radiat Oncol Biol Phys* 2006; **64**: 57-62.
- Bauman G, Yartsev S, Rodrigues G, Lewis C, Venkatesan VM, Yu E, et al. A prospective evaluation of helical tomotherapy. *Int J Radiat Oncol Biol Phys* 2007; **68**: 632-41.
- Lee N, Xia P, Quivey JM, Sultanem K, Poon I, Akazawa C, et al. Intensity-modulated radiotherapy in the treatment of nasopharyngeal carcinoma: an update of the UCSF experience. *Int J Radiat Oncol Biol Phys* 2002; **53**: 12-22.
- Fiorino C, Dell'Oca I, Pierelli A, Broggi S, Cattaneo GM, Chiara A, et al. Simultaneous integrated boost (SIB) for nasopharynx cancer with helical tomotherapy. A planning study. *Strahlenther Oncol* 2007; **183**: 497-505.
- Leung SW, Lee TF. Treatment of nasopharyngeal carcinoma by tomotherapy: five-year experience. *Radiat Oncol* 2013; **8**: 107-12.

Bevacizumab plus chemotherapy in elderly patients with previously untreated metastatic colorectal cancer: single center experience

Janja Ocvirk^{1,2}, Maja Ebert Moltara¹, Tanja Mesti¹, Marko Boc¹, Martina Rebersek¹, Neva Volk¹, Jernej Benedik¹, Zvezdana Hlebanja¹

¹ Department of Medical Oncology, Institute of Oncology Ljubljana, Ljubljana, Slovenia

² Faculty of Medicine, University of Ljubljana, Ljubljana, Slovenia

Radiol Oncol 2016; 50(2): 226-231.

Received 3 September 2014

Accepted 7 October 2014

Correspondence to: Assoc. Prof. Janja Ocvirk, M.D., Ph.D., Institute of Oncology Ljubljana, Zaloška 2, Ljubljana. Phone: +386 1 5879 220; Fax: +386 1 5879 305; E-mail: jocvirk@onko-i.si

Disclosure: No potential conflicts of interest were disclosed.

Background. Metastatic colorectal cancer (mCRC) is mainly a disease of elderly, however, geriatric population is underrepresented in clinical trials. Patient registries represent a tool to assess and follow treatment outcomes in this patient population. The aim of the study was with the help of the patients' register to determine the safety and efficacy of bevacizumab plus chemotherapy in elderly patients who had previously untreated metastatic colorectal cancer. **Patients and methods.** The registry of patients with mCRC was designed to prospectively evaluate the safety and efficacy of bevacizumab-containing chemotherapy as well as selection of patients in routine clinical practice. Patient baseline clinical characteristics, pre-specified bevacizumab-related adverse events, and efficacy data were collected, evaluated and compared according to the age categories.

Results. Between January 2008 and December 2010, 210 patients with mCRC (median age 63, male 61.4%) started bevacizumab-containing therapy in the 1st line setting. Majority of the 210 patients received irinotecan-based chemotherapy (68%) as 1st line treatment and 105 patients (50%) received bevacizumab maintenance therapy. Elderly (≥ 70 years) patients presented 22.9% of all patients and they had worse performance status (PS 1/2, 62.4%) than patients in < 70 years group (PS 1/2, 35.8%). Difference in disease control rate was mainly due to inability to assess response in elderly group (64.6% in elderly and 77.8% in < 70 years group, $p = 0.066$). The median progression free survival was 10.2 (95% CI, 6.7–16.2) and 11.3 (95% CI, 10.2–12.6) months in elderly and < 70 years group, respectively ($p = 0.58$). The median overall survival was 18.5 (95% CI, 12.4–28.9) and 27.4 (95% CI, 22.7–31.9) months for elderly and < 70 years group, respectively ($p = 0.03$). Three-year survival rate was 26% and 37.6% in elderly vs. < 70 years group ($p = 0.03$). Overall rates of bevacizumab-related adverse events were similar in both groups: proteinuria 21/22 %, hypertension 25/19 %, haemorrhage 2/4 % and thromboembolic events 10/6 %, for elderly and < 70 years group, respectively.

Conclusions. In routine clinical practice, the combination of bevacizumab and chemotherapy is effective and well-tolerated regimen in elderly patients with metastatic colorectal cancer.

Key words: metastatic colorectal cancer; bevacizumab; chemotherapy; elderly

Introduction

As with many cancers, metastatic colorectal cancer (mCRC) is mainly a disease of elderly population. However, geriatric population is underrepresented in clinical trials. The median age at diagnosis

for patients with CRC is 72 years, while the median age of patients in clinical trials is 63 years.¹ In Slovenia, 44% of colorectal cancer cases were diagnosed in people aged 70 years and over.² Age together with performance status and comorbidities is one of the most important factors when deciding

on treatment regimen.³ Studies show that close to half of the elderly patients with stage III colon cancer do not receive chemotherapy, although most of the studies and meta-analysis have reported similar response rate (ORR), overall survival (OS), time to progression (TTP) and tolerability for elderly and younger patients in adjuvant and metastatic setting.^{4,6}

Addition of bevacizumab, a humanized monoclonal antibody against vascular endothelial growth factor, to the chemotherapy backbone regimens improves progression-free survival (PFS) and overall survival in first-line and second-line treatment and when continued beyond first progression in mCRC.⁷ Data from large observational studies, subgroup analysis and pooled analysis of randomized trials have suggested that the survival benefits associated with the use of bevacizumab in the first-line treatment are similar in elderly and general population.⁸⁻¹³ With the introduction of bevacizumab as standard of care for mCRC patients in Slovenia¹⁴, our centre has created patient registry to prospectively assess patient selection as well as efficacy and safety of bevacizumab containing chemotherapy in routine clinical practice. This registry enabled data capturing of the mCRC management in geriatric population that is usually excluded in clinical research and comparison of clinical outcomes to their younger counterparts.

The aim of the study was with the help of the patients' register to determine the safety and efficacy of bevacizumab plus chemotherapy in elderly patients who had previously untreated metastatic colorectal cancer.

Patients and methods

Patient clinical baseline characteristics, pre-specified bevacizumab-related adverse events, and efficacy data were prospectively collected within local patient registry from 210 mCRC patients who started bevacizumab-containing chemotherapy in the 1st line setting. Patient clinical characteristics (primary tumour treatments, an Eastern Cooperative Oncology Group [ECOG] performance status [PS], metastatic burden), rate of bevacizumab-related toxicities, metastasectomy rate, ORR, PFS and OS were evaluated.

The study was done in accordance with the principles of Good Clinical Practice and the Declaration of Helsinki and was approved by national ethics committee. All patients provided written informed consent for data collection.

Statistical analysis

Statistical analyses were performed on the intent-to-treat (ITT) population e.g. patients who received at least one dose of bevacizumab. Patient characteristics and toxicity data were summarized descriptively by the age group. Proportions of categorical variables were compared using the chi-square test. Survival analyses were performed using the Kaplan-Meier method, which provided medians and 95% confidence intervals (CIs). The differences in survival were evaluated using the log rank test; the follow-up time for this comparison was limited to 3 years, which is the minimum period available for all the patients.

Results

Patient characteristics

The data from 210 patients (median age 63, males 61.4%) treated with bevacizumab-containing chemotherapy (B-CTX) in the 1st line setting in routine clinical practice were included in the evaluation. The patients with mCRC started B-CTX treatment between January 2008 and December 2010 and were followed for outcomes at our centre until December 2013. The ECOG PS at baseline was 0 in 58%, 1 in 38% and 2 in 4% of all patients. Subgroup Elderly patients (≥ 70 years, $n = 48$) presented 22.9% of all patients and they had worse performance status (PS1/2 62.4%) than patients in < 70 years group (PS1/2 35.8%). Patient characteristics are described in Table 1. Metastatic disease was the first diagnosis in 63% of patients < 70 years old, while in the elderly patients only 45.8% had mCRC as the first diagnosis of CRC.

Treatment

Bevacizumab 5 mg/kg every two weeks or 7.5 mg/kg every three weeks was administered in combination with chemotherapy (CTX) to the patients with mCRC. Majority of 210 patients received irinotecan-based chemotherapy (68%) as 1st line treatment and 105 patients (50%) received bevacizumab maintenance therapy. The patients in < 70 years group received mainly irinotecan-based chemotherapy (66%) - capecitabine plus irinotecan (XELIRI) 58.6%, capecitabine plus oxaliplatin (XELOX) 27.8%, leucovorin, fluorouracil plus irinotecan (FOLFIRI) 6.8%, leucovorin, fluorouracil plus oxaliplatin (FOLFOX) 4.9%, monotherapy capecitabine or irinotecan 1.8%. Median duration

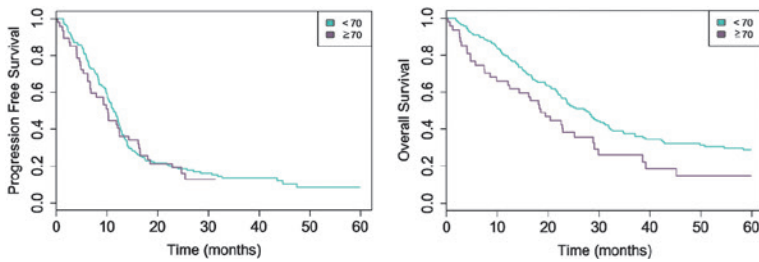


FIGURE 1. Kaplan-Meier survival curves for Progression Free Survival and Overall Survival in patients aged < 70 years and ≥ 70 years.

TABLE 2. Efficacy outcomes

Outcomes	Age < 70 y (n = 162)	Age ≥ 70 y (n = 48)
Best response, n (%)		
Complete	9 (6)	4 (8)
Partial	60 (37)	13 (27)
Stable disease	57 (35)	14 (29)
Progressive disease	21 (13)	6 (13)
Not evaluable	7 (4)	6 (13)
Overall response rate, % (95% CI)	69 (43)	17 (35)
Disease-control rate, % (95% CI)	126 (78)	31 (65)
Progression free survival, months		
Median (95% CI)	11.3 (10.2–12.6)	10.2 (6.7–16.2)
Overall survival, months		
Median (95% CI)	27.4 (22.7–31.9)	18.5 (12.4–28.9)
Metastasectomy, n (%)		
	32 (21.2)	6 (15)

CI = confidence interval

of B-CTX was 24 weeks (range 3 to 36) and the median number of treatment cycles was 8 (range 1 to 16). In this group of patients, maintenance bevacizumab was administered to 83 patients (51%), with median number of cycles 6 (range 1 to 70). The backbone chemotherapy in patients aged ≥ 70 years was also mostly irinotecan (75%) - XELIRI 60.4%, XELOX 14.6%, FOLFIRI 10.4%, FOLFOX 6.2%, monotherapy capecitabine or irinotecan 8.4%. Median duration of B-CTX in elderly was 17 weeks (range 3 to 36) and the median number of treatment cycles was 6 (range 1 to 12). Twenty one patients (44%) received maintenance bevacizumab with median number of cycles 5 (range 1 to 51).

Treatment interruption was reported in 20.4% of patients in < 70 years group and 14.6% of patients ≥ 70 years group. Two main reasons for bevacizumab discontinuation in < 70 years group were disease

TABLE 1. Patient characteristics at baseline

Characteristics	Age < 70 y (n = 162)	Age ≥ 70 y (n = 48)
Gender, n (%)		
Men	96 (60)	33 (70)
Women	64 (40)	14 (30)
Age		
Median, years	59	72
Range, years	24–69	70–81
ECOG performance status, n (%)		
0	104 (64)	18 (38)
1	52 (32)	27 (56)
2	6 (4)	3 (6)
3	0	0
Site of metastatic disease, n (%)		
Liver	112 (69)	35 (73)
Lung	39 (24)	12 (25)
Lymph nodes	42 (26)	12 (25)
Bones	6 (4)	3 (6)
Other	64 (40)	13 (27)
Primary tumour location, n (%)		
Colon only	106 (65)	31 (65)
Rectum only	56 (35)	16 (33)
Colon and rectum	0	1 (2)
Adjuvant chemotherapy, n (%)		
	50 (31)	18 (38)
Previous radiotherapy, n (%)		
	30 (19)	9 (19)
Surgical resection, n (%)		
	132 (82)	42 (88)

progression (49% of all patients that discontinued) and adverse events (25%). In ≥ 70 years group bevacizumab was discontinued due to disease progression (35%) and adverse events (20%), but 15% of patients were lost to follow-up.

Efficacy

Efficacy data are summarized in Table 2. Difference in disease control rate (DCR) was mainly due to inability to assess response in elderly group (64.6% in elderly and 77.8% in < 70 years group).

ORR and DCR did not differ significantly between the two groups ($p = 0.375$ and $p = 0.066$, respectively). The median PFS was 10.2 (95% CI, 6.7–16.2) and 11.3 (95% CI, 10.2–12.6) months in elderly and < 70 years group, respectively ($p = 0.58$) (Figure 1). The median OS was 18.5 (95% CI,

12.4–28.9) and 27.4 (95% CI, 22.7–31.9) months for elderly and <70 years group, respectively ($p = 0.03$) (Figure 1).

Metastasectomy was performed in 6 (15%) of elderly patients and 32 (21.2%) patients in <70 years group. Three-year survival rate was 26% (95% CI, 15.3–44.2) and 37.6% (95% CI, 30.7–46.1) in elderly *vs.* <70 years group ($p = 0.03$).

In elderly patients, 15 patients received second-line therapy, all of them receiving bevacizumab in combination with subsequent chemotherapy. In patients aged <70 years, 101 patients received second-line therapy, out of which 76% contained bevacizumab.

Toxicity

Adverse events related to bevacizumab were reported in 123 (75.9%) and 38 (79.2%) patients in <70 years and ≥ 70 years group, respectively. Adverse events of special interest to bevacizumab are summarized in Table 3 (epistaxis excluded). A case of vesico-rectal fistula was reported in the patient aged <70 years (rectal cancer with previous radiotherapy). One case of acute myocardial infarction was reported in each group. One patient on capecitabine monotherapy from elderly group presented with adverse event with an outcome death (heart failure).

The incidence of adverse event that led to bevacizumab discontinuation was 19% in both age groups. The incidence of adverse event that led to bevacizumab dose interruption was 10.5% and 10% in patients aged <70 and ≥ 70 years, respectively.

Discussion

Randomized studies, subgroup and pooled analysis, along with large observational studies suggest that bevacizumab containing first-line chemotherapy is efficacious and safe in elderly patients with mCRC. Randomized phase II trial of bevacizumab or placebo added to 5-FU in elderly patients not suitable for irinotecan treatment reported significantly longer PFS in patients who received bevacizumab *versus* placebo (9.2 months *versus* 5.5 months, respectively, hazard ratio, 0.5; $p = 0.0002$).¹⁵ Furthermore, results from phase III trial AVEX showed that in patients over age of 70 years and non-fit for oxaliplatin or irinotecan-based chemotherapy, PFS was significantly longer in the group of patients who received bevacizumab plus capecitabine *versus* the capecitabine alone group

TABLE 3. Targeted adverse events

Adverse event	No. of patients (%)				Total
	Grade1	Grade2	Grade3	Grade4	
< 70 years (n = 162)					
Hypertension	11 (6.8)	15 (9.3)	5 (3.1)	0 (0)	30 (18.5)
Thromboembolism	1 (0.6)	4 (2.5)	4 (2.5)	0 (0)	9 (5.6)
Proteinuria	23 (14.2)	11 (6.8)	2 (1.2)	0 (0)	36 (22.2)
Hemorrhage	4 (2.5)	1 (0.6)	0 (0)	1 (0.6)	6 (3.7)
Infection	4 (2.5)	1 (0.6)	4 (2.5)	0 (0)	8 (4.9)
> 70 years (n = 48)					
Hypertension	3 (6.2)	6 (12.5)	2 (4.2)	0 (0)	12 (25)
Thromboembolism	0 (0)	1 (2.1)	2 (4.2)	2 (4.2)	5 (10.4)
Proteinuria	7 (14.6)	3 (6.2)	0 (0)	0 (0)	10 (20.8)
Hemorrhage	0 (0)	0 (0)	1 (2.1)	0 (0)	1 (2.1)
Infection	0 (0)	1 (2.1)	0 (0)	0 (0)	1 (2.1)

(9.1 *versus* 5.1 months, $p < 0.0001$).¹⁶ The subanalysis of the BICC-C study (bevacizumab + FOLFIRI or mFL) reported no difference in efficacy and safety for mCRC patients >70 years compared with patients ≤ 70 years (PFS 7.6 months compared to 10.7 months, $p = 0.14$, with FOLFIRI/Bev ORR 57% >70 years and 58% ≤ 70 years).¹¹ Pooled analysis of four randomized trials (three first-line and one second-line treatment, $n = 3,007$), where patients were treated with fluoropyrimidine-based chemotherapy with or without bevacizumab, showed that addition of bevacizumab to CTX significantly prolonged PFS in older and younger patients with similar magnitude of PFS benefit (hazard ratios were 0.59, 0.58 and 0.54 in patients aged <65 years, ≥ 65 years and ≥ 70 years, respectively). In addition, OS in both older and younger patients was statistically significantly prolonged by addition of bevacizumab to CTX (median OS was 19.9 months in patients aged <65 years, 17.9 months in patients ≥ 65 years and 17.4 months in those aged ≥ 70 years).¹³ Recent results from phase II study BECOX suggest that bevacizumab plus XELOX is effective and well tolerated in elderly mCRC patients with time to progression of 11.1 months, median OS of 20.4 months and ORR of 46%.¹⁷

Bevacizumab-containing CTX outcomes from routine clinical practice were monitored and/or reported in mCRC patients registries such as prospective US BRiTE registry ($n = 1,953$)⁹ or retrospective Czech ($n = 3,187$) and French ($n = 1,322$) registries.^{10,18} These large first-line setting registries confirmed similarity of clinical benefit between

younger and older patients, previously reported in randomized clinical trials and pooled analysis.

Safety profile for all these studies is generally similar in older and younger patients, except for thromboembolic events, which were more common in the older group.

Within local registry of patients with metastatic colorectal cancer, we have assessed efficacy and safety of bevacizumab in combination with various chemotherapy regimens and compared data between two age groups - patients aged below and over 70 years.

While other registries as backbone chemotherapy reported use of primarily oxaliplatin-based first line chemotherapy (FOLFOX followed by XELOX or FOLFIRI) with trend of increased monotherapy use in elderly population, in our centre backbone chemotherapy was in majority of patients (68%) irinotecan-based. Specifically, bevacizumab was administered mainly with XELIRI (58.6% in <70 years group and 60.4% in ≥70 years group) followed by XELOX (27.8% in <70 years group and 14.6% in ≥70 years group) with low rate of monotherapy use (1.8% and 8.4% for <70 years and ≥70 years, respectively). Although median duration of B-CTX in elderly was 17 weeks and in patients aged <70 years was 24 weeks, maintenance with bevacizumab was well tolerated in both groups with median number of cycles 6 and 5 for <70 years (51% of patients) and ≥70 years group (44% of patients), respectively. ORR and DCR did not differ significantly between the two groups ($p = 0.375$ and $p = 0.066$, respectively) which is in concordance with other studies. The median PFS of 10.2 and 11.3 months in elderly and <70 years group, respectively ($p = 0.58$) is also comparable to findings in other studies. In BRiTE registry, even after adjusting for significant baseline covariates such as ECOG PS or site and surgical resection of primary tumour, decreasing median OS in older age cohorts was observed.⁹ Similarly, in our study median OS was 18.5 and 27.4 months for elderly and <70 years group, respectively ($p = 0.03$). This can be partially explained by worse PS in elderly (PS1/2 62.4%) than patients in <70 years group (PS1/2 35.8%). Selection bias and influence of comorbidities and presence of synchronous metastasis that were not captured cannot be excluded.

In the registry, only bevacizumab-associated adverse event information was collected. A disadvantage of our registry was lack of data for chemotherapy induced adverse events. This was not in scope of the registry, as in an earlier retrospective study from our group, where we compared XELIRI/

bevacizumab to FOLFIRI/bevacizumab (age range 31–77 years), we have reported similar efficacy and safety data between two chemotherapy regimens, but with more grade 3/4 neutropenia in FOLFIRI/bevacizumab combination, and more grade 3/4 diarrhoea in XELIRI/bevacizumab, findings confirmed also by other studies.^{19,20}

The rates of most bevacizumab-targeted adverse events in the older patient group were similar to rates in the patients aged <70 years. They were also comparable to previously reported overall rates of adverse events.^{9,13,15} The most common bevacizumab-associated adverse events were hypertension and proteinuria, with hypertension being slightly more observed in elderly (25% *vs.* 18.5%). No grade 4 or 5 hypertensive events were recorded. Thromboembolic events were reported in 10.4% of elderly patients compared to 5.6% in patients aged <70 years. The increase of arterial thromboembolism in elderly treated with bevacizumab, but no change in venous thromboembolic events, was previously reported in pooled analysis of four randomized trials as well as in large patient registry.^{9,13}

Conclusions

Our single centre experience present new set of data confirming PFS and OS benefit of bevacizumab containing, predominantly irinotecan-based first-line chemotherapy in mCRC patients in routine clinical practice. This benefit was observed in both elderly and patients aged <70 years with manageable safety profile. Proper selection of patients with mCRC can result in a safe and beneficial B-CTX treatment results in older patients with similar outcomes to their younger counterparts, therefore, chronological age does not present exclusion to treatment with bevacizumab.

Acknowledgements

The independent analysis of data was performed by Institute for Biostatistics and Medical Informatics at University of Ljubljana, Slovenia. This research was partially supported by Roche.

References

1. Schmoll HJ, Van Cutsem E, Stein A, Valentini V, Glimelius B, Haustermans K, et al. ESMO consensus guidelines for management of patients with colon and rectal cancer. A personalized approach to clinical decision making. *Ann Oncol* 2012; **23**: 2479-516.

2. Cancer in Slovenia 2010. Ljubljana: Institute of Oncology Ljubljana, Epidemiology and Cancer Registry, Cancer Registry of Republic of Slovenia; 2013.
3. Zwitter M, Kovac V, Rajer M, Vrankar M, Smerdel U. Two schedules of chemotherapy for patients with non-small cell lung cancer in poor performance status: a phase II randomized trial. *Anticancer Drugs* 2010; **21**: 662-8.
4. Sundararajan V, Mitra N, Jacobson JS, Grann VR, Heitjan DF, Neugut AI. Survival associated with 5-fluorouracil-based adjuvant chemotherapy among elderly patients with node positive colon cancer. *Ann Intern Med* 2002; **136**: 349-57.
5. Folprecht G, Cunningham D, Ross P, Glimelius B, Di Costanzo F, Wils J, et al. Efficacy of 5-fluorouracil-based chemotherapy in elderly patients with metastatic colorectal cancer: A pooled analysis of clinical trials. *Ann Oncol* 2004; **15**: 1330-8.
6. Köhne CH, Folprecht G, Goldberg RM, Mitry E, Rougier P. Chemotherapy in elderly patients with colorectal cancer. *Oncologist* 2008; **13**: 390-402.
7. Ocvirk J. Advances in the treatment of metastatic colorectal carcinoma. *Radiol Oncol* 2009; **43**: 1-8.
8. Van Cutsem E, Rivera F, Berry S, Kretzschmar A, Michael M, DiBartolomeo M, et al. Safety and efficacy of first-line bevacizumab with FOLFOX, XELOX, FOLFIRI and fluoropyrimidines in metastatic colorectal cancer: the BEAT study. *Ann Oncol* 2009; **29**: 1842-7.
9. Kozloff MF, Berlin J, Flynn PJ, Kabbinavar F, Ashby M, Dong W, et al. Clinical outcomes in elderly patients with metastatic colorectal cancer receiving bevacizumab and chemotherapy: results from the BRITE observational cohort study. *Oncology* 2010; **78**: 329-39.
10. Slavicek L, Pavlik T, Tomasek J, Bortlicek Z, Buchler T, Melichar B, et al. Efficacy and safety of bevacizumab in elderly patients with metastatic colorectal cancer: results from the Czech population-based registry. *BMC Gastroenterology* 2014; **14**: 53.
11. Jackson NA, Barrueco J, Soufi-Mahjoubi R, Marshall J, Mitchell E, Zhang X, et al. Comparing safety and efficacy of first-line irinotecan/fluoropyrimidine combinations in elderly versus nonelderly patients with metastatic colorectal cancer. *Cancer* 2009; **115**: 2617-29.
12. Price TJ, Zannino D, Wilson K, Simes J, Cassidy J, Van Hazel GA, et al. Bevacizumab is equally effective and no more toxic in elderly patients with advanced colorectal cancer: a subgroup analysis from the AGITG MAX trial: an international randomised controlled trial of capecitabine, bevacizumab and mytomycin C. *Ann Oncol* 2012; **23**: 1531-6.
13. Cassidy J, Saltz LB, Giantonio BJ, Kabbinavar FF, Hurwitz HI, Rohr UP. Effect of bevacizumab in older patients with metastatic colorectal cancer: pooled analysis of four randomized studies. *J Cancer Res Clin Oncol* 2010; **136**: 737-43.
14. Mesti T, Boshkoska BM, Kos M, Tekavčič M, Ocvirk J. The cost of systemic therapy for metastatic colorectal carcinoma in Slovenia: Discrepancy analysis between cost and reimbursement. *Radiol Oncol* 2015; **49**: 200-8.
15. Kabbinavar FF, Schulz J, McCleod, Patel T, Hamm JT, Hecht JR, et al. Addition of bevacizumab to bolus fluorouracil and leucovorin in first-line metastatic colorectal cancer: results of randomized phase II trial. *J Clin Oncol* 2005; **23**: 3697-705.
16. Cunningham D, Lang I, Marcuello E, Lorusso V, Ocvirk J, Shin DB, et al. Bevacizumab plus capecitabine versus capecitabine alone in elderly patients with previously untreated metastatic colorectal cancer (AVEX): an open label, randomized phase 3 trial. *Lancet Oncol* 2013; **14**: 1077-85.
17. Feliu J, Salud A, Safont MJ, Garcia-Girón C, Aparicio J, Vera R, et al. First-line bevacizumab and capecitabine-oxaliplatin in elderly patients with mCRC: GEMCAD phase II BECOX study. *Br J Cancer* 2014; **111**: 241-8.
18. Doat S, Thiébaud A, Samson S, Ricordeau P, Guillemont D, Mitry E. Elderly patients with colorectal cancer: treatment modalities and survival in France. National data from the ThInDIT cohort study. *Eur J Cancer* 2014; **50**: 1276-83.
19. Ocvirk J, Rebersek M, Boc M. Bevacizumab in first-line therapy of metastatic colorectal cancer: a retrospective comparison of FOLFIRI and XELIRI. *Anticancer Res* 2011; **31**: 1777-82.
20. Ducreux M, Adenis A, Pignon J-P, François E, Chauffert B, Ichanté JL, et al. Efficacy and safety of bevacizumab-based combination regimens in patients with previously untreated metastatic colorectal cancer: Final results from a randomised phase II study of bevacizumab plus 5-fluorouracil, leucovorin plus irinotecan versus bevacizumab plus capecitabine plus irinotecan (FNCLCC ACCORD 13/0503 study). *Eur J Cancer* 2013; **49**: 1236-45.

The dosimetric significance of using 10 MV photons for volumetric modulated arc therapy for post-prostatectomy irradiation of the prostate bed

Henry Kleiner^{1,2}, Matthew B. Podgorsak^{1,2}

¹ Department of Physiology and Biophysics, SUNY University at Buffalo, Buffalo, NY, USA

² Department of Radiation Medicine, Roswell Park Cancer Institute, Buffalo, NY, USA

Radiol Oncol 2016; 50(2): 232-237.

Received 21 September 2015
Accepted 8 January 2016

Correspondence to: Henry Kleiner, MS, Department of Physiology and Biophysics, SUNY University at Buffalo, Buffalo, NY, USA and Department of Radiation Medicine, Roswell Park Cancer Institute, Buffalo, NY, USA. E-mail: henry.kleiner@gmail.com

Disclosure: No potential conflicts of interest were disclosed.

Background. The purpose of the study was to analyse the dosimetric differences when using 10 MV instead of 6 MV for VMAT treatment plans for post-prostatectomy irradiation of the prostate bed.

Methods and materials. Ten post-prostatectomy prostate bed irradiation cases previously treated using 6 MV with volumetric modulated arc therapy (VMAT) were re-planned using 10 MV with VMAT. Prescription dose was 66.6 Gy with 1.8 Gy per fraction for 37 daily fractions. The same structure set, number of arcs, field sizes, and minimum dose to the Planning Target Volume (PTV) were used for both 6 MV and 10 MV plans. Results were collected for dose to Organs at Risk (OAR) constraints, dose to the target structures, number of monitor units for each arc, Body V_5 , Conformity Index, and Integral Dose. The mean values were used to compare the 6 MV and 10 MV results. To determine the statistical significance of the results, a paired Student *t* test and power analysis was performed.

Results. Statistically significant lower mean values were observed for the OAR dose constraints for the rectum, bladder-Clinical Target Volume (bladder-CTV), left femoral head, and right femoral head. Also, statistically significant lower mean values were observed for the Body V_5 , Conformity Index, and Integral Dose.

Conclusions. Several dosimetric benefits were observed when using 10 MV instead of 6 MV for VMAT based treatment plans. Benefits include sparing more dose from the OAR while still maintaining the same dose coverage to the PTV. Other benefits include lower Body V_5 , Conformity Index, and Integral Dose.

Key words: volumetric modulated arc therapy (VMAT); prostate bed; 10 MV; 6 MV; radiation therapy

Introduction

In radiation therapy, high energy photons are used to deliver x-rays to a tumor target. It is known that as the energy of the photons is increased, they will penetrate deeper into tissue resulting in more radiation dose being delivered to the tumor target. This has been observed when treating prostate cancer with three dimensional conformal radiation therapy (3DCRT).¹

However, as the photon energy is increased, two issues arise: an increase in the penumbra and the

production of secondary neutrons from the head of the linac when using photon energies greater than or equal to 10 MV.²⁻⁴ As the technology of radiation therapy has changed, 3DCRT has given way to Intensity Modulated Radiation Therapy (IMRT), with 6 MV being the most commonly used beam energy in IMRT treatment planning. IMRT allows more dose to be delivered to the tumor target with less dose being deposited to adjacent organs at risk (OAR), as seen in two studies of prostate cancer.^{5,6} For treatment plans using IMRT, numerous studies have been conducted about the impact of differ-

ent photons energies in treating prostate cancer.⁷⁻¹⁴ Some of these studies show no clear benefit to using higher energy photons.

Volumetric Modulated Arc Therapy (VMAT) has now begun to replace IMRT for treating prostate cancer, and numerous studies show that using VMAT instead of IMRT for prostate cancer results in dosimetric benefits, such as reduced treatment time and more dose sparing to OAR.¹⁵⁻²⁰ Therefore, it is relevant to investigate if using higher energy photons has greater potency than using the traditional 6 MV for VMAT. To deal with the issue of neutron contamination, 10 MV photons were used for this work since the issue of neutron production for higher photon energies is negligible at that energy.²¹

When deciding which cancer type would be appropriate for conducting this study, we chose prostate cancer patients who were undergoing post-prostatectomy irradiation of the prostate bed. The reason for this selection is two-fold. The first reason is that we wanted a location with a deep seated target volume. This would ensure that using photon beam energies higher than 6 MV would result in x-rays that would penetrate into the target; photon beam energies greater than 6 MV would not be useful for a shallower target. The second reason is due to there being no requirement for additional boost plans. This allows the same plan to be used during the entire course of patient treatment, requires less treatment planning time per patient, and reduces the complexity of the plan.

Materials and methods

Ten cases of prostate cancer patients who had undergone a prostatectomy and received irradiation of the prostate bed using 6 MV photons with VMAT at Roswell Park Cancer Institute were selected for a retrospective study. These cases were re-planned using 10 MV photons with VMAT, and were compared to the clinically used 6 MV plans. The prescription dose was kept the same at 66.6 Gy for all ten cases for both beam energies, with 1.8 Gy per fraction in 37 daily fractions. Treatment plans were created with the Varian Eclipse version 11 treatment planning system (Varian Medical Systems, Inc., Palo Alto, CA, USA). The Varian implementation of VMAT is known as RapidArc and used Anisotropic Analytical Algorithm version 10 and Progressive Resolution Optimizer version 10. Two complete arcs were used for all ten cases for both beam energies. For each patient, the field sizes for the 10 MV plan were kept the same as the cor-

responding 6 MV plan. Structure sets containing regions of interest were generated using CT based contouring, and the same structure set was used for both sets of treatment plans for dose measurement purposes. For each patient, the same minimum dose to the planning target volume (PTV) structure that existed for each 6 MV plan was used for the corresponding 10 MV plan. This was done as a baseline to compare the 6 MV and 10 MV plans for each patient. It should be noted that this study was performed using only a treatment planning system. There was no actual treatment plan verification of dose delivery by the linear accelerator.

Plan evaluation was based on the OAR dose constraint categories provided in Radiation Therapy Oncology Group (RTOG) protocol 0534.²² Based on this protocol, values were collected for the following OAR dose constraint categories: Bladder-Clinical Target Volume (Bladder-CTV) $D_{50\%}$, Bladder-CTV $D_{70\%}$, Rectum $D_{35\%}$, Rectum $D_{55\%}$, Right Femoral Head $D_{10\%}$, and Left Femoral Head $D_{10\%}$. Bladder-CTV was created by cropping out the part of the bladder that overlaps with the CTV structure. For each plan, the cumulative dose volume histogram was used to collect these values. We also collected the minimum dose, maximum dose, and mean dose for the CTV and PTV, and the volume percentages of the CTV and the PTV that receives 95% of the prescription dose of 66.6 Gy. We also collected values for the Body V_5 , the number of monitor units for the first and second arcs, the Conformity Index, and the Integral Dose. The Body V_5 provided a measurement of low dose exposure to the Body as contoured in the treatment planning system. The International Committee for Radiation Units (ICRU) report 62 defined the Conformity Index as the ratio between the treated volume receiving a selected dose and the PTV volume receiving a selected dose.²³ Based on ICRU report 62, we defined the Conformity Index in our study as the ratio between the Body volume receiving 66.6 Gy and the PTV volume receiving 66.6 Gy. We defined the Integral Dose as the volume of the Body-PTV structure multiplied by the mean dose to the Body-PTV. The Body-PTV structure was created by cropping out the section of the Body structure that overlapped with the PTV. For each category of interest, the results collected for both energies were used to generate a mean along with a standard deviation of the mean for 6 MV and 10 MV. To determine the statistical significance of our results, a paired Student t test and power analysis was conducted using the R statistical software package version 3.2.3.²⁴ The OAR dose constraint limits were adapted from RTOG protocol 0534, and

are presented in Table 1. We did not want the dose to the OAR to exceed these limits.

Additional optimization structures were used for the 10 MV treatment plans in order to spare dose to the OAR and increase dose to the PTV. These structures were labeled PTV_x, Bladder-PTV_x, Rectum-PTV_x, Penile Bulb-PTV_x, Rectum 7 mm, and Rectum Mid. The PTV_x is created from the PTV with a margin expansion of 1 mm in all directions. The Bladder-PTV_x structure is created by cropping out the portion of the bladder that overlaps with the PTV_x with a 3 mm separation between the new structure and the PTV_x. The Rectum-PTV_x structure is created by cropping out the portion of the rectum that overlaps with the PTV_x with a 3 mm separation between the new structure and the PTV_x. The Penile Bulb-PTV_x structure is created by cropping out the portion of the penile bulb that overlaps with the PTV_x with a 3 mm separation between the new structure and the PTV_x. Not every plan had this structure due to the possibility that the penile bulb completely overlaps with the PTV_x. The Rectum 7 mm structure was created through several steps. First, the Rectum-PTV_x structure is created with no additional separation. Then, this structure is expanded by 5 mm on all sides. This new structure is cropped out from the PTV_x with an additional margin of 7 mm. Any instances of the Rectum 7 mm structure on slices where the PTV_x structure did not exist were erased. The Rectum Mid structure was created through several steps. First, the Rectum-PTV_x structure is created with no additional separation. This structure is expanded the margin by 5 mm on all sides. Then, using a Boolean operation, this structure is cropped from the Rectum 7 mm structure. This new structure is then cropped from the PTV_x structure with an additional separation of 3 mm. Any instances of the Rectum Mid structure on CT slices where the PTV_x structure did not exist were erased. These two structures Rectum Mid and Rectum 7 mm were created to move the 50% isodose line away from the posterior portion of the rectum. This is due to a study that showed an increased complication risk if the 50% isodose line falls outside the rectum.²⁵ Additionally, we want the 90% isodose line to fall at half the width posteriorly in the rectum and the 50% isodose line should fall at less than half the full width posteriorly in the rectum.

Results

For each category in Table 2, the mean, standard deviation of the mean (SDOM), the percent in-

TABLE 1. Dose constraint limits adapted from RTOG protocol 0534

Category	Dose Constraint
Bladder-CTV D ₅₀	65 Gy
Bladder-CTV D ₇₀	40 Gy
Rectum D ₃₅	65 Gy
Rectum D ₅₅	40 Gy
Right Femoral Head D ₁₀	50 Gy
Left Femoral Head D ₁₀	50 Gy

CTV = Clinical Target Volume

crease, the *p*-value, and the power of the statistical test are presented below. The percent increase is the increase (or decrease) when transitioning from the 6 MV mean to the corresponding 10 MV mean. A negative sign in the percent increase column indicates a percent decrease going from 6 MV to 10 MV. A *p*-value less than or equal to 0.05 is considered statistically significant.

Looking at Table 2, we see that all the values for the OAR dose constraint categories show a lower dose when using 10 MV in place of 6 MV. We also see more than 10% reduction in the mean dose for the categories Bladder-CTV D₇₀, Right Femoral Head D₁₀, and Left Femoral Head D₁₀. Note that the 6 MV and 10 MV results for all OAR dose constraint categories were much lower than the dose limits set by the RTOG 0534 protocol displayed in Table 1.

For the two categories CTV Percent Volume Covered by the 95% Isodose Line and PTV Percent Volume Covered by the 95% Isodose Line, we observed that 100% of the respective target structure received 95% of the prescription dose of 66.6 Gy for all ten patients for both 6 MV and 10 MV. Therefore, there is no standard deviation of the mean and no *p*-value to be found for these two categories.

Looking at the *p*-values less than or equal to 0.05 in Table 2, we see that the 10 MV results are statistically significant for the following categories: Bladder-CTV D₅₀, Bladder-CTV D₇₀, Rectum D₃₅, Rectum D₅₅, Right Femoral Head D₁₀, Left Femoral Head D₁₀, CTV Mean Dose, Body V₅, Conformity Index, and Integral Dose. The following categories had a *p*-value greater than 0.05, and therefore are not statistically significant: CTV Min Dose, CTV Max Dose, PTV Min Dose, PTV Max Dose, PTV Mean Dose, Global Max Dose, Arc 1 Monitor Units, and Arc 2 Monitor Units. It should be noted that for the number of MU for the first arc, eight of the ten

TABLE 2. Mean, standard deviation of the mean, percent increase, p-value, and power for both 6 MV and 10 MV are displayed

Category	6 MV Mean \pm SDOM	10 MV Mean \pm SDOM	Percent Increase	p-value	Power
Bladder-CTV D ₅₀	32.5 \pm 4.3 Gy	29.7 \pm 3.9 Gy	-8.62%	0.013	0.79
Bladder-CTV D ₇₀	18.5 \pm 3.7 Gy	16.2 \pm 3.2 Gy	-12.4%	0.011	0.81
Rectum D ₃₅	49.5 \pm 3.3 Gy	46.8 \pm 3.9 Gy	-5.45%	6.6 \times 10 ⁻³	0.88
Rectum D ₅₅	28.5 \pm 2.7 Gy	26.7 \pm 2.7 Gy	-6.32%	0.023	0.68
Right Femoral Head D ₁₀	34.12 \pm 0.86 Gy	29.80 \pm 0.99 Gy	-12.66%	1.2 \times 10 ⁻⁴	1.0
Left Femoral Head D ₁₀	32.74 \pm 0.94 Gy	29.4 \pm 1.1 Gy	-10.20%	8.3 \times 10 ⁻⁵	1.0
CTV Min Dose	65.53 \pm 0.38 Gy	65.29 \pm 0.21 Gy	-0.3662%	0.41	0.12
CTV Max Dose	71.01 \pm 0.37 Gy	70.53 \pm 0.31 Gy	-0.6760%	0.10	0.37
CTV Mean Dose	68.30 \pm 0.29 Gy	67.68 \pm 0.27 Gy	-0.9078%	0.019	0.72
CTV Percent Volume Covered by the 95% Isodose Line	100%	100%	0%	N/A	N/A
PTV Min Dose	64.42 \pm 0.29 Gy	64.42 \pm 0.29 Gy	0%	0.10	0.37
PTV Max Dose	71.78 \pm 0.29 Gy	71.76 \pm 0.33 Gy	-0.02786%	0.94	0.051
PTV Mean Dose	68.39 \pm 0.38 Gy	67.94 \pm 0.28 Gy	-0.6580%	0.063	0.47
PTV Percent Volume Covered by the 95% Isodose Line	100%	100%	0%	N/A	N/A
Body V ₅	(27.0 \pm 1.0)%	(26.5 \pm 1.0)%	-1.85%	2.2 \times 10 ⁻³	0.96
Global Max Dose	71.80 \pm 0.38 Gy	71.76 \pm 0.33 Gy	-0.05571%	0.89	0.052
Arc 1 Monitor Units	325 \pm 17 MU	311.8 \pm 9.8 MU	-4.06%	0.41	0.12
Arc 2 Monitor Units	330 \pm 15 MU	312 \pm 10 MU	-5.5%	0.19	0.24
Conformity Index	1.127 \pm 0.013	1.091 \pm 0.015	-3.194%	6.8 \times 10 ⁻⁴	0.99
Integral Dose	207 \pm 12 Gy-L	191 \pm 11 Gy-L	-7.73%	1.1 \times 10 ⁻⁵	1.0

CTV = Clinical Target Volume; N/A = not applicable for that category; PTV = Planning Target Volume

cases had lower MU when using 10 MV, and for the number of MU for the second arc, eight of the ten cases had lower MU when using 10 MV. For the Global Max Dose, six of the ten cases had lower Global Max Dose when using 10 MV. Further analysis of our power results are presented in the Discussion section below.

Discussion

Our results have shown that using 10 MV photons instead of 6 MV photons for irradiation of the prostate bed will result in statistically significant lower values for the OAR dose constraint categories, Body V₅, Conformity Index, and Integral Dose. We also observed that using 10 MV results in 95% of the prescription dose of 66.6 Gy covering 100% of the CTV and PTV volumes for all ten patients; this is the same coverage as using 6 MV for all ten patients. This is important because OAR dose sparing should not occur at the expense of tumor target coverage.

It should be noted that the mean results for both 6 MV and 10 MV plans were well below the dose constraints outlined in the RTOG 0534 protocol and posted in Table 1 above. RTOG 0534 was developed as a phase 3 trial for androgen deprivation with pelvic lymph node or prostate bed only radiation therapy after a prostatectomy. We used this protocol for our study because it is used at Roswell Park Cancer Institute for plan evaluation when using 6 MV for post-prostatectomy prostate bed irradiation.

For our study, we used a sample size of ten cases. Even though this is a small sample size, there is no minimum size requirement in using a paired Student t test. Research in the methodology of statistical testing has shown that a possible limitation for using a small sample size exists in the power of the statistical test that was performed.^{26,27} However, it has also been shown that this limitation regarding small sample sizes does not exist for experiments where there is a large effect size present.²⁸ For our study, the null hypothesis is that for each category listed above in Table 2, the difference

between the respective means for 6 MV and 10 MV are 0. The alternative hypothesis is that there is a difference between the respective means for 6 MV and 10 MV. The probability of committing a Type II error is the probability of failing to reject a false null hypothesis, and is denoted by β . The probability of rejecting a false null hypothesis is known as the power of the statistical test, and is denoted by $1-\beta$. Looking at our power results in Table 2, we see that for the categories where the p -values are statistically significant, there is a high probability that we will reject a false null hypothesis, and therefore will not commit a Type II error. Another issue is the possibility of committing a Type I error. The probability of committing a Type I error is the probability of rejecting a true null hypothesis, and is denoted by α . By setting $\alpha = 0.05$, and obtaining a p -value less than or equal to 0.05 means that there is a high probability (greater than or equal to 95%) that we will not commit a Type I error.

In making a comparison between the 6 MV and 10 MV plans used for this study, it should be noted that the 6 MV and 10 MV cases were created by different planners. The 6 MV cases were created by an experienced dosimetrist, while the 10 MV cases were created by a non-experienced planner. This can introduce some biases regarding the 10 MV plan outcomes. However, looking at the 10 MV results, we argue that if the same 6 MV planner had worked on the 10 MV plans, the same or better results could be obtained due to planner experience. The 6 MV plans were created with time constraints imposed by real-world clinical conditions; this was not the case for the 10 MV plans. However, it can be argued that 10 MV plans with the same or better outcomes could be created by an experienced dosimetrist using the same time constraints as the 6 MV plans.

Our results for OAR dose sparing contrast with other studies of IMRT treatment plans using higher photon beam energies for intact prostate where there is no improvement in dose reduction to OAR and no better Conformity Index.^{9,11,13} Work done by Pirzkall *et al.* has shown that when the number of IMRT static fields are increased, the effects of using higher photon energy are downplayed.¹³ This same study wondered if higher photon energies would play less of a role in rotational IMRT, *i.e.* VMAT. Studies performed by Pasler *et al.*¹² and Ost *et al.*²⁹ looked at VMAT planning for prostate cancer for ten and twelve patients, respectively. The study by Pasler *et al.* found that using photon energies of 10 MV and 15 MV versus 6 MV resulted in a statistically significant lower Integral Dose; however,

monitor units were not investigated in that study. The study by Ost *et al.* found that using 18 MV instead of 6 MV resulted in statistically significant lower monitor units; however, Integral Dose was not investigated in that study.

Furthermore, a recent study by Mattes *et al.* using 6 MV and 10 MV with VMAT to treat intact prostate cancer also found a lower Conformity Index, lower Integral Dose, and lower monitor units, while having minimal dose sparing to the OAR.³⁰ However, that VMAT study purposely uses the same optimization constraints for both 6 MV and 10 MV treatment plans, thereby not allowing the optimizer to make full use of the 10 MV photons. It can be argued that using 10 MV may allow the optimizer in the Eclipse treatment planning system more leeway to shift more dose from the OAR. Therefore, setting higher dose constraints on the optimization structures may prove useful. In that same study, 10 MV resulted in a more than 16% decrease in maximum dose to the skin structure. While our work did not measure dose to the skin, the possibility of lower skin dose would be another benefit to using 10 MV photons due to the greater penetrating power and longer dose build-up of 10 MV. Skin sparing effects have been noted in a study by Chow *et al.* of prostate irradiation using IMRT.³¹ This topic could be investigated in a future work.

For our study, most of the OAR dose constraint categories that exhibited the largest dose reduction of more than 10% were to the shallow OAR, *i.e.* the left and right femoral heads. It stands to reason that using 10 MV photons can result in large dose reductions to OAR that are shallowly located relative to the tumor target. Other cancer sites that one may wish to investigate should possess deep seated target volumes. This ensures that much of the dose is deposited into the target, and not to adjacent healthy tissue. Therefore, cancers located in the pelvic or abdominal regions should be investigated into whether using 10 MV photons provide similar benefits.

Another possible benefit for using 10 MV rather than 6 MV could be the reduced chance of a patient having a secondary cancer malignancy. Work done by Kry *et al.* has shown that the lifetime risk of developing a fatal secondary cancer is 39% higher when using 6 MV compared to 10 MV for IMRT.³² It is possible that this finding carries over into VMAT when using 10 MV instead of 6 MV. A system that tracks future occurrences of cancer in patients treated with prostate bed irradiation may prove useful for future studies.

Conclusions

In this retrospective study of treatment plans comparing 6 MV to 10 MV for post-prostatectomy irradiation of the prostate bed, we have shown that using 10 MV photons can result in statistically significant better outcomes for our OAR dose constraints, Body V_{5r} , Conformity Index, and Integral Dose. We also have shown that 10 MV can be used in our treatment plans without compromising dose coverage to the CTV and PTV. In addition, neutron contamination from the linac head is not a major concern when choosing 10 MV over 6 MV. From these observations, it can be argued that using 10 MV rather than 6 MV can result in better treatment plans for patients undergoing prostate bed irradiation after a prostatectomy.

References

- Laughlin JS, Mohan R, Kutcher GJ. Choice of optimum megavoltage for accelerators for photon beam treatment. *Int J Radiat Oncol* 1986; **12**: 1551-7.
- NCRP. Report No. 79: *Neutron contamination from medical electron accelerators*. Bethesda, Maryland: NCRP; 1987.
- Westermarck M, Arndt J, Nilsson B, Brahme A. Comparative dosimetry in narrow high-energy photon beams. *Phys Med Biol* 2000; **45**: 685-702.
- Howell RM, Ferenci MS, Hertel NE, Fullerton GD. Investigation of secondary neutron dose for 18 MV dynamic MLC IMRT delivery. *Med Phys* 2005; **32**: 786-93.
- Xu N, Rossi PJ, Jani AB. Toxicity analysis of dose escalation from 75.6 Gy to 81.0 Gy in prostate cancer. *Am J Clin Oncol* 2011; **34**: 11-5.
- Zelevsky MJ, Yamada Y, Fuks Z, Zhang Z, Hunt M, Cahlon O, et al. Long-term results of conformal radiotherapy for prostate cancer: impact of dose escalation on biochemical tumor control and distant metastases-free survival outcomes. *Int J Radiat Oncol* 2008; **71**: 1028-33.
- Soderstrom S, Eklof A, Brahme A. Aspects on the optimal photon beam energy for radiation therapy. *Acta Oncol* 1999; **38**: 179-87.
- Park JM, Choi CH, Ha SW, Ye SJ. The dosimetric effect of mixed-energy IMRT plans for prostate cancer. *J Appl Clin Med Phys* 2011; **12**: 3563.
- Sun M, Ma L. Treatments of exceptionally large prostate cancer patients with low-energy intensity-modulated photons. *J Appl Clin Med Phys* 2006; **7**: 43-9.
- Sung W, Park JM, Choi CH, Ha SW, Ye SJ. The effect of photon energy on intensity-modulated radiation therapy (IMRT) plans for prostate cancer. *Radiat Oncol J* 2012; **30**: 27-35.
- de Boer SF, Kumek Y, Jaggernauth W, Podgorsak MB. The effect of beam energy on the quality of IMRT plans for prostate conformal radiotherapy. *Technol Cancer Res Treat* 2007; **6**: 139-46.
- Pasler M, Georg D, Wirtz H, Lutterbach J. Effect of photon-beam energy on VMAT and IMRT treatment plan quality and dosimetric accuracy for advanced prostate cancer. *Strahlenther Onkol* 2011; **187**: 792-8.
- Pirzkall A, Carol MP, Pickett B, Xia P, Roach M, 3rd, Verhey LJ. The effect of beam energy and number of fields on photon-based IMRT for deep-seated targets. *Int J Radiat Oncol* 2002; **53**: 434-42.
- Welsh JS, Mackie TR, Limmer JP. High-energy photons in IMRT: uncertainties and risks for questionable gain. *Technol Cancer Res Treat* 2007; **6**: 147-9.
- Palma D, Vollans E, James K, Nakano S, Moiseenko V, Shaffer R, et al. Volumetric modulated arc therapy for delivery of prostate radiotherapy: comparison with intensity-modulated radiotherapy and three-dimensional conformal radiotherapy. *Int J Radiat Oncol* 2008; **72**: 996-1001.
- Wolff D, Stieler F, Welzel G, Lorenz F, Abo-Madyan Y, Mai S, et al. Volumetric modulated arc therapy (VMAT) vs. serial tomotherapy, step-and-shoot IMRT and 3D-conformal RT for treatment of prostate cancer. *Radiother Oncol* 2009; **93**: 226-33.
- Shaffer R, Morris WJ, Moiseenko V, Welsh M, Crumley C, Nakano S, et al. Volumetric modulated Arc therapy and conventional intensity-modulated radiotherapy for simultaneous maximal intraprostatic boost: a planning comparison study. *Clin Oncol* 2009; **21**: 401-7.
- Zhang P, Happersett L, Hunt M, Jackson A, Zelevsky M, Mageras G. Volumetric modulated arc therapy: planning and evaluation for prostate cancer cases. *Int J Radiat Oncol* 2010; **76**: 1456-62.
- Cozzi L, Dinshaw KA, Shrivastava SK, Mahantshetty U, Engineer R, Deshpande DD, et al. A treatment planning study comparing volumetric arc modulation with RapidArc and fixed field IMRT for cervix uteri radiotherapy. *Radiother Oncology* 2008; **89**: 180-91.
- Guckenberger M, Richter A, Krieger T, Wilbert J, Baier K, Flentje M. Is a single arc sufficient in volumetric-modulated arc therapy (VMAT) for complex-shaped target volumes? *Radiother Oncol* 2009; **93**: 259-65.
- NCRP. Report No. 151: *Structural shielding design and evaluation for megavoltage x-and gamma-ray radiotherapy facilities*. Bethesda, Maryland: NCRP; 2006.
- RTOG. RTOG 0534: *A phase III trial of short term androgen deprivation with pelvic lymph node or prostate bed only radiotherapy (spport) in prostate cancer patients with a rising psa after radical prostatectomy*. Philadelphia, Pennsylvania: RTOG; 2013.
- ICRU. Report No. 62: *Prescribing, recording and reporting photon beam therapy (supplement to ICRU report 50)*. Bethesda, Maryland: ICRU; 1999.
- R Core Team. R: *A Language and Environment for Statistical Computing*. Vienna, Austria: R Foundation for Statistical Computing; 2015.
- Skwarchuk MW, Jackson A, Zelevsky MJ, Venkatraman ES, Cowen DM, Levegrun S, et al. Late rectal toxicity after conformal radiotherapy of prostate cancer (I): multivariate analysis and dose-response. *Int J Radiat Oncol* 2000; **47**: 103-13.
- Rossi JS. Statistical power of psychological research: What have we gained in 20 years? *J Consult Clin Psych* 1990; **58**: 646-56.
- Cohen J. Approximate power and sample size determination for common one-sample and two-sample hypothesis tests. *Educ Psychol Meas* 1970; **30**: 811-31.
- de Winter JC. Using the Student's t-test with extremely small sample sizes. *Practical Assessment, Research & Evaluation* 2013; **18**: 1-12.
- Ost P, Speleers B, De Meerleer G, De Neve W, Fonteyne V, Villeirs G, et al. Volumetric arc therapy and intensity-modulated radiotherapy for primary prostate radiotherapy with simultaneous integrated boost to intraprostatic lesion with 6 and 18 MV: a planning comparison study. *Int J Radiat Oncol* 2011; **79**: 920-6.
- Mattes MD, Tai C, Lee A, Ashamalla H, Ikoro NC. The dosimetric effects of photon energy on the quality of prostate volumetric modulated arc therapy. *Pract Radiat Oncol* 2014; **4**: e39-44.
- Chow JC, Grigorov GN, Barnett RB. Study on surface dose generated in prostate intensity-modulated radiation therapy treatment. *Med Dosim* 2007; **31**: 249-58.
- Kry SF, Followill D, White RA, Stovall M, Kuban DA, Salehpour M. Uncertainty of calculated risk estimates for secondary malignancies after radiotherapy. *Int J Radiat Oncol* 2007; **68**: 1265-71.

Effect of photon energy spectrum on dosimetric parameters of brachytherapy sources

Mahdi Ghorbani¹, Mohammad Mehrpouyan², David Davenport³, Toktam Ahmadi Moghaddas⁴

¹ Medical Physics Research Center, Mashhad University of Medical Sciences, Mashhad, Iran

² Bioinformatics Research Center, Sabzevar University of Medical Sciences, Sabzevar, Iran

³ Comprehensive Cancer Centers of Nevada, Las Vegas, Nevada, USA

⁴ Department of Basic Medical Sciences, Neyshabur University of Medical Sciences, Neyshabur, Iran

Radiol Oncol 2016; 50(2): 238-246.

Received 2 November 2015

Accepted 29 January 2016

Correspondence to: Mohammad Mehrpouyan, Bioinformatics Research Center, Sabzevar University of Medical Sciences, Sabzevar, Iran. Phone: +98 51 4444 6070, +98 51 4444 6234; Fax: +98 51 4444 5648; E-mail: mehrpouyan.mohammad@gmail.com; or Toktam Ahmadi Moghaddas, Department of Basic Medical Sciences, Neyshabur University of Medical Sciences, Neyshabur, Iran. E-mail: toktamt.moghaddas@gmail.com

Disclosure: No potential conflicts of interest were disclosed.

Aim. The aim of this study is to quantify the influence of the photon energy spectrum of brachytherapy sources on task group No. 43 (TG-43) dosimetric parameters.

Background. Different photon spectra are used for a specific radionuclide in Monte Carlo simulations of brachytherapy sources.

Materials and methods. MCNPX code was used to simulate ¹²⁵I, ¹⁰³Pd, ¹⁶⁹Yb, and ¹⁹²Ir brachytherapy sources. Air kerma strength per activity, dose rate constant, radial dose function, and two dimensional (2D) anisotropy functions were calculated and isodose curves were plotted for three different photon energy spectra. The references for photon energy spectra were: published papers, Lawrence Berkeley National Laboratory (LBNL), and National Nuclear Data Center (NNDC). The data calculated by these photon energy spectra were compared.

Results. Dose rate constant values showed a maximum difference of 24.07% for ¹⁰³Pd source with different photon energy spectra. Radial dose function values based on different spectra were relatively the same. 2D anisotropy function values showed minor differences in most of distances and angles. There was not any detectable difference between the isodose contours.

Conclusions. Dosimetric parameters obtained with different photon spectra were relatively the same, however it is suggested that more accurate and updated photon energy spectra be used in Monte Carlo simulations. This would allow for calculation of reliable dosimetric data for source modeling and calculation in brachytherapy treatment planning systems.

Key words: photon energy spectrum; brachytherapy; TG-43 dosimetric parameters; dose distribution

Introduction

Monte Carlo (MC) codes are currently used to verify brachytherapy sources while utilizing the photon energy spectrum of a specific radionuclide for calculations. There exist some common energy spectrum databases which are used by researchers. Some use the recommendation of the American

Association of Physicists in Medicine (AAPM) from task group No. 43 updated report (TG-43 U1) which was prepared for low energy photon emitting radionuclides such as ¹²⁵I and ¹⁰³Pd.¹ In a report by the AAPM and the European Society for Therapeutic Radiology and Oncology (ESTRO)², the use of the energy spectrum database of the National Nuclear Data Center (NNDC)³ was rec-

ommended for photon emitting radionuclides higher than 50 keV.

There are various methods to determine the energy spectra of photon emitting radionuclides. One widely used technique is high-purity germanium detectors, especially for low energy sources.⁴⁻⁶ Chen *et al.*⁷, have used a high purity germanium detector to measure the photon energy spectrum emitted by a ¹²⁵I brachytherapy source. Rivard *et al.*⁸ have studied the influence of photon energy spectrum on kerma and dose rate for ¹²⁵I, ¹⁰³Pd, and ¹⁹²Ir sources. They calculated the water kerma proportion for each photon energy to the total energy and plotted the obtained data for different distances. It was concluded that the differences in photon energy spectra do not have a considerable impact on the dose rate constant because of the compensatory effect of dividing dose rate to air kerma strength. In a study by Aryal *et al.*⁹, TG-43 dosimetry parameters were calculated for IAI ¹²⁵I brachytherapy source by variation of some factors such as photon energy spectrum. They found that the photon energy spectrum can change dose rate constant by up to 3% and can alter radial dose function about 12% (at $r = 10$ cm where the dose rate is very low).

It is necessary to implement TG-43 dosimetric parameters in treatment planning systems.¹⁰ ¹²⁵I brachytherapy source models are widely used in prostate cancer treatments wherein the dose received by organs at risk such as rectum and urinary bladder is important. To quantify the dose to these organs, treatment planning systems use the appropriate TG-43 dosimetric parameters which were reported in the literature. Treatment planning systems do not use energy spectrum directly, but they use TG-43 parameters reported by a published study. Therefore, the energy spectrum used in that study can effect on the calculation accuracy of the treatment planning systems indirectly. So the precision of energy spectrum of the radionuclide can have influences on the calculated dose to the tumor and the related organs at risk. Therefore, it is important to provide accurate energy spectra of radionuclides. In the previously mentioned studies, only some dosimetric parameters were evaluated from the energy spectrum point of view. To the best of our knowledge, a comprehensive study considering the influence of photon energy spectrum on the dosimetric parameters of brachytherapy sources was not performed.

The aim of this study is to evaluate the influence of photon energy spectrum on TG-43 dosimetric parameters and isodose curves for three common

photon energy spectra; for ¹²⁵I, ¹⁰³Pd, ¹⁶⁹Yb, and ¹⁹²Ir brachytherapy sources.

Materials and methods

In this study, MCNPX code (version 2.4.0) was used to simulate brachytherapy sources.¹¹ Four brachytherapy sources were studied: MED 3631-A/M ¹²⁵I, Optiseed ¹⁰³Pd, a hypothetical ¹⁶⁹Yb, and Flexisource ¹⁹²Ir sources. In the selection of these radionuclides, there was an attempt to evaluate various brachytherapy sources within a relatively wide range of photon energies. The MED 3631-A/M ¹²⁵I source consists of four polystyrene spheres coated with active ¹²⁵I with an active length of 4.2 mm. The Optiseed ¹⁰³Pd is composed of two polystyrene cylinders containing active ¹⁰³Pd. The active length of ¹⁰³Pd is assumed to be 3.8 mm. The ¹⁶⁹Yb and ¹⁹²Ir sources have the same geometries with 3.5 mm active core, including radioactive ¹⁶⁹Yb and ¹⁹²Ir, respectively. The geometry properties of simulated sources were described in details in the previous published article.¹² The simulations of the sources were verified in that study and the same input files were applied for the mentioned brachytherapy sources in the current study. In that study¹² the verification was based on calculation and comparison of dose rate constant and radial dose function with the corresponding published data on these source models.

Dosimetric parameters

The updated report of TG-43U¹ was followed to calculate the dosimetric parameters of low energy brachytherapy sources. For higher energy brachytherapy sources the recommendations by the report of AAPM and ESTRO² were applied. Based on the report of TG-43 U1, dose rate is calculated from the following formula:

$$\dot{D}(r, \theta) = S_k \left\langle \frac{G(r, \theta)}{G(r_0, \theta_0)} g(r) F(r, \theta) \right\rangle \quad [1]$$

Geometry function with line-source approximation ($G_L(r, \theta)$), radial dose function ($g_L(r, \theta)$) and two dimensional (2D) anisotropy function ($F(r, \theta)$) are calculated from the following formulas:

$$G_L(r, \theta) = \begin{cases} \frac{\beta}{Lr \sin \theta} & \text{if } \theta \neq 0 \\ \left(r^2 - \frac{L^2}{4} \right)^{-1} & \text{if } \theta = 0 \end{cases} \quad [2]$$

$$g_L(r) = \frac{\dot{D}(r, \theta_0) G(r, \theta_0)}{\dot{D}(r_0, \theta_0) G(r_0, \theta_0)} \quad [3]$$

$$F(r, \theta) = \frac{\dot{D}(r, \theta) G_L(r, \theta_0)}{\dot{D}(r_0, \theta_0) G_L(r_0, \theta_0)} \quad [4]$$

where β is the angle between the tips of the ends of the active part of source and point of calculation; L is the active length of the source; r is the radial distance from the source and the calculation point; and θ is the polar angle specifying the calculation point.

Monte Carlo simulations

MCNPX code (version 2.4.0) was used for the simulations. MCNPX is a general purpose Monte Carlo code and is able to transport neutrons, photons, electrons and other particles in various geometries. It includes a geometry modeling tool and various tallies related to energy deposition, particle current, and particle flux. The 2.4.0 version of this code, which was used in the present study, uses MCPLIB02 cross section library for transport of photons.¹³⁻¹⁴ In the MC calculations both photons and electrons were transported. Line-source approximation was used in the MC simulations. The energy cut-off for photons and electrons was considered 1 keV for ¹²⁵I and ¹⁰³Pd sources and 5 keV for ¹⁶⁹Yb and ¹⁹²Ir sources in all input files. No other variance reduction method was applied in this study.

To calculate air kerma strength, air toroid cells were defined in a 100 cm radius vacuum sphere. The brachytherapy source was located at the center of this sphere. The torus cells were in the range of 1–50 cm and their thickness was assumed 1 mm. An F6 tally was scored in these torus cells and the outputs were multiplied by r^2 (where r is the distance from the center of the source). There are different tallies in MCNP (including F4, *F4, F6, etc.) which can be utilized to score various dosimetric parameters such as particle flux, energy flux, kerma, etc. In various versions of MCNP code F6 tally is used to score energy deposition averaged over a cell in terms of MeV/g per particle¹¹. In other words, kerma is calculated by this tally type. The average of $F6 \times r^2$ versus r on the flat region of the curve was calculated to obtain air kerma strength. After obtaining air kerma strength, its value per mCi was calculated for each photon energy spectrum and source. The number of particles transported was 5×10^7 and type A statistical uncertainty was less than 1.4% in this step.

To obtain the dose rate constant, an *F4 tally was calculated at $r_0 = 1$ cm and $\theta_0 = \pi/2$. *F4 tally is en-

ergy flux of a particle type averaged over a cell (in terms of MeV/cm²).¹¹ It should be noticed that with F4 and *F4 tallies in MCNP, it is possible to score particle flux and energy flux in a cell, respectively. In other words, the asterisk sign determines that energy flux be scored by the code, and not particle flux. The outputs of this tally were multiplied by mass energy absorption coefficients at various energy bins and the dose was obtained. The dose was divided to air kerma strength value for each source. Additionally, the dose rate at $r = 1$ cm per mCi for each photon energy spectrum and each source was calculated. Radial dose function was calculated in 1 mm thickness torus cells at radial distances of 0.5–15 cm in a spherical water phantom. The phantom radius was assigned 50 cm and an *F4 tally was scored and then converted to dose. The number of particle histories for the dose rate constant and radial dose function calculations was 10^8 for ¹²⁵I, ¹⁶⁹Yb, and ¹⁹²Ir and 3×10^8 for ¹⁰³Pd source. The maximum type A statistical uncertainty was 4.16%.

The 2D anisotropy function was calculated at 0°–180° with a degree interval of 10° at radial distances of 0.5, 1, 5, 10, and 15 cm. The source was located at the center of a spherical water phantom with a 50 cm radius and an *F4 tally was calculated. Spherical cells were used for 0° and 180° polar angles while torus cells were defined for the other polar angles. The number of particles for this section was assumed as 2×10^8 for ¹⁶⁹Yb and ¹⁹²Ir sources; 9×10^8 for ¹²⁵I source; and 2×10^9 for ¹⁰³Pd source. In all of the data points, the Type A statistical uncertainty was less than 4.18%, with exceptions for two points with 13.8% uncertainty at 0° and 180° angles in 15 cm distance for the ¹⁰³Pd source. These uncertainties could not be reduced because it was not possible to exceed the maximum particle history of 2×10^9 in MCNP.

To plot isodose curves for a source, a mesh grid was defined in a 50 cm spherical water phantom. The sources were defined in the phantom, separately. For the purpose of output calculation, “pedep” option of type 1 mesh tally type in MCNP was applied in the grid. In MCNP, there are various mesh tallies (including type 1, type 2, type 3, etc.) which can be used to score different dosimetric variables in a grid. Each mesh tally has various options, by which the user defines that which variable should be scored by the code. As an example, type 1 tally is track-average mesh tally. With “pedep” option in this mesh tally type, the average energy deposition per unit volume (in terms of MeV/cm per source particle) for a specified particle type is calculated. This option allows the user to score the equivalent

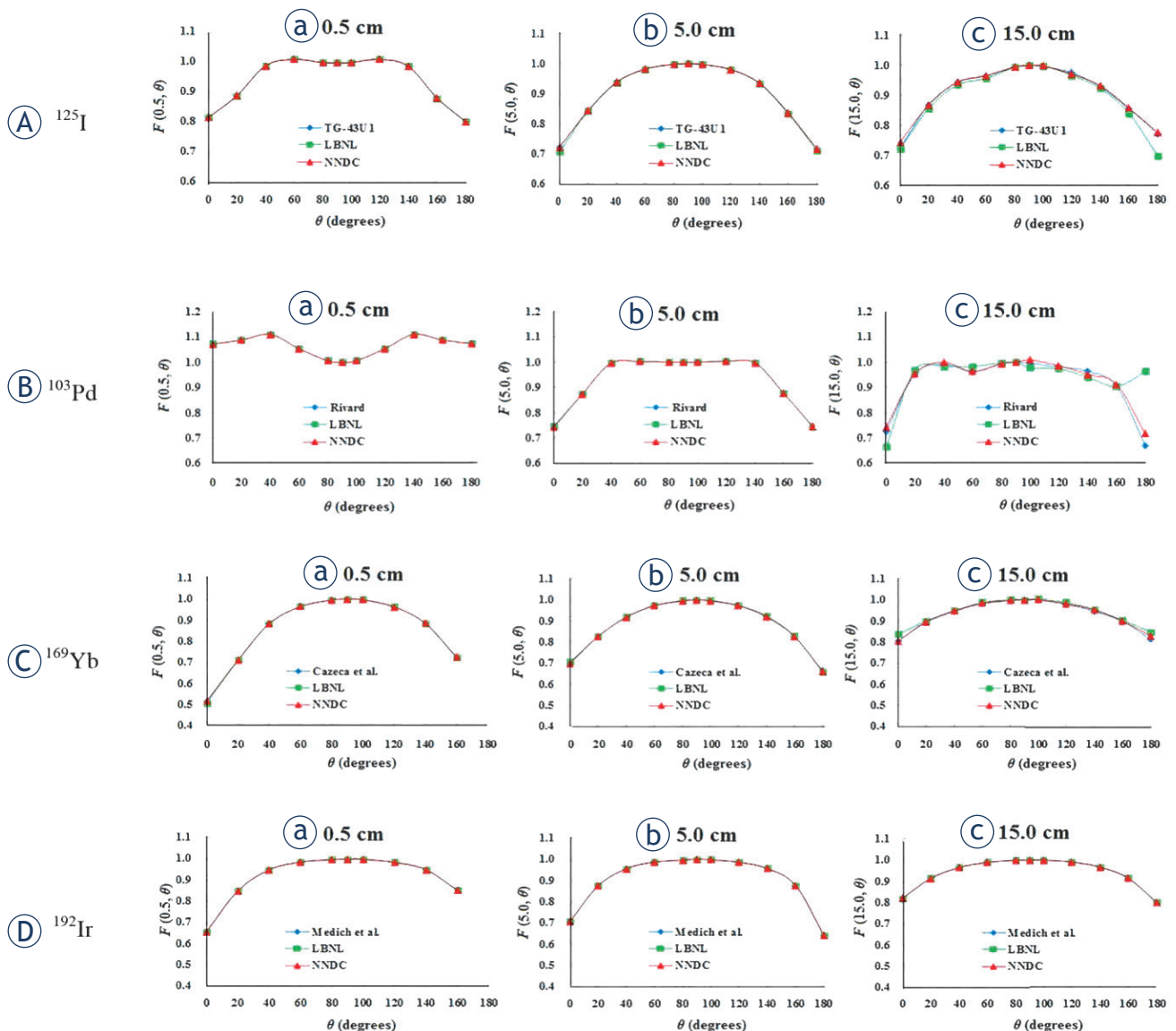


FIGURE 1. 2D anisotropy function values for (A) ^{125}I , (B) ^{103}Pd , (C) ^{169}Yb and (D) ^{192}Ir sources at $r = 0.5$ cm (a), 5.0 cm (b), and 15.0 cm (c) distances.

of F6 tally. The grid included $2 \times 2 \times 2$ mm³ and the obtained data was plotted in the Y-Z plane using MATLAB software (version: 8.3.0.532, The Mathworks, Inc., Natick, MA).¹⁵ The number of particles for ^{125}I , ^{169}Yb , and ^{192}Ir sources was 6×10^8 photons while it was 1.5×10^9 for the ^{103}Pd source. The type A statistical uncertainty in these mesh voxels was less than 6.5% in the output files.

The effect of photon energy spectrum

The effect of energy spectrum on dosimetric parameters of ^{125}I , ^{103}Pd , ^{169}Yb , and ^{192}Ir radionuclides was evaluated for three different spectra.

As the first spectrum and via a common method in brachytherapy Monte Carlo studies, the reported photon energy spectra by previous papers were used for the radionuclides.^{1,16-18} As the second spectrum database, Lawrence Berkeley National Laboratory (LBNL) was chosen.¹⁹ We applied version 2.1 (January 2004) for all radionuclides in the LBNL database. The third spectrum applied for each radionuclide was extracted from the National Nuclear Data Center (NNDC) database³ as it was suggested by the report of AAPM and ESTRO.² The NNDC database reports a number of energy spectra for a radionuclide. In the present study, these numbers of datasets were chosen from NNDC

TABLE 1. Information on photon energy spectra of the ^{125}I and ^{103}Pd , ^{169}Yb , and ^{192}Ir radionuclides reported by different databases

	^{125}I			^{103}Pd		
Reference	TG-43 U1 ¹	LBNL ¹⁹	NNDC ²⁰	Rivard ¹⁶	LBNL ¹⁹	NNDC ²¹
Energy range (keV)	27.202-35492	3.335-35.4919	3.77-35.4925	22.074-497.054	2.377-497.08	2.7-487.08
Total photons per disintegration	1.4757	1.60482	1.5767	0.7713825	0.851569801	0.857582605
Average energy (keV)	28.370	27.541	26.059	21.319	19.038	18.889
	^{169}Yb			^{192}Ir		
Reference	Cazeca <i>et al.</i> ¹⁷	LBNL ¹⁹	NNDC ²²	Medich and Munro ¹⁸	LBNL ¹⁹	NNDC ²³
Energy range (keV)	49.77-307.74	6.341-781.64	7.18-781.64	61.49-884.54	7.822-1378.3	9.44-1378.50
Total photons per disintegration	3.322	3.779	3.771	2.301	2.359	2.214
Average energy (keV)	92.797	82.622	82.781	354.356	346.736	369.525

LBNL = Lawrence Berkeley National Laboratory; NNDC = National Nuclear Data Center; TG-43 U1 = Recommendation of the American Association of Physicists in Medicine from task group No. 43 updated report

TABLE 2. Air kerma strength, dose rate constant, and dose rate at 1 cm for ^{125}I , ^{103}Pd , ^{169}Yb , and ^{192}Ir sources based on different photon energy spectra reported by other studies, LBNL, and NNDC databases

Source	Other studies ^{1, 16-18}	LBNL ¹⁹	NNDC ²⁰⁻²³	Diff. (%) Other study-NNDC	Diff. (%) LBNL-NNDC
^{125}I	1.035	1.169	1.121	-7.67	4.28
^{103}Pd	1.132	1.428	1.404	-19.37	1.71
^{169}Yb	1.094	1.094	1.097	-0.27	-0.27
^{192}Ir	3.622	3.631	3.496	3.60	3.86
Dose rate constant (cGy/hU)					
^{125}I	1.115	0.961	1.013	10.07	-5.13
^{103}Pd	0.830	0.658	0.669	24.06	-1.64
^{169}Yb	1.222	1.226	1.222	0.00	0.33
^{192}Ir	1.117	1.117	1.117	0.00	0.00
Dose rate at 1 cm (cGy/hmCi)					
^{125}I	1.154	1.123	1.136	1.60	-1.07
^{103}Pd	0.939	0.940	0.939	0.00	0.09
^{169}Yb	1.338	1.341	1.341	-0.23	0.00
^{192}Ir	4.045	4.054	3.904	3.59	3.84

LBNL = Lawrence Berkeley National Laboratory; NNDC = National Nuclear Data Center

database: dataset No. 1 for ^{125}I ²⁰, dataset No. 1 for ^{103}Pd ²¹, dataset No. 2 for ^{169}Yb ²² and dataset No. 4 for ^{192}Ir ²³ radionuclides.

The photon energy spectra of ^{125}I , ^{103}Pd , ^{169}Yb , and ^{192}Ir radionuclides reported by various databases are listed in Table 1. The photon energy spectra applied for the ^{125}I source are: AAPM TG-43 U1 report¹, LBNL database¹⁹, and NNDC database²⁰. For the ^{103}Pd source, the photon energy spectra reported by a study by Rivard¹⁶, LBNL database¹⁹,

and NNDC database²¹ were used. The photon energy spectra applied for the ^{169}Yb source are: the study by Cazeca *et al.*¹⁷, LBNL database²⁰, and NNDC database²². For the ^{192}Ir source, we extracted the photon energy spectra reported by Medich and Munro¹⁸, LBNL database¹⁹, and NNDC database²³.

In MCNPX code, the photon energy spectrum should be introduced for a source in terms of energies of photons (MeV) emitted by the radionuclide and their intensities. For the four sources, it was

TABLE 3. Radial dose function for ¹²⁵I, ¹⁰³Pd, ¹⁶⁹Yb, and ¹⁹²Ir sources based on different photon energy spectra reported by other studies^{1,16-18}, Lawrence Berkeley National Laboratory (LBNL)¹⁹, and National Nuclear Data Center (NNDC)²⁰⁻²³ databases

Source	r (cm)	Other studies (A)	LBNL (B)	NNDC (C)	Diff. (%) A-C	Diff. (%) B-C	Source	Other studies (A)	LBNL (B)	NNDC (C)	Diff. (%) A-C	Diff. (%) B-C
¹²⁵ I	0.5	0.996	0.996	0.996	0.00	0.00	¹⁰³ Pd	1.196	1.196	1.196	0.00	0.00
	1	1.000	1.000	1.000	0.00	0.00		1.000	1.000	1.000	0.00	0.00
	1.5	0.955	0.955	0.954	0.11	0.10		0.789	0.789	0.789	0.00	0.00
	2	0.890	0.890	0.890	0.00	0.00		0.609	0.609	0.608	0.16	0.16
	2.5	0.816	0.815	0.816	0.00	-0.12		0.465	0.465	0.464	0.22	0.22
	3	0.740	0.740	0.740	0.00	0.00		0.352	0.352	0.352	0.00	0.00
	3.5	0.667	0.666	0.667	0.00	-0.15		0.265	0.265	0.264	0.38	0.38
	4	0.596	0.596	0.595	0.17	0.17		0.199	0.199	0.198	0.50	0.51
	4.5	0.530	0.530	0.530	0.00	0.00		0.150	0.150	0.149	0.67	0.68
	5	0.470	0.469	0.470	0.00	-0.21		0.112	0.112	0.112	0.00	0.00
	5.5	0.415	0.415	0.415	0.00	0.00		0.084	0.084	0.083	1.20	1.21
	6	0.365	0.365	0.365	0.00	0.00		0.063	0.062	0.062	1.61	0.00
	6.5	0.320	0.319	0.319	0.31	0.00		0.047	0.047	0.047	0.00	0.00
	7	0.279	0.279	0.279	0.00	0.00		0.035	0.035	0.035	0.00	0.00
	10	0.120	0.120	0.120	0.00	0.00		0.0066	0.0066	0.0065	1.54	1.54
15	0.029	0.029	0.029	0.00	0.00	0.0010	0.0010	0.0010	0.00	0.00		
¹⁶⁹ Yb	0.5	0.950	0.949	0.951	-0.11	-0.21	¹⁹² Ir	0.996	0.996	0.996	0.00	0.00
	1	1.000	1.000	1.000	0.00	0.00		1.000	1.000	1.000	0.00	0.00
	1.5	1.042	1.041	1.041	0.10	0.00		1.003	1.003	1.003	0.00	0.00
	2	1.079	1.079	1.077	0.19	0.19		1.006	1.006	1.006	0.00	0.00
	2.5	1.113	1.111	1.110	0.27	0.09		1.008	1.008	1.008	0.00	0.00
	3	1.136	1.137	1.133	0.27	0.35		1.010	1.010	1.009	0.10	0.10
	3.5	1.157	1.156	1.155	0.17	0.09		1.011	1.011	1.010	0.10	0.01
	4	1.169	1.171	1.168	0.09	0.26		1.011	1.011	1.010	0.10	0.10
	4.5	1.183	1.181	1.180	0.25	0.09		1.010	1.010	1.010	0.00	0.00
	5	1.189	1.185	1.185	0.34	0.00		1.008	1.008	1.007	0.10	0.10
	5.5	1.193	1.191	1.191	0.17	0.00		1.005	1.005	1.005	0.00	0.00
	6	1.195	1.189	1.190	0.42	-0.08		1.002	1.002	1.001	0.10	0.10
	6.5	1.189	1.185	1.186	0.25	-0.08		0.998	0.998	0.998	0.00	0.00
	7	1.182	1.181	1.181	0.09	0.00		0.995	0.994	0.994	0.10	0.00
	10	1.089	1.091	1.090	-0.09	0.09		0.949	0.949	0.949	0.00	0.00
15	0.860	0.865	0.862	-0.23	0.35	0.836	0.836	0.835	0.12	0.12		

not feasible to list all the energies and the related probabilities in a single table or figure. Therefore, some information including the energy range, total intensity, and average energy are listed in Table 1.

TG-43 parameters were calculated for ¹²⁵I, ¹⁰³Pd, ¹⁶⁹Yb, and ¹⁹²Ir sources with three specific photon energy spectra to evaluate whether the photon energy spectrum effect the dosimetric parameters.

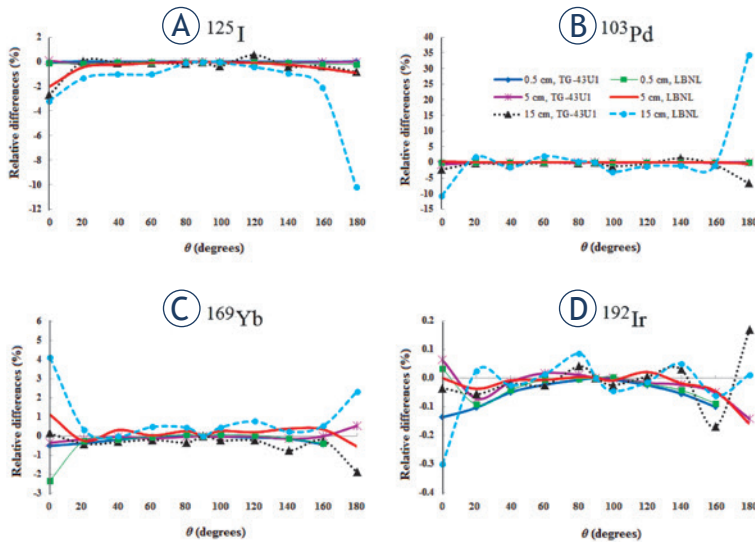


FIGURE 2. Percentage differences (%) between the 2D anisotropy function obtained from National Nuclear Data Center (NNDC) and other references of energy spectra for (A) ^{125}I , (B) ^{103}Pd , (C) ^{169}Yb , and (D) ^{192}Ir sources.

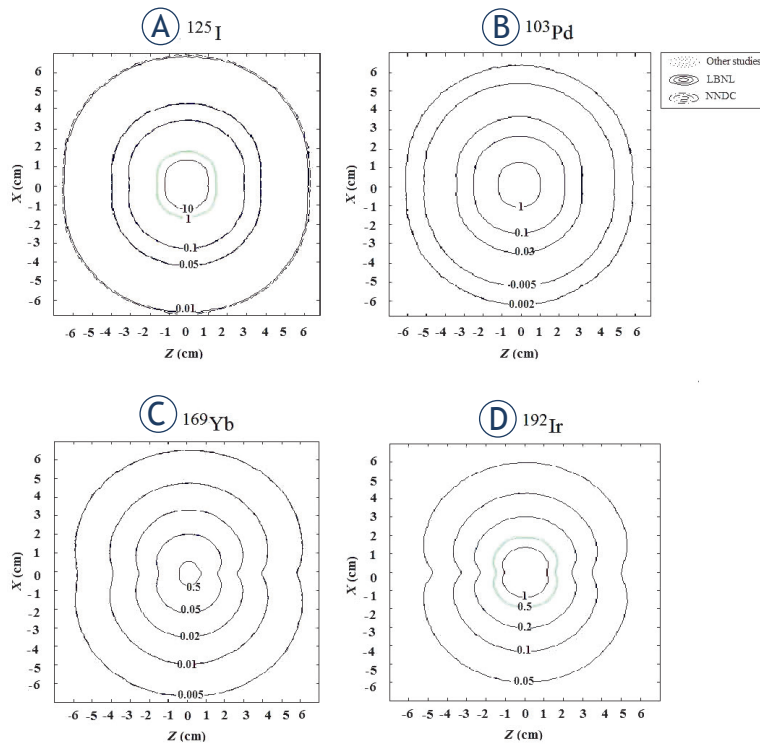


FIGURE 3. Isodose curves for (A) ^{125}I , (B) ^{103}Pd , (C) ^{169}Yb , and (D) ^{192}Ir sources obtained by different photon energy spectra. The contours for various spectra are not clearly distinguishable due to their overlapping.

Results

The values of air kerma strength per activity were calculated for MED 3631-A/M ^{125}I , Optiseed ^{103}Pd , a hypothetical ^{169}Yb , and Flexisource ^{192}Ir sources. These values are presented in Table 2 for three

photon energy spectra for each of these sources. Furthermore, dose rate constant and dose rate at $r = 1$ cm are presented in Table 2. The values of radial dose function at $r = 0.5$ – 15 cm with the three photon energy spectra for ^{125}I , ^{103}Pd , ^{169}Yb , and ^{192}Ir sources are listed in Table 3.

2D anisotropy function calculated at $\theta = 0^\circ$ – 180° angles for $r = 0.5$, 5 , and 15 cm distances for ^{125}I , ^{103}Pd , ^{169}Yb , and ^{192}Ir sources are illustrated in Figure 1. The differences between the anisotropy function data based on NNDC photon energy spectrum and the other spectra are shown in Figure 2. The isodose curves for ^{125}I , ^{103}Pd , ^{169}Yb , and ^{192}Ir sources based on different energy spectra reported by articles^{1,16–18}, LBNL¹⁹ and NNDC^{20–23} are contoured in Figure 3. In this figure the dose values are related to the values in the Z-X plane while the source's longitudinal axis is along the Z-axis. The dose values are normalized to the dose at $r = 1$ cm for each source.

Discussion

In the current study, the influence of photon energy spectrum on dosimetric parameters of ^{125}I , ^{103}Pd , ^{169}Yb , and ^{192}Ir brachytherapy sources was evaluated. Dose rate constant is the ratio of dose rate at 1 cm to air kerma strength. All these quantities are presented in Table 2 for the considered sources. The relative difference values of dose rate constant with regard to NNDC based data, shows a maximum value of 24.06% and 10.07% for the ^{103}Pd and ^{125}I brachytherapy sources, respectively (Table 2). These percentage differences are related to the photon energy spectra by TG-43 U1 protocol¹ and NNDC²⁰ database for the ^{125}I source; and LBNL¹⁹ and NNDC database²¹ for the ^{103}Pd source. There are non-negligible differences between the dose rate constant values obtained by different photon energy spectra databases for the ^{125}I and ^{103}Pd sources. Table 2 demonstrates that the cause of these differences is due to air kerma strengths. The effect for air kerma strength to the differences in total number of photons per disintegration (Table 1) and the differences in photon energy in various spectra demonstrate their main cause is air kerma strength. In other words, for calculation of air kerma strength the environment is void and minor differences in photon energy have a major effect on the kerma rate. This effect is not seen for dose rate at 1 cm in which the media is water.

The radial dose function calculated by different photon energy spectra does not show a consider-

able difference between brachytherapy sources. The differences do not show a general trend with distance. The minor effect of energy spectrum on radial dose function is in agreement with the results by Rivard *et al.*⁸ In that study, the effect of energy spectrum on dose rate constant and radial dose function ranged from 0.1% to 2%. The values of anisotropy function illustrated in Figure 1 show a similar trend for all applied photon energy spectra of brachytherapy sources. As illustrated in Figure 2, there are some points that a non-negligible difference is observable. This figure refers a larger difference at $\theta = 0^\circ$ and 180° at far distances from the ^{103}Pd , ^{125}I and ^{169}Yb sources, respectively. Furthermore, as it can be seen from the range of vertical axis of Figure 2, the difference of anisotropy function values with regard to the values calculated by NNDC spectra databases, ^{103}Pd , ^{125}I , and ^{169}Yb show the maximum differences. For the ^{103}Pd source, about 35% difference was observed between anisotropy function calculated based on the photon energy spectra reported by LBNL and NNDC databases. The reason for the differences in the 0° and 180° degrees for ^{103}Pd is related to the uncertainty in the Monte Carlo calculations (13.8%), therefore they may be independent of the effect of photon spectrum. In the current study no variance reduction method was applied except for energy cut offs. For future studies, it is suggested to apply such methods to reduce the statistical uncertainties, especially for the ^{103}Pd source.

As it is seen in Figure 3, there is no observable difference in isodose curves of ^{125}I , ^{103}Pd , ^{169}Yb , and ^{192}Ir sources with different photon energy spectra. However, this doesn't mean that the photon energy spectrum choice for a radionuclide doesn't affect dose distribution around the source. As it was implied from the obtained data of TG-43 dosimetric parameters, such as air kerma strength and dose rate constant values, this effect is not negligible. On the other hand, isodose contours cannot show such differences. Relying only on isodose curves for clinical application of brachytherapy sources may induce some errors in quantification of dose values.

For different photon energy spectra the calculated mean energies were in relatively good agreement for both LBNL and NNDC databases. A maximum of 24.06% difference was observed between dose rate constant of different energy databases. Ignoring the differences in the anisotropy function values at $\theta = 0^\circ$ and 180° degrees, especially for the ^{103}Pd source which originate from the Monte Carlo calculation uncertainties, there are minor differences in dosimetric parameters of the

studied sources for various energy spectrum references. Additionally no considerable difference was observed in isodose curves of different photon energy spectra. Generally it can be concluded that while these differences are not considerable, due the fact that the total uncertainty in dose delivery in radiotherapy should not exceed $\pm 5\%$ (ICRU report No. 24²⁴), it is recommended that more accurate and updated photon energy spectrum databases be used in Monte Carlo simulation and other radiotherapy applications of brachytherapy sources. This is to minimize the related uncertainties in clinical applications of the sources and is in accordance with the AAPM and ESTRO guideline on simulation of brachytherapy sources.²

Acknowledgment

The authors would like to thank Sabzevar University of Medical Sciences for financial support of this work.

References

- Rivard MJ, Coursey BM, DeWerd LA, Hanson WF, Huq MS, Ibbott GS, et al. Update of AAPM task group No. 43 report: a revised AAPM protocol for brachytherapy dose calculations. *Med Phys* 2004; **31**: 633-74.
- Perez-Calatayud J, Ballester F, Das RK, Dewerd LA, Ibbott GS, Meigooni AS, et al. Dose calculation for photon-emitting brachytherapy sources with average energy higher than 50 keV: Report of the AAPM and ESTRO. *Med Phys* 2012; **39**: 2904-29.
- National Nuclear Data Center (NNDC); 2007, Available at: <http://www.nndc.bnl.gov>. [Accessed 22 Jan 2016].
- Keillor ME, Aalseth CE, Day AR, Fast JE, Hoppe EW, Hyronimus BJ, et al. Design and construction of an ultra-low-background 14-crystal germanium array for high efficiency and coincidence measurements. *J Radioanal Nucl Chem* 2009; **282**: 703-8.
- Nedera H, Heussera G, Laubensteinb M. Low level γ -ray germanium-spectrometer to measure very low primordial radionuclide concentrations. *Appl Radiat Isotopes* 2000; **53**: 191-5.
- Karamanis D. Efficiency simulation of HPGe and Si (Li) detectors in γ - and X-ray spectroscopy. *Nucl Instr Meth Phys Res* 2003; **505**: 282-5.
- Chen Z, Bongiorno P, Nath R. Experimental characterization of the dosimetric properties of a newly designed I-Seed model AgX100 ^{125}I interstitial brachytherapy source. *Brachytherapy* 2012; **11**: 476-82.
- Rivard MJ, Granero D, Perez-Calatayud J, Ballester F. Influence of photon energy spectra from brachytherapy sources on Monte Carlo simulations of kerma and dose rates in water and air. *Med Phys* 2010; **37**: 869-76.
- Aryal P, Molloy JA, Rivard MJ. A modern Monte Carlo investigation of the TG-43 dosimetry parameters for an ^{125}I seed already having AAPM consensus data. *Med Phys* 2014; **41**: 021702.
- Luse RW, Blasko J, Grimm P. A method for implementing the American Association of Physicists in Medicine Task Group-43 dosimetry recommendations for ^{125}I transperineal prostate seed implants on commercial treatment planning systems. *Int J Radiat Oncol Biol Phys* 1997; **37**: 737-41.
- Waters LS. *MCNPX user's manual*. Version 2.4.0. Report LA-CP-02-408 (Los Alamos, New Mexico: Los Alamos National Laboratory; 2000.

12. Moghaddas TA, Ghorbani M, Haghparast A, Flynn RT, Eivazi MT. A Monte Carlo study on dose enhancement effect of various paramagnetic nanoshells in brachytherapy. *J Med Biol Eng* 2014; **34**: 559-67.
13. Gifford KA, Mourtada F, Cho SH, Lawyer A, Horton JL Jr. Monte Carlo calculations of the dose distribution around a commercial gynecologic tandem applicator. *Radiother Oncol* 2005; **77**: 210-5.
14. Bahreyni Toossi MT, Abdollahi M, Ghorbani M. A Monte Carlo study on dose distribution validation of GZP6 ⁶⁰Co stepping source. *Rep Pract Oncol Radiother* 2013; **18**: 112-6.
15. MathWorks Inc., Available at: <http://www.mathworks.com/matlabcentral/>. [Accessed 22 Jan 2016].
16. Rivard MJ. A discretized approach to determining TG-43 brachytherapy dosimetry parameters: case study using Monte Carlo calculations for the MED3633 ¹⁰³Pd source. *Appl Radiat Isotopes* 2001; **55**: 775-82.
17. Cazeca MJ, Medich DC, Munro JJ 3rd. Monte Carlo characterization of a new Yb-169 high dose rate source for brachytherapy application. *Med Phys* 2010; **37**: 1129-36.
18. Medich DC, Munro JJ 3rd. Monte Carlo characterization of the M-19 high dose rate Iridium-192 brachytherapy source. *Med Phys* 2007; **34**: 1999-2006.
19. LBNL Isotopes Project - LUNDS Universitet. Available at: <http://ie.lbl.gov/toi/index.asp>. [Accessed 22 Jan 2016].
20. National Nuclear Data Center (NNDC); 2007. Available at: <http://www.nndc.bnl.gov/chart/decaysearchdirect.jsp?nuc=125I&unc=nds>. [Accessed 22 Jan 2016].
21. National Nuclear Data Center (NNDC); 2007. Available at: <http://www.nndc.bnl.gov/chart/decaysearchdirect.jsp?nuc=103PD&unc=nds>. [Accessed 22 Jan 2016].
22. National Nuclear Data Center (NNDC); 2007, Available at (<http://www.nndc.bnl.gov/chart/decaysearchdirect.jsp?nuc=169YB&unc=nds>), [accessed at 22 January 2016].
23. National Nuclear Data Center (NNDC); 2007. Available at: <http://www.nndc.bnl.gov/chart/decaysearchdirect.jsp?nuc=192IR&unc=nds>. [Accessed 22 Jan 2016].
24. International Commission on Radiation Units and Measurements. *Determination of absorbed dose in a patient irradiated by beams of X or gamma rays in radiotherapy procedures*. Washington, Bethesda: ICRU; 1976. Report No: ICRU-24.

Radiol Oncol 2016; 50(2): 129-138.
doi:10.1515/raon-2015-0003

Sistemsko zdravljenje malignih gliomov

Mesti T, Ocvirk J

Izhodišča. Maligni gliomi so hitro napredujoči možganski tumorji z zelo izrazitimi znaki bolezni in visoko smrtnostjo. Do nedavna so bile možnosti njihovega zdravljenja omejene in enake za vse podtipe. Zdravili smo jih predvsem kirurško in z radioterapijo. Kemoterapijo smo uporabljali kot dopolnilno zdravljenje in ob ponovitvi bolezni; imela je precej omejeno učinkovitost.

Zaključki. Tudi danes je zdravljenje malignih gliomov multidisciplinarno ter vključuje kirurgijo, radioterapijo in kemoterapijo. Izbrano zdravljenje je bolj celovito in ga prilagajamo posamezniku. Vpliv na preživetje in kakovost življenja je opazno večji.

Radiol Oncol 2016; 50(2): 139-144.
doi:10.1515/raon-2015-0004

Zgodnja medicinska rehabilitacija po nevrokirurškem zdravljenju malignih možganskih tumorjev v Sloveniji

Kos N, Kos B, Benedičič M

Izhodišča. Število bolnikov z malignimi možganskimi tumorji je v porastu. Zaradi novih metod zdravljenja je preživetje daljše. Kljub daljšemu preživetju pa so posledice tumorja in zdravljenja pogosto hude in vplivajo na kakovost bolnikovega življenja. Ustrezna in dovolj zgodaj uvedena rehabilitacija predstavlja pomemben del obravnave bolnikov. Njen najpomembnejši cilj je preprečevanje zapletov, ki lahko imajo negativni vpliv na funkcijske sposobnosti bolnika

Zaključki. Z izvajanjem individualno prilagojenih postopkov zgodnje medicinske rehabilitacije je pogosto možno doseči bolnikovo samostojnost pri gibanju in opravljanju osnovnih dnevnih aktivnosti že pred odpustom iz bolnišnice. Potrebno je redno in natančno ocenjevanje bolnikov ob odpustu s ciljem ugotoviti, kateri bolniki poleg onkološkega zdravljenja potrebujejo tudi kompleksno rehabilitacijsko obravnavo. Pri teh bolnikih lahko z zgodnjo medicinsko rehabilitacijo povečamo možnost dobrega funkcijskega izida.

Radiol Oncol 2016; 50(2): 145-152.

doi:10.1515/raon-2016-0020

Ob presejanju ugotovljen duktalni rak *in situ*, odkrit pri stereotaktični vakuumski biopsiji sumljivih mikrokalcinacij brez tumorske formacije. Radiološko-histološka primerjava

Szynglarewicz B, Kasprzak P, Biecek P, Halon A, Matkowski R

Izhodišča. Mikrokalcinacije, ki jih običajno odkrijemo s presejalno mamografijo, so najpogostejši znak duktalnega raka *in situ* (DCIS). Cilj raziskave je bil ugotoviti povezavo med klinično-radiološkimi značilnostmi in histološkim rezultatom pri bolnicah z netipnim duktalnim rakom *in situ*.

Bolniki in metode. V raziskavo smo vključili 127 bolnic z netipnim duktalnim rakom *in situ*, odkritim s stereotaktično vakuumsko biopsijo sumljivih mikrokalcinacij brez tumorske formacije. Ugotavljali smo starost bolnikov, tip in razporeditev mikrokalcinacij, stopnjo malignosti in prisotnost komedonekroze. Naredili smo statistično analizo povezanosti posameznih dejavnikov; vrednost $P < 0,05$ smo upoštevali kot statistično značilno.

Rezultati. Mikrokalcinacije v obliki prahu (»powdery«) so bile najpogosteje razvrščene v skupine, medtem ko so bile intraduktalne polimorfne mikrokalcinacije (»casting-type«) običajno razporejene regionalno ($P < 0,001$). Visoka, srednja in nizka stopnja malignosti je bila najpogostejša pri intraduktalnih polimorfnih mikrokalcinacijah (»casting«), kalcinacijah v obliki lomljenega kamna (»crushed stone-like«) in mikrokalcinacijah v obliki prahu ($P < 0,01$). Duktalni rak *in situ* nizke in srednje stopnje malignosti je bil najpogostejši pri mikrokalcinacijah razvrščenih v skupine, medtem ko je bil duktalni rak *in situ* visoke stopnje malignosti najpogostejši pri regionalni razporeditvi mikrokalcinacij ($P < 0,05$). Komedonekroza je bila statistično značilno pogostejša pri duktalnem raku *in situ* visoke stopnje malignosti ($P < 0,01$). Povezava med komedonekrozo in tipom mikrokalcinacij ni bila statistično pomembna, povezava z njihovo razporeditvijo pa je bila blizu meje statistične značilnosti ($P = 0,07$). Povezava med starostjo bolnikov in slikovnimi ali histološkimi ugotovitvami ni bila statistično značilna.

Zaključki. Povezava med mamografskim izgledom mikrokalcinacij in histološkim rezultatom, ki jo pogosteje najdemo pri bolj agresivni bolezni, je lahko v pomoč pri optimalnem načrtovanju kirurgije pri bolnicah z netipnim duktalnim rakom *in situ* in sicer pri obsegu operacije in možnosti istočasne odstranitve varovalne bezgavke.

RadiolOncol 2016; 50(2): 153-158.

doi:10.1515/raon-2016-0022

Privzem ^{18}F -FET in ^{18}F -FCH v celicah humanega glioblastoma T98G

Persico MG, Buroni FE, Pasi F, Lodola L, Aprile C, Nano R, Hodolič M

Izhodišča. Kljub zdravljenju s kombinacijo operacije, obsevanja in kemoterapije se gliomi visoke stopnje malignosti pogosto ponovijo. Razlikovanje med spremembami po zdravljenju in ponovitvijo bolezni je težko. ^{18}F -metil-holin (^{18}F -FCH) pogosto uporabljamo za odkrivanje in določanje stadija bolezni pri ponavljajočih rakah prostate, kot tudi nekaterih možganskih tumorjih; vendar količina vnetja zmanjšuje specifičnost te preiskovalne metode. Maligne celice možganskih tumorjev pa, verjetno zaradi povečanega izražanja prenašalcev aminokislin ali zaradi prehajanja preko možgansko-krvne bariere, specifično privzemajo ^{18}F -etil-tirozin (^{18}F -FET). ^{18}F -FET se slabše izraža v makrofagih in drugih vnetnih celicah. Cilj naše raziskave je bil primerjati privzem ^{18}F -FCH in ^{18}F -FET v celični liniji humanega glioblastoma T98G.

Material in metode. Celicam humanega glioblastoma T98G in kožnim fibroblastomom gostote 2×10^5 , ki so rastle pritrjene na dnu gojitvene posode ob 37°C in 5% CO_2 smo dodali ekvimolarno količino radioaktivnih označevalcev ^{18}F -FCH oz. ^{18}F -FET in jih nato gojili od 20 do 120 minut. Količino privzetega radioaktivnega označevalca v celicah smo določili s števcem gama. Vse poskuse smo izvedli v dvojniku in jih ponovili trikrat. Rezultate privzema radioaktivnega označevalca smo izrazili kot odstotek doze označevalca na 2×10^5 celic. Rezultate izražene kot povprečne vrednosti v odstotkih privzema smo analizirali z uporabo parametričnih ali neparametričnih testov, za značilne so veljale vrednosti $p < 0,05$.

Rezultati. Rezultati so pokazali statistično značilne razlike v privzemu ^{18}F -FCH v celicah T98G po 60, 90 in 120 minutah. Privzem ^{18}F -FET je bil v primerjavi s privzemom ^{18}F -FCH ob različni farmakokinetični krivulji nižji za več kot trikrat. Privzem ^{18}F -FET je pokazal hitrejši začetni privzem z največjimi vrednostmi do 40 minut, medtem ko je bil pri ^{18}F -FCH viden postopen dvig z najvišjimi vrednostmi po 90 minutah.

Zaključki. ^{18}F -FCH in ^{18}F -FET sta primerna za nevroonkološko slikanje PET. Uporabnost ^{18}F -FET kot onkološkega označevalca PET je zlasti velika ob prisotnosti sprememb po zdravljenju, saj je zaradi večje afinitete vnetnih celic za ^{18}F -FCH težko razlikovati med ostanki tumorja in nerakastimi spremembami. Potrebne so dodatne raziskave o vplivu vnetnih tkiv in nekroze na radiofarmakološki privzem obeh označevalcev.

Radiol Oncol 2016; 50(2): 159-167.

doi:10.1515/raon-2016-0017

Vizualizacija celic človeškega glioblastoma in njihovih interakcij z mezenhimskimi matičnimi celicami v možganih zarodkov cebric (*Danio rerio*)

Vittori M, Breznik B, Gredar T, Hrovat K, Bizjak Mali L, Lah TT

Izhodišča. Novo zanimivo proučevanje raka pri človeku je uporaba prosojnih zarodkov rib cebric, ki omogoča opazovanje napredovanja raka v živih živalih.

Materiali in metode. Mešanice fluorescentno označenih celic glioblastoma in mezenhimskih matičnih celic smo vsadili v zarodke rib cebric, da bi preučevali njihove poti celične invazije in interakcije med tema dvema vrstama celic *in vivo*.

Rezultati. Razvili smo protokol bistrenja tkiv, ki je kompatibilen z uporabo karbocianinskih barvil, ker je omogočil mikroskopijsko fluorescentno označenih celic globoko v tkivih. Na ta način smo pokazali, da sta tako glioblastomska celična linija U87 kot tudi U373 hitro agregirali v tumorsko maso v ventriklih in hemisferah srednjih možganov, od koder sta se širili predvsem preko ventriklov in osrednjega kanala hrbtnjače, vendar pri tem celice glioblastoma niso zapustile osrednjega živčevja. Ko smo v možgane vnesli različno označene glioblastomske celice skupaj z mezenhimskimi matičnimi celicami, so se v možganih rib oblikovali mešani tumorji. Med glioblastomskimi celicami in mezenhimskimi matičnimi celicami smo opazili tesne povezave in tudi fuzije različnih vrst celic. Glioblastomske celice in mezenhimske matične celice so v osrednje živčevje invadirale po podobnih poteh.

Zaključki. Ta preprost model lahko uporabimo za proučevanje molekularnih poti v celičnih procesih pri invaziji glioblastomskih celic in njihovih interakcijah z različnimi celicami strome v dvojnih ali trojnih sokulturah. To lahko vodi k razvoju novih celičnih terapij glioblastoma z uporabo mezenhimskih matičnih celic kot celičnih vektorjev.

Radiol Oncol 2016; 50(2): 168-174.

doi:10.1515/raon-2016-0010

Identifikacija diferencialno izraženih genov povezanih s povečanjem občutljivosti na rentgenske žarke z RITA na celični liniji ploščatoceličnega raka ustnega žrela (FaDu)

Luan J, Li X, Guo R, Liu S, Luo H, You Q

Izhodišča. Za raziskovanje mehanizma reaktivacije p53 in indukcije apoptoze tumorskih celic (RITA), ki poveča občutljivost celic FaDu na rentgenske žarke, smo uporabili sekvenciranje nove generacije in bioinformatično analizo.

Materiali in metode. Molekule cDNA smo izolirali iz celic FaDu, ki smo jih izpostavili obsevanju z 0 Gy, 8 Gy ali 8 Gy + RITA. Nato smo pripravili cDNA knjižnice in jih sekvencirali s sekvenciranjem nove generacije. Poskus smo ponovili dvakrat. Nato smo ugotavljali diferencialno izražene gene (DEG) s pomočjo algoritma *Cuffdiff* v *Cufflinks* in njihove funkcije napovedali z obogatitveno analizo različnih poti. Gene, ki so bili stalno povečano ali zmanjšano izraženi pri celicah FaDu, izpostavljenih obsevanju z 8 Gy ali 8 Gy + RITA, smo vzeli za gene RITA. Nato smo določili interakcije protein-protein (PPI) z bazo podatkov STRING in zgradili njihovo mrežo s Cytoscape programom. Za obogatitveno analizo za gene v mreži PPI smo uporabili algoritem ClueGO.

Rezultati. V celicah FaDu izpostavljenih obsevanju z 8 Gy smo ugotovili 2040 DEG, v celicah FaDu izpostavljenih obsevanju z 8 Gy + RITA pa 297. Pri popravljanju z izrezovanjem baz sta bil najbolj obogatena gena *PARP3* in *NEIL1*, pri signalni poti p53 pa smo *CDK1*, *RFC2* in *EZH2* prepoznali kot gene RITA. V mreži PPI smo ugotovili več interakcij med proteini (*RFC2*-*CDK1*, *EZH2*-*CDK1* in *PARP3*-*EZH2*). Z analizo ClueGO smo pokazali, da sta *RFC2* in *EZH2* povezana s celičnim ciklom.

Zaključki. *RFC2*, *EZH2*, *CDK1*, *PARP3* in *NEIL1* so verjetno med seboj povezani in skupaj povečajo občutljivost celic FaDu, ki smo ji izpostavili RITA, na škodljive vplive rentgenskih žarkov.

Radiol Oncol 2016; 50(2): 175-187.

doi:10.1515/raon-2016-0018

Magnetnoresonančna mikroskopija difuzijskega tenzorja tkiv z nizko difuzijsko anizotropijo

Bajd F, Mattea C, Stapf S, Serša I

Izhodišča. Magnetnoresonančno slikanje difuzijskega tenzorja izkorišča preferenčne smeri difuzijskega gibanja vodnih molekul v opazovanem tkivu za oceno stopnje strukturne anizotropije tkiva. Vendar je izračun difuzijskega tenzorja močno obremenjen z mersko napako, ki ima izvor v instrumentalnem šumu. V raziskavi smo analizirali številne dejavnike, ki vplivajo na točnost izračuna difuzijskega tenzorja.

Materiali in metode. Proučili smo učinke razmerja signal-šum in konfiguracije uporabljenih difuzijskih gradientov na točnost določitve frakcijske anizotropije z uporabo numeričnih simulacij. Rezultate simulacije smo preverili tudi z magnetnoresonančno mikroskopijo difuzijskega tenzorja izotropnega vodnega vzorca in strukturno neizotropnega vzorca govejega sklepnega hrustanca *ex vivo*.

Rezultati. Tako v rezultatih simulacije kot tudi v poskusih smo s pomočjo uporabe multivariatne linearne regresije dobili precejšnje vrednosti frakcijske anizotropije za majhne vrednosti razmerja med signalom in šumom ter pri majhnem številu smeri difuzijskih gradientov.

Zaključki. Povečanje frakcijske anizotropije zaradi neugodnih eksperimentalnih pogojev je mogoče zmanjšati z uporabo večjega števila smeri difuzijskih gradientov, kakor tudi z zmanjšanjem pogojnega števila difuzijske transformacijske matrike. To je zlasti pomembno pri magnetnoresonančni mikroskopiji, kjer uporabljamo močne slikovne gradientne in je razmerje med signalom in šumom običajno nizko.

Radiol Oncol 2016; 50(2): 188-196.
doi:10.1515/raon-2015-0027

Prognostična vloga izražanja mRNA *SOX2*, *NANOG* in *OCT4* v celotni krvi pri napredovalem drobnoceličnem pljučnem raku

Sodja E, Rijavec M, Koren A, Sadikov A, Korošec P, Čufer T

Izhodišča. Izražanje in klinični vpliv označevalcev rakavih matičnih celic *SOX2*, *NANOG* in *OCT4* pri pljučnem raku še vedno nista znana. Namen raziskave je bil primerjati ravni izražanja mRNA *SOX2*, *NANOG* in *OCT4* v celotni krvi med bolniki z napredovalim drobnoceličnim pljučnim rakom in zdravimi posamezniki ter povezati njihovo izražanje s preživetjem brez napredovanja bolezni po prvem redu kemoterapije in s celokupnim preživetjem pri bolnikih z napredovalo obliko drobnoceličnega pljučnega raka.

Bolniki in metode. Prospektivno smo vključili 50 bolnikov z napredovalim drobnoceličnim pljučnim rakom, ki smo jih v letih med 2009 in 2013 zdravili s kemoterapijo v Univerzitetni bolnišnici Golnik. Raven izražanja *SOX2*, *NANOG* in *OCT4* smo določili s kvantitativnim testom RT-PCR in tehnologijo TaqMan v vzorcih celotne krvi, odvzetih pred začetkom zdravljenja. Za primerjavo smo testirali tudi vzorce celokupne krvi 34 zdravih posameznikov.

Rezultati. Raven izražanja *SOX2* je bila statistično značilno višja v celotni krvi bolnikov z drobnoceličnim pljučnim rakom v primerjavi z zdravimi posamezniki ($p = 0,006$). Prav tako smo opazili statistično značilno povezavo med izražanjem *SOX2* in številom oddaljenih metastatskih mest ($p = 0,027$). Bolniki s povišano ravno izražanja *SOX2* so imeli krajše celokupno preživetje ($p = 0,017$) in krajše preživetje brez napredovanja bolezni ($p = 0,046$). V multivariatni analizi Cox smo potrdili neodvisno vlogo izražanja *SOX2* za celokupno preživetje ($p = 0,002$). V primerjavi ravni izražanja *NANOG* in *OCT4* med bolniki z drobnoceličnim pljučnim rakom in zdravimi posamezniki nismo opazili statistično značilnih razlik, prav tako za oba omenjena označevalca nismo opazili statistično pomembnih povezav v analizi preživetja bolnikov z drobnoceličnim pljučnim rakom.

Zaključki. Izražanje *SOX2* v celotni krvi je obetaven neinvaziven označevalac za molekularno presejanje drobnoceličnega pljučnega raka in pomemben napovedni označevalac pri bolnikih z napredovalim drobnoceličnim pljučnim rakom zdravljenih s kemoterapijo, kar nakazuje pomembno vlogo regulatorjev rakavih matičnih celic pri širjenju raka. Potrebne so dodatne raziskave, ki bi ovrednotile izražanje *SOX2* kot potencialnega presejalnega/napovednega označevalca in terapevtsko tarčo pri drobnoceličnem pljučnem raku.

Radiol Oncol 2016; 50(2): 197-203.

doi:10.1515/raon-2016-0002

Vstavljanje Tenckhoffovega tunelskega peritonealnega katetra pri paliativnem zdravljenju malignega ascitesa. Tehnični rezultati in skupni klinični izid

Maleux G, Indesteege I, Laenen A, Verslype C, Vergote I, Prenen H

Izhodišča. Namen raziskave je bil ovrednotiti tehnični in klinični izid perkutanega vstavljanja tunelskega peritonealnega katetra pri paliativnem zdravljenju neodzivnega malignega ascitesa ter določiti varnost in izvedljivost intraperitonealne uporabe citostatikov skozi tunelski kateter.

Bolniki in metode. V raziskavo smo vključili zaporedno zdravljene bolnice, ki smo jim s tunelskim peritonealnim katetrom drenirali maligni ascites. Podatke o zdravljenju, klinično sledenje, vključno z zapleti in predvidenim preživetjem smo ugotavljali pri vsaki bolnici. Poleg tega smo opravili analizo pri tistih bolnicah, ki so imele razširjeni rak jajčnikov in smo jih ali pa ne zdravili z intraperitonealno aplikacijo citostatikov.

Rezultati. Pri vseh 94 bolnicah je bilo tehnično možno izvesti vstavev peritonealnega katetra in skozi kateter se je izločilo 3260 cm³ srednje vrednosti (razpon 100–850 cm³) malignega ascitesa. Zapleti po postopku so predstavljali infekcijo katetra (n = 2; 2 %), uhajanje tekočine okoli mesta vstavitve (n = 4; 4 %), zaporo katetra (n = 2; 2 %), nastanek rokava okoli konice katetra (n = 1; 1 %) in nenamerno izgubo katetra (n = 1; 1 %). Pri bolnicah, ki so bile ali pa ne zdravljene z intraperitonealno aplikacijo citostatikov ni bilo povečanega tveganja za infekcijo katetra. Srednja vrednost celokupnega preživetja po vstavitvi katetra je bila 1,7 meseca.

Zaključki. Perkutano vstavljanje Tenckhoffovega tunelskega katetra za paliativno odstranjevanje malignega ascitesa in intraperitonealna infuzija citostatikov je izvedljiva metoda, ki je povezana z zelo nizko stopnjo zapletov, vključno z infekcijami katetra. Tunelski katetri so koristni pri simptomatskem paliativnem zdravljenju neodzivnih ascitesov in omogočajo varno intra-peritonealno kemoterapijo.

Radiol Oncol 2016; 50(2): 204-211.

doi:10.1515/raon-2015-0025

Serumski nivo CA19-9 napoveduje mikrometastaze pri bolnikih z rakom želodca

Jagrič T, Potrč S, Miš K, Plankl M, Marš T

Izhodišča. Namen raziskave je bil ugotoviti, ali lahko povišan nivo karbohidratnega antigena 19-9 (CA19-9) napoveduje mikrometastaze pri bolnikih z želodčnim rakom in negativnimi bezgavkami.

Bolniki in metode. Mikrometastaze smo določili s kvantitativno reverzno transkripcijsko polimerazno verižno reakcijo (RT-qPCR) pri 30 bolnikih z želodčnim rakom in negativnimi bezgavkami. Skupina je določala mejne vrednosti predoperativnega serumskega nivoja antigena CA19-9 kot nadomestnega pokazatelja za mikrometastaze. Nato smo pri 187 bolnikih z želodčnim rakom stadija T1 do T4 in N0 preverili napovedno vrednost antigena CA19-9 za mikrometastaze.

Rezultati. Bolniki z mikrometastazami so imeli značilno višje predoperativne vrednosti CA19-9 v serumu v primerjavi z bolniki brez mikrometastaz (p = 0,046). Serumski nivo CA19-9 je bil soodvisen z lokacijo tumorja, njegovim premerom in perinevralno invazijo. Čeprav razlika ni bila statistično značilna, je bilo petletno preživetje bolnikov s serumskimi vrednostmi CA19-9 pod mejno vrednostjo boljše v primerjavi z bolniki, ki so imeli vrednosti CA19-9 nad mejno vrednostjo. Kumulativno preživetje bolnikov stadija T2 do T4 in N0 je bilo značilno boljše pri tistih bolnikih, ki so imeli serumske vrednosti CA19-9 pod mejnimi vrednostmi (p = 0,04).

Zaključki. Predoperativni serumski nivo CA19-9 kaže na visoko tveganje za nastanek hematogene razširitve in mikrometastaz pri bolnikih z želodčnim karcinomom z negativnimi bezgavkami. Vendar pa ugotavljanje serumskega nivoja CA19-9 nima dovolj visoke občutljivosti in specifičnosti, da bi zanesljivo napovedoval mikrometastaze.

Radiol Oncol 2016; 50(2): 212-217.
doi:10.2478/raon-2014-0040

Jetrna splenoza pri bolniku z anamnezo nezrelega teratoma v otroštvu, ki na videz posnema jetrne zasevke

Jereb S, Trotovšek B, Škrbinc B

Izhodišča. Jetrna splenoza je prisotnost vsadkov normalnega vraničnega tkiva v jetrnem parenhimu. Je redka in nastane po splenektomiji ali poškodbi vranice. Predvsem pri bolnikih z anamnezo malignega obolenja jo lahko zmotno ocenimo kot zasevke, kar vodi v nepotrebne diagnostične postopke in neustrezno zdravljenje.

Prikaz primera. 22-letnega bolnika so po rojstvu operativno zdravili zaradi nezrelega teratoma, povezanega z nespuščenim desnim testisom. Na rednih kontrolnih pregledih onkologi niso ugotavljali ponovitve bolezni ali dolgotrajnih posledic. Zaradi suma na levostransko dimeljsko kilo so naredili elektivni operativni poseg, tvorbo v kilni vreči pa so histološko opredelili kot policističen zrel teratom. Ocenili so, da so odstranili zasevek teratoma iz otroštva. Origo bolezni v preostalem, levem testisu niso našli. Slikovne diagnostične metode, opravljene v nadaljevanju, so pokazale prisotnost jetrnih sprememb, ki so bile radiološko sumljive za zasevke. Naredili so dve ultrazvočno vodeni tankoigelnji aspiracijski biopsiji omenjenih sprememb, ki nista bili diagnostični. Laparoskopsko pridobljen histološki vzorec sumljivega tkiva je pokazal normalno vranično tkivo. Tako so potrdili diagnozo jetrne splenoze.

Zaključki. Kljub temu, da je jetrna splenoza redek pojav, jo moramo vključiti med diferencialne diagnoze nodularnih jetrnih sprememb. Njihova natančna opredelitev je ključnega pomena za ustrezno obravnavo bolnika. Če citološka punkcija ne da ustreznega odgovora, je pred obsežnejšo jetrno resekcijo laparoskopka ekscizija nodularne spremembe najboljša rešitev.

Radiol Oncol 2016; 50(2): 218-225.
doi:10.1515/raon-2016-0001

Zdravljenje raka nosnega žrela s sočasnim moduliranim in pospešenim obsevanjem s helično tomoterapijo. Raziskava II. faze

Du L, Zhang XX, Feng LC, Chen J, Yang J, Liu HX, Xu SP, Xie CB, Ma L

Izhodišča. Namen raziskave je bil oceniti kratkoročno varnost in učinkovitost sočasnega moduliranega in pospešenega obsevanja (SMART) s helično tomoterapijo pri bolnikih z rakom nosnega žrela.

Metode. V prospektivno raziskavo II. faze smo med avgustom 2011 in septembrom 2013 vključili 132 novoodkritih bolnikov z rakom nosnega žrela. Predpisane doze na volumen primarnega tumorja (pGTV_{nx}) in prizadete bezgavke (pGTV_{nd}), na planirni tarčni volumen visokega tveganja (PTV1) in planirni tarčni volumen nizkega tveganja (PTV2) so bile 67,5 Gy (2,25 Gy/frakcijo), 60 Gy (2,0 Gy/frakcijo) in 54 Gy (1,8 Gy/frakcijo). Akutne neželene učinke smo ocenili z uveljavljenimi kriteriji RTOG/EORTC. To skupino bolnikov smo primerjali z 190 bolniki iz retrospektivne raziskave P70, ki smo jih zdravili med septembrom 2004 in avgustom 2009 s helično tomoterapijo in dozo na pGTV_{nx} in pGTV_{nd} 70–74 Gy/33 frakcij/v 6,5 tednih.

Rezultati. Srednji čas spremljanja je bil 23,7 (12–38) mesecev. Akutni, z obsevanjem povezani stranski učinki so bili poglavitna težava in smo jih ocenili s stopnjo 1 ali 2. Le manjše število bolnikov je imelo levkopenijo (4,5 %) ali trombocitopenijo (2,3 %) stopnje 4. Preživetje brez lokalne ponovitve (LRFS), preživetje brez področne ponovitve (NRFS), preživetje brez lokalne in področne ponovitve (LNRFS), preživetje brez oddaljenih zasevkov (DMFS) in celokupno preživetje (OS) je bilo po dveh letih sledenja 96,7 %, 95,5 %, 92,2 %, 92,7 % in 93,2 % ter brez pomembnih razlik glede na raziskavo P70.

Zaključki. Dosedanji rezultati kažejo, da ima pri bolnikih z rakom nosnega žrela SMART s helično tomoterapevtsko tehniko sprejemljivo akutno toksičnost in ugoden kratkoročen izid zdravljenja. Kasno toksičnost in preživetje bolnikov še ugotavljamo.

Bevacizumab s kemoterapijo pri starejših bolnikih s predhodno nezdravljenim metastatskim rakom debelega črevesa in danke. Izkušnje posamičnega centra

Ocvirk J, Maja Ebert Moltara M, Mesti T, Boc M, Reberšek M, Volk N, Benedik J, Hlebanja Z

Izhodišča. Metastatski rak debelega črevesa in danke je predvsem bolezen starejših. Geriatrična populacija pa je premalo zastopana v kliničnih raziskavah. Registri bolnikov predstavljajo orodje za ocenjevanje in sledenje rezultatov zdravljenja tudi pri tej populaciji bolnikov. Namen raziskave je bil s pomočjo registra bolnikov ugotoviti varnost in učinkovitost zdravljenja z bevacizumabom in kemoterapijo pri starejših bolnikih, ki so imeli predhodno nezdravljen rak debelega črevesa in danke.

Bolniki in metode. Register bolnikov z metastatskim rakom debelega črevesa in danke smo zasnovali zaradi prospektivnega ocenjevanja varnosti in učinkovitosti kemoterapije in bevacizumaba. Z njim smo tudi ugotavljali izbor bolnikov za takšno zdravljenje v vsakodnevni klinični praksi. Zbirali in ovrednotili smo osnovne klinične značilnosti bolnikov, vnaprej opredeljene neželene dogodke, povezane z bevacizumabom, in podatke o učinkovitosti zdravljenja ter naredili primerjavo glede na starostne kategorije.

Rezultati. Od januarja 2008 do decembra 2010 smo 210 bolnikov z metastatskim rakom debelega črevesa in danke (srednja starost 63, moški 61,4 %) začeli zdraviti z bevacizumabom. To je bilo njihovo prvo zdravljenje. Večina bolnikov je prejela ob bevacizumabu kemoterapijo prvega reda, ki je temeljila na irinotekanu (68 %), 105 bolnikov (50 %) pa je prejelo vzdrževalno zdravljenje z bevacizumabom. Starejših (≥ 70 let) bolnikov je bilo 22,9 % in so imeli slabše stanje zmogljivosti (PS 1–2 v 62,4%) kot bolniki v skupini <70 let (PS 1–2 v 35,8 %). Ugotovili smo razliko v deležu nadzora bolezni, ki smo jo pripisali nezmožnosti ocenitve odziva na zdravljenje pri skupini starejših bolnikov (64,6 % pri starejših in 77,8 % v skupini < 70 let, $p = 0,066$). Srednje preživetje brez napredovanja bolezni je bilo 10,2 (95% interval zaupanja [CI] 6,7–16,2) mesecev pri starejših in 11,3 (95% CI 10,2–12,6) v skupini < 70 let ($p = 0,58$). Srednje celokupno preživetje je bilo 18,5 (95% CI 12,4–28,9) mesecev za starejše in 27,4 (95% CI 22,7–31,9) za skupino < 70 let ($p = 0,03$). Triletno preživetje je bilo 26 % pri starejših in 37,6 % pri skupini < 70 let ($p = 0,03$). Stopnje neželenih učinkov, povezanih z bevacizumabom je bila v obeh skupinah podobna: proteinurija 21 % pri starejših vs. 22 % pri skupini < 70 let, hipertenzija 25 vs. 19 %, krvavitev 2 vs. 4% in tromboembolični dogodki 10 vs 6%.

Zaključki. Kombinacija bevacizumaba in kemoterapije, ki jo uporabljamo v vsakodnevni klinični praksi, je učinkovita in jo starejši bolniki z metastatskim rakom debelega črevesa in danke dobro prenašajo.

Radiol Oncol 2016; 50(2): 232-237.
doi:10.1515/raon-2016-0012

Dozimetrični pomen uporabe fotonov 10 MV pri obsevanju prostatične lože po prostatektomiji z volumetrično modulirano ločno terapijo (VMAT)

Kleiner H, Podgorsak M

Izhodišča. Namen raziskave je bil analiza dozimetričnih razlik ob uporabi 10 MV namesto 6 MV obsevalnih načrtov VMAT pri obsevanju prostatične lože po prostatektomiji.

Metode. Pri desetih primerih obsevanja prostatične lože po prostatektomiji, ki smo jih predhodno že zdravili s 6 MV VMAT, smo ponovno naredili obsevalni načrti za obsevanje z 10 MV VMAT. Predpisana doza je bila 66,6 Gy, razdeljena v 37 dnevni odmerkov po 1,8 Gy. Za načrtovanje s 6 MV in 10 MV smo uporabili enak nabor struktur, število lokov, velikost polj in minimalno dozo na planini tarčni volumen (PTV). Zbrali smo dozimetrične rezultate za rizične organe, doze na tarčne strukture, število monitorskih enot za vsak lok, odstotek volumna, ki je prejel 5 Gy ($Body V_5$), konformnostni indeks in integralno dozo. Za primerjavo rezultatov obsevanja 6 MV in 10 MV smo uporabili povprečne vrednosti. Za ugotavljanje statističnega pomena rezultatov pa smo uporabili parni Studentov t test.

Rezultati. Statistično pomembno nižje povprečne vrednosti smo ugotovili za rizične organe: danko, klinični tarčni volumen, ki je zajemal mehur, levo glavico stegenice in desno glavico stegenice. Statistično pomembno nižje povprečne vrednosti smo ugotovili tudi za $Body V_5$, konformnostni indeks in integralno dozo.

Zaključki. Pri uporabi obsevalnih načrtov VMAT 10 MV namesto 6 MV smo ugotovili več dozimetričnih prednosti. Te so vključevale obvarovanje rizičnih organov pred višjo dozo, pri čemer smo ohranili dozo na PTV. Ostale prednosti so se nanašale na $Body V_5$, konformnostni indeks in integralno dozo.

Radiol Oncol 2016; 50(2): 238-246.
doi:10.1515/raon-2016-0019

Vpliv spektra fotonovskih energij na dozimetrične lastnosti brahiterapevtskih virov

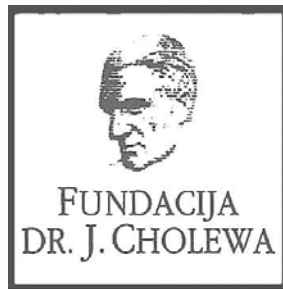
Ghorbani M, Mohammad M, David D, Ahmadi Moghaddas T

Izhodišča. Namen raziskave je bil kvantitativno opredeliti vpliv fotonovskega energijskega spektra brahiterapevtskih virov na parametre dozimetričnega sistema TG-43. Za posamezne radionuklide v simulacijah Monte Carlo namreč uporabljamo različne fotonovske energijske spektre.

Materiali in metode. Za numerično simulacijo brahiterapevtskih virov ^{125}I , ^{103}Pd , ^{169}Yb in ^{192}Ir smo uporabili kodo MCNPX. Tako smo izračunali: moč vira glede na aktivnost, konstanto hitrosti doze, funkcijo radialne doze in dvodimenzionalno (2D) anizotropijsko funkcijo. Izodozne krivulje smo izrisali za tri različne fotonovske energijske spektre. Pri izračunu spektrov fotonovskih energij smo upoštevali: objavljene članke, Nacionalni laboratorij Lawrence Berkeley (NBNL) in Nacionalni center za nuklearne podatke (NNDC). Podatke, ki smo jih izračunali s pomočjo teh spektrov fotonovskih energij smo primerjali med seboj.

Rezultati. Največja razlika med vrednostmi konstant hitrosti doze je bila 24,07 % pri viru ^{103}Pd z različnimi spektri fotonovskih energij. Vrednosti funkcije radialne doze so bile dokaj podobne po različnih spektrih. Vrednosti funkcije 2D anizotropije so pokazale le majhne razlike pri večini razdalj in kotov. Med izodzoznimi krivuljami nismo ugotovili nobene opazne razlike.

Zaključki. Dozimetrični parametri, dobljeni z različnimi fotonovskimi spektri, so si podobni. Vseeno priporočamo za simulacije Monte Carlo uporabo bolj natančnih in posodobljenih spektrov fotonovskih energij. To bi omogočilo zanesljivejše dozimetrične podatke pri modeliranih virov in izračunavanjih v brahiterapevtskih načrtovalnih sistemih.



FUNDACIJA "DOCENT DR. J. CHOLEWA"
JE NEPROFITNO, NEINSTITUCIONALNO IN NESTRANKARSKO
ZDRUŽENJE POSAMEZNIKOV, USTANOV IN ORGANIZACIJ, KI ŽELIJO
MATERIALNO SPODBUJATI IN POGLABLJATI RAZISKOVALNO
IN IZOBRAŽEVALNO DEJAVNOST V ONKOLOGIJI.

FUNDACIJA »DOCENT DR. JOSIP CHOLEWA« V SODELOVANJU Z
MEDICINSKO FAKULTETO LJUBLJANA, MEDICINSKO FAKULTETO MARIBOR,
UNIVERZITETNIM KLINIČNIM CENTROM LJUBLJANA, UNIVERZITETNIM
KLINIČNIM CENTROM MARIBOR IN ONKOLOŠKIM INŠTITUTOM LJUBLJANA

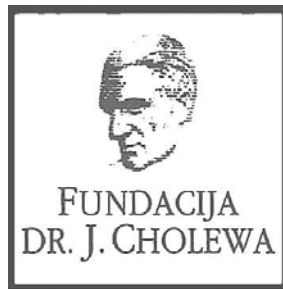
PRIREJA STROKOVNI SIMPOZIJ Z NASLOVOM:

DIAGNOSTIKA IN ZDRAVLJENJE ZGODNJEGA RAKA

SIMPOZIJ BO POTEKAL V LJUBLJANI, DNE 7. OKTOBRA 2016
V MODRI DVORANI DOMUS MEDICA, DUNAJSKA CESTA 162.

DUNAJSKA 106
1000 LJUBLJANA

TRR: 02033-0017879431



Activity of "Dr. J. Cholewa" Foundation for Cancer Research and Education - a report for the second quarter of 2016

Dr. Josip Cholewa Foundation for cancer research and education continues with its planned activities in the second quarter of 2016. Its primary focus remains the provision of grants and scholarships and other forms of financial assistance for basic, clinical and public health research in the field of oncology. In parallel, it also makes efforts to provide financial and other support for the organisation of congresses, symposia and other forms of meetings to spread the knowledge about prevention and treatment of cancer, and finally about rehabilitation for cancer patients. In Foundation's strategy the spread of knowledge should not be restricted only to the professionals that treat cancer patients, but also to the patients themselves and to the general public.

The Foundation continues to provide support for »Radiology and Oncology«, a quarterly scientific magazine with a long tradition and with a respectable impact factor that publishes research and review articles about all aspects of cancer. The magazine is edited and published in Slovenia.

The Foundation will continue with its activities in the future, especially since the problems associated with cancer affect more and more people in Slovenia and elsewhere. Ever more successful treatment results in longer survival in many patients with previously incurable cancer conditions, thus adding many new dimensions in life of cancer survivors and their families.

Borut Štabuc, M.D., Ph.D.
Tomaž Benulič, M.D.
Andrej Plesničar, M.D., M.Sc.
Viljem Kovač M.D., Ph.D.

Neulasta®:

Zaščitite bolnike, optimizirajte zdravljenje s citostatiki¹



NEULASTA® 6 mg raztopina za injiciranje (pegfilgrastim) – SKRAJŠAN POVZETEK GLAVNIH ZNAČILNOSTI ZDRAVILA

Samo za strokovno javnost. Pred predpisovanjem si preberite celoten Povzetek glavnih značilnosti zdravila. **SESTAVA ZDRAVILA:** Ena napolnjena injekcijska brizga vsebuje 6 mg pegfilgrastima v 0,6 ml (10 mg/ml) raztopine za injiciranje. **TERAPEVTSKE INDIKACIJE:** Skrajšanje trajanja nevropenije in zmanjšanje incidence febrilne nevropenije pri odraslih bolnikih, zdravljenih s citotoksično kemoterapijo za maligne bolezni (z izjemo kronične mieloidne levkemije in mielodisplastičnih sindromov). **ODMERJANJE IN NAČIN UPORABE:** Zdravljenje z zdravilom Neulasta® morajo uvesti in nadzorovati zdravniki, izkušeni v onkologiji in/ali hematologiji. Za vsak cikel kemoterapije priporočajo en 6 mg odmerek (eno napolnjeno injekcijsko brizgo) zdravila Neulasta®, ki je dana vsaj 24 ur po citotoksični kemoterapiji. Zdravilo Neulasta® se injicira subkutano. Injekcije se morajo dati v stegno, trebuh ali zgornji del roke. Varnost in učinkovitost zdravila Neulasta® pri otrocih še nista bili dokazani in priporočil o odmerjanju ni mogoče dati. Pri bolnikih z okvaro ledvic in s končno odpovedjo ledvic odmerek ni treba spreminjati. **KONTRAINDIKACIJE:** Preobčutljivost za zdravilo učinkovino ali katerokoli pomožno snov. **POSEBNA OPOZORILA IN PREDVIDNOSTNI UKREPI:** Pri bolnikih z *de novo* akutno mieloidno levkemijo omejeni klinični podatki kažejo primerljiv učinek pegfilgrastima in filgrastima na čas do okrevanja po hudi nevropeniji. Dolgoročni učinki zdravila Neulasta® pri akutni mieloidni levkemiji niso ugotovljeni, zato ga je treba pri tej populaciji bolnikov uporabljati previdno. Varnost in učinkovitost zdravila Neulasta® nista raziskani pri bolnikih z mielodisplastičnim sindromom, s kronično mielogeno levkemijo in s sekundarno akutno mieloidno levkemijo (AML), zato ga pri takšnih bolnikih ne smete uporabljati. Posebno pozornost je treba nameniti razlikovanju diagnoze blastne transformacije kronične mieloidne levkemije od akutne mieloidne levkemije. Varnost in učinkovitost uporabe zdravila Neulasta® pri bolnikih z *de novo* AML, mlajših od 55 let in s citogenetiko t(15;17), nista ugotovljeni. Varnosti in učinkovitosti zdravila Neulasta® niso raziskovali pri bolnikih, ki prejemajo kemoterapijo v velikih odmerkih. Teža zdravila ne smete uporabljati za zvečevanje odmerka citotoksične kemoterapije preko uveljavljenih shem odmerjanja. Neželene reakcije na pljučih: Bolj ogroženi so lahko bolniki z nedavno anamnezo pljučnih infiltratov ali pljučnice. Pojav pljučnih znakov, kot so kašelj, zvišana telesna temperatura in dispneja v povezavi z radiološkimi znaki pljučnih infiltratov, in poslabšanje pljučne funkcije skupaj z zvečanim številom nevтроfilcev utegnejo biti preliminarni znaki sindroma akutne dihalne stiske (ARDS - *Acute Respiratory Distress Syndrome*). V takih primerih je treba zdravilo Neulasta® po presoji zdravnika prenehati dajati in poskrbeti za ustrezno zdravljenje. Glomerulonefritis: Na splošno so primeri glomerulonefritisa minili po zmanjšanju odmerka ali prenehanju uporabe filgrastima ali pegfilgrastima. Priporočljivo je spremljanje laboratorijskih izvidov urina. Sindrom kapilarne prepustnosti: Bolniki, ki se jim pojavijo simptomi sindroma kapilarne prepustnosti, je treba natančno kontrolirati in deležni morajo biti standardnega simptomatskega zdravljenja, ki lahko vključuje potrebo po intenzivni negi. Splenomegalija in ruptura vranice: Skrbno je treba spremljati velikost vranice (s kliničnim pregledom, ultrazvokom). Na diagnozo rupture vranice moramo misliti pri bolnikih, ki poročajo o bolečini v zgornjem levem delu trebuha ali v predelu lopatic. Trombocitopenija in anemija: Zdravljenje s samim zdravilom Neulasta® ne prepreči trombocitopenije in anemije, ker se hkrati vzdržuje mielosupresivna kemoterapija s polnimi odmerki po predpisani shemi. Priporočajo redno spremljanje števila trombocitov in hematokrita. Posebna previdnost je potrebna med uporabo posameznih kemoterapevtikov ali njihovih kombinacij, za katere je znano, da povzročajo hudo trombocitopenijo. Srpastocelična anemija: Pri bolnikih s srpastocelično dispozicijo ali s srpastocelično anemijo je bila uporaba pegfilgrastima povezana s srpastocelično krizo, zato se mora pri teh bolnikih zdravilo Neulasta® predpisovati previdno in spremljati ustrezne klinične parametre in laboratorijski status in biti pozoren na morebitno povezavo tega zdravila z zvečanjem vranice in vazookluzivno krizo. Levkocitoza: Zaradi kliničnih učinkov zdravila Neulasta® in zaradi možnosti levkocitoze je treba med zdravljenjem redno kontrolirati število belih krvničk. Če število levkocitov po pričakovanem najmanjšem številu preseže $50 \times 10^9/l$, je treba nemudoma prenehati z zdravljenjem s tem zdravilom. Preobčutljivost: Dokončno prenehajte z zdravljenjem z zdravilom Neulasta® pri bolnikih s klinično znakovno preobčutljivostjo. Zdravilo Neulasta® ne dajate bolnikom z anamnezo preobčutljivosti na pegfilgrastim ali filgrastim. V primeru resne alergijske reakcije je treba poskrbeti za ustrezno zdravljenje in pazljivo spremljanje bolnika še nekaj dni. Imunogenost: Kot pri vseh terapevtskih beljakovinah obstaja možnost imunogenosti. Stopnja nastajanja protiteles proti pegfilgrastimu je na splošno nizka. Vezavna protitelesa se pojavijo po pričakovanih pri vseh bioloških zdravilih, vendar jih doslej niso povezali z nevtralizacijskim delovanjem. Varnosti in učinkovitosti zdravila Neulasta® za mobilizacijo matičnih krvotvornih celic pri bolnikih ali zdravih dajalcih niso primerno ovrednotili. Pokrovček igle pri napolnjeni injekcijski brizgi vsebuje suho naravno gumo (derivat lateksa), ki lahko povzroča alergične reakcije. Povečana hemopoetična aktivnost kostnega mozga zaradi zdravljenja z rastnimi dejavniki je bila povezana s prehodnimi pozitivnimi izvidi pri slikanju kosti, kar je treba upoštevati pri interpretaciji izvidov na podlagi slikanja kosti. Zdravilo Neulasta® vsebuje sorbitol. Bolniki z redko prirojeno motno intoleranco za fruktozo ne smejo dobiti tega zdravila. Zdravilo Neulasta® vsebuje manj kot 1 mmol (23 mg) natrija na 6 mg odmerek, kar v bistvu pomeni "brez natrija". Za izboljšanje sledljivosti granulocitne kolonije spodbujajočih faktorjev (G-CSF) je treba v bolnikovi dokumentaciji jasno zabeležiti zaščiteno ime uporabljenega zdravila. **MEDSEBOJNO DELOVANJE ZDRAVIL IN DRUGE OBLIKE INTERAKCIJ:** Zaradi možne občutljivosti hitro se delčih mieloidnih celic za citotoksično kemoterapijo je treba zdravilo Neulasta® dati vsaj 24 ur po aplikaciji citotoksične kemoterapije. Sočasne uporabe zdravila Neulasta® s katerimkoli kemoterapevtskim zdravilom pri bolnikih niso ovrednotili. **NEZELENI UČINKI:** Podatki opisujejo neželene učinke, zabeležene v kliničnih preskušanjih in med spontanim poročanjem. Zelo pogosti ($\geq 1/10$): glavobol, navzea, bolečina v kosteh. Pogosti ($\geq 1/100$ do $< 1/10$): trombocitopenija, levkocitoza, mišično-skeletna bolečina (mialgija, artralgija, bolečina v okončinah, bolečina v hrbtu, mišično-skeletna bolečina, bolečina v vratu), bolečina na mestu injiciranja, bolečina v prsih, ki ne izvira od srca. Občasni ($\geq 1/1.000$ do $< 1/100$): srpastocelična kriza, splenomegalija, ruptura vranice, preobčutljivostne reakcije, anafilaksija, zvišanje sečne kisline, sindrom kapilarne prepustnosti, sindrom akutne dihalne stiske, pljučne neželene reakcije (intersticijska pljučnica, pljučni edem, pljučni infiltrati in pljučna fibroza), Sweetov sindrom (akutna febrilna dermataza), kožni vaskulitis, reakcije na mestu injiciranja, zvišanje laktat-dehidrogenaze in alkalne fosfataze, prehodno zvišanje jetrnih funkcijskih testov za ALT ali AST, glomerulonefritis. **FARMACEVTSKI PODATKI:** Shranjujte v hladilniku (2°C – 8°C). Ne zamrzujte. Zdravilo Neulasta® sme biti izpostavljeno sobni temperaturi (ne nad 30°C) za enkratno obdobje, ki ne sme preseči 72 ur. Zdravilo Neulasta® ni kompatibilno z raztopinami natrijevega klorida. **NAČIN IN REŽIM PREDPISOVANJA TER IZDAJE ZDRAVILA:** Predpisovanje in izdaja zdravila je le na recept s posebnim režimom – H/Rp. **IMETNIK DOVOLJENJA ZA PROMET:** Amgen Europe B.V., 4817 ZK Breda, Nizozemska. Dodatna pojasnila lahko dobite v lokalni pisarni: Amgen zdravila d.o.o., Šmartinska 140, SI-1000 Ljubljana. **DATUM ZADNJE REVIZIJE BESEDILA:** Maj 2015. **DATUM PRIPRAVE INFORMACIJE:** April 2016. Podrobni podatki o tem zdravilu so na voljo na spletni strani Evropske agencije za zdravila <http://www.ema.europa.eu/>. **Literatura:** 1.) Povzetek glavnih značilnosti zdravila Neulasta®, Amgen, 2015.

SHR-SLP-003-0416-129220

AMGEN®

 **Neulasta®**
(pegfilgrastim)

Zaščitite bolnike, optimizirajte
zdravljenje s citostatiki.



Iclusig® (ponatinib)

Ključ do učinkovitega zdravljenja bolnikov s KML in Ph + ALL



Zdravilo Iclusig® je peroralni zaviralec tirozin-kinaze (TKI) za doziranje enkrat dnevno z učinkovitim delovanjem pri odraslih bolnikih s KML in Ph+ ALL¹



Za bolnike s kronično mieloidno levkemijo (KML) v kronični, pospešeni ali blastni fazi, ki:

- so odporni na dasatinib ali nilotinib **ali**
- ne prenašajo dasatiniba ali nilotiniba in pri katerih nadaljnje zdravljenje z imatinibom ni klinično ustrezno **ali**
- imajo mutacijo T3151

Za bolnike z akutno limfoblastno levkemijo s prisotnim kromosomom Philadelphia (Ph+ ALL), ki:

- so odporni na dasatinib **ali**
- ne prenašajo dasatiniba in pri katerih nadaljnje zdravljenje z imatinibom ni klinično ustrezno **ali**
- imajo mutacijo T3151

SKRAJŠAN POVZETEK GLAVNIH ZNAČILNOSTI ZDRAVILA Iclusig 15 mg, 30 mg in 45 mg filmsko obložene tablete

Pred predpisovanjem natančno preberite celoten Povzetek glavnih značilnosti zdravila.

Samo za strokovno javnost.

▼ Za to zdravilo se izvaja dodatno spremljanje varnosti. Tako bodo hitreje na voljo nove informacije o njegovi varnosti. Zdravstvene delavce naprošamo, da poročajo o katerem koli domnevnem neželenem učinku zdravila.

Sestava: Ena filmsko obložena tableta vsebuje 15mg, 30mg ali 45 mg ponatiniba (v obliki ponatinibijevga klorida). **Indikacije:** Zdravilo Iclusig je indicirano pri odraslih bolnikih s kronično mieloidno levkemijo (KML) v kronični fazi, pospešeni fazi ali blastni fazi, ki so odporni na dasatinib ali nilotinib; ki ne prenašajo dasatiniba ali nilotiniba in pri katerih nadaljnje zdravljenje z imatinibom ni klinično ustrezno; ali ki imajo mutacijo T3151. **Odmernjevanje in način uporabe:** Terapijo mora uvesti zdravnik z izkušnjami v diagnosticiranju in zdravljenju bolnikov z levkemijo. Med zdravljenjem se lahko bolniku nudi hematološka podpora, če je to klinično indicirano. Pred začetkom zdravljenja s ponatinibom je treba oceniti kardiovaskularni status bolnika, vključno z anamnezo in telesnim pregledom, in aktivno obravnavati kardiovaskularne dejavnike tveganja. Kardiovaskularni status je treba še naprej spremljati in med zdravljenjem s ponatinibom optimizirati zdravljenje z zdravili in podporno zdravljenje stanj, ki prispevajo h kardiovaskularnim tveganjem.

Odmernjevanje: Priporočeni začetni odmerek ponatiniba je 45 mg enkrat na dan. Potrebno je razmisliti o ukinitvi ponatiniba, če v 3 mesecih ni celovitega hematološkega odgovora. Z zdravljenjem je treba prenehati, če se pojavijo znaki napredovanja bolezni ali v primeru hudih neželenih učinkov. **Prilagoditev odmerjanja:** tveganje za žilni okluzivni dogodek je verjetno povezano z odmerkom. Zdravljenje z zdravilom Iclusig je treba pri sumu, da se je pri bolniku razvil arterijski ali venski okluzivni dogodek, takoj prekiniti. Ko se dogodek razreši, je treba pri odločitvi o ponovni uvedbi zdravljenja upoštevati oceno koristi in tveganj. Pri obravnavi hematoloških in nehematoloških toksičnosti je treba razmisliti o prilagoditvi ali prekinitvi odmerjanja. V primeru hudih neželenih učinkov je treba z zdravljenjem prekiniti. Prilaganje odmerka je priporočljivo v primeru nevotropenije ali trombocitopenije, ki nista povezani z levkemijo, pri pankreatitisu in zvišani ravni lipaze/amilaze. **Način uporabe:** tablete je treba pogottniti cele, ne sme se jih drobiti ali raztapljati, lahko pa se jih jemlje s hrano ali brez nje. **Kontraindikacije:** Preobčutljivost na ponatinib ali katero koli pomožno snov. **Posebna opozorila in previdnostni ukrepi:** **Mielosupresija** – Zdravilo Iclusig je povezano s hudo trombocitopenijo, nevotropenijo in anemijo. Prve 3 mesece je treba vsaka 2 tedna opraviti pregled celotne krvne slike, nato pa mesečno ali kot je klinično indicirano. **Žilna okluzija** – Pojavilo se je arterijska in venska tromboza in okluzija, vključno s smrtnim miokardnim infarktom, možgansko kapjo, retinalna žilna okluzija, v nekaterih primerih povezana s trajno okvaro vida ali slepoto, stenozo velikih arterijskih žil v možganih, hudo periferno žilno bolezenjo in potrebo po nujnem postopku

revaskularizacije. Zdravilo Iclusig se ne sme uporabljati pri bolnikih z miokardnim infarktom, predhodno revaskularizacijo ali možgansko kapjo v anamnezi, razen če so možne koristi zdravljenja večje od možnih tveganj. Med zdravljenjem s ponatinibom je treba spremljati znake tromboembolije in žilne okluzije in zdravljenje je treba takoj prekiniti, če se pojavi žilna okluzija. V primeru, da se pojavi poslabšanje vida ali zamegljen vid, je treba opraviti oftalmološki pregled (vključno s fundoskopijo). **Hipertenzija** – Pri zdravljenju z zdravilom Iclusig, se je pojavila z zdravljenjem povezana hipertenzija (vključno s hipertenzivno krizo), ki lahko prispeva k tveganju arterijskih trombotičnih dogodkov. Zato je treba ob vsakem obisku zdravnika spremljati krvni tlak. Zdravljenje z zdravilom Iclusig je treba prekiniti, če hipertenzija ni pod zdravniškim nadzorom. **Kongestivno srčno popuščanje** – Pojavilo se je smrtno in resno srčno popuščanje ter dogodki, povezani s predhodnimi vaskularnimi okluzivnimi dogodki. Bolnike je treba spremljati in jih zdraviti, kot je klinično ustrezno, vključno s prekinitvijo zdravljenja z zdravilom Iclusig. Pri bolnikih, pri katerih se razvije resno srčno popuščanje, je treba razmisliti o ukinitvi ponatiniba. **Pankreatitis in serumska lipaza** – Pogostnost pojava pankreatitisa je večja prva 2 meseca uporabe. Prva 2 meseca vsaka 2 tedna preverjajte serumsko lipazo, nato pa periodično. Morda bo treba odmerek prekiniti ali zmanjšati. Če zvišanje ravni lipaz spremljajo abdominalni simptomi, je treba z uporabo zdravila Iclusig prenehati in preveriti, ali ima bolnik pankreatitis. Pri bolnikih s pankreatitisom ali zlorabo alkohola v anamnezi se priporoča previdnost. Bolnike s hudo ali zelo hudo hipertrigliceridemijo je treba ustrezno obravnavati. **Laktatoza** – Zdravilo Iclusig vsebuje laktozo monohidrat. Bolniki z redkimi dednimi težavami neprenašanja galaktoze, laptosko obliko zmanjšane aktivnosti laktaze ali slabo absorpcijo glukoze-galaktoze ne smejo jemati tega zdravila. **Podaljšanje intervala QT** – Klinično pomembnih učinkov na interval QT ni mogoče izključiti. **Hepatotoksičnost** – Lahko se zvišajo ravni ALT, AST, bilirubina in alkalne fosfataze. Opazili so jetrno odpoved (vključno s smrtnim izidom). Teste delovanja jeter je treba opraviti pred uvedbo zdravljenja in nato periodično, kot je klinično indicirano. **Krvavitve** – Pojavili so se smrtni ter resni hemoragični dogodki. Pri resni ali hudi krvavitvi je treba zdravljenje z zdravilom Iclusig prekiniti. **Okvara jeter** – Pri bolnikih s hudo okvaro jeter se priporoča previdnost. **Okvara ledvic** – Pri bolnikih z ocenjenim očistkom kreatinina < 50 ml/min ali ledvično bolezenjo v zadnjem stadiju se priporoča previdnost. **Starostni bolniki** – Verjetnost neželenih učinkov je večja. **Pediatrska populacija** – Varnost in učinkovitost zdravila Iclusig pri bolnikih, starih do 18 let, se nista bili dokazani. **Medsebojno delovanje z drugimi zdravili in druge oblike interakcij:** Sočasni uporabi zdravila Iclusig z močnimi induktorji CYP3A4 se je treba izogniti; pri sočasni uporabi močnih zaviralcev CYP3A4 je potrebna previdnost, razmisliti pa je treba tudi o uporabi zdravila Iclusig z začetnim odmerkom 30 mg; potrebna je previdnost pri sočasno uporabljenih substratih P-glikoproteina (P-gp) ali beljakovine rezistence za raka dojke (BCRP). Pri sočasni uporabi ponatiniba z zdravili proti strjevanju krvi pri bolnikih, pri katerih obstaja tveganje za krvavitve, je potrebna previdnost. **Plodnost, nosečnost in dojenje:** Zenskam v rodni dobi je treba svetovati, da naj v času zdravljenja z zdravilom Iclusig ne zanosi, možkim pa, da naj v času zdravljenja ne zaplodijo otroka. Med zdravljenjem je treba uporabljati

alternativno ali dodatno metodo kontracepcije. Ni zadostnih podatkov o uporabi zdravila Iclusig pri nosečnicah. Študije na živalih so pokazale vpliv na sposobnost razmnoževanja. Če se zdravilo uporablja med nosečnostjo, je treba bolnico obvestiti o možnem tveganju za plod. Z dojenjem je treba med zdravljenjem z zdravilom Iclusig prenehati. **Vpliv na sposobnost vožnje in upravljanja s stroji:** Pri vožnji ali upravljanju strojev je potrebna previdnost. **Neželeni učinki:** Zelo pogosti (≥ 1/10): okužba zgornjih dihal, nespečnost, anemija, zmanjšanje števila trombocitov, zmanjšanje števila nevtrofilcev, zmanjšan apetit, glavobol, omotica, hipertenzija, dispneja, kašelj, bolečine v trebuhu, driska, bruhanje, zaprtje, navzea, zvišanje ravni lipaz, zvišanje ravni alanin aminotransferaze, zvišanje ravni aspartat-aminotransferaze, izpuščaji, suha koža, bolečine v kosteh, artralgija, mialgija, bolečine v okončinah, bolečine v hrbtu, mišični krči, utrujenost, astenija, periferni edem, piroksija, bolečine. Pogosti (≥ 1/100 do < 1/10): pljučnica, sepsa, folikulitis, pancitopenija, febrilna nevropenija, zmanjšanje števila levkocitov, dehidracija, zastajanje tekočine, hipokalcemija, hiperglikemija, hiperurikemija, hipofosfatemija, hipertrigliceridemija, hipokalemija, zmanjšanje telesne mase, cerebrovaskularni dogodek, cerebralni infarkt, periferna nevropatija, letargija, migrena, hiperestezija, hipopostezija, parestezija, prehodni ishemični napad, zamegljen vid, suhe oči, periorbitalni edem, edem veke, srčno popuščanje, miokardni infarkt, kongestivno srčno popuščanje, bolezen koronarnih arterij, angina pectoris, perikardni izliv, atrijska fibrilacija, zmanjšanje iztisnega deleža, periferna arterijska okluzivna bolezen, periferna ishemija, stenozna periferna arterija, intermitentna kladikacija, globoka venska tromboza, vročinski oblivi, zariplot, mišična embolija, pleuralni izliv, epistaksa, disfonija, pljučna hipertenzija, pankreatitis, zvišanje amilaz v krvi, gastroezofagealna refluksna bolezen, stomatitis, dispepsija, trebušna distenzija, nelagodje v trebuhu, suha usta, zvišanje ravni bilirubina v krvi, zvišanje ravni alkalne fosfataze v krvi, zvišanje ravni gama-glutamilttransferaze, pruritični izpuščaji, ekfoliativni izpuščaji, eritem, alopecija, pruritis, ekfoliativna koža, nočno potenje, hiperhidroza, petehija, ekhimoza, boleča koža, ekfoliativni dermatitis, mišično-skeletne bolečine, bolečine v vratu, mišično-skeletne bolečine v prsnem košu, erektilna disfunkcija, mrzlica, gripi podobna bolezen, nekardiogena bolečina v prsnem košu, tipljiv vozilci, obrazni edem. Občasni (≥ 1/1000 do < 1/100): sindrom tumorske lize, cerebralna arterijska stenozna, tromboza mrežnične vene, okluzija mrežnične vene, okluzija mrežnične arterije, okvara vida, miokardna ishemija, akutni koronarni sindrom, kardialno nelagodje, ishemična kardiomiopatija, spazem koronarnih arterij, disfunkcija levega prekata, atrijska disfunkcija, mrzlica, gripi podobna bolezen, vrenični infarkt, venska embolija, venska tromboza, hipertenzivna kriza, krvavitve v želodcu, hepatotoksičnost, odpoved jeter, zlatenica. **Režim izdaje zdravila:** Predpisovanje in izdaja zdravila je le na recept. **Imetnik dovoljenja za promet z zdravilom:** ARIAD Pharma Ltd., Riverbridge House, Guildford Road, Leatherhead, Surrey KT22 9AD, Velika Britanija. **Zadnja revizija besedila:** marec 2016. **Informacija pripravljena:** april 2016. **Podrobnejše informacije o zdravilu Iclusig so na voljo pri predstavniku imetnika dovoljenja za promet z zdravilom:** Angelini Pharma d.o.o., Koprška ulica 108A, 1000 Ljubljana, tel.: +386 1 544 65 79, E-pošta: info@angelini.si



Predstavnik:
Angelini Pharma d.o.o.
Koprška ulica 108 A, Ljubljana

➤ PRVA REGISTRIRANA TERAPIJA
V 2. LINIJI ZA ZDRAVLJENJE
ADENOKARCINOMA ŽELODCA ALI
GASTRO-EZOFAGEALNEGA PREHODA¹


CYRAMZA™
(ramucirumab)

UKREPAJTE ZDAJ



**USPOSOBLJENI
ZA SPREMEMBE,
ZA NEPRIMERLJIVE
IZKUŠNJE**

Skrajšjan povzetek glavnih značilnosti zdravila

▼ Za to zdravilo se izvaja dodatno spremljanje varnosti. Tako bodo hitreje na voljo nove informacije o njegovi varnosti. Zdravstvene delavce naprošamo, da poročajo o katerem koli domnevnem neželenem učinku zdravila.

Cyramza 10 mg/ml koncentrat za raztopino za infundiranje

En mililiter koncentrata za raztopino za infundiranje vsebuje 10 mg ramucirumaba. Ena 10-mililitrska viala vsebuje 100 mg ramucirumaba. **Terapevtske indikacije** Zdravilo Cyramza je v kombinaciji s paklitakselom indicirano za zdravljenje odraslih bolnikov z napredovalim rakom želodca ali adenokarcinomom gastro-efozagealnega prehoda z napredovalo boleznijo po predhodni kemoterapiji, ki je vključevala platino in fluoropirimidin. Monoterapija z zdravilom Cyramza je indicirana za zdravljenje odraslih bolnikov z napredovalim rakom želodca ali adenokarcinomom gastro-efozagealnega prehoda z napredovalo boleznijo po predhodni kemoterapiji s platino ali fluoropirimidinom, za katere zdravljenje v kombinaciji s paklitakselom ni primerno. Zdravilo Cyramza je v kombinaciji s shemo FOLFIRI indicirano za zdravljenje odraslih bolnikov z metastatskim kolorektalnim rakom (mCRC), z napredovanjem bolezni ob ali po predhodnem zdravljenju z bevacizumabom, oksaliplatinom in fluoropirimidinom. Zdravilo Cyramza je v kombinaciji z docetakselom indicirano za zdravljenje odraslih bolnikov z lokalno napredovalim ali metastatskim nedrobnočeličnim pljučnim rakom, z napredovanjem bolezni po kemoterapiji na osnovi platine. **Odmerjanje in način uporabe** Zdravljenje z ramucirumabom morajo uvesti in nadzirati zdravniki z izkušnjami v onkologiji. **Odmerjanje Rak želodca in adenokarcinom gastro-efozagealnega prehoda** Priporočeni odmerek ramucirumaba je 8 mg/kg 1. in 15. dan 28-dnevnega cikla, pred infuzijo paklitaksela. Priporočeni odmerek paklitaksela je 80 mg/m² in se daje z intravenskim infundiranjem, ki traja približno 60 minut, 1., 8. in 15. dan 28-dnevnega cikla. Pred vsakim infundiranjem paklitaksela je treba pri bolnikih pregledati celotno krvno sliko in izvide kemičnih preiskav krvi, da se oceni delovanje jeter. Priporočeni odmerek ramucirumaba kot monoterapije je 8 mg/kg vsaka 2 tedna. **Kolorektalni rak** Priporočeni odmerek ramucirumaba je 8 mg/kg vsaka 2 tedna, dan z intravensko infuzijo pred dajanjem sheme FOLFIRI. Pred kemoterapijo je treba bolnikom odvzeti kri za popolno krvno sliko. **Nedrobnočelični pljučni rak (NSCLC)** Priporočeni odmerek ramucirumaba je 10 mg/kg na 1. dan 21-dnevnega cikla, pred infuzijo docetakselo. Priporočeni odmerek docetakselo je 75 mg/m², dan z intravensko infuzijo v približno 60 minutah na 1. dan 21-dnevnega cikla. **Premedikacija** Pred infundiranjem ramucirumaba je priporočljiva premedikacija z antagonistom histaminskih receptorjev H1. **Način uporabe** Po redčenju se zdravilo Cyramza daje kot intravenska infuzija v približno 60 minutah. Zdravila ne dajajte v obliki intravenskega bolusa ali hitre intravenske injekcije. Da boste dosegli zahtevano trajanje infundiranja približno 60 minut, največja hitrost infundiranja ne sme preseči 25 mg/minuto, saj morate sicer podaljšati trajanje infundiranja. Bolnika je med infundiranjem treba spremljati glede znakov reakcij, povezanih z infuzijo, zagotoviti pa je treba tudi razpoložljivost ustrezne opreme za oživiljanje. **Kontraindikacije** Pri bolnikih z NSCLC je ramucirumab kontraindiciran, kjer gre za kavitacijo tumorja ali prepletenost tumorja z glavnimi žilami. **Posebna opozorila in previdnostni ukrepi** Trajno prekinite zdravljenje z ramucirumabom pri bolnikih, pri katerih se pojavijo resni arterijski tromboembolični dogodki, gastrointestinalne perforacije, krvavitve stopnje 3 ali 4, če zdravstveno pomembne hipertenzije ni mogoče nadzirati z antihipertenzivnim zdravljenjem ali če se pojavi fistula, raven beljakovin v urinu > 3 g/24 ur ali v primeru nefrotskega sindroma. Pri bolnikih z neuravnavano hipertenzijo zdravljenja z ramucirumabom ne smete uvesti, dokler oziroma v kolikor obstoječa hipertenzija ni uravnavana. Pri bolnikih s ploščatocelično histologijo obstaja večje tveganje za razvoj resnih pljučnih krvavitev. Če se pri bolniku med zdravljenjem razvijejo zapleti v zvezi s celjenjem rane, prekinite zdravljenje z ramucirumabom, dokler rana ni povsem zaceljena. V primeru pojava stomatitisa je treba takoj uvesti simptomatsko zdravljenje. Pri bolnikih, ki so prejimali ramucirumab in docetaksel za zdravljenje napredovalnega NSCLC z napredovanjem bolezni po kemoterapiji na osnovi platine, so opazili trend manjše učinkovitosti z naraščajočo starostjo. **Plodnost, nosečnost in dojenje** Ženskam v rodni dobi je treba svetovati, naj se izognejo zanositvi med zdravljenjem z zdravilom Cyramza in jih je treba seznaniti z možnim tveganjem za nosečnost in plod. Ni znano, ali se ramucirumab izloča v materino mleko. **Neželeni učinki** **Želo pogosti** ($\geq 1/10$) nevtropenija, levkopenija, trombocitopenija, hipoalbuminemija, hipertenzija, epistaksa, gastrointestinalne krvavitve, stomatitis, driska, proteinurija, utrujenost/astenija, periferni edem, bolečina v trebuhu. **Pogosti** ($\geq 1/100$ do $< 1/10$) hipokaliemija, hiponatriemija, glavobol. **Rok uporabnosti** 3 leta **Posebna navodila za shranjevanje** Shranjujte v hladilniku (2 °C–8 °C). Ne zamrzujte. Vialo shranjujte v zunanji ovojnini, da zagotovite zaščito pred svetlobo. **Pakiranje** 2 viali z 10 ml **IMETNIK DOVOLJENJA ZA PROMET Z ZDRAVILOM** Eli Lilly Nederland B.V., Papendorpseweg 83, 3528 BJ Utrecht, Nizozemska **DATUM ZADNJE REVIZIJE BESEDILA** 25.01.2016

Režim izdaje: Predpisovanje in izdaja zdravila je le na recept, zdravilo pa se uporablja samo v bolnišnicah.

Pomembno obvestilo:

Pričujoče gradivo je namenjeno **samo za strokovno javnost**. Zdravilo Cyramza se izdaja le na recept. Pred predpisovanjem zdravila Cyramza vas vljudno prosimo, da preberete celotni Povzetek glavnih značilnosti zdravila Cyramza. Podrobnejše informacije o zdravilu Cyramza in o zadnji reviziji besedila Povzetka glavnih značilnosti zdravila so na voljo na sedežu podjetja Eli Lilly (naslov podjetja in kontaktni podatki spodaj) in na spletni strani European Medicines Agency (EMA): www.ema.europa.eu. in na spletni strani European Commission <http://ec.europa.eu/health/documents/community-register/html/alfregister.htm>.

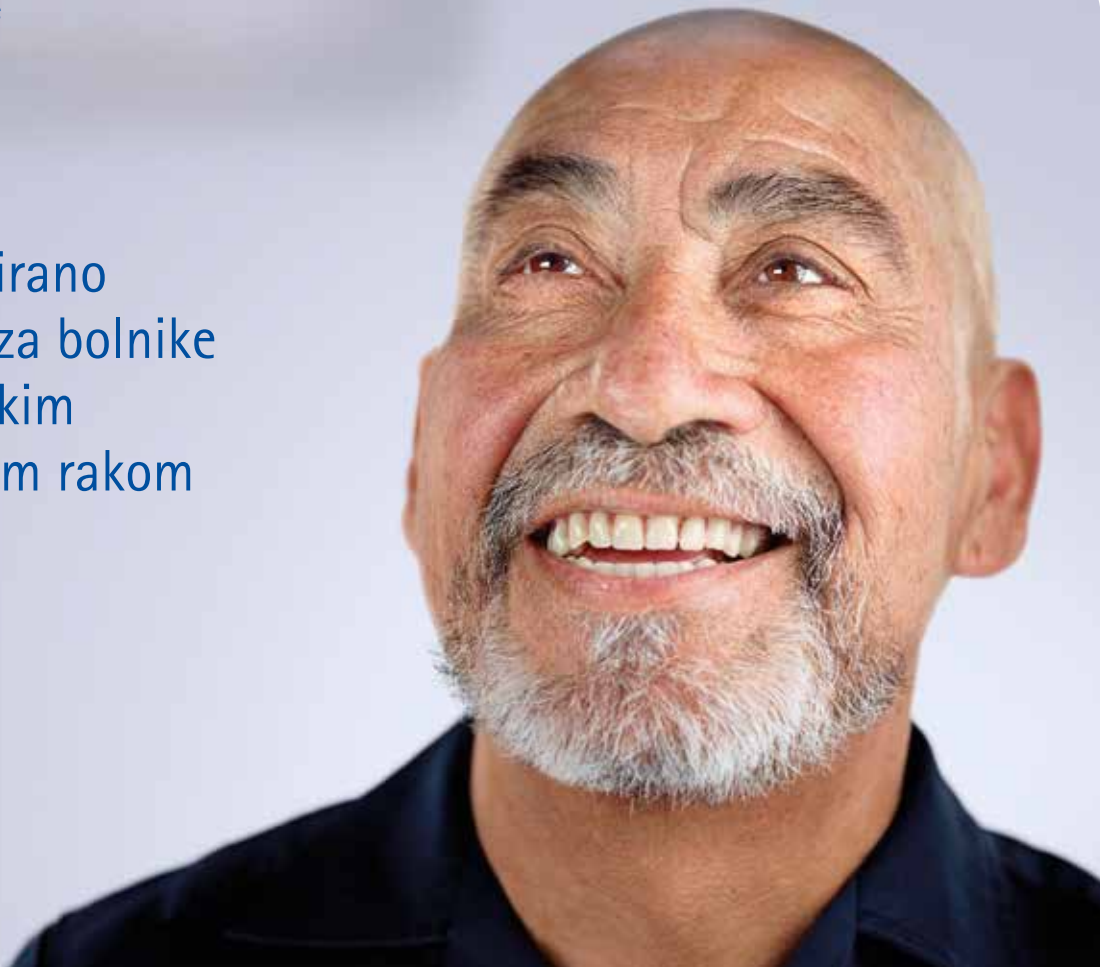
Eli Lilly farmacevtska družba, d.o.o., Dunajska cesta 167, 1000 Ljubljana, telefon: (01) 5800 010, faks: (01) 5691 705

Referenca: 1. Cyramza, Povzetek glavnih značilnosti zdravila, zadnja odobrena verzija.

EERAM00010a, 12.02.2016.



Individualizirano zdravljenje za bolnike z metastatskim kolorektalnim rakom



Merck Serono Onkologija | *Ključ je v kombinaciji*

Erbitux 5 mg/ml raztopina za infundiranje

Skrajšan povzetek glavnih značilnosti zdravila

Sestava: En ml raztopine za infundiranje vsebuje 5 mg cetuksimaba in pomožne snovi. Cetuksimab je himerno monoklonsko IgG₁ protitelo. **Terapevtske indikacije:** Zdravilo Erbitux je indicirano za zdravljenje bolnikov z metastatskim kolorektalnim rakom z ekspresijo receptorjev EGFR in nemutiranim tipom RAS v kombinaciji s kemoterapijo na osnovi irinotekana, kot primarno zdravljenje v kombinaciji s FOLFFOX in kot samostojno zdravilo pri bolnikih, pri katerih zdravljenje z oksaliplatinom in zdravljenje na osnovi irinotekana ni bilo uspešno in pri bolnikih, ki ne prenašajo irinotekana. Zdravilo Erbitux je indicirano za zdravljenje bolnikov z rakom skvamoznih celic glave in vratu v kombinaciji z radioterapijo za lokalno napredovalo bolezen in v kombinaciji s kemoterapijo na osnovi platine za ponavljajočo se in/ali metastatsko bolezen. **Odmerjanje in način uporabe:** Zdravilo Erbitux pri vseh indikacijah infundirajte enkrat na teden. Pred prvo infuzijo mora bolnik prejeti premedikacijo z antihistaminikom in kortikosteroidom najmanj 1 uro pred uporabo cetuksimaba. Začetni odmerek je 400 mg cetuksimaba na m² telesne površine. Vsi naslednji tedenski odmerki so vsak po 250 mg/m². **Kontraindikacije:** Zdravilo Erbitux je kontraindicirano pri bolnikih z znano hudo preobčutljivostno reakcijo (3. ali 4. stopnje) na cetuksimab. Kombinacija zdravila Erbitux s kemoterapijo, ki vsebuje oksaliplatin, je kontraindicirana pri bolnikih z metastatskim kolorektalnim rakom z mutiranim tipom RAS ali kadar status RAS ni znan. **Posebna opozorila in previdnostni ukrepi:** Pojav hude reakcije, povezane z infundiranjem, zahteva takojšnjo in stalno ukinitve terapije s cetuksimabom. Če pri bolniku nastopi blaga ali zmerna reakcija, povezana z infundiranjem, lahko zmanjšate hitrost infundiranja. Priporočljivo je, da ostane hitrost infundiranja na nižji vrednosti tudi pri vseh naslednjih infuzijah. Če se pri bolniku pojavi kožna reakcija, ki je ne more prenašati, ali huda kožna reakcija (≥ 3. stopnje po kriterijih CTCAE), morate prekiniti terapijo s cetuksimabom. Z zdravljenjem smete nadaljevati le, če se je reakcija izboljšala do 2. stopnje. Če ugotovite intersticijsko bolezen pljuč, morate zdravljenje s cetuksimabom prekiniti, in bolnika ustrezno zdraviti. Zaradi možnosti pojava znižanja nivoja elektrolitov v serumu se pred in periodično med zdravljenjem s cetuksimabom priporoča določanje koncentracije elektrolitov v serumu. Pri bolnikih, ki prejemajo cetuksimab v kombinaciji s kemoterapijo na osnovi platine, obstaja večje

tevanje za pojav hude nevropenije. Takšne bolnike je potrebno skrbno nadzorovati. Pri predpisovanju cetuksimaba je treba upoštevati kardiovaskularno stanje in indeks zmogljivosti bolnika in sočasno dajanje kardiotoksičnih učinkovin kot so fluoropirimidini. Če je diagnoza ulcerativnega keratitisa potrjena, je treba zdravljenje s cetuksimabom prekiniti ali ukiniti. Cetuksimab je treba uporabljati previdno pri bolnikih z anamnezo keratitisa, ulcerativnega keratitisa ali zelo suhih oči. Cetuksimaba ne uporabljajte za zdravljenje bolnikov s kolorektalnim rakom, če imajo tumorje z mutacijo RAS ali pri katerih je tumorski status RAS neznan. **Interakcije:** Pri kombinaciji s fluoropirimidini se je v primerjavi z uporabo fluoropirimidinov, kot monoterapije, povečala pogostnost srčne ishemije, vključno z miokardnim infarktom in kongestivno srčno odpovedjo ter pogostnost sindroma dlani in stopal. V kombinaciji s kemoterapijo na osnovi platine se lahko poveča pogostnost hude levkopenije ali hude nevropenije. V kombinaciji s kapecitabinom in oksaliplatinom (XELOX) se lahko poveča pogostnost hude driske. **Neželeni učinki:** Zelo pogosti (≥ 1/10): hipomagnezija, povečanje ravnih jetrnih encimov, kožne reakcije, blage ali zmerne reakcije povezane z infundiranjem, mukozitis, v nekaterih primerih resen. Pogosti (≥ 1/100 do < 1/10): dehidracija, hipokalcemija, anoreksija, glavobol, konjunktivitis, driska, navzeja, bruhanje, hude reakcije povezane z infundiranjem, utrujenost. **Posebna navodila za shranjevanje:** Shranjujte v hladilniku (2 °C - 8 °C). **Pakiranje:** 1 viala z 20 ml ali 100 ml raztopine. **Način in režim izdaje:** Izdaja zdravila je le na recept-H. **Imetnik dovoljenja za promet:** Merck KGaA, 64271 Darmstadt, Nemčija.

Datum zadnje revizije besedila: november 2014.

Pred predpisovanjem zdravila natančno preberite celoten Povzetek glavnih značilnosti zdravila.

Samo za strokovno javnost.

Podrobnejše informacije so na voljo pri predstavniku imetnika dovoljenja za promet z zdravilom:
Merck d.o.o., Ameriška ulica 8, 1000 Ljubljana, tel.: 01 560 3810, faks: 01 560 3830, el. pošta: info@merck.si
www.merckserono.net
www.Erbitux-international.com

Skrajšan povzetek glavnih značilnosti zdravila COTELLIC:

Za to zdravilo se izvaja dodatno spremljanje varnosti. Tako bodo hitreje na voljo nove informacije o njegovi varnosti. Zdravstvene delavce naprošamo, da poročajo o katerem koli domnevem neželenem učinku zdravila. Kako poročati o neželenih učinkih, si pogledajte skrajšani povzetek glavnih značilnosti zdravila pod "Poročanje o domnevih neželenih učinkih".

Ime zdravila: Cotellic 20 mg filmsko obložene tablete. **Kakovostna in količinska sestava:** Ena filmsko obložena tableta vsebuje kobimetinib hemifumarat, kolikor ga ustreza 20 mg kobimetiniba. **Pomožna snov z znanim učinkom:** Ena filmsko obložena tableta vsebuje 36 mg laktaze monohidrata. **Terapevtske indikacije:** Zdravilo Cotellic je v kombinaciji z zdravilom imidancinor indicirano za zdravljenje odraslih bolnikov z neoperabilnim ali metastatskim melanomom, ki ima mutacijo BRAF V600. **Odmerjanje in način uporabe:** Zdravljenje z zdravilom Cotellic v kombinaciji z vemurafenibom sme uvesti in nadzorovati le usposobljen zdravnik, ki ima izkušnje z uporabo zdravil proti raku. Pred začetkom zdravljenja je treba z validirano preiskavo potrditi, da ima bolnik melanom z mutacijo BRAF V600. **Udmerjanje:** Vsak odmerek obsega tri 20-mg tablete (60 mg) in ga je treba vzeti enkrat na dan 21 dni zapored, temu sledi 7-dnevni premor. Zdravljenje z zdravilom Cotellic je treba nadaljevati, dokler bolniku ne koristi več oziroma do pojava nesprejemljive toksičnosti. Če bolnik izpusti odmerek, ga lahko vzame do 12 ur pred naslednjim učinkom zdravila, da ohrani shemo enkrat na dan. Če bolnik po uporabi zdravila Cotellic bruha, tisti dan ne sme vzeti dodatnega odmerka, temveč mora zdravljenje nadaljevati naslednji dan, kot je predpisano. **Splaisne prilagoditve odmerka:** Odlučitev za zmanjšanje odmerka zdravila Cotellic ali vemurafeniba mora temeljiti na zdravnikovi oceni varnosti in prenašanju pri posameznem bolniku. Ko je bil odmerek enkrat zmanjšan, se ga kasneje ne sme več povečati. **Nasvet za prilagoditev odmerka v primeru disfunkcije levega prekata:** Če so srčni simptomi posledica zdravila Cotellic in se po prehodni prekinitvi njegove uporabe ne izboljšajo, je treba razmisliti o trajnem prenehanju zdravljenja z zdravilom Cotellic. **Nasvet za prilagoditev odmerka zdravila Cotellic med uporabo z zaviralcem BRAF:** **Jetna laboratorijska odstopanja:** Stopnja 3: Zdravilo Cotellic je treba nadaljevati v predpisanim odmerku. Odmerek vemurafeniba je mogoče zmanjšati, kot je klinično primerno. Stopnja 4: Zdravljenje z zdravilom Cotellic in zdravljenje z vemurafenibom se lahko pojavita tudi v kombinaciji z zdravilom Cotellic in zdravljenje z vemurafenibom se lahko pojavita tudi v kombinaciji z zdravilom Cotellic in zdravljenjem z vemurafenibom. **Udmerjanje vemurafeniba:** Bolnik, stari > 65 let, odmerka ni treba prilagoditi. Pri bolnikih s hudo okvaro ledvic je treba zdravilo Cotellic uporabljati previdno. Pri bolnikih z zmerno do hudo okvaro jeter je treba zdravilo Cotellic uporabljati previdno. Varnost in učinkovitost zdravila Cotellic pri otrocih in mladostnikih, mlajših od 18 let, nista ugotovljeni. **Način uporabe:** Zdravilo Cotellic je za peroralno uporabo. Tablete je treba zaviti cele, z vodo. Lahko se jemljejo skupaj s hrano ali brez nje. **Kontraindikacije:** Preobčutljivost na zdravilno učinkovino ali katero koli pomožno snov. **Posebna opozorila in previdnostni ukrepi:** Zdravilo Cotellic v kombinaciji z vemurafenibom pri bolnikih, katerih bolezen je napredovala med zdravljenjem z zaviralcem BRAF: **Podatki pri teh bolnikih je malo.** To je učinkovita kombinacija pri teh bolnikih manjša. Zato je treba razmisliti o drugih možnostih zdravljenja pred uvedbo kombinacije. **Zdravilo Cotellic v kombinaciji z vemurafenibom pri bolnikih z zapestji v možganih:** Varnost in učinkovitost kombinacije zdravila Cotellic in vemurafeniba pri teh bolnikih ni bila ocenjena. Intraokularna aktivnost kobimetiniba trenutno ni poznana. **Serозна retinopatija:** Pri bolnikih, zdravljenih z zaviralci MEK, vključno z zdravilom Cotellic, so opažali serozno retinopatijo. Večina primerov je bila opisana kot horioretinopatija ali odstop mrežnice. Večina dogodkov, opazanih v kliničnih preskušanjih, je po prekinitvi ali zmanjšanju odmerka izvenela ali se izboljšala na nesimptomatsko stopnjo 1. Bolnike je treba na vsakem pregledu ugotoviti glede simptomov novih motenj vida ali poslabšanja obstoječih motenj vida ali poslabšanja obstoječih motenj vida. V primeru simptomov novih motenj vida ali poslabšanja obstoječih motenj vida je treba zdravljenje z zdravilom Cotellic in vemurafenibom prekiniti. **Disfunkcija levega prekata:** Pri bolnikih, ki so prejeli zdravilo Cotellic, so poročali o zmanjšanju citrsnega dela levega prekata (LVEF) v primerjavi z izhodiščem. LVEF je treba izmeriti pred začetkom zdravljenja za določitev izhodiščne vrednosti, nato pa ga kontrolirati po prvem mesecu zdravljenja ter vsaj na 3 mesece oziroma kot je klinično indicirano, do prenehanja zdravljenja. Zmanjšanje LVEF od izhodišča je mogoče obvladati s prekinitvijo zdravljenja, zmanjšanjem odmerka ali prenehanjem zdravljenja. Bolnikov z izhodiščnim LVEF pod splošno mejo normalne vrednosti (SMN) za ustanovo ali pod 50 % niso proučevali. **Jetna laboratorijska odstopanja:** Jetna laboratorijska odstopanja se lahko pojavijo tudi med uporabo zdravila Cotellic v kombinaciji z vemurafenibom kot samostojnim zdravljenjem z vemurafenibom. Pri bolnikih, zdravljenih s kombinacijo zdravila Cotellic in vemurafeniba, so opažali jetna laboratorijska odstopanja, zlasti zvišanje ALT, AST in AF. Jetna laboratorijska odstopanja je treba kontrolirati z laboratorijskimi preiskavami jeter pred začetkom kombiniranega zdravljenja in vsak mesec med zdravljenjem, lahko pa tudi pogosteje, če je klinično indiciirano. Laboratorijska odstopanja stopnje 3 je treba obvladati s prekinitvijo uporabe vemurafeniba ali zmanjšanjem odmerka. Jetna laboratorijska odstopanja stopnje 4 se obvlada s prekinitvijo zdravljenja, zmanjšanjem odmerka ali prenehanjem zdravljenja z zdravilom Cotellic in vemurafenibom. **Disleksija:** Pri bolnikih, zdravljenih z zdravilom Cotellic, so poročali o primerih disleksije stopnje > 3 in resni disleksiji. Disleksija je treba obvladati z antidiaroidi in podpornim zdravljenjem. V primeru disleksije stopnje > 3, ki se pojavi kljub podpornemu zdravljenju, je treba obvladati Cotellic in vemurafenib, prekiniti, dokler se disleksija ne izboljša na stopnjo < 1. Če se disleksija stopnje > 3 ponovi, je treba odmerek zdravila Cotellic in vemurafeniba zmanjšati. **Intoleranca za laktazo:** Zdravilo vsebuje laktazo. Bolniki z redko dedno intoleranco za galaktozo, lakposno obliko pomanjkanja laktaze ali malabsorpcijo glukoze/galaktoze se morajo posvetovati z zdravnikom in se z njim pogovoriti, ali zanje koristi zdravljenje odtehtajo tveganje. **Podaljšanje intervala QTc:** Če interval QTc med zdravljenjem preseže 500 ms, prosimo, glejte povzetka glavnih značilnosti vemurafeniba. **Medsebojno delovanje z drugimi zdravili in druge oblike interakcij:** **Učinki drugih zdravil na kobimetinib:** **Zaviralci CP3A4:** Med zdravljenjem s kobimetinibom se izogibajte sočasni uporabi močnih zaviralcev CP3A4. Če se sočasni uporabi močnega zaviralca CP3A4 ni mogoče izogniti, je treba bolnike skrbno nadzirati glede varnosti. Previdnosti je potrebna, če se kobimetinib uporablja sočasno z zmernimi zaviralci CP3A4. Če se kobimetinib uporablja sočasno z zmernimi zaviralci CP3A4, je treba bolnike skrbno nadzirati glede varnosti. **Induktorji CP3A4:** Treba se izogibati sočasni uporabi z zmernimi in močnimi induktorji CP3A4. Razmisliti je treba o uporabi drugih zdravil, ki CP3A4 inducirajo le malo ali sploh ne. Ker se med sočasno uporabo zmernih do močnih induktorjev CP3A4 koncentracija kobimetiniba verjetno bistveno zniža, se lahko njegova učinkovitost pri bolniku poslabša. **Zaviralci P-glikoproteina:** Sočasna uporaba zaviralcev P-gp, npr. ciklospolina in verapamila, lahko zviša koncentracijo kobimetiniba in plazmi. **Učinki kobimetiniba na druga zdravila:** **Substrati CP3A in CP2D6:** Klinična študija medsebojnega delovanja zdravil pri onkoloških bolnikih je pokazala, da se koncentraciji midazolama in dekstrometofanila v plazmi v prisotnosti kobimetiniba nista spreminjali. **Substrati CYP1A2:** *In vitro* je kobimetinib potencialen induktor CYP1A2 in lahko zato zmanjša izpostavljenost substratom tega encima, npr. teofilinu. **Substrati BCRP:** *In vitro* kobimetinib zmerno zavrača BCRP. Klinično pomembnega zavrta BCRP na ravni črevesja ni mogoče izključiti. **Druga zdravila proti raku:** vemurafenib: Pri bolnikih z neoperabilnim ali metastatskim melanomom ni dokazov o klinično pomembnem medsebojnem delovanju med kobimetinibom in vemurafenibom, zato prilagoditev odmerkov niso potrebne. **Vpliv kobimetiniba na transportne sisteme zdravil:** Študije *in vitro* kažejo, da kobimetinib ni substrat jernih priveznih prenašalcev OATP1B1, OATP1B3 in OCT1, vendar pa jih lahko zavira. Klinični pomen teh izsledkov ni raziskan. **Pediatrična populacija:** Študije medsebojnega delovanja so izvedli le pri odraslih. **Neželeni učinki:** Neželeni učinki pri bolnikih, zdravljenih z zdravilom Cotellic v kombinaciji z vemurafenibom: **Zelo pogosti:** anemija, serozna retinopatija, hipertenzija, krvavitve, driska, navzea, bruhanje, fotosenzibilnost, izpuščaj, makulopapulozen izpuščaj, akneliformni dermatitis, hiperkeratoza, zvišana telesna temperatura, zvišanja CPK, ALT, AST, gama-glutamitranferaze (GGT) in AF v krvi. **Pogosti:** bazilocelularni karcinom, ploščatocelularni karcinom, keratokatantom, dehidracija, hipofosfatemija, hiponatriemija, hiperglikemija, zamegljen vid, okvara vida, pnevmonitis, mrzlica, zmanjšanje izsni delež in zvišanje bilirubina v krvi. **Poročanje o domnevih neželenih učinkih:** Poročanje o domnevih neželenih učinkih zdravila po izdaji dovoljenja za promet je pomembno. Omogoča namreč stalno spremljanje razmerja med koristimi in tveganji zdravila. Od zdravstvenih delavcev se zahteva, da poročajo o katerem koli domnevem neželenem učinku zdravila na: Univerzitetni klinični center Ljubljana, Interna klinika, Center za zastrupitve, Zaloška cesta 2, SI-1000 Ljubljana, Faks: + 386 (0)1 434 76 46, e-pošta: farmakovigilanca@kclj.si. **Režim izdaje zdravila:** Rp/Spec. **Imetnik dovoljenja za promet:** Roche Registration Limited, 6 Falcon Way, Shire Park, Welwyn Garden City, AL7 1TW, Velika Britanija. **Verzija:** 1.0/15. **Informacija pripravljena:** april 2016. Samo za strokovno javnost.

Skrajšan povzetek glavnih značilnosti zdravila ZELBORAF:

Za to zdravilo se izvaja dodatno spremljanje varnosti. Tako bodo hitreje na voljo nove informacije o njegovi varnosti. Zdravstvene delavce naprošamo, da poročajo o katerem koli domnevem neželenem učinku zdravila. Kako poročati o neželenih učinkih, si pogledajte skrajšani povzetek glavnih značilnosti zdravila pod "Poročanje o domnevih neželenih učinkih".

Ime zdravila: Zelboraf 240 mg filmsko obložene tablete. **Kakovostna in količinska sestava:** Ena tableta vsebuje 240 mg vemurafeniba (v obliki precipitata vemurafeniba in hipromeloze acetat sukcinata). **Terapevtske indikacije:** Vemurafenib je indiciran za samostojno zdravljenje odraslih bolnikov z neresektabilnim ali metastatskim melanomom, s pozitivno mutacijo BRAF V600. **Odmerjanje in način uporabe:** Zdravljenje z vemurafenibom mora uvesti in nadzorovati usposobljen zdravnik, ki ima izkušnje z uporabo zdravil za zdravljenje raka. **Udmerjanje:** Priporočeni odmerek vemurafeniba je 960 mg (4 tablete po 240 mg) dvakrat na dan (to ustreza celotnemu dnevnemu odmerku 1920 mg). Vemurafenib lahko vzamemo s hrano ali brez nje, izogibati pa se moramo stalnemu jemanju obnih dnevnih odmerkov na prazen želodec. Zdravljenje z vemurafenibom mora nadaljevati do napredovanja bolezni ali pojava nesprejemljive toksičnosti. Če bolnik izpusti odmerek, ga lahko vzame do 4 ure pred naslednjim odmerkom za ohranitev sheme dvakrat na dan. Obel odmerek pa ne sme vzeti hkrati. Če bolnik po zaužitju vsakega odmerka, brusno, ne sme vzeti dodatnega odmerka zdravila, ampak mora z zdravljenjem normalno nadaljevati. **Prilagoditve odmerjanja:** Za obvladovanje neželenih učinkov ali ob podaljšanju intervala QTc je potrebno zmanjšanje odmerka, zlasti pri bolnikih z zapestji v možganih. Zmanjšanje odmerka po 480 mg zdravila na dan ni priporočljivo. Če se pri bolniku pojavi ploščatocelularni karcinom kože, priporočamo nadaljevanje zdravljenja brez zmanjšanja odmerka vemurafeniba. **Posebne populacije:** Za bolnike, starejše od 65 let, prilaganje odmerka ni potrebno. O bolnikih z okvaro ledvic ali jeter je na voljo malo podatkov. Bolnike s hudo okvaro ledvic ali z zmerno do hudo okvaro jeter je treba pozorno spremljati. Varnost in učinkovitost vemurafeniba pri otrocih in mladostnikih, mlajših od 18 let, nista bili dokazani. Podatki ni na voljo. **Način uporabe:** Tablete vemurafeniba je treba zaviti cele, z vodo. Ne sme se jih žvečiti ali zdrobiti. **Kontraindikacije:** Preobčutljivost na zdravilno učinkovino ali katero koli pomožno snov. **Posebna opozorila in previdnostni ukrepi:** Pred uporabo vemurafeniba je treba z validirano preiskavo potrditi, da ima bolnik tumor s pozitivno mutacijo BRAF V600. Dokazani o učinkovitosti in varnosti vemurafeniba pri bolnikih s tumorji z izrazno redko BRAF V600 mutacijo, ki ni V600E ali V600K, niso prepričljivi. Vemurafeniba se ne sme uporabljati pri bolnikih z malignim melanomom, ki ima divjo tip mutacijo BRAF. **Preobčutljivostne reakcije:** V povezavi z vemurafenibom so bile opisane resne preobčutljivostne reakcije, vključno z anafilaksijo. Hude preobčutljivostne reakcije lahko vključujejo Stevens-Johnsonov sindrom, generaliziran izpuščaj, eritem ali hipotenzijo. Pri bolnikih, pri katerih se pojavijo resne preobčutljivostne reakcije, je treba zdravljenje z vemurafenibom dokončno opustiti. **Kažne reakcije:** Pri bolnikih, ki so prejeli vemurafenib, so v ključnem kliničnem preskušanju poročali o hudih kožnih reakcijah, vključno z redkim Stevens-Johnsonovim sindromom in toksično epidermalno nekrozo. Po prihodu vemurafeniba na trg so v povezavi z njim poročali o reakcijah na zdravilo z eozinofilijo in sistemskimi simptomi (DRESS, *Drug Reaction with Eosinophilia and Systemic Symptoms*). Pri bolnikih, pri katerih se pojavi huda kažna reakcija, je treba zdravljenje z vemurafenibom dokončno opustiti. **Povečanje toksičnosti obsevanja:** Pri bolnikih, ki so se pred, med ali po zdravljenju z vemurafenibom zdravili z obsevanjem, so poročali o primerih *in vivo* povečanih reakcij na mestu obsevanja (t.i. *radiation recall*) in povečane občutljivosti na obsevanje. Večina primerov je bila po naravi kožnih, a nekaj primerov, ki je vključevalo visceralne organe, je imelo smrtni izid. Pri sočasni ali zaporedni uporabi vemurafeniba in obsevanja je potrebna previdnost. **Podaljšanje intervala QTc:** V nekontrolirani, odprti študiji faze II pri predhodno zdravljenih bolnikih z metastatskim melanomom, so opažali podaljšanje intervala QTc, odvisnega od izpostavljenosti vemurafenibu. Podaljšanje intervala QTc lahko poveča tveganje za ventrikularne aritmije, vključno s t. i. *Torsade de Pointes*. Z vemurafenibom ni priporočljivo zdravljenje bolnikov z elektrolitskimi motnjami (vključno z magnezijem), ki jih ni mogoče odpraviti. Bolnike s sindromom dolgega intervala QTc in bolnikov, zdravljenih z zdravili, ki podaljšajo interval QTc, pred zdravljenjem z vemurafenibom, in mesec po zdravljenju in po spremembi odmerka je treba pri vseh bolnikih posneti elektrokardiogram (EKG) in kontrolirati elektrolite (vključno z magnezijem). Nadaljnje kontrole so priporočljive predvsem pri bolnikih z zmerno do hudo jetno okvaro, in sicer mesečno prve 3 mesece zdravljenja, potem pa na 3 mesece oziroma pogosteje, če je to klinično indicirano. Zdravljenje z vemurafenibom ni priporočljivo vstati pri bolnikih, ki imajo interval QTc > 500 milisekund (ms). **Bolzni oči:** Poročali so o resnih neželenih učinkih na oči, vključno z uveitisom, iritisom in zaporo mrežnice vne. Bolnikom je treba redno kontrolirati glede morebitnih neželenih učinkov na oči. **Ploščatocelularni karcinom kože:** Pri bolnikih, zdravljenih z vemurafenibom, so bili opisani primeri ploščatocelularnega karcinoma kože, vključno s ploščatocelularnim karcinomom, opredeljenim kot keratokatantom ali mešanji keratokatantom. Priporočljivo je, da vsi bolniki pred uvedbo zdravljenja opravijo dermatološki pregled in da se med zdravljenjem delžni rednih kontrol. Vsako sumljivo spremembo je treba izrezati, poslati na histopatološko oceno in jo zdraviti v skladu z lokalnimi smernicami. Med zdravljenjem in do šest mesecev po zdravljenju ploščatocelularnega karcinoma mora zdravnik mesečno pregledati bolnika. Pri bolnikih, ki se jim pojavijo ploščatocelularni karcinom kože, je priporočljivo nadaljevati zdravljenje brez zmanjšanja odmerka. Nadzor se mora nadaljevati še 6 mesecev po prenehanju zdravljenja z vemurafenibom ali do uvedbe drugega antineoplastičnega zdravljenja. Bolnikom je treba naročiti, naj svojega zdravnika obvestijo o pojavi kakršnih koli sprememb na koži. **Ploščatocelularni karcinom, ki se ne nahaja na koži:** Pri bolnikih, ki so prejeli vemurafenib v kliničnih preskušanjih, so poročali o primerih ploščatocelularnega karcinoma, ki se ne nahaja na koži. Bolnikom je treba pred uvedbo zdravljenja in na 3 mesece med zdravljenjem pregledati glavo in vrat (pregled mora obsegati vsaj ogleđ usne sluznice in palpacijo bezgavk). Poleg tega morajo bolniki pred zdravljenjem in na 6 mesecev med zdravljenjem opraviti računalniško tomografijo (CT) prsnega koša. Pred in po končanem zdravljenju ali kadar je klinično indicirano, je priporočljivo opraviti pregled zrakovalca in ginekološki pregled (pri ženskah). Po prenehanju zdravljenja z vemurafenibom se mora nadzor glede ploščatocelularnega karcinoma, ki se ne nahaja na koži, nadaljevati še 6 mesecev ali do dveh druge antineoplastičnega zdravljenja. Normalne spremembe je treba obravnavati v skladu s klinično prakso. **Novi primarni melanom:** V kliničnih preskušanjih so poročali o novih primarnih melanomih. Bolnike s takimi primeri so zdravili z ekscizijo, bolniki pa so nadaljevali z zdravljenjem brez prilagoditve odmerka. Nadzor nad pojavom kožnih lezij je treba izvajati, kot je navedeno zgoraj pri ploščatocelularnem karcinomu kože. **Druge malignosti:** Glede na mehanizem delovanja lahko vemurafenib povzroči napredovanje raka, povezanih z mutacijo RAS. Pred dajanjem vemurafeniba bolnikom, ki so imeli ali imajo raka, povezanega z mutacijo RAS, skrbno razmisli o koristih in tveganjih. **Pankreatitis:** Pri bolnikih, zdravljenih z zdravilom Zelboraf, so poročali o pankreatitisu. Neopojasniva bolečina v trebuhu je treba nemudoma preiskati. Bolnike je treba skrbno spremljati, ko po epizodi pankreatitisa ponovno uvedemo vemurafenib. **Poslabšanje jeter:** Med uporabo vemurafeniba so poročali o poslabšanju jeter, vključno s primeri hudih poškodb. Pred uvedbo zdravljenja in mesečno med zdravljenjem oz. kot je klinično indicirano, je treba kontrolirati jetrne encime (transaminaze in alkalne fosfataze) ter bilirubin. Laboratorijske nepravilnosti je treba obvladati z zmanjšanjem odmerka, prekinitvijo zdravljenja ali prenehanjem zdravljenja (za podrobnosti o prilagoditvi odmerka, prosimo glejte SmPC zdravila). **Jetna okvara:** Bolnikom z jetno okvaro začetnih odmerkov ni treba prilagoditi. Bolnike, ki imajo zaradi metastaz v jetrih blago jetno okvaro in nimajo hiperbilirubinemije, se lahko nadzoruje v skladu s splošnimi priporočili. Podatki o bolnikih z zmerno do hudo jetno okvaro je le malo; pri takih bolnikih je izpostavljenost lahko večja. Tako je posebej po prvih tednih zdravljenja potreben skrben nadzor, saj lahko po daljšem obdobju (več tednih) pride do kopičenja. **Ledvična okvara:** Bolnikom z blago ali zmerno ledvično okvaro začetnih odmerkov ni treba prilagoditi. Pri bolnikih z hudo ledvično okvaro je treba vemurafenib uporabljati previdno ter jih pozorno spremljati. **Fotosenzibilnost:** Pri bolnikih, ki so v kliničnih študijah prejeli vemurafenib, je bila opisana blaga do huda fotosenzibilnost. Vsem bolnikom je treba naročiti, naj se med jemanjem vemurafeniba ne izpostavljajo soncu. V primeru fotosenzibilnosti stopnje 2 (nepresojljivi) ali več so priporočljive prilagoditve odmerka. Ženske v rodni dobi morajo med zdravljenjem in vsaj še 6 mesecev po zdravljenju uporabljati učinkovito kontracepcijsko zaščito. Vemurafenib lahko zmanjša učinkovitost hormonskih kontraceptivov. **Sočasna dajanja ipilimumaba:** Pri sočasni uporabi ipilimumaba in vemurafeniba so v preskušanju jeta I poročali o asimptomatskih zvišanih transaminaz in bilirubina stopnje 3. Glede na te preliminarne podatke sočasna uporaba ipilimumaba in vemurafeniba ni priporočljiva. **Medsebojno delovanje z drugimi zdravili in druge oblike interakcij:** **Vpliv vemurafeniba na substrata CYP** Vemurafenib lahko poveča izpostavljenost v plazmi tistih snovi, ki se presnavljajo pretežno s CYP1A2, v takem primeru se lahko razmisli o prilagoditvi odmerka, če je klinično indicirano. Vemurafenib lahko zmanjša plazemsko izpostavljenost zdravilom, ki se presnavljajo pretežno s CYP3A4. Tako je lahko učinkovitost kontracepcijskih tablet, ki se presnavljajo s CYP3A4 in se uporabljajo sočasno z vemurafenibom, zmanjšana. Pri substratih CYP3A4, ki imajo ozko terapevtsko okno, se lahko razmisli o prilagoditvi odmerka, če je klinično indiciirano. Znakert 3 ni znano ali lahko vemurafenib pri 100 µM koncentraciji v plazmi, ki je bila opazna pri bolnikih s stabilno dinamičnega ravnovesja (približno 50 µg/ml), zmanjša plazemsko koncentracijo sočasno dajanih substratov CYP2B6, kot je bupropion. Kadar se vemurafenib pri bolnikih z melanomom uporablja hkrati z varfarinom (CYP2C9), je potrebna previdnost. Tveganja za klinično pomembne učinke na sočasno uporabe učinkovine, ki so substrati CYP2C8, pa ni mogoče izključiti. Zaradi dolge razpolovne dobe vemurafeniba je mogoče, da popolnega inhibitorstva učinkov vemurafeniba na sočasno dajano zdravilo ne opazimo, dokler ne mine 8 dni zdravljenja z vemurafenibom. Po končanem zdravljenju z vemurafenibom bo morda potrebno 8-dnevni premor, da se izognemo interakcijam z nadaljnjim zdravljenjem. **Zdravljenje z obsevanjem:** Pri bolnikih, zdravljenih z vemurafenibom, so poročali o povečanju toksičnosti obsevanja. V večini primerov so bolniki prejeli protokole obsevanja z 2 Gy/dan ali več (hipofrakcionirane protokole). **Vpliv vemurafeniba na transportne sisteme zdravil:** Ob sočasni uporabi vemurafeniba in substrata P-gp je potrebna previdnost. Pri uporabi zdravil, ki so substrati P-gp in imajo ozko terapevtsko okno (npr. digoksina, dabigatran eteksilata, aliskirena), je treba razmisliti o dodatnem spremljanju koncentracije zdravila. Učinki vemurafeniba na zdravila, ki so substrati BCRP, niso znani. Možnost, da vemurafenib morda poveča izpostavljenost zdravil, ki se presnavljajo s BCRP, ni mogoče izključiti. Možni vplivi vemurafeniba na druge prenašalce trenutno ni znan. **Vpliv sočasne uporabe drugih zdravil na vednost študije in vitro** kažejo, da sta presnova s CYP3A4 in glukuronidacija odgovori za presnovo vemurafeniba. Zdi se, da je tudi izločanje z žolcem pomembna pot izločanja. Vemurafenib je treba uporabljati previdno v kombinaciji z močnimi inhibitorji CYP3A4, glukuronidacija in/ali prenašalci beljakovin (npr. ritonavirjem, sakniravirjem, telitromicinom, ketokonazolom, itrakonazolom, vorikonazolom, posazonazolom, nefazodonom, atazanavirjem). Sočasna uporaba močnih induktorjev P-gp, glukuronidacije, in/ali CYP3A4 (npr. rifampicina, rifabutina, karbamazepina, fenitoina ali fenitoina) lahko vodi v suboptimalno izpostavljenost vemurafenibu in se je je treba izogibati. **Študije in vitro so pokazale, da je vemurafenib substrat sekretornih prenašalcev P-gp in BCRP. Vpliv induktorjev in inhibitorjev P-gp in BCRP na izpostavljenost vemurafenibu niso znani. Ne moremo pa izključiti možnosti, da imajo lahko učinki, ki vplivajo na P-gp (npr. verapamil, ciklospirin, ritonavir, kinidin, itrakonazol) ali BCRP (npr. ciklospirin, gefitinib), vpliv na farmakokinetiko vemurafeniba. Za zdaj ni znano, ali je vemurafenib substrat tudi za druge beljakovinske prenašalce. **Neželeni učinki:** Med najpogostejšimi neželenimi učinki (> 30 %) o, o katerih so poročali v zvezi z vemurafenibom, so artralgija, utrujenost, kožni izpuščaj, fotosenzibilnostna reakcija, navzea, alopecija in srbenje. Zelo pogosto je bil opisan ploščatocelularni karcinom kože. Sledijo najpogostejši neželeni učinki, ki so se pojavili pri bolnikih, zdravljenih z vemurafenibom v študiji faze II in III in dogodki iz vrstnih poročil vseh preskušanj in obdobja po prihodu zdravila na trg. **Zelo pogosti:** ploščatocelularni karcinom kože, seboroični karcinomi, kožni papilomi, zmanjšanje teka, glavobol, dispepsija, kašelj, driska, bruhanje, slabost, zaprtost, fotosenzibilna reakcija, aktinična keratoza, kožni izpuščaj, makulo-papulozen izpuščaj, papulozen izpuščaj, srbenje, hiperkeratoza, eritem, alopecija, suha koža, sončne opelkine, artralgija, mialgija, bolečina v okončinah, mišično-skletne bolečine, bolečine v hrbtu, utrujenost, prekijska, periferi edem, astenija, zvišanje GGT. **Pogosti:** folikulitis, bazilocelularni karcinom, novi primarni melanom, ohromelost sedmega žveca, omotica, uveitis, sindrom palmarno-plantarne eritrodostozije, pankulitis (vključno z nodoznim eritemom), plikna keratoza, artritis, zvišanje ALT, alkalne fosfataze, bilirubina in izguba telesne mase, podaljšanje QTc. **Posebne populacije:** Pri starejših bolnikih (> 65 let) je mogoče večja verjetnost neželenih učinkov, vključno s ploščatocelularnim karcinomom kože, zmanjšanjem teka in motnjami srčnega ritma. Med neželenih učinkov stopnje 3, ki so bili med kliničnimi preskušnji vemurafeniba pri ženskah opazni pogosteje kot pri moških, spadajo kožni izpuščaj, artralgija in fotosenzibilnost. **Poročanje o domnevih neželenih učinkih:** Poročanje o domnevih neželenih učinkih zdravila po izdaji dovoljenja za promet je pomembno. Omogoča namreč stalno spremljanje razmerja med koristimi in tveganji zdravila. Od zdravstvenih delavcev se zahteva, da poročajo o katerem koli domnevem neželenem učinku zdravila na: Univerzitetni klinični center Ljubljana, Interna klinika, Center za zastrupitve, Zaloška cesta 2, SI-1000 Ljubljana, Faks: + 386 (0)1 434 76 46, e-pošta: farmakovigilanca@kclj.si. **Režim izdaje zdravila:** Rp/Spec. **Imetnik dovoljenja za promet:** Roche Registration Limited, 6 Falcon Way, Shire Park, Welwyn Garden City, AL7 1TW, Velika Britanija. **Verzija:** 4.0/15. **Informacija pripravljena:** april 2016. Samo za strokovno javnost.**

SKUPAJ

MOČNEJŠA



Kombinacija zdravil
Cotellic[®] ▼ in **Zelboraf**[®] ▼
za zdravljenje odraslih bolnikov
z neoperabilnim ali metastatskim
melanomom, ki ima mutacijo
BRAF V600.^{1,2}

1 Povzetek glavnih značilnosti zdravila Cotellic. Dostopano april 2016 na: http://www.ema.europa.eu/docs/sl_SI/document_library/EPAR_-_Product_Information/human/003960/WC500198563.pdf

2 Povzetek glavnih značilnosti zdravila Zelboraf. Dostopano april 2016 na: http://www.ema.europa.eu/docs/sl_SI/document_library/EPAR_-_Product_Information/human/002409/WC500124317.pdf

Instructions for authors

The editorial policy

Radiology and Oncology is a multidisciplinary journal devoted to the publishing original and high quality scientific papers and review articles, pertinent to diagnostic and interventional radiology, computerized tomography, magnetic resonance, ultrasound, nuclear medicine, radiotherapy, clinical and experimental oncology, radiobiology, radiophysics and radiation protection. Therefore, the scope of the journal is to cover beside radiology the diagnostic and therapeutic aspects in oncology, which distinguishes it from other journals in the field.

The Editorial Board requires that the paper has not been published or submitted for publication elsewhere; the authors are responsible for all statements in their papers. Accepted articles become the property of the journal and, therefore cannot be published elsewhere without the written permission of the editors.

Submission of the manuscript

The manuscript written in English should be submitted to the journal via online submission system Editorial Manager available for this journal at: www.RadiolOncol.com.

In case of problems, please contact Sašo Trupej at saso.trupej@computing.si or the Editor of this journal at gsera@onko-i.si

All articles are subjected to the editorial review and when the articles are appropriated they are reviewed by independent referees. In the cover letter, which must accompany the article, the authors are requested to suggest 3-4 researchers, competent to review their manuscript. However, please note that this will be treated only as a suggestion; the final selection of reviewers is exclusively the Editor's decision. The authors' names are revealed to the referees, but not vice versa.

Manuscripts which do not comply with the technical requirements stated herein will be returned to the authors for the correction before peer-review. The editorial board reserves the right to ask authors to make appropriate changes of the contents as well as grammatical and stylistic corrections when necessary. Page charges will be charged for manuscripts exceeding the recommended length, as well as additional editorial work and requests for printed reprints.

Articles are published printed and on-line as the open access (www.degruyter.com/view/j/raon).

All articles are subject to 700 EUR + VAT publication fee. Exceptionally, waiver of payment may be negotiated with editorial office, upon lack of funds.

Manuscripts submitted under multiple authorship are reviewed on the assumption that all listed authors concur in the submission and are responsible for its content; they must have agreed to its publication and have given the corresponding author the authority to act on their behalf in all matters pertaining to publication. The corresponding author is responsible for informing the coauthors of the manuscript status throughout the submission, review, and production process.

Preparation of manuscripts

Radiology and Oncology will consider manuscripts prepared according to the Uniform Requirements for Manuscripts Submitted to Biomedical Journals by International Committee of Medical Journal Editors (www.icmje.org). The manuscript should be written in grammatically and stylistically correct language. Abbreviations should be avoided. If their use is necessary, they should be explained at the first time mentioned. The technical data should conform to the SI system. The manuscript, excluding the references, tables, figures and figure legends, must not exceed 5000 words, and the number of figures and tables is limited to 8. Organize the text so that it includes: Introduction, Materials and methods, Results and Discussion. Exceptionally, the results and discussion can be combined in a single section. Start each section on a new page, and number each page consecutively with Arabic numerals.

The Title page should include a concise and informative title, followed by the full name(s) of the author(s); the institutional affiliation of each author; the name and address of the corresponding author (including telephone, fax and E-mail), and an abbreviated title (not exceeding 60 characters). This should be followed by the abstract page, summarizing in less than 250 words the reasons for the study, experimental approach, the major findings (with specific data if possible), and the principal conclusions, and providing 3-6 key words for indexing purposes. Structured abstracts are preferred. Slovene authors are requested to provide title and the abstract in Slovene language in a separate file. The text of the research article should then proceed as follows:

Introduction should summarize the rationale for the study or observation, citing only the essential references and stating the aim of the study.

Materials and methods should provide enough information to enable experiments to be repeated. New methods should be described in details.

Results should be presented clearly and concisely without repeating the data in the figures and tables. Emphasis should be on clear and precise presentation of results and their significance in relation to the aim of the investigation.

Discussion should explain the results rather than simply repeating them and interpret their significance and draw conclusions. It should discuss the results of the study in the light of previously published work.

Charts, Illustrations, Images and Tables

Charts, Illustrations, Images and Tables must be numbered and referred to in the text, with the appropriate location indicated. Charts, Illustrations and Images, provided electronically, should be of appropriate quality for good reproduction. Illustrations and charts must be vector image, created in CMYK color space, preferred font "Century Gothic", and saved as .AI, .EPS or .PDF format. Color charts, illustrations and Images are encouraged, and are published without additional charge. Image size must be 2.000 pixels on the longer side and saved as .JPG (maximum quality) format. In Images, mask the identities of the patients. Tables should be typed double-spaced, with a descriptive title and, if appropriate, units of numerical measurements included in the column heading. The files with the figures and tables can be uploaded as separate files.

References

References must be numbered in the order in which they appear in the text and their corresponding numbers quoted in the text. Authors are responsible for the accuracy of their references. References to the Abstracts and Letters to the Editor must be identified as such. Citation of papers in preparation or submitted for publication, unpublished observations, and personal communications should not be included in the reference list. If essential, such material may be incorporated in the appropriate place in the text. References follow the style of Index Medicus. All authors should be listed when their number does not exceed six; when there are seven or more authors, the first six listed are followed by "et al.". The following are some examples of references from articles, books and book chapters:

Dent RAG, Cole P. In vitro maturation of monocytes in squamous carcinoma of the lung. *Br J Cancer* 1981; **43**: 486-95.

Chapman S, Nakielny R. *A guide to radiological procedures*. London: Bailliere Tindall; 1986.

Evans R, Alexander P. Mechanisms of extracellular killing of nucleated mammalian cells by macrophages. In: Nelson DS, editor. *Immunobiology of macrophage*. New York: Academic Press; 1976. p. 45-74.

Authorization for the use of human subjects or experimental animals

When reporting experiments on human subjects, authors should state whether the procedures followed the Helsinki Declaration. Patients have the right to privacy; therefore the identifying information (patient's names, hospital unit numbers) should not be published unless it is essential. In such cases the patient's informed consent for publication is needed, and should appear as an appropriate statement in the article. Institutional approval and Clinical Trial registration number is required.

The research using animal subjects should be conducted according to the EU Directive 2010/63/EU and following the Guidelines for the welfare and use of animals in cancer research (*Br J Cancer* 2010; 102: 1555 – 77). Authors must state the committee approving the experiments, and must confirm that all experiments were performed in accordance with relevant regulations.

These statements should appear in the Materials and methods section (or for contributions without this section, within the main text or in the captions of relevant figures or tables).

Transfer of copyright agreement

For the publication of accepted articles, authors are required to send the License to Publish to the publisher on the address of the editorial office. A properly completed License to Publish, signed by the Corresponding Author on behalf of all the authors, must be provided for each submitted manuscript.

The non-commercial use of each article will be governed by the Creative Commons Attribution-NonCommercial-NoDerivs license.

Conflict of interest

When the manuscript is submitted for publication, the authors are expected to disclose any relationship that might pose real, apparent or potential conflict of interest with respect to the results reported in that manuscript. Potential conflicts of interest include not only financial relationships but also other, non-financial relationships. In the Acknowledgement section the source of funding support should be mentioned. The Editors will make effort to ensure that conflicts of interest will not compromise the evaluation process of the submitted manuscripts; potential editors and reviewers will exempt themselves from review process when such conflict of interest exists. The statement of disclosure must be in the Cover letter accompanying the manuscript or submitted on the form available on www.icmje.org/coi_disclosure.pdf

Page proofs

Page proofs will be sent by E-mail to the corresponding author. It is their responsibility to check the proofs carefully and return a list of essential corrections to the editorial office within three days of receipt. Only grammatical corrections are acceptable at that time.

Open access

Papers are published electronically as open access on www.degruyter.com/view/j/raon, also papers accepted for publication as E-ahead of print.



XALKORI® - prvi zaviralec ALK, odobren za I. linijo zdravljenja napredovalega, ALK pozitivnega nedrobnoceličnega pljučnega raka¹

ALK = anaplastična limfomska kinaza

BISTVENI PODATKI IZ POVZETKA GLAVNIH ZNAČILNOSTI ZDRAVILA

XALKORI 200 mg, 250 mg trde kapsule

▼ Za to zdravilo se izvaja dodatno spremljanje varnosti. Tako bodo hitreje na voljo nove informacije o njegovi varnosti. Zdravstvene delavce naprošamo, da poročajo o kateremkoli domnevnem neželenem učinku zdravila. Glejte poglavje 4.8 povzetka glavnih značilnosti zdravila, kako poročati o neželenih učinkih.

Sestava in oblika zdravila: Ena kapsula vsebuje 200 mg ali 250 mg krizotiniba. **Indikacije:** Zdravljenje odraslih bolnikov z napredovalim nedrobnoceličnim pljučnim rakom (NSCLC - non-small cell lung cancer), ki je ALK (anaplastična limfomska kinaza) pozitiven. Zdravljenje odraslih bolnikov s predhodno zdravljenim, napredovalim NSCLC, ki je ALK pozitiven. **Odmerjanje in način uporabe:** Zdravljenje mora uvesti in nadzorovati zdravnik z izkušnjami z uporabo zdravil za zdravljenje rakavih bolezni. **Preverjanje prisotnosti ALK:** Pri izbiri bolnikov za zdravljenje z zdravilom XALKORI je treba opraviti točno in validirano preverjanje prisotnosti ALK. **Odmerjanje:** Priporočeni odmerki je 250 mg dvakrat na dan (500 mg na dan), bolniki pa morajo zdravilo jemati brez prekinitev. Če bolnik pozabi vzeti odmerka, ga mora vzeti takoj, ko se spomni, razen če do naslednjega odmerka manjka manj kot 6 ur. V tem primeru bolnik pozabljenega odmerka na sme vzeti. **Prilaganja odmerkov:** Glede na varnost uporabe zdravila pri posameznem bolniku in kako bolnik zdravljenje prenaša, utegne biti potrebna prekinitev in/ali zmanjšanje odmerka zdravila na 200 mg dvakrat na dan; če je potrebno še nadaljnje zmanjšanje, pa znaša odmerki 250 mg enkrat na dan. **Prilaganje odmerkov pri hematološki in nehematološki (povečanje vrednosti AST, ALT, bilirubina; ILD/pnevmonitis; podaljšanje intervala QTc, bradikardija) toksičnosti:** Glejte preglednici 1 in 2 v povzetku glavnih značilnosti zdravila. **Okvara jeter:** Pri blagi in zmerni okvari je zdravljenje treba izvajati previdno, pri hudi okvari se zdravila ne sme uporabljati. **Okvara ledvic:** Pri blagi in zmerni okvari prilaganje začetnega odmerka ni priporočeno. Pri hudi okvari ledvic (ki ne zahteva peritonealne dialize ali hemodialize) je začetni odmerki 250 mg peroralno enkrat na dan; po vsaj 4 tednih zdravljenja se lahko poveča na 200 mg dvakrat na dan. **Starejši bolniki (U 65 let):** Prilaganje začetnega odmerka ni potrebno. **Pediatrična populacija:** Varnost in učinkovitost nista bili dokazani. **Način uporabe:** Kapsule je treba pogoltniti cele, z nekaj vode, s hrano ali brez nje. Ne sme se jih zdrobiti, raztopiti ali odpreti. Izogibati se je treba uživanju grenivk, grenivkinega soka ter uporabi šentjanževke. **Kontraindikacije:** Preobčutljivost na krizotinib ali katerokoli pomožno snov. Huda okvara jeter. **Posebna opozorila in previdnostni ukrepi:** **Določanje statusa ALK:** Pomembno je izbrati dobro validirano in robustno metodologijo, da se izognemo lažno negativnim ali lažno pozitivnim rezultatom. **Hepatotoksičnost:** V kliničnih študijah so poročali o hepatotoksičnosti, ki jo je povzročilo zdravilo (vključno s primeri s smrtnim izidom). Delovanje jeter, vključno z ALT, AST in skupnim bilirubinom, je treba preveriti enkrat na teden v prvih 2 mesecih zdravljenja, nato pa enkrat na mesec in kot je klinično indicirano. Ponovite preverjanj morajo biti pogostejše pri povečanih vrednosti stopnje 2, 3 ali 4. **Intersticijska bolezen pljuč/**

pnevmonitis: Lahko se pojavi huda, življenjsko nevarna in/ali smrtna intersticijska bolezen pljuč (ILD - interstitial lung disease)/pnevmonitis. Bolnike s simptomi, ki nakazujejo na ILD/pnevmonitis, je treba spremljati, zdravljenje pa prekiniti ob sumu na ILD/pnevmonitis. **Podaljšanje intervala QTc:** Opažali so podaljšanje intervala QTc. Pri bolnikih z obstoječo bradikardijo, podaljšanjem intervala QTc v anamnezi ali predispozicijo zanj, pri bolnikih, ki jemljejo antiaritmike ali druga zdravila, ki podaljšujejo interval QT, ter pri bolnikih s pomembno obstoječo srčno boleznijo in/ali motnjami elektrolitov je treba zdravilo uporabljati previdno; potrebno je redno spremljanje EKG, elektrolitov in delovanja ledvic; preiskavi EKG in elektrolitov je treba opraviti čim bližje uporabi prvega odmerka, potem se priporoča redno spremljanje. **Bradikardija:** Lahko se pojavi simptomatska bradikardija (lahko se razvije več tednov po začetku zdravljenja); izogibati se je treba uporabi krizotiniba v kombinaciji z drugimi zdravili, ki povzročajo bradikardijo; pri simptomatski bradikardiji je treba prilagoditi odmerki. **Srčno popuščanje:** Poročali so o hudih, življenjsko nevarnih ali smrtnih neželenih učinkih srčnega popuščanja. Bolnike je treba spremljati glede pojavov znakov in simptomov srčnega popuščanja in ob pojavu simptomov zmanjšati odmerjanje ali prekiniti zdravljenje. **Nevtropenija in levkopenija:** V kliničnih študijah so poročali o neutropeniji, levkopeniji in febrilni neutropeniji (pri manj kot 0,5 % bolnikov); spremljati je treba popolno krvno sliko (pogostejše preiskave, če se opazijo abnormalnosti stopnje 3 ali 4 ali če se pojavi povišana telesna temperatura ali okužba). **Perforacija v prebavilih:** V kliničnih študijah so poročali o perforacijah v prebavilih, v obdobju trženja pa o smrtnih primerih perforacij v prebavilih. Krizotinib je treba pri bolnikih s tveganjem za nastanek perforacije v prebavilih uporabljati previdno; bolniki, pri katerih se razvije perforacija v prebavilih, se morajo prenehati zdraviti s krizotinibom; bolnike je treba poučiti o prvih znakih perforacije in jim svetovati, naj se nemudoma posvetujejo z zdravnikom. **Vplivi na vid:** Opažali so motnje vida; če so trdovratne ali se poslabšajo, je treba razmisliti o oftalmološkem pregledu. **Histološka preiskava, ki ne nakazuje adenokarcinoma:** Na voljo so le omejeni podatki pri NSCLC, ki je ALK pozitiven in ima histološke značilnosti, ki ne nakazujejo adenokarcinoma, vključno s skvamoznoceličnim karcinomom (SCC). **Medsebojno delovanje z drugimi zdravili in druge oblike interakcij:** Zdravila, ki lahko povečajo koncentracije krizotiniba v plazmi (atazanavir, indinavir, neflavin, ritonavir, sakvinavir, itraconazol, ketokonazol, vorikonazol, klaritromicin, telitromicin, troleanomicin), tudi grenivke in grenivkin sok. Zdravila, ki lahko zmanjšajo koncentracije krizotiniba v plazmi (karbamazepin, fenobarbital, fenitoin, rifabutin, rifampicin, šentjanževka). Zdravila, katerih koncentracije v plazmi lahko krizotinib spremeni (midazolam, alfentanil, cisaprid, ciklosporin, derivati ergot alkaloidov, fentanyl, pimozid, kinidin, sirilimus, takrolimus, bupropion, efavirenz, peroralni kontraceptivi, raltegravir, irinotekan, morfin, nalokson, digoksin, dabigatran, kolhicin, pravastatin, metformin, prokainamid). Zdravila, ki podaljšujejo interval QT ali ki lahko povzročijo Torsades de pointes (kinidin, disopiramid, amiodaron, sotalol, dofetilid, ibutilid, metadon, cisaprid, moksifloksacin, antipsihotiki). Zdravila, ki



povzročajo bradikardijo (verapamil, diltiazem, antagonisti adrenergičnih receptorjev beta, klonidin, guanfacin, digoksin, meflokin, antiholinesteraze, pilokarpin). **Plodnost, nosečnost in dojenje:** Ženske v rodni dobi se morajo izogibati zanositvi. Med zdravljenjem in najmanj 90 dni po njem je treba uporabljati ustrezno kontracepcijo (velja tudi za moške). Zdravilo lahko škoduje plodu in se ga med nosečnostjo ne sme uporabljati, razen če klinično stanje matere ne zahteva takega zdravljenja. Matere naj se med jemanjem zdravila dojenju izogibajo. Zdravilo lahko zmanjša plodnost moških in žensk. **Vpliv na sposobnost vožnje in upravljanja s stroji:** Lahko se pojavijo simptomatska bradikardija (npr. sinkopa, omotica, hipotenzija), motnje vida ali utrujenost; potrebna je previdnost. **Neželeni učinki:** Najresnejši neželeni učinki so hepatotoksičnost, ILD/pnevmonitis, neutropenija in podaljšanje intervala QT. Najpogostejši neželeni učinki (U 25 %) so motnje vida, navzea, diareja, bruhanje, edem, zaprtje, povečane vrednosti transaminaz, pomanjkanje apetita, utrujenost, omotica in nevropatija. Ostali zelo pogosti (U 1/10 bolnikov) neželeni učinki so: neutropenija, anemija, levkopenija, disgevgzija, bradikardija, bolečina v trebuhu in izpuščaji. **Način in režim izdaje:** Predpisovanje in izdaja zdravila je le na recept, zdravilo pa se uporablja samo v bolnišnicah. Izjemoma se lahko uporablja pri nadaljevanju zdravljenja na domu ob odpustu iz bolnišnice in nadaljnjem zdravljenju. **Imetnik dovoljenja za promet:** Pfizer Limited, Ramsgate Road, Sandwich, Kent, CT13 9NJ, Velika Britanija. **Datum zadnje revizije besedila:** 31.12.2015

Pred predpisovanjem se seznanite s celotnim povzetkom glavnih značilnosti zdravila.

Vir: 1. Povzetek glavnih značilnosti zdravila Xalkori, 23.11.2015



Pfizer Luxembourg SARL, GRAND DUCHY OF LUXEMBOURG, 51, Avenue J.F. Kennedy, L-1855, Pfizer podružnica Ljubljana, Letališka cesta 3c, 1000 Ljubljana

